To the Graduate Council:

I am submitting herewith a dissertation written by Elizabeth Ann McClellan entitled "Tectonic Evolution of the Einunnfjellet-Savalen Area, Hedmark Fylke, Central-Southern Norwegian Caledonides." I have examined the final copy of this dissertation for form and content and recommend that it be accepted in partial fulfillment of the requirements for the degree of Doctor of Philosophy, with a major in Geology.

Robert D. Hatcher, Jr., Major Professor

We have read this dissertation
and recommend its acceptance:

Steven G. Driese

Carl J. Remenyik

Accepted for the Council:

Associate Vice Chancellor
and Dean of the Graduate School

# TECTONIC EVOLUTION OF THE EINUNNFJELLET-SAVALEN AREA, HEDMARK FYLKE, CENTRAL-SOUTHERN NORWEGIAN CALEDONIDES

A Dissertation

Presented for the

Doctor of Philosophy

Degree

The University of Tennessee, Knoxville

Elizabeth Ann McClellan

December, 1993

Copyright © Elizabeth Ann McClellan, 1993
All rights reserved

Dedicated to the memory of my father,
Roy C. McClellan

his great curiosity and child-like wonder of the world around him,
his profound gentleness,
his love for his family and friends,
these things live on forever

# ACKNOWLEDGEMENTS

First and foremost, I thank my committee chair, Prof. Robert D. Hatcher, Jr., for giving me the opportunity to go to Norway and tackle this project, and for having faith that I could successfully complete this dissertation. In the eight years that I have known Bob, I not only learned a wealth of geology, but also much about being a professional and a scientist. Committee members Steve Driese, Hap McSween, and Carl Remenyik were always available for help and discussion, and I am very grateful for their assistance and comments . In addition, I thank Drs. Bill Dunne and Ted Labotka for taking time out to discuss various aspects of my research. Technical assistance was provided by Allan Patchen (microprobe) and Don McClanahan (drafting)—thanks to both for calmly ignoring my attacks of panic! Others who answered my questions, listened to my ranting and raving, or otherwise helped me through the process are Landon Davidson, Lauren Browning, Ian Richards, Marvin Bennet, Gina Keeling, and all the "trailer folks". My gratitude goes to them, and others too numerous to mention.

Field work for this project was supported by Norges Geologiske Undersøkelse (NGU), the University of Tennessee Science Alliance Center of Excellence Distinguished Scientist stipend for Prof. Robert D. Hatcher, Jr., the Geological Society of America, Sigma Xi, and the Discretionary Fund of the Department of Geological Sciences, University of Tennessee. A nine–month research term at NGU was made possible through an American–Scandinavian Foundation Research Fellowship, with generous support from NGU. My extreme gratitude goes to Brian A. Sturt and Fredrik Chr. Wolff of NGU for their help during this period, and to Dr. Hatcher for his continued guidance.

During my stay in Norway, stimulating field excursions and/or geologic discussions with David Roberts, Odd Nilsen, David Gee, Allan Krill, and Tor Grenne provided many insights into Caledonian tectonostratigraphy. In particular, I thank Tor Grenne of NGU for first suggesting that some of my mafic samples with "weird" geochemical signatures might be boninites, and then patiently steering me toward some key references when it was obvious that I had never heard of a such a rock. I also thank Ivar Killi and Folldal Kraftwerk for access to shallow cores from the Folldal and Savalen area.

I will never forget Fru Larsson's lovely cabin, my "home away from home" in the Einunnfjellet-Savalen area, or my wonderful field neighbors, Olav and Eli Anne Strypet. Allan Krill and geology students Ingunn, Bente Laugtug, Trond Watne, Anna Metta Brøseth, Marianne Langedal, and Berit Fjerdingøy, from Norges Tekniske Høgskole, provided friendship as well as invaluable logistical and field assistance. I would also like to thank

Allan and his family for helping me get settled in Trondheim, and for hospitality and many fine meals during my stay.

Last, but far from least, I thank my family for having faith in me all these years—my mother and sister, and my father who always believed in me, even when I didn't. During the course of this project, my husband, Darcy Morey, has served at various times as housekeeper, technician, typist, artist, and counselor, and always as loving husband. To him I owe just about everything!

# ABSTRACT

The central Scandinavian Caledonides comprise a historic area for the study of thrust and nappe tectonics and metamorphic petrology, and more recently have been an important site for studies of Paleozoic plate tectonics. Reconstruction of the tectonic history of the Iapetus Ocean basin between Greenland and Baltica, prior to and during its final closure in the Siluro-Devonian Scandian orogeny, largely depends upon deciphering the tectonic history of the upper allochthon, a composite thrust complex containing elements of an accreted terrane. Although final emplacement of the upper allochthon occurred during the Siluro-Devonian Scandian orogeny, the complex experienced an intricate and still debatable early Paleozoic history. In the central Norwegian Caledonides the upper allochthon comprises the Trondheim nappe complex (TNC). Determination of the nature of internal contacts and timing of assembly of the TNC has been hampered by wide variations in lithology, strain, and metamorphic grade, and scanty age constraints in some rock units. In the Einunnfjellet-Savalen area, southeastern TNC, a polydeformed continental margin quartzite-schist sequence occurs in the core of the Einunnfjellet dome. These rocks, which can be linked to the Baltoscandian miogeocline, were overthrust by the Savalen thrust complex (STC), containing fragments of oceanic crust and associated sediments, then eroded and unconformably succeeded by polymict conglomerate and fine-grained clastic sediment. Regional correlations indicate that tectonostratigraphic relationships similar to the Einunnfjellet-Savalen area are widespread in the TNC and throughout the upper allochthon, and isotopic age dates or faunal control in these areas imply that thrusting of the STC onto the underlying quartzite-schist sequence occurred prior to the Scandian orogeny.

The Einunnfjellet dome is defined by a major NE-SW doubly plunging antiformal axis, and a minor axis that plunges gently NW-SE. A complex interference structure, the dome resulted from several phases of deformation. The first, $D_1$, involved structures present only in rocks stratigraphically below the unconformity. $F_1$ isoclinal, recumbent folds are indicated by a type-2 refold pattern in the core of the dome, and mesoscopic refolded $F_1$ folds occur in pelitic and amphibolitic rocks in the STC. Detailed petrologic study of the rocks in the Einunnfjellet-Savalen area, however, does not reveal firm evidence of metamorphism related to this event.

The Scandian orogenic phase, $D_2$, which produced the NNE-striking antiformal structure of the dome, was a progressive deformation that can be divided into two main phases: a flattening phase ($D_{2a}$) followed by a phase of pervasive shearing ($D_{2b}$). The earliest mesoscopic $F_{2a}$ folds are inclined isoclinal folds with an axial planar schistosity, and are overprinted by pervasive $D_{2b}$ deformation that produced tight flexural flow buckle folds in

quartzite and other competent rocks, and crenulations in schist. In some rocks two distinct foliations related to these phases can be distinguished, although locally the regional foliation is a composite foliation that formed during a single metamorphic event. Textural zoning in garnet indicates that garnet growth began late during $D_{2a}$ in some samples, although the dominant period of growth was synkinematic with respect to $D_{2b}$, suggesting that metamorphism peaked after the transition from flattening to a simple shear regime. Temperatures remained high after deformation ceased, however, as indicated by garnet rims that overgrew the crenulated foliation. Garnet-biotite thermometry and amphibole composition indicate a progressive metamorphic increase from greenschist to amphibolite facies across the area. The transition zone between the two facies (i.e., the epidote-amphibolite facies) is characterized by a change from albite to oligoclase and presence of coexisting calcic amphiboles in mafic rocks, and strong compositional zoning of garnet in pelitic rocks. Mineral assemblages and compositions are consistent with medium-pressure regional metamorphism.

Late gentle warping of the Einunnfjellet antiform about a NW-SE axis accentuated the elongate dome structure, and reoriented fold axes and mineral lineations to a NE plunge on the north side of the dome. The thrust contact between the STC and the underlying quartzite-schist sequence is entirely overprinted by Scandian metamorphism—no metamorphic break occurs at the contact and $D_2$ structures occur in both the hangingwall and footwall rocks—consistent with the STC having been emplaced prior to Scandian orogenesis. In contrast, the eastern contact of the STC with the Fundsjø Group (Meråker nappe) is a prograde $D_{2b}$ shear zone that developed at greenschist facies conditions. Kinematic analysis indicates a clockwise (dextral) sense of movement on the shear zone, although the amount of displacement may be relatively minor.

Much of the areal extent of the TNC comprises the central Gula nappe, a thick sequence of metasedimentary rocks that contains subordinate and discontinuous mafic/ultramafic horizons termed the Gula greenstone. Although much work has been done on metavolcanic sequences that border the Gula nappe on the west (Støren and related complexes) and east (Fundsjø/Hersjø complexes), the tectonic environments of the Gula nappe have remained speculative. Field and geochemical evidence from two metaigneous complexes that occur in the Einunnfjellet-Savalen area, indicates that both complexes formed in a suprasubduction-zone setting. Metabasalts of the Lomsjødalen complex, directly correlative with the Gula greenstone, are primitive arc tholeiites. Overlying metalliferous sediments and possible remnants of black smokers suggest a spreading ridge environment, probably either an opening marginal basin or the earliest stage of island arc development. Mafic rocks of the Bangardsvola complex, previously correlated with either the Fundsjø Group or with rocks equivalent to the

structurally lower Seve nappe, have boninitic affinities uniquely characteristic of subduction-related settings. Although isotopic dating is not yet available for the metaigneous rocks of the Einunnfjellet-Savalen area, they are lithologically and geochemically similar to dated Early Ordovician Norwegian ophiolites that formed in a suprasubduction-zone environment. The association of primitive IAT, boninite, and Fe- and Mn-rich metalliferous sediments is strongly analogous to the upper parts of the Troodos ophiolite, Cyprus. Although the tectonic setting of Troodos is still highly debated, Moores*et al.* (1984) suggested that an actualistic model for this and other Mideast ophiolites is provided by the Andaman Sea region of the Indian Ocean, where short spreading segments formed above an oblique subduction zone. Some variation of this model could account for the field and geochemical features of the metavolcanic rocks of the southeastern TNC, and other Norwegian ophiolites that have similar characteristics.

# TABLE OF CONTENTS


| Chapter | | Page |
|---|---|---|
| I. | Introduction | 1 |
| | The Einunnfjellet-Savalen Area | 1 |
| | Regional Geology | 5 |
| | Upper Allochthon | 7 |
| | Trondheim Nappe Complex | 9 |
| | Regional Problems | 11 |
| II. | Contact Relationships in the Southeastern Trondheim Nappe Complex, Central-Southern Norway: Implications for Early Paleozoic Tectonism in the Scandinavian Caledonides | 13 |
| | Introduction | 13 |
| | The Einunnfjellet-Savalen Area—Stratigraphy and Contact Relationships | 14 |
| | Savalen Area | 19 |
| | Einunnfjellet Dome Area | 25 |
| | Discussion | 28 |
| | The Pre-Scandian Unconformity in the Southeastern Trondheim Nappe | 28 |
| | Comparison with the Otta Nappe—Timing Constraints on Tectonic Evolution | 31 |
| | Tectonic Evolution of the Einunnfjellet-Savalen Area, and Implications for the Trondheim Nappe Complex | 33 |
| | Regional Implications—Contact Relationships within the Upper Allochthon | 37 |
| | Conclusions | 38 |
| III. | Subduction-Related Volcanism in the Gula Nappe, Trondheim Nappe Complex | 39 |
| | Introduction | 39 |
| | Metavolcanic Sequences in the Trondheim Region | 40 |
| | Mafic Metavolcanic Rocks in the Gula Nappe Complex | 44 |
| | Einunnfjellet-Savalen Area | 45 |
| | Lomsjødalen Complex | 46 |
| | Bangardsvola Complex | 48 |
| | Geochemistry | 50 |
| | Analytical Methods | 50 |
| | Major and Trace Elements | 50 |
| | Tectonic Discrimination Diagrams | 54 |
| | Boninite vs. Komatiitic Basalt | 60 |
| | Trace Element Patterns | 62 |
| | Discussion | 67 |
| | Paleotectonic Setting | 67 |
| | Regional Comparisons | 71 |
| | Conclusions | 73 |

| Chapter | | Page |
|---|---|---|
| IV. | Deformational and Metamorphic History of the Einunnfjellet-Savalen Area, Southeastern Trondheim Nappe Complex | 75 |
| | Introduction | 75 |
| | Regional Structural Relationships | 76 |
| | Einunnfjellet-Savalen Area | 77 |
| | Meso- and Macroscopic Structure | 78 |
| | Folds and Lineations | 82 |
| | Mesoscopic Foliations | 97 |
| | Microscopic Structures | 100 |
| | Garnet Zoning | 103 |
| | Textural Zoning | 103 |
| | Compositional Zoning | 111 |
| | Conditions of Metamorphism | 117 |
| | Garnet-biotite Thermometry | 117 |
| | Amphibole Chemistry | 118 |
| | Barometry | 128 |
| | Greenschist-Amphibolite Facies Transition | 129 |
| | Regional Implications | 132 |
| | Summary | 133 |
| Conclusions | | 135 |
| References Cited | | 138 |
| Appendices | | 156 |
| | Appendix 1: Electron Microprobe Analyses | 157 |
| | Appendix 2: Structural Data | 190 |
| | Appendix 3: Mineral Assemblages | 204 |
| | Appendix 4: XRF Analytical Techniques | 207 |
| Vita | | 209 |

# LIST OF FIGURES


| Figure | | Page |
|---|---|---|
| I-1 | Tectonic map of the Scandinavian Caledonides | 2 |
| I-2 | Simplified tectonic map of the central-southern and southwestern Caledonides of Norway, illustrating the extent of the Seve and Köli divisions of the upper allochthon, and the Trondheim nappe complex. | 3 |
| I-3 | Schematic diagram of thrust stacking | 8 |
| II-1 | Geologic map of the Einunnfjellet–Savalen area | 15 |
| II-2 | Pillow structures in greenstone of the Lomsjødalen complex | 22 |
| II-3 | Volengsvola phyllite, Savalen area | 24 |
| II-4 | Felsic clast facies of conglomerate in the upper Savalen sequence | 26 |
| II-5 | Suggested correlations between the Einunnfjellet dome and Savalen areas | 32 |
| II-6 | Simple model for the tectonic evolution of the Einunnfjellet-Savalen area | 34 |
| III-1 | Tectonic map of the Trondheim nappe complex, showing locations of major metavolcanic sequences | 41 |
| III-2 | Photomicrographs of lithologies in the Lomsjødalen complex | 47 |
| III-3 | Photomicrographs of lithologies in the Bangardsvola complex | 49 |
| III-4 | Variation diagrams of major and trace elements versus wt. % MgO | 53 |
| III-5 | $TiO_2$ versus Zr plot | 56 |
| III-6 | Zr/Y versus Zr plot | 57 |
| III-7 | Ti–Zr–Y plot | 58 |
| III-8 | Ti–V plot | 59 |
| III-9 | $TiO_2$ versus MgO plot | 63 |
| III-10 | MORB-normalized trace element diagrams | 64 |

| Figure | | Page |
|---|---|---|
| III-11 | MORB-normalized trace element diagram for Lau basin basalts ..... | 68 |
| IV-1 | Simplified structural map of the Einunnfjellet-Savalen area , showing representative orientations of the dominant foliation and lineation, and trend of major structures ..... | 79 |
| IV-2 | Boudinage and refolded folds in amphibole schist of the Savalen thrust sheet (Einunna mafic complex, UTM 701 005) ..... | 83 |
| IV-3 | Lower hemisphere equal area projection of isoclinal folds, Einunnfjellet dome area .. ..... | 84 |
| IV-4 | Lower hemisphere equal area projection of a) poles to axial surfaces, and b) fold axes of tight folds in 5 subdomains in the Einunnfjellet dome area ..... | 85 |
| IV-5 | Lower hemisphere equal area projection of a) crenulation axes, and b) mineral lineations in 5 subdomains in the Einunnfjellet dome area..... | 87 |
| IV-6 | Lower hemisphere equal area projection of 31 asymmetric fold axes, Einunnfjellet dome area ..... | 90 |
| IV-7 | Lower hemisphere equal area projection of open folds, Einunnfjellet dome area ..... | 91 |
| IV-8 | Lower hemisphere equal area projection of tight folds, Savalen area ... | 92 |
| IV-9 | Crenulation axes and mineral lineations, Savalen area ..... | 93 |
| IV-10 | Outcrop photos of Stei-Langsætra shear zone ..... | 95 |
| IV-11 | Kinematic analysis of sense of movement in shear zone (Mies, 1991).... | 96 |
| IV-12 | Dominant foliation ..... | 98 |
| IV-13 | Poles to compositional layering, or bedding (?) compared to dominant schistosity in same outcrops ..... | 99 |
| IV-14 | Dominant schistosity vs. crenulation cleavage ..... | 101 |
| IV-15 | Photomicrographs of features of $D_{2b}$ deformation ..... | 102 |
| IV-16 | Photomicrograph of composite foliation..... | 104 |
| IV-17 | Photomicrographs of mylonitic foliation..... | 105 |
| IV-18 | Photomicrographs of garnets with inclusions..... | 107 |

| Figure | | Page |
|---|---|---|
| IV-19 | Photomicrographs of garnets with inclusion trails, various orientations | 108 |
| IV-20 | Photomicrographs of rimmed garnets | 110 |
| IV-21 | Sample location map | 112 |
| IV-22 | Zoning profiles of garnets from the Einunnfjellet-Savalen area | 113 |
| IV-23 | Fe-Mg-Mn (squares) and Fe-Mg-Ca (dots) ternary diagrams of garnet composition | 114 |
| IV-24 | Garnet-biotite temperatures, at various pressures, calculated using Hodges and Spear (1982) calibration | 120 |
| IV-25 | Examples of amphibole formula proportion diagrams by Laird and Albee (1981) | 122 |
| IV-26 | Leake classification for calcic amphiboles | 123 |
| IV-27 | Photomicrograph of fine-grained greenstone, sample A1463 | 124 |
| IV-28 | Formula proportion diagrams for amphibolites, Einunnfjellet-Savalen area | 125 |
| IV-29 | Photomicrographs of amphibolite | 127 |
| IV-30 | (100 N1)/(Ca + Na) vs. (100 Al)/(Si + Al) diagram for amphibolites | 130 |
| IV-31 | Metamorphic map of the Einunnfjellet-Savalen area | 131 |

# LIST OF TABLES


| Table | | Page |
|---|---|---|
| II-1 | Previous work in the Einunnfjellet-Savalen area and correlations in the Trondheim region | 18 |
| II-2 | Savalen area: Informal stratigraphy and correlations | 20 |
| II-3 | Einunnfjellet dome area: Informal stratigraphy and correlations | 21 |
| III-1 | Major and trace element concentrations of metavolcanic rocks in the Einunnfjellet–Savalen area | 51 |
| III-2 | Comparison of element concentrations and ratios between siliceous high-magnesian basalts, komatiitic basalts, boninites, Bangardsvola Group I, and Lomsjødalen metavolcanic rocks | 61 |
| IV-1 | Sequence of deformation in the Einunnfjellet-Savalen area | 81 |
| IV-2 | Comparison of garnet-biotite thermometry of pelitic schists from the Einunnfjellet-Savalen area | 119 |

# LIST OF PLATES


| Plate | | |
|---|---|---|
| I | Geologic map of the Einunnfjellet-Savalen area (scale 1:25,000) .... | In Pocket |
| II | Cross sections along lines A-A', B-B', and C-C' on Plate I ..... | In Pocket |
| III | Bedrock geology map of the Lomsjødalen area (scale 1:5,000) ..... | In Pocket |

# CHAPTER I

## Introduction

The Scandinavian Caledonides extend for 1800 km along the length of Scandinavia, and have a present-day width of up to 300 km (Fig. I-1). The orogen consists of Precambrian basement (approximately 1.8 Ga) and thin sedimentary cover of the Baltoscandian platform, over which a stack of thrust nappes were emplaced from west to east during the early to mid-Paleozoic continent-continent collision that closed the ancient Iapetus ocean. Now deeply eroded, the mountain chain has proven to be an excellent location to study the deep structure of a collisional orogen, and to address questions related to the deformational and metamorphic processes that operate at depth, the partitioning of deformation between inboard and outboard elements of an orogen, and the continuous vs. discontinous nature of orogenic events.

### *The Einunnfjellet-Savalen Area*

The Einunnfjellet-Savalen area in the central-southern Norwegian Caledonides (Fig. I-2) contains an eroded structural dome that provides an excellent opportunity to compare and contrast deformation, metamorphism, and tectonic histories of major tectonostratigraphic units. This composite structure exposes a section through several thrust complexes (commonly referred to as thrust nappes in Scandinavian literature), and offers a telescoped view of a number of critical contacts within a relatively small (approximately 300 $km^2$) area. A detailed study of this area is presented here, with the following overall objectives: 1) Make a detailed geologic map of the area (1:25,000 scale), and interpret the geometry of the dome and surrounding area through cross-section and mesofabric analysis; 2) Define the nature of critical contacts between major complexes, and suggest or substantiate regional correlations of the nappes; 3) Interpret the tectonic setting of metavolcanic rocks throughout the area utilizing field relationships and geochemical methods; 4) Determine relative timing of events, and compare deformation and metamorphic histories of the nappes. Satisfaction of these objectives could place important constraints on the evolution of the central-southern Scandinavian Caledonides, and enhance our knowledge of mountain-building processes related to collisional orogens.

This study consists of four major parts—three main chapters, and the plates, that include a detailed 1:25,000 scale geologic map (Plate I), accompanying cross sections (Plate II), and a

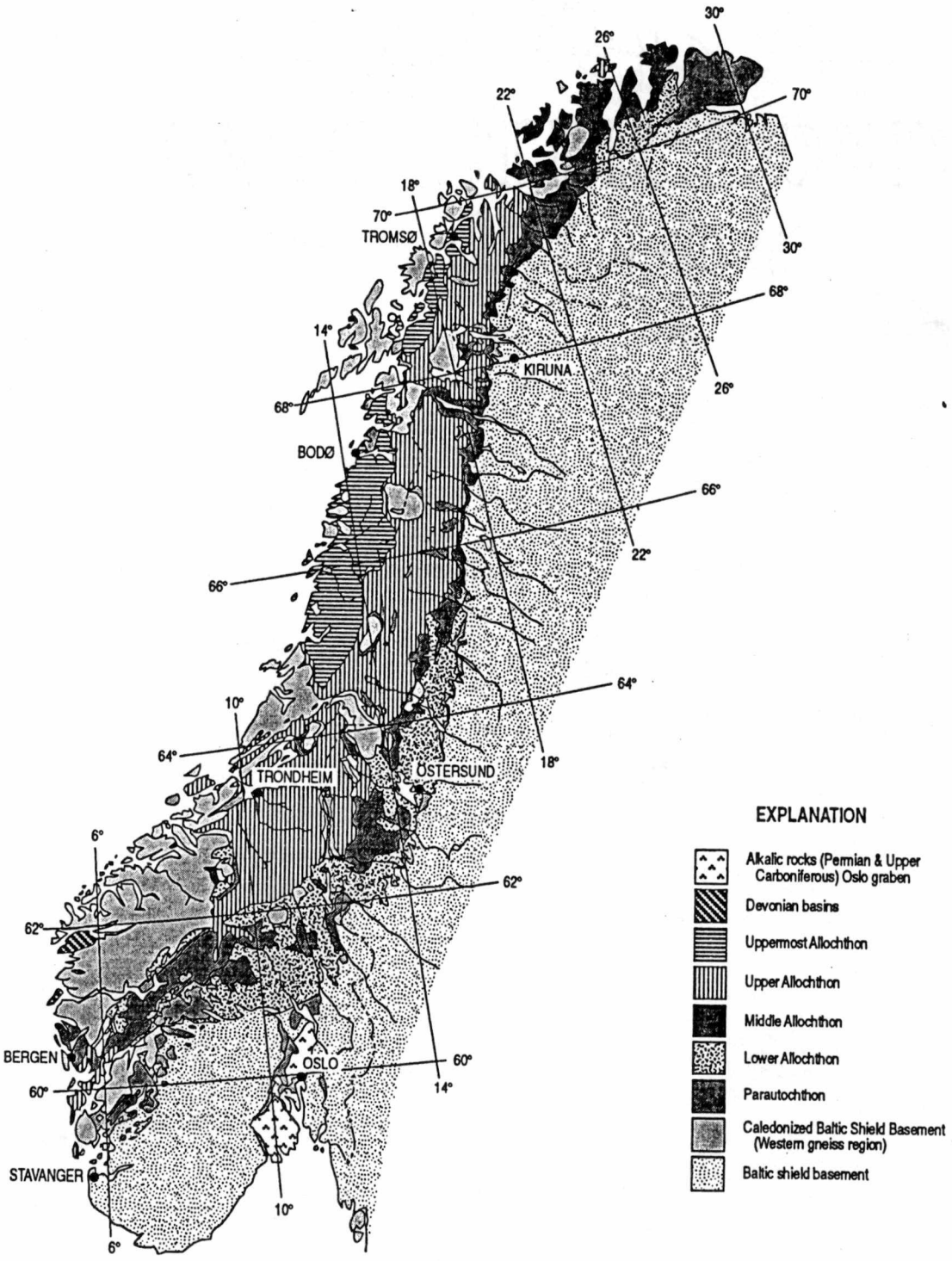
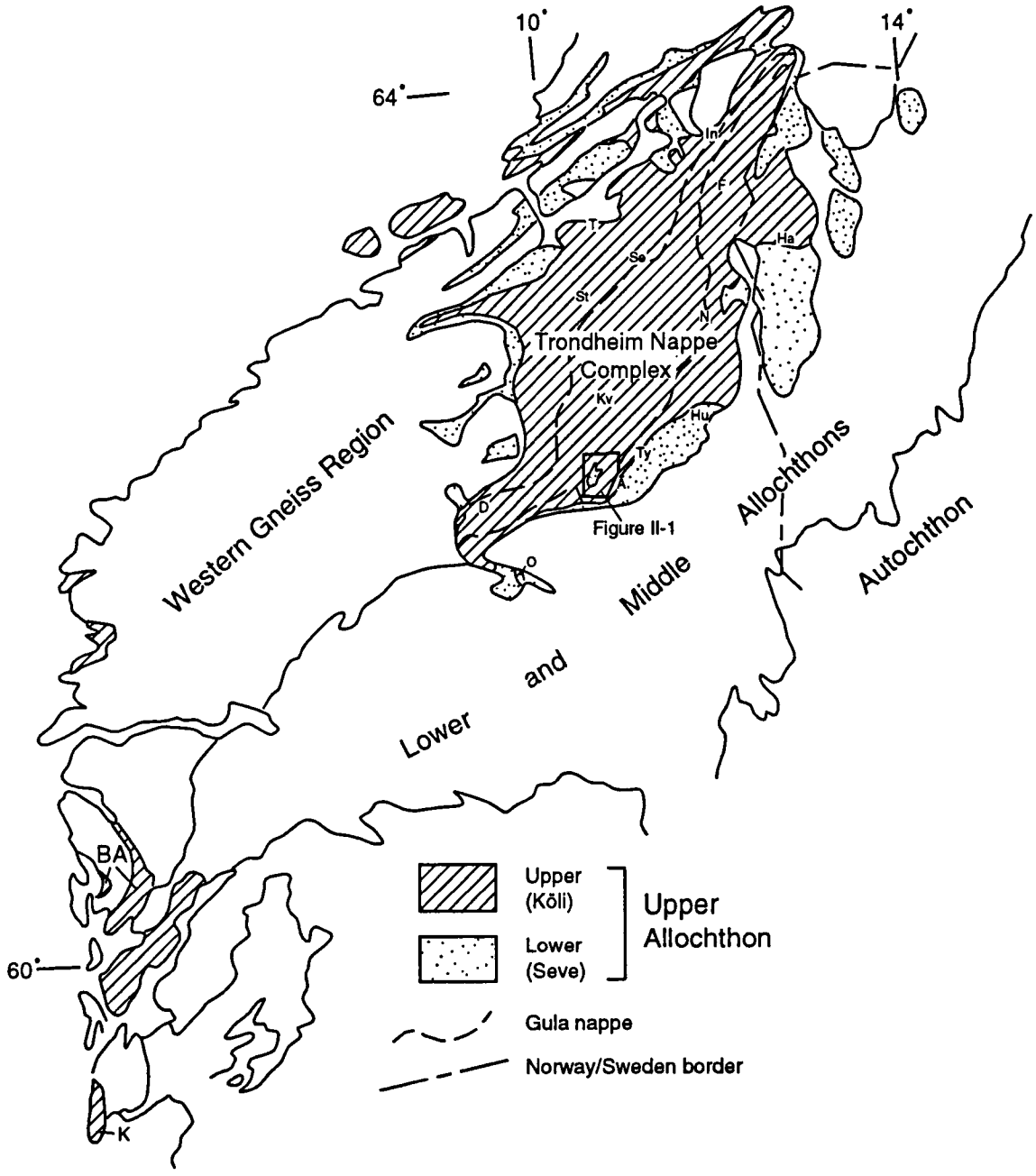



Figure I-1
Tectonic map of the Scandinavian Caledonides. (After Gee, *et al.*, 1985).

Figure I-2
Simplified tectonic map of the central-southern and southwestern Caledonides of Norway, illustrating the extent of the Seve and Köli divisions of the upper allochthon, and the Trondheim nappe complex. Place names and features referred to in the text: BA–Bergen arcs (major and minor); A–Alvdal; D–Dombås; F–Færen; Ha–Handöl; Hu–Hummellfjell; I–Inndalen; K–Karmøy; Kv–Kvikne; N–Nordaunevoll; O–Otta; Se–Selbusjøen; St–Støren; T–Trondheim; Ty–Tynset.


10°
14°
64°
60°
In
F
T
Se
St
N
Ha
Trondheim Nappe Complex
Kv
Hu
Ty
D
Figure II-1
Western Gneiss Region
Middle and Lower Allochthons
Autochthon
BA
K
Upper (Köli)
Lower (Seve)
Upper Allochthon
Gula nappe
Norway/Sweden border

1:5,000 scale geologic map of one part of the area that is critical to stratigraphic interpretation (Plate III). The chapters are basically written as manuscripts, although to avoid excessive repetition between the chapters, the regional geologic setting is summarized in Chapter I, and the chapters are cross-referenced where necessary.

In Chapter II, I describe the stratigraphy and contact relationships between rock units, and present evidence for a previously unrecognized unconformity in the area. In addition, I offer an alternative interpretation of the regional correlations, which places some constraints on the timing of deformation. In the third chapter, I discuss field relationships and whole-rock chemistry (XRF) of metavolcanic rocks from the study area. An exciting result of this part of the study is the recognition of a sequence of boninitic and primitive island-arc volcanites that points to a subduction-related setting for at least portions of the Gula nappe complex. Chapter IV delineates the deformational and metamorphic history of the area, based on macro- and meso-scale structures and fold patterns, microfabrics (including foliations and textural zoning in garnets), garnet and amphibole chemistry, and geothermometry. The geometry of the Einunnfjellet dome and surrounding area, as interpreted from a detailed geologic map of stratigraphic and tectonic contacts and structural data (Plate I), is shown in the accompanying cross sections (Plate II).

## *Regional Geology*

The Scandinavian Caledonides consist of Precambrian crystalline rocks with Late Proterozoic to Silurian, and locally Devonian, cover sedimentary and igneous rocks. The orogen was assembled during the Caledonian orogeny, which is thought to have culminated with closing of the Iapetus ocean basin (Harland and Gayer, 1972) and collision between the Baltoscandian and Laurentian (Greenland) continental margins (Gee, 1975). Several lines of evidence, however, point to a more complex history of deformation and metamorphism in the Caledonides, involving at least two distinct orogenic cycles. Earliest was the Finnmarkian event (530-490 Ma), first recognized in northern Norway (Sturt *et al.*, 1967; Ramsay and Sturt, 1977). Evidence for this event includes radiometric dating of synorogenic plutons (Sturt *et al.*, 1967, 1978); indications of ophiolite obduction in the earliest Ordovician (Furnes *et al.*, 1980); and recognition of a major unconformity cutting both ophiolites and metamorphosed continental rocks (Sturt, 1984), overlain by Middle Arenig to Ashgillian successions. Effects of the Finnmarkian phase are not evident everywhere, having been overprinted by a major period of Siluro-Devonian orogenic activity, termed the Scandian (Gee, 1975). Faunal and isotopic data bracket the main Scandian deformation to between approximately 425 and 400 Ma (Bryhni

and Andréasson, 1985). Mild deformation continued during deposition of Old Red Sandstone basins, and late orogenic sediments were involved in thrusting. Subsequent glaciation has deeply eroded the mountain chain, exposing Precambrian crystalline basement in an number of windows far into the internal zones of the orogen and along the Norwegian coast. Total shortening in the orogen has been estimated from 400-500 km (Gee, 1975; Hossack, 1985) to as much as 1000 km (Gee, 1978) at its widest point.

The nappe theory as traditionally applied to the Scandinavian Caledonides (i.e. large volumes of rock between major thrust faults; see Hossack, 1985) was first proposed by Törnebohm (1888). Since that time geologists have recognized and named a number of such units, and continue the quest to unravel the stratigraphy and internal features of these units. The autochthon and the various nappes have recently been grouped into five major composite thrust sheets (Roberts and Gee, 1985; as modified from Gee and Zachrisson, 1979): the autochthon/parautochthon, lower, middle, upper, and uppermost allochthons (Fig. I-1). A portion of the upper allochthon is the main focus of this study, and will be discussed in detail on page 7. The others are briefly described below.

The autochthon and parautochthon consists of a crystalline basement and cover sequence that occurs along most of the Caledonian foreland and in windows to the west coast of Norway. Precambrian basement rocks of the Scandinavian Caledonides are dominantly 3100 to 1550 Ma granites and gneisses that in some areas record evidence of at least two orogenic events, at 1400-1500 Ma and between 1250 and 850 Ma (Gorbatschev, 1985). Autochthonous basement in the east was unaffected by Caledonian deformation, but was increasingly metamorphosed and deformed toward the west. This has led some to believe that the rocks exposed in interior windows may have been laterally displaced; hence the term "parautochthonous" (Gee and Zachrisson, 1979).

The cover sequence of the autochthon/parautochthon consists of Vendian to Upper Cambrian sandstone and shale deposited directly on the crystalline basement, locally with a basal Varanger tillite. To the south, Ordovician limestones are preserved above the Cambrian shales. The Cambrian black shales served as the master detachment for the lower allochthon, thus controlling the thrust geometry (Roberts and Gee, 1985).

The lower allochthon is dominated by Vendian to Ordovician sandstone and quartzite, shale, and limestone. Some Late Proterozoic tillites are also present. At the frontal thrust zone of the orogen, Precambrian basement rocks occur only locally as thin slices at the base of the lower allochthon, and are believed to have been derived from preexisting irregularities on the basement (Roberts and Gee, 1985). Toward the interior of the orogen, however, the lower allochthon contains more and more Precambrian crystalline rocks, and it becomes increasingly

difficult to distinguish this unit from the autochthon/parautochthon.

The middle allochthon consists of Precambrian basement and a cover of unfossiliferous feldspathic sandstone, quartzite, and conglomerate. Effects of Caledonian deformation and metamorphism are generally more pronounced in this sequence than in the lower allochthon. Characteristic of the upper part of the middle allochthon (Särv nappe) is a suite of dolerite dikes that intruded undeformed sediments at a high angle to bedding. Claesson and Roddick (1983) obtained an $^{40}Ar/^{39}Ar$ date of 665±10 Ma for dikes from the essentially undeformed interior of the Särv nappe, and interpreted the date to represent time of intrusion and alteration of the dikes. In the Särv and equivalent rocks, internal penetrative deformation related to Caledonian orogenesis is limited (Gee, 1975), which Gilotti and Kumpulainen (1986) contributed to reinforcement by the competent dolerite dikes. During Caledonian thrusting the dikes were intensely mylonitized and rotated into discrete shear zones, although their original intrusive relationships are preserved away from thrust contacts (Gee, 1975; Kumpulainen, 1980; Gilotti and Kumpulainen, 1986).

The uppermost allochthon, located in north-central Norway, is dominated by amphibolite facies gneiss, schist, and migmatite with subordinate amphibolite, conglomerate, and marble. Rb-Sr whole rock dates for some of the rocks suggest that at least part of this sequence was metamorphosed prior to the Caledonian orogeny, possibly at 1000 Ma (Roberts and Gee, 1985).

*Upper Allochthon*

The upper allochthon, a complex unit containing heterogeneous lithologies with wide variations in strain and metamorphic grade, contains a majority of the exotic and suspect Caledonide terranes. It can be divided into two parts, the structurally lower Seve nappes and the overlying Köli nappes (Fig. I-1; I-3). The Köli nappes contain extensive metavolcanic units, representing a variety of oceanic tectonic environments, that have been interpreted to have developed outboard of the Baltoscandian platform and miogeocline (Stephens and Gee, 1985). Metamorphism in the Köli nappes is generally at greenschist facies, although epidote-amphibolite facies was reached in some areas. The Seve nappes comprise several thrust-bounded subunits of schist, gneiss, and amphibolite, metamorphosed from epidote-amphibolite to granulite, and locally eclogite, facies. The lower subunits appear to be in part correlative with Late Proterozoic dolerite-intruded sandstone of the underlying Särv nappe (middle allochthon), interpreted to represent the rifted Baltic margin (Gee, 1975; Solyom *et al.*, 1979; Gee *et al.*, 1985). The higher subunits, however, may contain higher-grade equivalents of

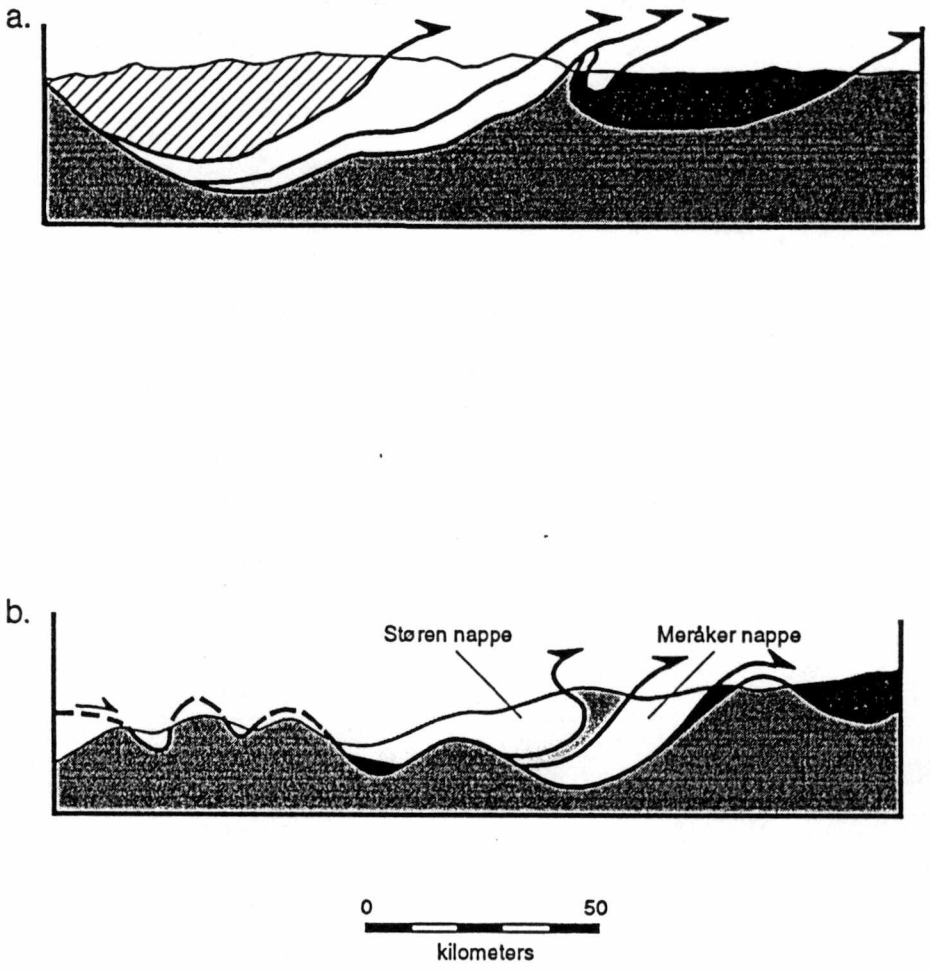



Figure I-3
Schematic diagram of thrust stacking. (a) Upper allochthon; (b) Trondheim nappe complex. White—Køli and equivalent nappes; black—Seve and equivalent nappes; dark gray—lower and middle allochthons; lined pattern—uppermost allochthon. Light gray in (b) is Gula nappe, which has been interpreted as both Seve- and Køli-equivalent (see text for discussion). (a) modified from Stephens and Gee (1985 ), central-northern Caledonides. (b) modified from Gee et al. (1985), Tømmerås area, central-southern Caledonides.

the Köli ocean crust sequences, indicating the transitional, composite nature of the Seve nappes (Andréasson and Gorbatschev, 1980).

Four generations of folds have been recognized within the Köli nappes (Williams and Zwart, 1977; Sjöstrom, 1983). Early tight-to-soclinal folds were overprinted by tight to open folds ($F_2$, $F_3$), commonly with an axial planar crenulation cleavage. Late kink folding has been recognized locally. Peak metamorphism occurred between $D_1$ and $D_2$ (Williams and Zwart, 1977). The sequence of internal deformation within the Seve and equivalent nappes is complicated by higher-grade metamorphism, higher strain, and by possible overprinting of Precambrian structures during Caledonian deformation (Sjöstrom, 1983). Williams and Zwart (1977) divided the internal structures into two groups: Group 1, several generations of tight to isoclinal folds; and Group 2, open or kink-like folds.

The Seve nappes were metamorphosed prior to emplacement onto the underlying Särv rocks, and the contact consistently juxtaposes rocks of contrasting metamorphic grade (Andréasson and Gorbatschev, 1980). Internal thrusts within the Seve nappes are also interpreted as occurring after peak metamorphism, based on discontinuities in metamorphic grade, presence of fault fabrics, and retrogression along contacts (Stephens *et al.*, 1985, and references therein). The Seve-Köli contact, on the other hand, is much more enigmatic. Although it has been traditionally interpreted as a thrust (Williams and Zwart, 1977; Gee *et al.*, 1985), and in some areas is marked by retrogressed mylonites (Sjöstrom, 1983), elsewhere no tectonic break is apparent (Stephens *et al.*, 1985) and the contact appears concordant and transitional (Gee, 1978). Lisle (1984) suggested that the contact was an unconformity, upon which only minor, local movement had occurred.

*Trondheim Nappe Complex*

In the area of this study, the upper allochthon comprises the Trondheim nappe (Wolff, 1967), or Trondheim nappe complex (Guezou, 1978) (Fig. I-2; I-3). Nilsen and Wolff (1989) represented the Trondheim nappe complex as a broad area of dominantly metasedimentary rocks flanked by metavolcanic sequences. Metamorphic grade is highest through the central Trondheim nappe complex—up to sillimanite grade in some pelitic rocks—and decreases to greenschist facies on either side. The central dominantly metasedimentary unit is known as the Gula Schist Group (Kjerulf, 1871; Wolff, 1967), Gula Group (Wolff, 1973) or Gula nappe complex (Gee *et al.*, 1985) (Fig. I-2). It is the least well-understood unit in the Trondheim nappe complex, having been variously correlated with the Seve (Roberts and Wolff, 1981) and Köli (Stephens and Gee, 1985) nappes. Kollung (1990) discussed the various and conflicting "Gula"

correlations. A two-fold division of the Gula Group (Törnebohm, 1896; Rui, 1972) was modified by Nilsen (1978), who divided the unit into three formations. The central Singsås Formation consists mainly of calcareous psammite and mica schist. Thin horizons of amphibolite, the Gula greenstone (Nilsen and Mukherjee, 1972; Nilsen, 1974), commonly associated with black schist and banded quartzite, occur sporadically throughout and bordering the Singsås Formation. The Undal Formation to the west and Åsli Formation to the east are made up of carbonaceous phyllite and biotite schist, and both units contain discontinuous horizons of Gula greenstone. In addition, a polymict conglomerate associated with a crystalline limestone horizon occurs within the Åsli Formation. Nilsen (1978) correlated this conglomerate with the Gudå conglomerate zone (see below).

Flanking the Gula Group to the west are rocks of the Støren Group. In the Støren area the Støren group predominantly consists of slightly metamorphosed pillow lava, breccia, and tuffite (Bugge, 1910), which to the south give way to a progressively more volcaniclastic facies (Nilsen, 1978). Geochemically, the mafic rocks are ocean-floor basalt (Gale and Roberts, 1974). The Støren Group is unconformably overlain by low-grade, locally fossiliferous metasedimentary rocks of the Hovin Group, ranging in age from Arenig–Llanvirn to Ashgill (Bruton *et al.*, 1985). Mafic and felsic volcanic horizons occur at various levels within the Hovin Group. The Støren Group was originally thought to stratigraphically overlie the Gula Group (Vogt, 1945; Wolff, 1967), but later interpretations incorporated a fault contact (Gale and Roberts, 1974), based on the difference in tectonic environments represented by the two groups. Horne (1979) described a mélange unit separating the Støren and Gula Groups in the Selbusjøen area (Fig. I-2) that has a primary contact with Støren metavolcanics, and partially tectonic, partially gradational contact with rocks typical of the Gula Group.

East of the Gula Group, the Meråker nappe contains a sequence of greenschist, quartz keratophyre, and black shale, the Fundsjø Group (Wolff, 1967) or Hersjø Formation (Rui, 1972). Mafic rocks from this unit have yielded both island-arc and MORB affinities (Grenne and Lagerblad, 1985; Grenne, 1988). The Fundsjø Group is overlain to the east by sandstone, siltstone, and phyllite. Locally, conglomerate derived from pebbles of the Fundsjø Group is present at the base of this sequence (Chaloupsky and Fediuk, 1967; Wolff, 1967). Fossils are scarce in this region, although Llandovery monograptids have been described from the black shale in the upper part of the overlying sequence (Getz, 1890).

The nature of the Gula–Fundsjø contact is equivocal, interpreted as either stratigraphic (Rui, 1972) or tectonic (Gee, 1975). Horne (1979) described one locality east of Selbusjøen where pillow lavas of the Fundsjø Group young westward into a fault contact with the Gula Group. Elsewhere, a zone of quartzite conglomerate associated with crystalline limestone—the Gudå

conglomerate of Wolff (1964)—separates the Fundsjø and Gula Groups. Wolff (1973) expanded the Gudå Formation to include metagraywacke, limestone, and mica schist (± amphibole). He considered it the basal portion of the Fundsjø Group, although it occurs along strike with, and is lithologically similar to portions of the Åsli Formation, which Nilsen (1978) assigned to the Gula Group. A potentially very important fossil locality, which has been ascribed to the transition zone between the Gula and Fundsjø (Hersjø) Groups (Rui, 1972), occurs at Nordaunevoll (Fig. I-2), where Vogt (1941) described the distinctive Tremodocian dendroid graptolite *Dictyonema flabelliforme* from highly organic black shale. Unfortunately, the stratigraphic position of this unit is still controversial.

Guezou (1978) reported a "marked tectonic contact" between his Tverråi Formation (Gudå equivalent) and rocks correlative with the Gula Group. Lagerblad (1984a, 1984b) concluded that the Gudå–Fundsjø contact in the Inndalen area (Fig. I-2) is primary, whereas the Gudå–Gula contact must be faulted, based on the supposition that the Gula rocks, which do not contain dikes related to Fundsjø volcanism, are the oldest unit. He presented strong evidence for a gradual increase in metamorphic grade from east to west across all three units, and surmised that the tectonic contact is an early structure, entirely overprinted by later deformation and metamorphism.

## *Regional Problems*

The central-southern Scandinavian Caledonides have been the site of many detailed, classic geologic studies (Gee *et al.*, 1985), but many questions remain. Unsolved problems, such as the nature of internal contacts and resolution of the timing of assembly of the Trondheim nappe complex and lack of age constraints within the central Gula Group, have led to much speculation concerning the internal structure of the complex. Early structural models were based on the apparent lithologic symmetry across the complex, and the authors debated whether the structure was anticlinal or synclinal (Wolff, 1964; Roberts, 1967; also numerous references in Gee *et al.*, 1985). More recent models suggest that the eastern and western flanking sequences may be parts of different thrust sheets within the nappe complex, and are not directly correlative (Gee and Zachrisson, 1974; Gee, 1978). This interpretation is shown in Figure I-3.

Correlations of units within the Gula nappe complex, and the nature of both internal and external contacts are also subject to debate (Gale and Roberts, 1974; Roberts and Wolff, 1981; Gee *et al.*, 1985). Solutions to these problems, along with determination of the tectonic history and setting of the Gula rocks, are crucial to our understanding of the evolution of the

Trondheim nappe complex. Rocks of the Gula nappe comprise a significant part of the Einunnfjellet-Savalen map area, making it an excellent location to try to shed some light on these problems.

# CHAPTER II

## Contact Relationships in the Southeastern Trondheim Nappe Complex, Central-Southern Norway: Implications for Early Paleozoic Tectonism in the Scandinavian Caledonides

### *Introduction*

Caledonian orogenesis in Scandinavia resulted from opening and closing of the Iapetus ocean (Harland and Gayer, 1972), and culminated with collision between the Baltoscandian and Laurentian continental masses during the Siluro-Devonian "Scandian" orogenic phase (Gee, 1975). Early plate tectonic models of the Caledonides (e.g., Gale and Roberts, 1974; Gee, 1975) assumed all major nappe translation, deformation, and metamorphism occurred during the Scandian event. Earlier Paleozoic orogenic episodes, recognized in the pioneering works of Holtedahl (1920) and Vogt (1945), were interpreted to be of only local importance (Roberts *et al.*, 1970; Gee and Wilson, 1974). Vogt (1945), however, considered the pre-Scandian "Trondheim" (Holtedahl, 1920) and "Ekne" disturbances (Vogt, 1945), which were based on the presence of hiatuses within the Caledonian eugeosynclinal tectonostratigraphy in the Trondheim region (Fig. I-2), as widespread episodes of considerable significance. Locally fossiliferous rocks above the unconformities date the Trondheim disturbance as early Arenig or older, and the Ekne disturbance as pre-Ashgill (Vogt, 1945). In the case of the Trondheim disturbance, the hiatus occurs conspicuously above the partially eroded Støren greenstone, and appears to have post-dated a weak metamorphic event (Vogt, 1945). Comparable relationships were later recognized in southwestern Norway (Kvale, 1960; Sturt and Thon, 1976; Naterstad, 1976), again involving greenstone and related rocks that appeared to have been deformed prior to erosion. The Støren and other greenstone sequences were subsequently shown to represent fragments of oceanic crust (Gale and Roberts, 1974; Furnes and Færseth, 1975; Gale, 1975; Furnes *et al.*, 1980), and a nearly complete ophiolite sequence was identified on the island of Karmøy (Sturt and Thon, 1978a; Sturt *et al.*, 1979) in southwestern Norway (Fig. I-2).

During the same time period, Sturt *et al.* (1967) determined that a Late Cambrian/Early Ordovician event, termed the Finnmarkian (Ramsay and Sturt, 1976), had affected the Baltoscandian margin of northern Norway. Based on Rb-Sr dates on supposed synorogenic plutons, the Finnmarkian was thought to have occurred betwen 540 and 490 Ma (Sturt *et al.*, 1978), and was equated with unconformities in southwestern and central Norway (Sturt *et al.*, 1967). Controversy still surrounds the basis for reasoning concerning the "Finnmarkian

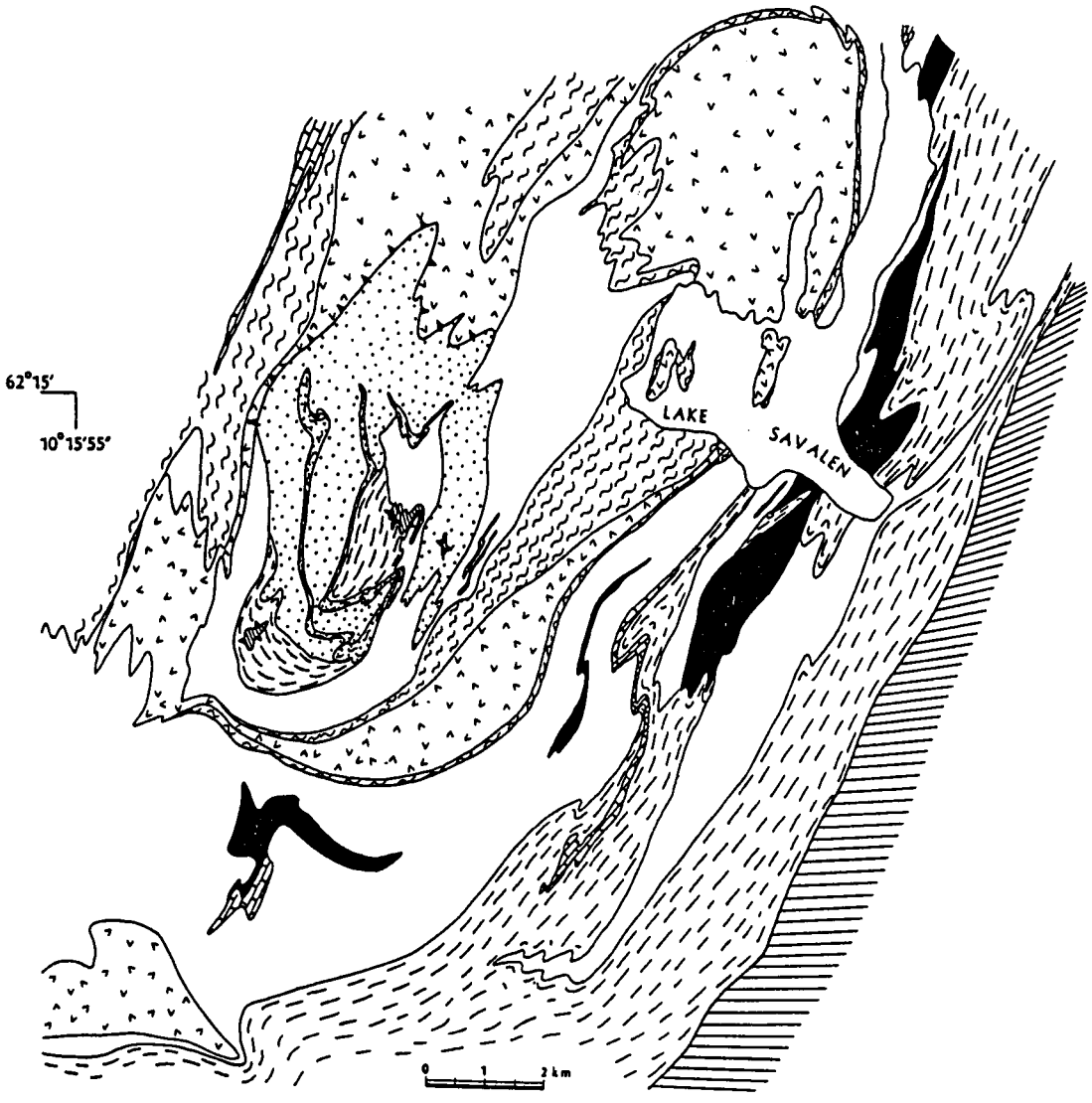
orogeny" (summarized in Townsend and Gayer, 1989), and the relationship of the Finnmarkian and Trondheim events (Bryhni, 1988; Gee, 1987). Evidence that has accumulated over the past two decades, however, clearly favors a period of ophiolite obduction and erosion prior to the Scandian orogeny (Furnes *et al.*, 1980). A major question now concerns the basement upon which the oceanic crust was emplaced (Sturt and Roberts, 1991): were the ophiolites initially thrust onto the Baltoscandian margin (Furnes *et al.*, 1980; Thon, 1985a; Sturt and Roberts, 1991)? Or, as suggested by faunal provinciality (Bruton and Bockelie, 1980), were some first emplaced upon Laurentia (Stephens and Gee, 1985) or an intervening microcontinent (Roberts *et al.*, 1984; Bruton and Harper, 1988) and later welded to Baltica during Siluro-Devonian continent-continent collision? One key piece to this puzzle is whether a belt-length, "terrane-linking" unconformity developed above the eroded ophiolite fragments prior to Scandian orogenesis (Sturt, 1984; Sturt and Roberts, 1991). Acceptance of such an unconformity hinges upon the difficult task of resolving contact relationships that have been overprinted by Scandian deformation, as well as recognition of pre-Scandian structures and/or metamorphism, and more precise age control through faunal or radiometric dating.

This study, based on detailed mapping in the Einunnfjellet-Savalen area, southeastern Trondheim nappe complex (Fig. II-1 & Plate I), provides additional evidence for the widespread nature of both pre-Scandian ophiolite obduction and subsequent development of a regional unconformity. The nature of this unconformity is addressed by detailed mapping of complex contact relationships in an intensely deformed rock sequence, coupled with recognition of early structures possibly related to ophiolite emplacement. The age of the early deformation is constrained by correlation with fossiliferous successions elsewhere within the Trondheim nappe complex. Situated to the east of these other successions, the Einunnfjellet-Savalen area also furnishes an important link between the tectonostratigraphy of the western Trondheim region and that of the Seve and Köli nappes in Sweden.

## *The Einunnfjellet-Savalen Area—Stratigraphy and Contact Relationships*

The Einunnfjellet-Savalen area (Fig. II-1 & Plate I) is located near lake Savalen, county Hedmark, 130 km south of Trondheim. The various stratigraphic interpretations of the region have been complicated by polyphase folding and differences in metamorphic grade, and uncertain age assignments that are based on lithologic correlations with other regions where age is constrained by fossil or radiometric data. Early work in and around the area includes that of Kleine-Hering (1969), Berthomier *et al.* (1970), Quenardel (1972), and Mosson *et al.* (1972). Lithostratigraphic correlations from these works, summarized in Table II-1, were based

Figure II-1
Geologic map of the Einunnfjellet–Savalen area. Location shown in Figure I-2. The map area is divided into two subareas, and, with the exception of the Fundsjø Group, all stratigraphic units are informal (descriptions and regional correlations in Tables II-2 and II-3). See text for discussion of interpreted unconformity in the two subareas. Lithologic contacts on the two islands in lake Savalen after Rui and Nilsen (1988) and Quenardel (1970).


62°15'
10°15'55"
LAKE
SAVALEN
0
1
2 km

## Explanation for Figure II-1

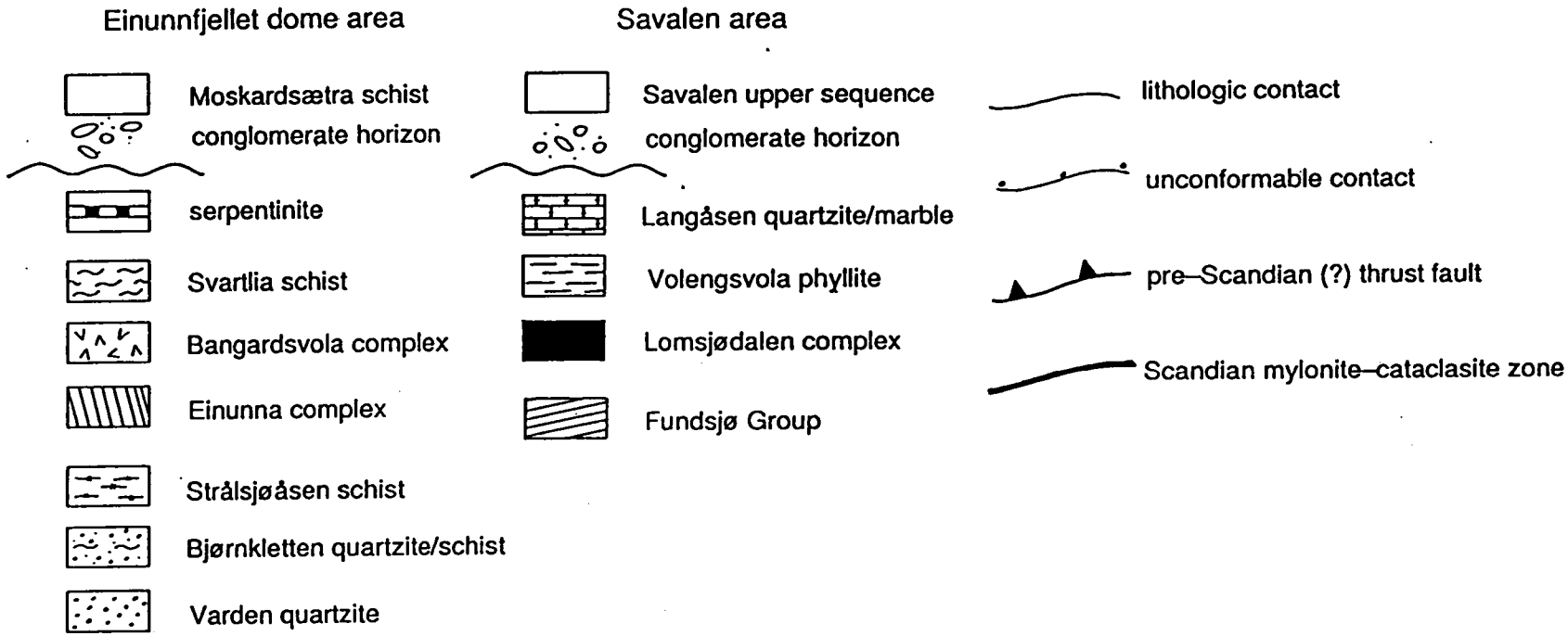


Table II-1: Previous work in the Einunnfjellet-Savalen area and correlations in the Trondheim region (modified from Mosson *et al.*, 1972)

| Presumed age | Western Trondheim sequence (Vogt, 1945; Chaloupsky, 1970) | Sel–Vågå area (SW) (Strand, 1951) | Einunnfjellet area (Mosson *et al.*, 1972) | Savalen–Alvdal area (Kleine–Hering, 1969) | Eastern sequence—Meråker (Getz, 1890; Wolff, 1967) |
|---|---|---|---|---|---|
| Silurian | Horg Group<br>schist and sandstone conglomerate | Absent | Absent | Absent | Slågån Group<br>graywacke |
| Ashgillian | Upper Hovin Group<br>black schist, sandstone, rhyolite | mica schist (?) | Naustervola group<br>gray mica schist, limestone | upper Naustervola series<br>graphitic phyllite, gray quartzite | Kjølhaugen Group<br>schist and metasandstone |
| Caradocian | conglomerate (Volla) | conglomerate (Skardshø) | conglomerate (Dølplass) | conglomerate | conglomerate (Kjølhaugen) |
| Llandeillian | Lower Hovin Group<br>rhyolitic tuff, sandstone, conglomerate limestone | mica schist with limestone (Sel) | Rødalshøa group<br>dark mica schist; limestone (w/fuchsite), amphibole–mica schist, amphibolite | lower Naustervola series<br>blue–gray phyllite, limestone | Sulåmo Group<br>amphibolite, sandstone and conglomerate, limestone (Brenna), schist |
| Llanvirnian<br>Arenigian | gray schist, greenstone conglomerate | serpentine conglomerate, greenstone cong. | absent (?) | absent (?) | conglomerate (Lille Fundsjø) |
| Tremodocian | Støren Group<br>greenstone | greenstone | Lomnesvola group<br>greenstone and metakeratophyre | Vesleåsen series<br>greenstone and metakeratophyre | Fundsjø Group<br>greenstone and metakeratophyre |
| Cambrian | ? | Heidal Series<br>? | *Einunnfjell group<br>mica-amphibole schist (serpentinite, amphibolite) | Røros Group<br>mica schist, cong., greenschist, serpentinite cong. (Brekkebakk) mica schist and quartzite | Sonvatn Group–Gula Group<br>mica schist, conglomerate (Gudå), limestone, mica schist |
| | | mica schist<br>banded mica schist and quartzite<br>conglomerate | mica schist and quartzite<br>graphitic schist<br>quartzite | | mica schist |
| Precambrian–Eocambrian | ? | Rudihø crystalline complex | ?<br>*(correlation with Gula Gp. uncertain) | Sparagmite | ? |

on the proposed equivalence of the western and eastern sequences of the Trondheim nappe complex (although, as noted in Chapter I, this correlation is now considered questionable). The stratigraphic position of the Gula Group remained uncertain in this interpretation. Lieungh (1970) offered an alternative interpretation, in which rocks of the Naustervola and Rødalshøa units (Table II-1) were correlated with the Gula Group. This correlation was retained in later work (Nilsen, 1978; Rui and Nilsen, 1988). A recent compilation (Nilsen and Wolff, 1989) depicts the Einunnfjellet structure as a window cored by quartzite of the Hummelfjell nappe, which is surrounded and in fault contact with various metasedimentary and metaigneous rocks of the Essandsjø (including Røros Group), Meråker, and Gula nappes.

Because interpretations of contact relationships and regional correlations of this study differ somewhat from those of Nilsen and Wolff (1989), and from earlier studies, I have named most units informally to facilitate discussion. The informal stratigraphy, lithologic descriptions, and UTM coordinates of key localities, as well as correlations with Nilsen and Wolff (1989) and with the Swedish nappe terminology, are given in Tables II-2 and II-3. Two sub-areas within the map area are critical to this study; the Einunnfjellet dome area to the west, and the Savalen area, south and east of lake Savalen (Fig. II-1).

*Savalen Area*

South and east of lake Savalen rocks are, in part, at lower metamorphic grade and less intensely deformed than rocks of the Einunnfjellet dome, and stratigraphic relationships are more easily discerned. The stratigraphy can be divided into lower and upper sequences, interpreted to be separated by a regional unconformity.

*Lower Sequence:* The lower Savalen sequence consists of three units, informally named the Lomsjødalen mafic complex, the Volengsvola phyllite, and the Langåsen quartzite/marble (Table II-2). The exact stratigraphic relationships of these units is uncertain, because of intense folding and lack of consistent facing criteria. The Lomsjødalen mafic complex occurs in several lensoid exposures in the Savalen area (Fig. II-1) To the east, the complex consists of massive and pillowed greenstone (Fig. II-2) and volcanic breccia overlain by a sequence of volcaniclastic and sedimentary rocks. At the contact with greenstone, the overlying sequence occurs as fine-grained, dark grey-green laminated tuffite. A unique feature of these rocks is abundant millimeter to centimeter-scale interlayers of fine-grained pink coticule, consisting of quartz and masses of tiny (0.01 to 0.20 mm) spessartine-rich garnets. Higher in the sequence, tuffite grades into coarser-grained, laminated and quartz-veined phyllite rich in chlorite and epidote, and

Table II-2: Savalen area: Informal stratigraphy and correlations

| Stratigraphy based on this study (informal unless otherwise noted) | Lithologic Summary | Regional Correlations | Correlative Nappes in Sweden |
|---|---|---|---|
| Upper Sequence | Conglomerate and pebbly sandstone grading into calcareous, feldspathic sandstone and greenish phyllite, then into homogeneous, slaty gray to black phyllite, in part graphitic. Conglomerate varies from polymict (UTM 774 997), with clasts of greenstone, quartz keratophyre, quartzite, and carbonate, to nearly monomict, dominated by greenstone (UTM 774 991) or keratophyre (UTM 762 004) clasts. Matrix contains chlorite, biotite, epidote, quartz, and feldspar, with metamorphic garnet in western-most exposures (UTM 762 004). To the north, in contact with the Langåsen marble, conglomerate contains clasts of fuchsite marble in amphibole-rich matrix (UTM 792 091). | Graphitic phyllite: Åsli Formation of Gula Nappe (Nilsen and Wolff, 1989);<br><br>Conglomerate: Gudå Formation (Wolff, 1967) or Gudå Group (Lagerblad, 1984); Skardshø conglomerate (Strand, 1951; Guezou, 1978) | Koli (?) |
| Lower Sequence | | | |
| Langåsen quartzite/marble | Quartzite and marble, typically with fuchsite (Cr-muscovite). White quartzite, fine-grained, with bright green fuchsite laminae. White calcite marble, with fuchsite flakes, or gray marble without fuchsite. | Åsli Formation of Gula Nappe (Nilsen and Wolff, 1989); Gudå Formation (Wolff, 1967) or Gudå Group (Lagerblad, 1984); Tverråi Formation (Guezou, 1978) | Köli? (Stephens and Gee, 1985) or Seve? (Roberts and Wolff, 1981) |
| Volengsvola phyllite | Laminated, quartz-veined gray phyllite. Alternating calcareous sandy layers, up to few cm in thickness, with thicker layers of variably graphitic phyllite (biotite + muscovite + chlorite + quartz with garnet to south and west). Rarely, graded bedding present. Locally, pebble conglomerate or broken zones contain clasts of same rock types. Quartz veins of 3 generations: early, bedding parallel; parallel to dominant foliation; and late, random veins. | Åsli Fm., in part Singsås Fm. of Gula Nappe (Nilsen and Wolff, 1989); or Gudå Formation (Wolff, 1967) or Gudå Group (Lagerblad, 1984) | Köli? (Stephens and Gee, 1985) or Seve? (Roberts and Wolff, 1981) |
| Lomsjødalen mafic complex | To east, greenstone (actinolitic hornblende+ chlorite + epidote + calcite), pillow lava (UTM 762 996), volcanic breccia. To west, amphibolite with fragments of metagabbro. Cap rock sequence of gray-green tuffite and quartz-veined phyllite, typically chlorite- and epidote-rich, interspersed with thin laminae of pink cherty coticule (Mn-garnet and quartz). Near greenstone contact also contains dark chert, fine-grained, laminated metalliferous rocks, keratophyre, and pods of siliceous ore-bearing "iron formation"(UTM 762 000; 738 993). | Gula Greenstone of Gula Nappe (Nilsen, 1978; Nilsen and Wolff, 1989) | Köli? (Stephens and Gee, 1985) or Seve? (Roberts and Wolff, 1981) |
| Fundsjø Group (Wolff, 1967) | Greenschist and mafic tuff interlayered with quartz keratophyre. Subordinate horizons of graphitic black phyllite and cherty layers associated with sulfide mineralization. Mylonitic textures common, particularly in quartz keratophyre. | Fundsjø Group of Meråker nappe (Nilsen and Wolff, 1989) | Köli |

Table II-3: Einunnfjellet dome area: Informal stratigraphy and correlations

| Stratigraphy of this study (informal unless otherwise noted) | Lithologic Summary | Correlations Nilsen and Wolff (1989) | Correlative Nappes in Sweden Roberts and Wolff, 1981) |
|---|---|---|---|
| Moskardsætra graphitic schist | Garnetiferous graphite schist of garnet in fine–grained matrix of muscovite, graphite, biotite, and quartz. Interlayers of dark gray to black graphitic quartzite common. Subordinate rock types are coarser–grained garnet–biotite–muscovite schist and feldspathic metasandstone. Locally at base is conglomerate containing mafic and carbonate clasts in amphibole–rich matrix (UTM 712 998), or alternatively serpentinite (possibly detrital–UTM 716 000) and actinolite–talc schist. | Essandsjø Nappe | Seve |
| Bangardsvola igneous complex | Bimodal to multimodal metaigneous suite. Amphibolite is dark green to black, schistose, and thinly banded with felsic laminae. Quartz keratophyre consists of very fine–grained quartz + feldspar groundmass, with larger albite grains (possibly relict phenocrysts) and porphyroblasts of amphibole and garnet. Coarse–grained amphibole–feldspar rock of intermediate composition, metagabbro and coarser–grained keratophyre also present. | Meråker Nappe (Fundsjø Group) | Köli |
| Svartlia mica schist | Laminated mica–quartz schist (± garnet) and garbenschiefer. Gray micaceous layers alternate with mm– to cm–scale quartz–rich laminae. Garbenschiefer is typically muscovite–rich, with amphibole rosettes visible on foliation surfaces. Near contact with Bangardsvola complex, it is rusty brown (more biotite–rich) and non–laminated. | Essandsjø Nappe | Seve |
| Einunna mafic complex | Heterogeneous unit containing sheared amphibole schist, metagabbro, and amphibolite, with minor mafic chlorite–biotite schist, quartz keratophyre, and carbonate. Amphibole schist locally contains lenses of coticule (UTM 701 005). Outcrop thickness of individual layers ranges from 0.5–15 m. | Essandsjø Nappe | Seve |
| Einunnfjellet quartzite/schist sequence | | Hummelfjell Nappe | Seve (higher–grade equivalent of Särv nappe) (Gee and others, 1985) |
| Strålsjøåsen calcarous schist | Silver to greenish garnet–muscovite–chlorite schist ± biotite ± amphibole. Accessory epidote and tourmaline. Commonly contains thin quartz–rich laminae. Locally thick interlayers of fine–grained garnetiferous quartzite (metachert?). | | |
| Bjørnkletten quartzite | Quartzite and feldspathic quartzite, alternating with thin interlayers of biotite–muscovite–quartz schist ± garnet. Gradational contact with Varden quartzite. | | |
| Varden quartzite | Sucrosic quartzite, locally feldspathic; light to medium gray, weathers white. Thick to massive layering. Foliation defined by very thin muscovite laminae. | | |



Figure II-2
Pillow structures in greenstone of the Lomsjødalen complex. (Locality: UTM 762 996)

containing some coticule intercalations. Sulfidic black phyllite is locally associated with the greenstone and the overlying rocks. Small pods (2-3 $m^2$) of ore mineralization typified by dark, siliceous "iron formation" occur within the sedimentary rocks near the greenstone contact. The westernmost exposures of the Lomsjødalen complex are more intensely deformed and metamorphosed, and consist of sheared greenstone and metagabbro surrounded by a thinned, heterogeneous cover of dark chert, coticule, fine-grained metalliferous sedimentary rocks, and tuffite, again with pods of iron formation.

A distinctive horizon of fuchsite-bearing quartzite and marble, informally designated the Langåsen quartzite/marble, commonly occurs either in contact with volcaniclastic/ sedimentary rocks of the Lomsjødalen complex, or with the Volengsvola phyllite (described below). The two lithologies of the Langåsen occur in approximately equal proportions, as fine-grained white quartzite with bright green fuchsite laminae, or as white calcite marble with fuchsite flakes. Gray marble without fuchsite is also present, although subordinate, and is generally interlayered with the other rocks.

The most widely exposed unit in the Savalen area is the Volengsvola phyllite, dominated by laminated and heavily quartz-veined grey phyllite. Original bedding ($S_0$) is recognizable as fine-grained, calcareous sandy layers, up to a few centimeters thick, alternating with thicker layers of slightly to moderately graphitic phyllite. Graded bedding is rarely recognizable in sandy layers, and thin "broken" zones appear to be intraformational breccia or rip-up clasts. Although $S_0$ is generally transposed into the regional foliation, locally the foliation crosscuts $S_0$ at a high angle. Abundant quartz veins of several different generations are characteristic of the Volengsvola phyllite, and impart a distinct "ribbony" appearance to the rock (Fig. II-3). The earliest veins are generally parallel to $S_0$ and are isoclinally folded along with the layering. Later millimeter-thick quartz veins parallel the dominant cleavage, refracting slightly through the sandy layers. A third vein set, with more random orientation, is also present.

*Upper Sequence:* The upper Savalen sequence is interpreted to unconformably overlie the lower sequence. Near the contact are discontinuous conglomerate horizons that alternately overlie Lomsjødalen, Volengsvola, or Langåsen lithologies. The largest mapped exposure of conglomerate, just south of the east end of lake Savalen (Fig. II-1), occurs in a tight antiform, and is bordered in two locations by greenstone or coticule-bearing phyllite. Clast composition of the conglomerate varies both between horizons and along strike within the same horizon. At the southern end of the exposure just mentioned, for instance, the conglomerate contains dominantly mafic clasts, including both fine-grained greenstone and metagabbro, in a green, chlorite and epidote-rich matrix, whereas toward the northern end it is finer-grained, the

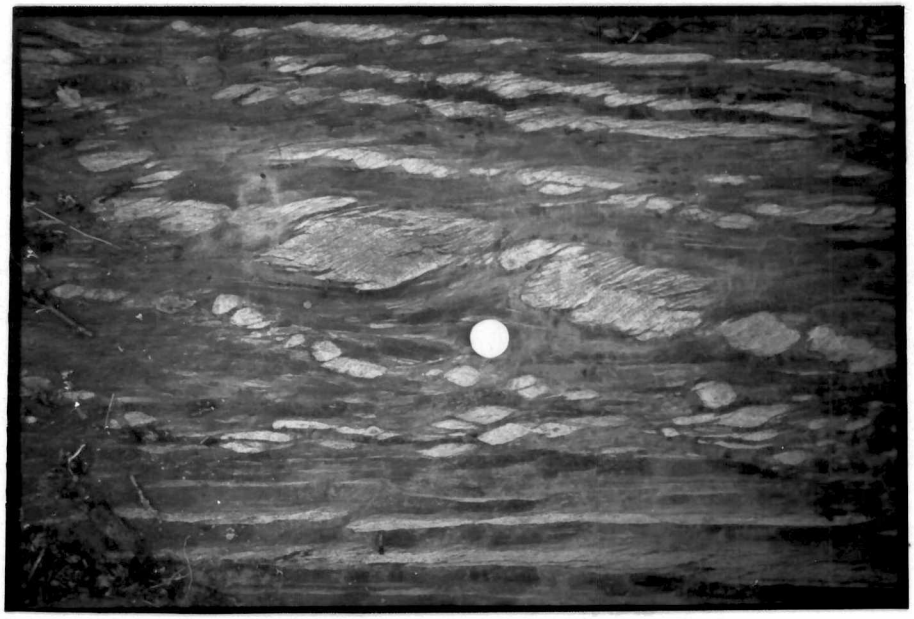


Figure II-3
Volengsvola phyllite, Savalen area. Incompletely transposed compositional layering and early quartz veins are transected by regional foliation and later set of veins which refract through sandy layers (UTM 756 939).

matrix is more sandy and calcareous, and the clast population includes a prominent felsic igneous component, with subordinate quartzite, chert, and carbonate (Fig. II-4). Elsewhere the conglomerate is nearly monomict, dominated by felsic clasts that generally appear to have been derived from fine-grained volcanic or hypabyssal intrusive rocks. In thin section these clasts are very similar to quartz keratophyre that occurs in the Bangardsvola igneous complex to the west (described below). North of lake Savalen, conglomerate containing clasts of fuchsite-bearing marble and chert in an amphibole-rich matrix is in direct contact with Langåsen marble.

The conglomerate grades upward into a thin zone of chlorite-rich, calcareous metasandstone and homogeneous gray phyllite. The metasandstone contains abundant detrital feldspar and isolated clasts of felsic igneous rocks similar to those in the conglomerate. The highest stratigraphic level, and most widely exposed lithology, is gray or black, variably graphitic phyllite. The phyllite is typically homogeneous, lacking sandy interlayers or abundant quartz veins such as in the Volengsvola phyllite, and has a characteristic slaty texture. This texture is present even in the westernmost exposures where metamorphic garnet has been identified in both the phyllite and conglomerate.

*Einunnfjellet Dome Area*

The Einunnfjellet dome is cored by a lower amphibolite facies sucession of three mappable units, here collectively referred to as the Einunnfjellet quartzite/schist sequence (Fig. II-1; Table II-3). Despite complex folding, the lowest stratigraphic unit appears to be the Varden quartzite, consisting of thickly layered to massive, partly feldspathic quartzite that contains a foliation defined by mm-scale muscovite laminae. In contrast, the Bjørnkletten quartzite comprises thinly layered quartzite and biotite-muscovite-quartz schist, ± garnet. The contact with the Varden quartzite is gradational. Overlying the quartzite is the Strålsjøåsen calcareous schist, dominated by silvery to greenish, chlorite-rich garnet-mica schist, locally containing amphibole, epidote, or tourmaline. Commonly, the schist contains thin, white quartz-rich laminae that possibly represent early veins, and thick layers of fine-grained garnet-bearing quartzite are interspersed throughout the unit.

Overlying the Einunnfjellet quartzite/schist sequence is a diverse assemblage of metaigneous and metasedimentary rocks. Structurally lowest in this assemblage is the Einunna mafic complex, a sheared and fragmented body of metagabbro, amphibolite, chlorite-biotite schist, amphibole schist, and dolomite. Thin, boudinaged layers of coticule locally occur in the amphibole schist. The Einunna complex is only sporadically preserved below the



Figure II-4
Felsic clast facies of conglomerate in the upper Savalen sequence. Clasts are dominantly quartz keratophyre, with minor quartzite and chert (UTM 762 004).

Moskardsætra graphitic schist (described below). A more widely occurring metaigneous sequence, a bimodal suite informally called the Bangardsvola complex, encircles the core of the dome and is in contact with the Varden quartzite on the northern side (Fig. II-1). Around the Einunnfjellet dome the dominant lithology of the Bangardsvola complex is dark green to black schistose amphibolite, typically pervasively banded with thin felsic laminae. Layers of quartz keratophyre up to several meters thick occur within the amphibolite. The ratio of keratophyre to amphibolite increases north of the dome, and keratophyre becomes the dominant lithology just northwest of lake Savalen. Fine-grained, layered keratophyre, the most common variety, appears to have had a volcanic origin. Slightly coarser-grained varieties that occasionally show intrusive relationships with amphibolite or metagabbro likely represent hypabyssal feeder dikes to the extrusive rocks.

The Bangardsvola igneous complex is intricately folded with a unit of laminated mica-quartz schist (± garnet ± graphite) and garnet-mica garbenschiefer, referred to as the Svartlia mica schist. The contact between the two units is continuously exposed in some areas (e.g., UTM 732 995 to 745 008), where a thin zone of amphibole-bearing quartz keratophyre occurs consistently between greenstone and obviously sedimentary amphibole-mica schist. The keratophyre appears to interfinger with the sedimentary rocks, suggesting a primary contact, although elsewhere zones of mylonite occur locally both within the Bangardsvola complex and near the contact. On the west side of Einunnfjellet dome, a thin horizon of gray carbonate separates the Bangardsvola complex from the Svartlia schist. This horizon occurs along strike with a more extensive exposure to the northeast (Fig. II-1) that consists of fuchsite-bearing quartzite and marble, identical to the Langåsen quartzite/marble in the Savalen area.

Overlying the various units described above from the Einunnfjellet area is a unit informally referred to as the Moskardsætra graphitic schist. The dominant lithology is graphite-garnet schist, with subordinate interlayers of graphitic quartzite, garnet-mica schist, and feldspathic metasandstone. At the base of the Moskardsætra schist, a thin serpentinite horizon occurs in an antiform within the graphitic schist. Despite pervasive alteration, clasts were tentatively identified in the serpentinite, suggesting a detrital origin. This interpretation is supported by the local occurrence of conglomerate at the same stratigraphic level, consisting of mafic and dolomitic clasts in an amphibole-rich matrix.

## *Discussion*

### *The Pre-Scandian Unconformity in the Southeastern Trondheim Nappe*

*Savalen Area:* Greenstone and amphibolite of the Lomsjødalen complex are correlative with the Gula greenstone (Table II-2). Geochemically, the Lomsjødalen metabasalts are primitive-arc tholeiites (discussed in Chapter III), and recognizable igneous features such as pillow lava and volcanic breccia are indicative of subaqueous volcanic activity. A primary contact exists between greenstone and the overlying volcaniclastic/sedimentary sequence of the Lomsjødalen complex. The cover sequence is very similar to the Torvastad Group (Solli, 1981) that overlies the Karmøy ophiolite complex of southwestern Norway (Sturt and Thon, 1978b) (Fig. I-2). Analogies to such ophiolite-capping sequences may be found in the pelagic mud and metalliferous sediment that blankets oceanic crust at modern-day spreading ridges (Jenkyns, 1986), or in the metalliferous sedimentary rocks overlying pillow lavas of the Troodos ophiolite, Cyprus (Robertson and Hudson, 1974).

The Volengsvola phyllite is correlative with the Åsli Formation of the Gula Group (Nilsen, 1978, 1988; Nilsen and Wolff, 1989). The phyllite and calcareous sandstone appear to represent a turbiditic succession, based on the laminated nature, mineralogy, presence of graded bedding, and association with deep-water lithologies. The similarity of the characteristic veining and accompanying deformational fabric in the Volengsvola phyllite to that in the quartz-veined chloritic phyllite of the Lomsjødalen complex, and the lack of a similar fabric in the Savalen upper sequence, leads me to suggest that the Volengsvola-Lomsjødalen contact is either stratigraphic or a tectonic contact that formed prior to deposition of the upper sequence. The hypothesis of an early tectonic contact is supported by the position of the Langåsen quartzite/marble, because although it generally appears as a horizon within the Volengsvola phyllite unit, it is in direct contact with sedimentary rocks of the Lomsjødalen complex in the southwest (Fig. II-1).

The contact between the lower and upper sequences of the Savalen area is best interpreted as an unconformity, based on the cross-cutting nature of the contact (Fig. II-1) and the clast population of the overlying conglomerate. Although the conglomerate horizon in the Savalen area was originally correlated with the Volla and Kjølhaugen conglomerates of probable Late Ordovician age (Kleine-Hering, 1969; Mosson *et al.*, 1972) (Table II-1) it was later included in the Åsli Formation of the Gula nappe (Rui and Nilsen, 1988; Nilsen and Wolff, 1989). The Gudå conglomerate or Gudå Formation (Wolff, 1967; Lagerblad 1984a, 1984b), not differentiated from

the Gula nappe on the 1:250,000 scale (Wolff, 1976), is characterized by a distinctive marble-conglomerate association similar to the Langåsen marble and upper Savalen conglomerate. Based on this lithologic similarity and along-strike stratigraphic position, correlation with the Gudå Formation appears most reasonable, although the stratigraphy should probably be revised to reflect units separated by both time and tectonic environment. In the Dombas area (Fig. I-2), fuchsite-bearing marble, the Tverråi Formation (Guezou, 1978), occurs just beneath the Skardshø conglomerate (Strand, 1951), that contains quartzitic and calcic pebbles in a green amphibole-rich matrix. Although Strand (1951) considered the stratigraphic position of the Skardshø conglomerate equivocal, he later (in Strand and Kulling, 1972) expressed the opinion that it was equivalent to the greenstone conglomerate in the Otta area (Fig. I-2; Table II-1). Calcite marble with associated graphitic schist and polymict conglomerate also overlies the Gula greenstone in the Kvikne district (Rui, 1973) (Fig. I-2). It should be noted that a distinctive fuchsite-bearing calcareous quartzite is associated with a possible ophiolitic complex at Handöl, Sweden (Bergman, 1987) (Fig. I-2), and similar lithologies have been reported from the Sulitjelma region (Nicholson, 1966), 600 km north of the area of this study. In addition, conglomerate with carbonate and fuchsite-bearing clasts occurs near the base of a pre-Scandian unconformity above the Lyngen Gabbro in the Troms region, northwestern Norway (Steltenpohl *et al.*, 1990). The presence over such a wide area of a succession that includes fragmented mafic assemblages associated with fuchsite-bearing marble, overlain by a distinctive polymict conglomerate that was derived from both oceanic and continental sources, is indicative of the regional nature of an unconformity developed above obducted oceanic crust.

*Einunnfjellet Dome Area:* The Einunnfjellet quartzite/schist sequence represents a miogeoclinal succession, based on the thickly layered to massive clean quartzite and associated muscovite-rich schist. Regional correlations suggest that these rocks can be linked to the Baltoscandian margin. The Einunnfjellet quartzite/schist has been correlated with the Hummelfjell quartzite to the east (Nilsen and Wolff, 1989). In the type area (Fig. I-2), the Hummelfjell Formation is characterized by abundant mafic dikes within quartzite, as well as the presence of blue quartz in psammitic rocks (Rui, 1972), neither of which are found in the Einunnfjellet quartzite. In the Alvdal area (Fig. I-2), however, two subdivisions of the Hummelfjell have been recognized (Nilsen and Wolff, 1989)—one of massive quartzite and the other a more schistose variety, probably corresponding to the Varden and Bjørnkletten units, respectively. In addition, in the Tynset district (Fig. I-2), a complex transition zone occurs above the Hummelfjell that includes conglomerate (polymict and quartzitic), marble, serpentinite, and graphitic or psammitic schist

(Rui, 1972). Thus, the proximity, tectonostratigraphic level, and overall lithological similarity argue that the correlation is correct. The Hummelfjell Formation is thought to represent a higher-grade equivalent of the Särv nappe, middle allochthon, that is characterized by Late Proterozoic, dominantly alluvial to shallow marine sandstone and quartzite (Kumpulainen, 1980), commonly intruded by numerous dolerite dikes. The dikes have abyssal tholeiitic to within-plate geochemical signatures (Solyom *et al.*, 1979), and are interpreted to mark rifting of the Baltic margin during the opening of Iapetus (Gee, 1975; Gee *et al.*, 1985).

The remainder of the Einunnfjellet dome succession was regarded by Nilsen and Wolff (1989) as correlating with the Essandsjø nappe or, in the case of parts of the Bangardsvola complex, with the Fundsjø Group (Tables II-2 & II-3). The Einunna mafic complex appears to sit in tectonic contact upon the Einunnfjellet quartzite/schist sequence, since the association of lithologies suggests an oceanic character, and no feeder dikes to the mafic igneous rocks occur in the Einunnfjellet sequence. Although the contact is presently concordant and no fault-related fabrics are specifically localized along the contact, lithologies of the Einunna complex appear more highly sheared and boudinaged than surrounding rocks. It is probable that early faulting has been pervasively overprinted by later Scandian deformation, as will be discussed more fully in Chapter IV. Similar reasoning can be used to interpret the Bangardsvola/Einunnfjellet sequence contact. In addition, geochemistry of Bangardsvola amphibolites suggests that they originated as oceanic crust in a suprasubduction-zone setting (Chapter III), and can, therefore, be regarded as exotic to the Baltoscandian margin.

The Moskardsætra schist locally truncates contacts within the Einunnfjellet sequence, as well as the Einunnfjellet sequence/Einunna complex contact and the boundary between the Bangardsvola complex and Svartlia schist. Although in a few areas graphitic schist appears gradational with Svartlia mica schist, this apparent relationship is complicated by the presence of some graphite in Svartlia lithologies. The truncated contacts could be explained by facies changes, an unconformable relationship, or faulting. Despite the apparently gradational contact in a few areas, the interpretation of the Moskardsætra schist lying unconformably above other units of the Einunnfjellet dome area best explains a number of other observations : 1) The outcrop pattern of the units within the lower sequence exhibits a complex refold pattern (Fig. II-1 & Plate I), indicating early folding that is not apparent in the Moskardsætra schist. Equivalent structures are also present on the mesoscopic scale in the lower sequence (Chapter IV), but have not been observed in rocks of the Moskardsætra schist; 2) The Moskardsætra schist is alternately in contact with rocks of the Einunnfjellet, Einunna, Svartlia, or Bangardsvola units, which could indicate deposition on an eroded surface; 3) Conglomerate is locally present at the base of the Moskardsætra unit (Fig. II-1); and 4) No evidence for faulting

is apparent—that is, although shear zones occur in the Einunnfjellet dome area, no zones of higher strain or mylonitization were observed to be localized along the contact between the Moskardsætra schist and other rocks, even where the contacts are well exposed.

*Comparison with Savalen Area:* The evidence for an unconformable contact in the Einunnfjellet dome area is intriguing, and comparison with the Savalen area (Fig. II-5) supports the interpretation. Similarities exist between lithologies of the Einunna complex and the volcaniclastic/sedimentary rocks of the Lomsjødalen complex, particularly in the presence of coticule-bearing rocks in both units, and the Svartlia laminated mica schist and garbenschiefer may represent higher-grade equivalents of the partly calcareous, laminated rocks of the Volengsvola phyllite. The Langåsen quartzite/marble serves as a distinctive marker horizon, and its presence in both areas especially supports a correlation between rocks of the the Einunnfjellet dome and Savalen areas. Although bimodal igneous rocks analogous to the Bangardsvola complex are not exposed in the Savalen area, the occurence of felsic clasts, identical to Bangardsvola keratophyre, in conglomerate of the upper Savalen sequence suggests proximity of the complex to the depositional basin. Based on these similarities, I propose that the units above, with the exception of conglomerate, represent fragments of oceanic crust, along with pelagic, volcaniclastic, and turbiditic sediments and carbonate, all transported in a major internally deformed thrust sheet that I term the Savalen thrust complex. Evidence was given in the previous sections to support the interpretation that both the upper Savalen sequence and the Moskardsætra schist unconformably overlie these rocks. If this hypothesis is correct, the unconformity oversteps both an exotic thrust complex and continental-type quartzite and schist, indicating that the oceanic sequence must have been emplaced upon the continental miogeocline, and partially eroded, prior to deposition of the overlying rocks.

*Comparison with the Otta Nappe—Timing Constraints on Tectonic Evolution*

The Einunnfjellet-Savalen tectonostratigraphy is very similar to the Otta nappe (Strand, 1961) at the southern termination of the Trondheim nappe complex (Fig. I-2), where a lower sequence of quartz-rich psammite, garnet-mica schist, and greenish chlorite-rich schist, the Heidal Series (Gjelsvik, 1946; Strand, 1951) is overlain, in ascending order, by greenstone, greenstone conglomerate, serpentinite conglomerate, and fine-grained mica schist of the Sel Series. Recent mapping (Sturt *et al.*, 1991b) has shown that the greenstone comprises features typical of an ophiolite complex, including gabbro, sheeted dikes, and pillow lava. This complex, the Vågåmo ophiolite, is interpreted to have been emplaced upon the Heidal rocks,

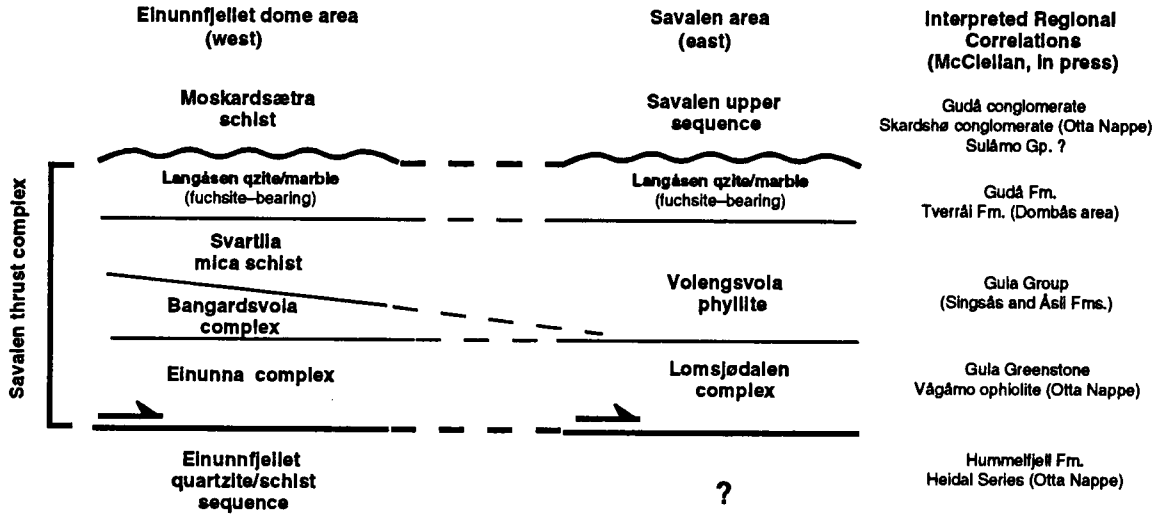



Figure II-5
Suggested correlations between the Einunnfjellet dome and Savalen areas.

eroded, and then overstepped by a "terrane-linking" unconformable sequence, the Sel, which was derived from both continental and ophiolitic sources. Finally, the entire package underwent deformation and metamorphism during the Siluro-Devonian Scandian orogenic phase (Sturt *et al.*, 1991a, 1991b; Hatcher *et al.*, 1991).

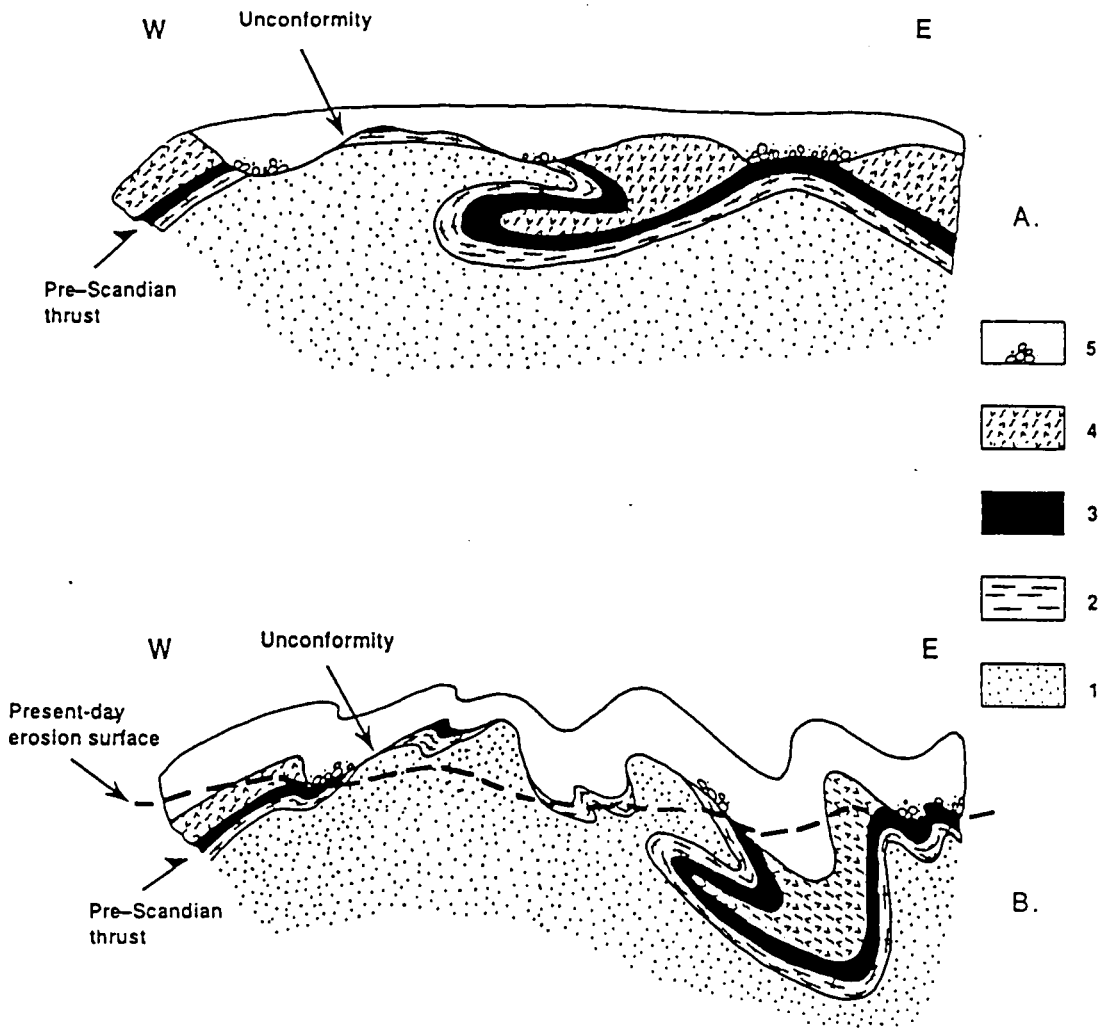
Two aspects of the Otta area are especially significant. First is an unconformable relationship of the Heidal Series to the underlying Rudihø Crystalline Complex (Gjelsvik, 1946; Strand, 1951), which has been interpreted as Baltoscandian basement (Sturt *et al.*, 1991a; 1991b). In addition, Heidal quartzite and flagstone are similar to the Vendian to Early Cambrian, autochthonous or parauthochthonous sparagmites (Strand and Kulling, 1972). These interpretations, if correct, suggest emplacement of the Vågåmo ophiolite onto the Baltoscandian margin. Second is the presence of a mixed faunal assemblage from serpentinite conglomerate that dates the horizon as late Arenig to Llanvirn (Hedström, 1930; Yochelson, 1963; Bruton and Harper, 1981). If the conglomerate occurs in the basal portion of the unconformable sequence, as interpreted by Sturt *et al.* (1991b), it provides a minimum age of Early Ordovician for ophiolite emplacement.

Lithologic similarity between the Heidal Series and the Einunnfjellet quartzite/schist sequence is striking, as is the comparable history involving thrusted oceanic assemblages overlain by unconformable sequences. Although no pelagic cover sequence to the Vågåmo ophiolite comparable to that in the Lomsjødalen complex has been identified, this may simply indicate that a higher part of the ophiolite stratigraphy is preserved in the Einunnfjellet-Savalen area.

### *Tectonic Evolution of the Einunnfjellet-Savalen Area, and Implications for the Trondheim Nappe Complex*

The development of the present-day outcrop pattern in the Einunnfjellet-Savalen area is illustrated schematically in Figure II-6. The deformational and metamorphic history of the area will be described in detail in Chapter IV, and lends support to the following interpretation of the tectonic evolution. In this scenario, early thrusting of the Savalen thrust complex onto the continental miogeocline, or possibly a microcontinent rifted from Baltica (Sturt and Roberts, 1991), was accompanied by large-scale isoclinal folding and possible weak metamorphism. The thrust sheets were unroofed during Early Ordovician uplift and erosion, and coarse oceanic and miogeoclinal detritus accumulated in local basins. The basins and their substrate were subsequently blanketed by finer-grained clastic material. Intermittent volcanism and hiatuses also occurred during this period (Roberts *et al.*, 1984; Furnes *et al.*, 1985; Roberts *et al.*, 1985),

Figure II-6
Simple model for the tectonic evolution of the Einunnfjellet–Savalen area. (See text for discussion.) A. Development of pre–Scandian unconformity. B. After Scandian deformation. 1–Quartzite units (Varden and Bjørnkletten); 2–Strålsjøåsen schist; Savalen thrust complex consisting of 3–Lower mafic complexes (Einunna, Lomsjødalen), and 4–Bangardsvola igneous complex combined with Svartlia schist, Volengsvola phyllite, and Langåsen quartzite/marble; 5–Post–unconformity sequences with conglomerate occurrences (Moskardsætra + upper Savalen sequence).


W
Unconformity
E
Pre–Scandian thrust
A.
5
4
3
2
1
W
Unconformity
E
Present-day erosion surface
Pre–Scandian thrust
B.

although the evidence is not now preserved in the immediate study area. Finally, the entire succession was tightly folded and thrust eastward during the Scandian orogeny. Pervasive Scandian metamorphism overprinted earlier structures and fault fabrics in the pre-unconformity sequence. At the present-day erosion level (Fig. II-6), post-unconformity rocks are preserved in plunging synclines above the lower sequence, similar to the situation described by Thon (1985b) from the Major Bergen Arc.

The age of the unconformity in the Otta and Einunnfjellet-Savalen areas closely corresponds to the "Trondheim disturbance" in the Støren area (Fig. I-2), where greenstone is unconformably overlain by metasedimentary rocks bearing Arenig fossils (Vogt, 1945). The timing of ophiolite emplacement and subsequent hiatus within the Trondheim nappe complex differs from that determined from southwestern Norway, however. It is intriguing that very similar successions, fragmented oceanic crustal complexes overlain by polymict or greenstone conglomerate, are known from the Major Bergen Arc (Færseth *et al.*, 1977; Heinriksen, 1981; Thon, 1985b; Ingdahl, 1989) and the Minor Bergen Arc (Fossen, 1989). The Karmøy ophiolite complex (Fig. I-2), which comprises a nearly complete ophiolite pseudostratigraphy and a well-developed pelagic cap rock sequence (Sturt *et al.*, 1979; Solli, 1981), lies unconformably beneath the sedimentary Skudeneset Group (Sturt and Thon, 1978b; Thon, 1980). In contrast to the Trondheim nappe complex, however, the oldest fossils found in the post-unconformity sequences of southwestern Norway are Ashgillian, a relationship that corresponds more closely with the Ekne disturbance (Vogt, 1945) in the Trondheim region. In addition, U/Pb zircon age dating of the Gullfjellet ophiolite (Major Bergen Arc) and the Karmøy ophiolite suggests that formation of these complexes occurred between approximately 490 and 470 Ma (Dunning and Pedersen, 1988; Pedersen *et al.*, 1988), a time which overlaps that of the Trondheim or Finnmarkian orogenic phases. While the relationships described above preclude direct temporal correlation of pre-Scandian events in the southwestern, central, and northern Caledonides, they could be accounted for by a diachronous, "scissors-like" closing of Iapetus, as suggested by Bryhni (1983), or by a more complex model involving separation of oceanic crustal segments by a system of transform faults (Sturt and Roberts, 1991). Alternatively, despite intriguing similarities the western (Bergen Arcs, Støren) and eastern (Vågåmo, Gula greenstone, Fundsjø) oceanic crustal sequences may have had quite different histories prior to the Scandian orogeny.

*Regional Implications—Contact Relationships within the Upper Allochthon*

The nature and significance of the contact between the lower and upper divisions of the upper allochthon, correlative with the Swedish Seve and Köli nappes, has proved difficult. Although frequently interpreted to be a major boundary separating rocks of contrasting tectonic setting and metamorphic grade, the actual contact often appears insignificant. In some areas in Sweden, the Seve-Köli contact is a prominent post-metamorphic thrust (Gee *et al.*, 1985), and Sjöstrom (1983) recognized retrogressed mylonites along the same contact. In many other areas no tectonic break is apparent (Stephens *et al.*, 1985), and the contact has been described as "generally concordant and transitional" (Gee, 1978). Williams and Zwart (1977) postulated that the Seve-Köli contact is a thrust based on truncation of rock units and contrast in metamorphic grade; however, they admitted that the fault was not well exposed and little information existed about it. Lisle (1984) suggested that the contact was an unconformity, upon which only minor, local movement had occurred.

Both Seve and Köli correlatives are represented in the Einunnfjellet-Savalen area (Tables II-2 & II-3). Contacts in the Einunnfjellet-Savalen tectonostratigraphy are interpreted to represent early thrusts involving ophiolitic rocks, and an overlying unconformity, all overprinted by Scandian deformation and metamorphism. Correlative rock units exist at different metamorphic grades, and it will be shown in Chapter IV that isograds cut across contacts without interruption. Extending relationships in this area to other parts of the orogen, some explanations for problematical or conflicting interpretations of contacts within the upper allochthon become apparent. Although the nappes have been metamorphosed, imbricated, and transported eastward during Scandian deformation, at least portions of the upper allochthon must have been assembled prior to Scandian orogenesis. Confusion over the boundary between the lower and upper divisions (i.e., the Seve-Köli contact) arises where the contact is mapped solely on the basis of metamorphic grade, or where pre-Scandian thrusts or unconformities go unrecognized. Identification of these early contacts in any one area may depend upon: 1) the depth of the erosion surface; 2) the presence or absence of conglomerate at the base of the post-unconformity sequence; 3) whether early faults, particularly at the base of the oceanic sequence, have been completely recrystallized during Scandian metamorphism; and 4) whether Scandian faulting has significantly overprinted or reactivated earlier structures.

## *Conclusions*

In summary, the southeastern Trondheim nappe complex contains an early Paleozoic unconformity that oversteps both a miogeoclinal sequence linked to the Baltoscandian margin, and a thrust sheet of oceanic crustal rocks. Regional correlations confirm the widespread nature of the hiatus, and, if interpretations of the Otta area are correct, indicate a minimum Arenig age for emplacement of the oceanic crust onto the continental margin, corresponding to the Trondheim disturbance of Holtedahl (1920). These relationships imply that portions of the upper allochthon were assembled prior to the Siluro-Devonian Scandian orogeny, and consisted of three major elements: 1) a lower sequence representing the outermost portions of the Baltoscandian continental margin; 2) a thrust complex of fragmented oceanic elements; and 3) a "terrane-linking" unconformable succession that overstepped both (1) and (2). During Scandian orogenesis, this composite mass was thrust eastward, imbricated, folded, and metamorphosed. In the present-day Caledonides, pre-Scandian faults or unconformities are often cryptic boundaries, concealed behind a pervasive overprint of Scandian deformation and metamorphism. Continued resolution of such boundaries through detailed investigations and documentation of contact relationships, however, will serve to better define the early Paleozoic tectonic history that affected much of the upper allochthon in the Scandinavian Caledonides.

# CHAPTER III

## Subduction-Related Volcanism in the Gula Nappe, Southeastern Trondheim Nappe Complex

### *Introduction*

Most of the exotic and suspect terranes identified in the Scandinavian Caledonides are included in the upper allochthon (Roberts and Gee, 1985). These terranes are represented by a multitude of dominantly basaltic greenstone units that occur particularly in the upper portions of the Allochthon, known collectively as the Köli nappes. The earliest geochemical investigations indentified these rocks as fragments of oceanic crust (Gale and Roberts, 1974; Furnes and Færseth, 1975; Gale, 1975), and in the ensuing years a variety of oceanic environments have been identified (Furnes *et al.*, 1980; 1985). This has made possible attempts at reconstruction of the Iapetus Ocean basin between Greenland and Baltica, and of the tectonic events affecting this segment prior to final closure during the Siluro-Devonian Scandian orogeny. Interpretations have been hindered, however, by possible disparate tectonic histories and uncertain age relationships within the nappes, and the commonly equivocal nature of internal contacts. These problems are particularly evident in the central-southern Caledonides, where the upper allochthon contains the Trondheim nappe (Wolff, 1967), or Trondheim nappe complex (Guezou, 1978). The central Trondheim nappe complex, as shown on the Røros 1:250,000 scale map (Nilsen and Wolff, 1989), comprises the dominantly metasedimentary Gula nappe, that contains subordinate discontinuous mafic/ultramafic horizons termed the Gula greenstone (Nilsen and Mukherjee, 1972). The Gula nappe is flanked by metavolcanic sequences, the Støren Group on the east and the Fundsjø Group on the west. Whereas the Lower Ordovician or older low-grade metavolcanic rocks in the Støren and Fundsjø Groups are distinctly of oceanic origin and represent marginal basin or island arc environments, the tectonic environments of the generally higher-grade rocks of the Gula nappe remain speculative. Insufficient knowledge of age relationships and tectonic affinities of rocks within the axial Gula nappe has long presented a major obstacle to understanding the structure and tectonic history of the Trondheim nappe complex.

Mafic and ultramafic rocks are also found in the the lower (Seve) nappes of the upper allochthon. The rocks are generally at a higher metamorphic grade than those of the Köli nappes, however, and the tectonic affinities are even less well-defined. Based on geochemistry and associated sedimentary rocks, some of the mafic horizons appear to be correlative with

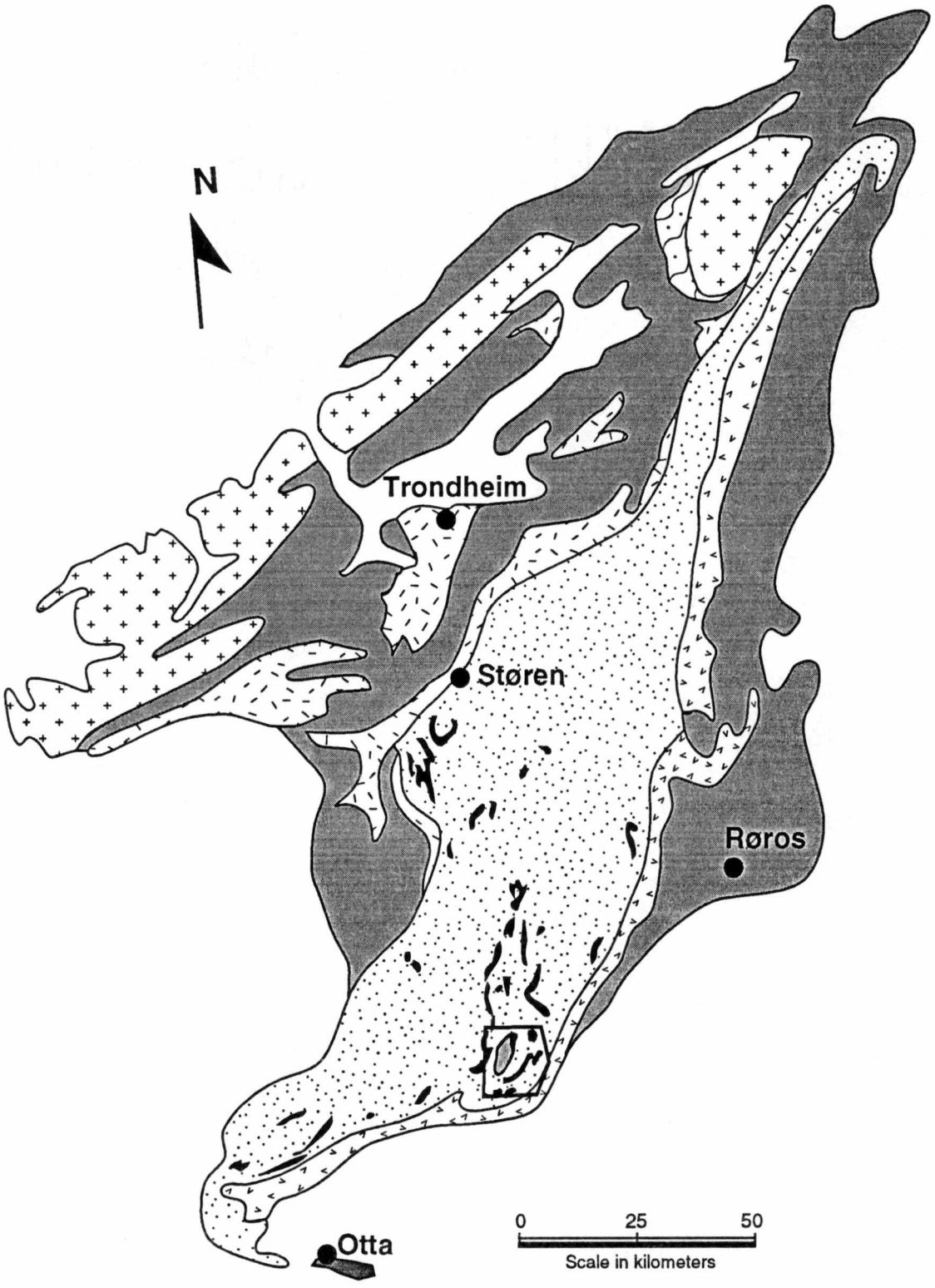
Late Proterozoic dolerite dikes in the Särv nappe, middle allochthon, that are interpreted to mark rifting of the Baltic margin during the opening of Iapetus (Gee, 1975; Solyom et *al.*, 1979; Gee *et al.*, 1985). Others, however, may be higher-grade equivalents of the oceanic crustal sequences in the upper nappes, indicating that the Seve nappes are a composite feature. In the western Trondheim region, possible Seve equivalent rocks, including mafic horizons, occur in the Blåhø nappe (Krill, 1980). Similar rocks were assigned to the Essandsjø nappe in the eastern part of the region (Nilsen and Wolff, 1989), and also surround the Einunnfjellet dome in the present study area.

This chapter presents field and geochemical investigations of two distinct metaigneous complexes that occur in the Einunnfjellet-Savalen area, southeastern Trondheim nappe complex (Fig. I-1). One, informally referred to here as the Lomsjødalen complex (Chapter II) is directly correlative with the Gula greenstone (Rui and Nilsen, 1988; Nilsen and Wolff, 1989). The other, informally the Bangardsvola complex (Chapter II), was previously shown as two separate units, correlative with the Essandsjø nappe and Fundsjø Group (Rui and Nilsen, 1988; Nilsen and Wolff, 1989). The tectonic affinities of the Lomsjødalen and Bangardsvola complexes, their mutual relationships, and associations with surrounding metasedimentary rocks have significant implications for the original tectonic setting of the Gula nappe, as well as for the relationship between rocks of the Trondheim nappe complex and those of the Seve nappes.

## *Metavolcanic Sequences in the Trondheim Region*

The Trondheim nappe complex contains three major metavolcanic sequences—the Støren and Fundsjø Groups that flank the Gula nappe complex on the west and east, respectively, and greenstone within the Gula nappe complex itself (Fig. III-1). The western Støren Group and possibly related metavolcanic complexes (Løkken, Vassfjell, Grefstadfjell, Jonsvatn, Forbordfjell) comprise the Hølonda terrane of Stephens and Gee (1985). The complexes are largely mafic and commonly preserve at least a partial ophiolite stratigraphy (Furnes *et al.*, 1985). Based on biostratigraphic control in the unconformably overlying sediments, the Støren Group is unambiguously mid-Arenig or older. Age relationships of the other complexes are less clear, however, and some, particularly Jonsvatn and Forbordfjell (Grenne and Roberts, 1980) and Løkken (Ryan *et al.*, 1980) have been interpreted as occurring higher in the Early to Middle Ordovician stratigraphy. Despite this suggestion, Stephens and Gee (1985, p. 966) preferred to consider the ophiolite fragments as "disrupted members of a single thrust sheet of oceanic crust". The Laurentian affinity of faunal assemblages in the overlying sedimentary

Figure III–1
Tectonic map of the Trondheim nappe complex, showing locations of major metavolcanic sequences. Cross-hatch pattern—Støren Group and related units (western sequence); "V" pattern—Fundsjø Group and related units (eastern sequence); Black—mafic horizons in central TNC [Gula greenstone and Seve-equivalent (?) units]; Dots—Gula nappe; Gray—Upper allochthon (undifferentiated); Dot and curved line pattern—Middle allochthon; Crosses—Lower allochthon/parautochthon. Box—location of Einunnfjellet–Savalen map area. Modified from Grenne (1988), with data from Nilsen and Wolff (1989).


N
Trondheim
Støren
Røros
Otta
0
25
50
Scale in kilometers

units (Bruton and Bockelie, 1980) has led some (Stephens and Gee, 1985; Pedersen *et al.*, 1988) to suggest that this oceanic crust formed on the Laurentian side of Iapetus, although the significance of the faunal provinciality has been questioned by others (Roberts *et al.*, 1984; Sturt and Roberts, 1991). The western Trondheim metavolcanites are considered to have been tectonically emplaced upon the Gula nappe prior to mid-Arenig time. In the Selbusjøen area, the Støren Group is separated from the Gula nappe by a mélange unit that has an apparently primary contact with Støren metavolcanics, and partially tectonic, partially gradational contact with typical Gula rocks (Horne, 1979).

Metavolcanics of the eastern Trondheim district form an essentially continuous belt that includes the Fundsjø Group (Wolff, 1967) in the Meråker area, the Hersjø Formation (Rui, 1972) in the Røros-Folldal district, and the Musadal Group (Guezou, 1978) near Dombås, at the southern termination of the Trondheim nappe complex. Although lithologically more diverse than the metavolcanic rocks of the western district, all the units are characterized by greenstone or amphibolite interlayered with variable amounts of quartz keratophyre and tuffaceous rocks. Mafic rocks in both the Fundsjø Group (Grenne and Lagerblad, 1985) and the Hersjø Formation (Grenne, 1988) display geochemical heterogeneity as well, and can be divided into island-arc, MORB, and transitional types. Deformation and metamorphism have largely obscured the interrelationships and relative ages of the different types, but the heterogeneities have been explained by models involving either an incipient rifted arc or an arc-related marginal basin setting (Grenne and Lagerblad, 1985; Grenne, 1988).

Age constraints in the eastern Trondheim district are limited. The metavolcanic rocks are overlain by a thick sequence of clastic rocks, the highest of which contains graptolite-bearing black phyllite of Llandoverian age (Getz, 1890). A potentially very important fossil locality occurs at Nordaunevoll, where Vogt (1941) described the distinctive Tremodocian dendroid graptolite *Dictyonema flabelliforme* from highly organic black shale. Unfortunately, the stratigraphic position of this unit is still controversial, having been variously ascribed to the Gula (Nilsen, 1971), the Hersjø (Gee, 1981), or a transition zone between the two groups (Rui, 1972). The nature of the contact between metavolcanites of the eastern district and the Gula nappe is equivocal, interpreted as either stratigraphic (Rui, 1972) or tectonic (Gee, 1975). Commonly, the contact is marked by a transition zone of quartzite conglomerate, crystalline limestone, metagraywacke, tuffite, and mica schist (± amphibole)—the "heterogeneous banded rock sequence" of Rui (1972) or the Gudå Formation of Wolff (1973). Lagerblad (1984a, 1984b) concluded that the Gudå-Fundsjø contact in the Inndalen area (Fig. I-1) is primary, whereas the Gudå-Gula contact is tectonic. He presented strong evidence for a gradual increase in

metamorphic grade from east to west across all three units, and surmised that the tectonic contact is an early structure, entirely overprinted by later deformation and metamorphism.

Based on overall lithologic similarities and the apparent symmetry across the Trondheim nappe complex, metavolcanic sequences of the eastern and western Trondheim districts were traditionally assumed to be correlative (Wolff, 1967). More recent models, however, propose that the sequences may be parts of different thrust sheets within the nappe complex, and are not directly correlative (Gee and Zachrisson, 1974; Gee, 1978). This is supported by distinct differences in geochemistry, and the inferred paleotectonic environment (Grenne and Lagerblad, 1985) and nature of associated massive sulfide deposits (Grenne, 1988). Although the possibility exists that the Fundsjø and Støren volcanism occurred at roughly the same time, they represent distinctly different tectonic environments (Grenne and Lagerblad, 1985).

*Mafic Metavolcanic Rocks in the Gula Nappe Complex*

The central unit of the Trondheim nappe complex is referred to as the Gula nappe complex (Gee *et al.*, 1985). A two-fold division of the Gula Group (Törnebohm, 1896; Rui, 1972) was modified by Nilsen (1978), who divided the unit into three formations. The central Singsås Formation consists mainly of calcareous psammite and mica schist, and is bordered on the west and east by carbonacous phyllite and biotite schist of the Undal and Åsli Formations, respectively. The Gula nappe complex is likely a composite tectonic unit and age constraints are few, although Klingspor and Gee (1981) reported an Early Ordovician isotopic age from syntectonic trondhjemite that intruded Gula mica schist. In Chapter II, I suggested a possible correlation of greenstone in the Gula nappe complex (see below) with the Vågåmo ophiolite in the Otta nappe (Sturt *et al.*, 1991), indicating an Early Ordovician or older age for the correlative Gula rocks.

Perhaps the least well-studied sequence of mafic metavolcanic rocks in the Trondheim nappe complex is the Gula greenstone (Nilsen and Mukherjee, 1972; Nilsen, 1974). Occurring as discontinuous horizons throughout the Gula nappe (Fig. III-1), and concentrated particularly at the contact between the Singsås and Åsli Formations, the Gula greenstone consists of amphibolite with subordinate metagabbroic and ultramafic lenses (Nilsen, 1974). The amphibolite horizons are commonly associated with black schist and banded quartzite, and contain numerous pyritic sulfide deposits capped by cherty iron formation (Nilsen, 1978). On the basis of the apparently exhalative nature of the stratabound sulfide deposits, the mafic rocks are considered to have resulted from submarine volcanic activity (Rui, 1973; Nilsen, 1974; 1978; 1988), although primary igneous structures have been obscured by polyphase

deformation and the typical amphibolite facies metamorphism. From the area of this study, however, I reported pillow lava and volcanic breccia from relatively low-grade horizons correlative with the Gula greenstone (Chapter II).

Based on the association of mafic volcanics with thick clastic sequences, Nilsen (1978) suggested that the Gula greenstone represented volcanism in an island-arc related environment. This suggestion was supported by mafic rock geochemistry (Rainey, 1980). In that study, Gula amphibolites plot consistently as island arc tholeiites on discriminant diagrams utilizing Ti, Zr, Y, and Zr/Y. Nilsen (1974), however, had previously noted a striking resemblance in the AFM diagram between Gula amphibolite and Archaean high-Mg basalts or komatiites. The relatively high concentrations of Cr and Ni are also worthy of note, because these features are uncharacteristic of typical island-arc tholeiites. Rainey's analyses (1980) yield similar results when plotted on the AFM diagram, and average approximately 400 ppm Cr, as compared to an average of 111 ppm in island-arc tholeiites (Pearce, 1982). Given the significant geochemical contrasts with typical IAT, the absence of associated intermediate or felsic lithologies, and the nature of the sulfide deposits, it appears that the tectonic setting of the Gula greenstone cannot be adequately explained by a simple island-arc model. On the basis of lithologic similarities and comparable deformational and intrusive phases, Stephens and Gee (1985) suggested that the higher-grade parts of the Gula nappe are correlative with the Krutfjellet nappe farther north, which they interpreted as representing a fore-arc basin. In the present study, this and other possible interpretations of the tectonic setting of the Gula nappe are considered from the standpoint of both field and geochemical characteristics.

## *Einunnfjellet-Savalen Area*

Two major metavolcanic sequences in the Einunnfjellet-Savalen area, the subjects of this study, are informally referred to as the Lomsjødalen and Bangardsvola complexes (Chapter II). The Lomsjødalen complex is directly correlative with the Gula greenstone (Nilsen and Wolff, 1989) (Table II-2), while the Bangardsvola complex encompasses rocks correlated with both the Essandsjø nappe and the Fundsjø Group (Mosson *et al.*, 1972; Nilsen and Wolff, 1989) (Table II-3). Considering lithologies, field appearance, and geochemical similarities, there appears to be little justification for separating the unit, with the exception of lenses of mafic and volcaniclastic rocks that occur near the core of the Einunnfjellet dome (Fig. II-1). These rocks, formerly referred to as the Einunna complex (Chapter II), were suggested to be higher-grade equivalents of the Lomsjødalen complex (Fig. II-5).

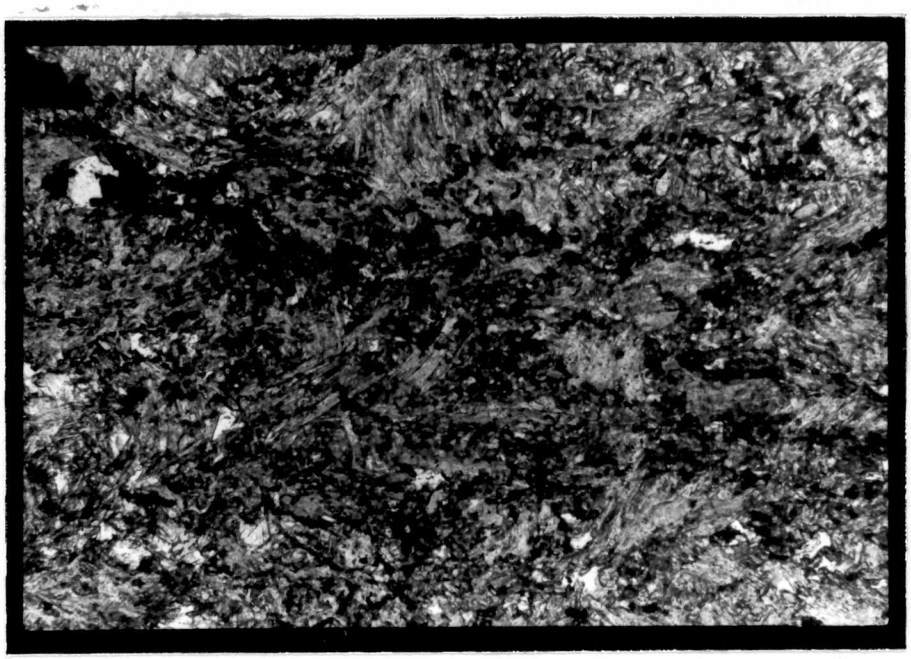
The Lomsjødalen and Bangardsvola complexes are interpreted to have been transported together with sedimentary and volcaniclastic rocks in the Savalen thrust complex (STC). The interpreted stratigraphic order within the STC is shown in Figure II-5, although contact relationships are uncertain, due to internal deformation and lack of consistent facing criteria. I interpret the Bangardsvola complex to overlie the Lomsjødalen complex, and both metavolcanic complexes are in turn overlain by mica schist and garbenschiefer, or calcareous phyllite at lower metamorphic grade (Plate II). Locally, however, both complexes are in contact with distinctive fuchsite-bearing marble and quartzite. The Bangardsvola complex appears to pinch out toward the east; whether this signifies internal faulting or original volcanic stratigraphy is uncertain. In the study area, the contact between the STC and metavolcanic rocks of the Fundsjø Group is characterized by a prograde shear zone, that will be described in detail in Chapter IV.

*Lomsjødalen Complex*

The Lomsjødalen mafic complex consists of greenstone or amphibolite and overlying volcaniclastic and sedimentary rocks. Detailed mapping at the scale of 1:5,000 in the Lomsjødalen area south of lake Savalen (Plate III) shows that the complex occurs in several lenticular exposures as a result of intense folding (Plate II, and discussed in Chapter IV). The largest complete exposure is located on Lomsjøvola, where fine-grained greenstone is generally massive to schistose, but commonly contains calcite and epidote segregations giving the impression of pillow shapes. Indisputable pillow lavas occur in a few outcrops (Fig. II-2), and are associated with volcanic breccia apparently derived from the pillow material. In thin section, fine-grained felted masses of amphibole and feldspar are interspersed with epidote and chlorite, with accessory sphene and rutile (Fig. III-2a). Larger amphiboles are generally hornblende in composition, while smaller grains range from actinolitic hornblende to hornblende (Chapter IV).

Greenstone is overlain by fine-grained, dark grey-green laminated tuffite . A unique feature of these rocks is abundant millimeter to centimeter-scale interlayers of fine-grained pink coticule (Fig. III-2b), consisting of quartz and masses of tiny (0.01 to 0.20 mm) garnets. Despite the small size of the garnets, they are strongly zoned, with spessartine-rich cores ($Sp_{39}Al_{43}$) and almandine-spessartine rims ($Sp_{27}Al_{60}$). Higher in the overlying sequence, tuffite grades into coarser-grained, laminated and quartz-veined phyllite rich in chlorite and epidote, and containing some coticule intercalations. Sulfidic black phyllite is locally associated with the greenstone and the overlying rocks. Small pods (2-3 $m^2$) of ore mineralization within the

a.



b.

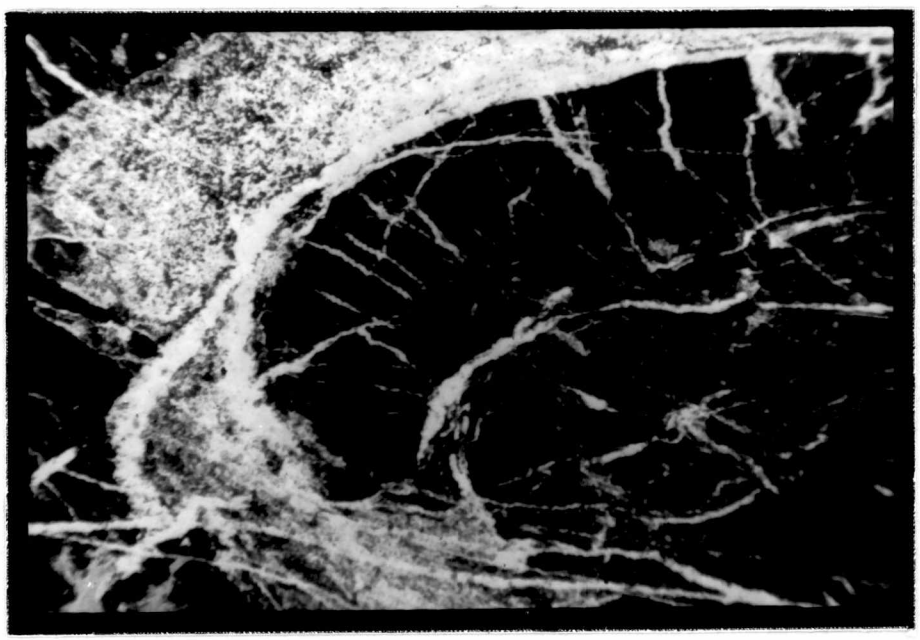


Figure III-2
Photomicrographs of lithologies in the Lomsjødalen complex. a) Fine-grained greenstone. Long dimension of photograph 1.7 mm; and b) Coticule layer from phyllite in Lomsjødalen cover sequence. Long dimension of photograph 10 mm.

sedimentary/volcaniclastic rocks near the greenstone contact consist of siliceous "iron formation", as described in detail by Nilsen (1978, pp. 47–51).

On Lomnesvola (Plate III), the Lomsjødalen complex is more intensely deformed and tectonically thinned. Sheared amphibolite and metagabbro are surrounded by a heterogeneous cover of dark chert, coticule, fine-grained metalliferous sedimentary rocks, and tuffite, again with pods of iron formation. Texturally, all rocks are coarser-grained and more schistose than those on Lomsjøvola, and consequently appear to represent a higher metamorphic grade. In the sampled mafic rocks, amphibole composition is consistently hornblende despite a wide variation in size and morphology of the amphibole grains.

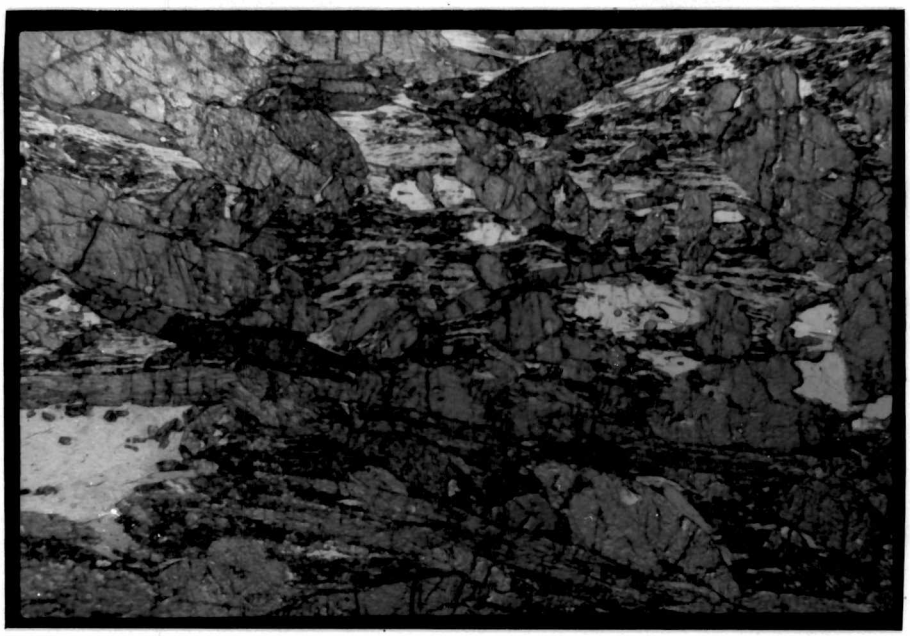
Of the metaigneous and related rocks surrounding the Einunnfjellet dome (included in the Essandsjø nappe by Nilsen and Wolff, 1989), the structurally lowest rocks comprise a sheared and fragmented body of metagabbro, amphibolite, chlorite-biotite schist, and amphibole schist locally containing thin, boudinaged layers of coticule. This unit, referred to informally as the Einunna mafic complex (Fig. II-1, Table II-3), was suggested to be correlative with the Lomsjødalen complex on the basis of lithologic similarity and the presence of the distinctive coticule interlayers (Chapter II). In addition, conglomerate with mafic and carbonate clasts locally overlies the Einunna complex, a situation that is very similar to that on Lomsjøvola (Plate III).

*Bangardsvola Complex*

A bimodal igneous suite, informally called the Bangardsvola complex (Chapter II), encircles the core of the Einunnfjellet dome (Fig. II-1 & Plate I). The dominant lithology of the Bangardsvola complex is dark green to black schistose amphibolite, typically pervasively banded with thin felsic laminae. The medium to coarse-grained amphibolite consists of hornblende, epidote, feldspar, and quartz, with accessory rutile and minor secondary chlorite (Fig. III-3a). Grains of muscovite on foliation surfaces are a unique feature in some samples. Metagabbroic rocks form a subordinate component of the Bangardsvola complex; the fine-grained, banded amphibolite, however, is typically basaltic in composition (see following section), and is interpreted to have formed from an extrusive volcanic protolith.

Layers of quartz keratophyre up to several meters thick occur within the amphibolite. In thin section (Fig. III-3b), it is seen to consist of a fine-grained groundmass of interlocking quartz and feldspar surrounding larger plagioclase porphyroclasts. Varying amounts of hornblende and chlorite are present, and the subparallel alignment of these minerals defines the foliation. Layered keratophyre, which becomes more abundant just northwest of lake Savalen, appears to

a.



b.

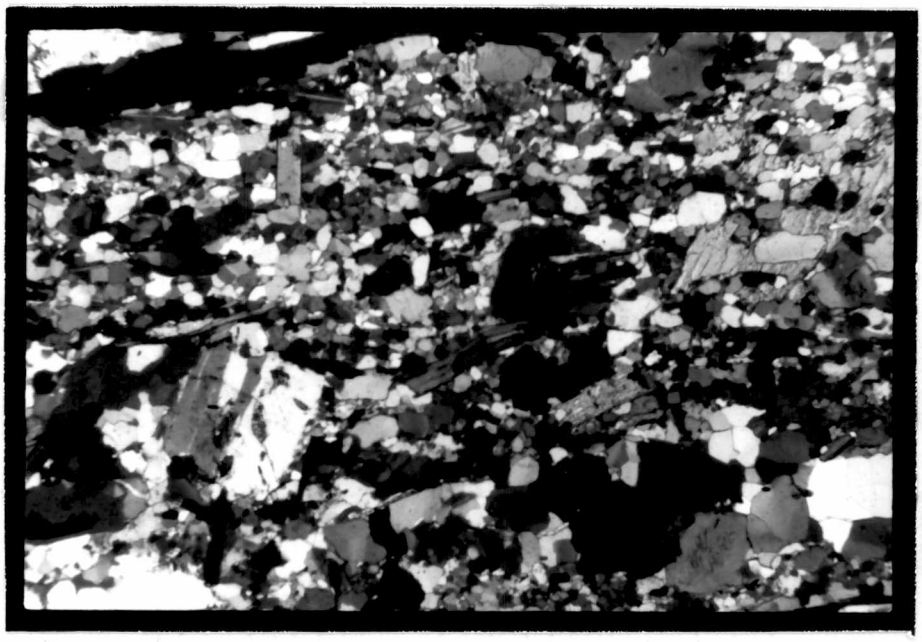


Figure III-3
Photomicrographs of lithologies in the Bangardsvola complex. a) Amphibolite. Long dimension of photograph 4.5 mm; and b) Quartz keratophyre. Long dimension of photograph 4.5 mm.

have had a volcanic, or possibly volcanoclastic, origin, whereas slightly coarser-grained varieties that occasionally show intrusive relationships with amphibolite or metagabbro likely represent hypabyssal feeder dikes to the extrusive rocks.

The Bangardsvola igneous complex is in contact, and locally intricately folded, with mica-quartz schist, metasandstone, and garbenschiefer. The contact between the two units is continuously exposed in some areas (e.g., UTM 732 995 to 745 008), and appears to be a primary stratigraphic contact. In a few places near the contact, mafic layers are present in the metasedimentary rocks and possibly represent dikes. These mafic layers, which range from a few centimeters up to three meters thick, are geochemically distinct from the Bangardsvola layered metavolcanic rocks (see below). A homogeneous amphibolite layer with similar major element geochemistry was also identified from a core sample of the metavolcanic rocks.

## *Geochemistry*

### *Analytical Methods*

A total of 26 samples were analyzed for this study (Table III-1). Ten metabasalts are from the Bangardsvola complex, 2 samples represent the dike-like layers from within the Svartlia metasedimentary rocks, and 1 sample is a possible dike from the Bangardsvola rocks. Nine metabasalts from the Lomsjødalen complex, including pillow lavas, were also analyzed, and four Fundsjø Group samples are included for comparison. Major and trace elements were analyzed by Bjørn Nilsen and the technical staff at the Analytical Chemistry Section, Norges Geologiske Undersøkelse, Trondheim, using a Philips PW 1480 XRF. Major elements were analyzed on fused disks melted with lithium tetraborate in the proportions 1:7, and trace elements were determined on pressed pellets. FeO, $H_2O+$, $H_2O-$, and $CO_2$ were determined by standard wet chemical methods.

### *Major and Trace Elements*

Because the samples were all metamorphosed to greenschist or lower amphibolite facies, it can be expected that some elements, such as K, Ca, Na, and Si, may have been selectively mobilized. When plotted against MgO as a differentiation index (Fig. III-4), however, good igneous trends are present for most elements; for instance, CaO, Cr, and Ni tend to increase with increasing MgO, while $Al_2O_3$, FeO (total), Zr, and $Na_2O$ decrease. $Na_2O$ is particularly surprising in its consistent covariation with MgO, because it is considered mobile during both

Table III-1: Major and trace element concentrations of metavolcanic rocks in the Einunnfjellet–Savalen area

| | Bangardsvola Group I | | | | | | Bangardsvola Group II | | Dikes (?) | | | | *BAS |
|---|---|---|---|---|---|---|---|---|---|---|---|---|---|
| Sample | Fiskt–2 | Slia–2 | Slia–3 | A114 | A1145 | Gruv | Slia–1 | Slia–7 | K283 | K47 | A112A | Fiskt–4 | K2201 |
| $SiO_2$ | 49.60 | 48.20 | 54.67 | 47.35 | 51.54 | 57.28 | 48.84 | 51.18 | 46.58 | 46.65 | 45.64 | 52.35 | 50.90 |
| $Al_2O_3$ | 9.79 | 11.58 | 13.76 | 10.27 | 12.60 | 15.47 | 16.40 | 15.64 | 17.67 | 14.87 | 14.88 | 15.25 | 15.14 |
| $Fe_2O_3$ | 0.82 | 0.65 | 1.49 | 1.17 | 2.99 | 1.43 | 1.58 | 1.76 | 1.57 | 0.69 | 1.14 | 0.92 | 3.05 |
| FeO | 7.00 | 7.27 | 6.45 | 6.98 | 6.14 | 5.34 | 8.56 | 7.46 | 8.20 | 9.36 | 9.41 | 7.63 | 10.07 |
| $TiO_2$ | 0.08 | 0.10 | 0.15 | 0.13 | 0.16 | 0.21 | 0.57 | 0.52 | 0.51 | 1.04 | 1.01 | 1.12 | 1.55 |
| MgO | 10.47 | 9.69 | 9.22 | 11.45 | 8.38 | 6.35 | 7.08 | 8.56 | 9.46 | 8.92 | 7.22 | 9.28 | 5.10 |
| CaO | 11.28 | 12.40 | 8.28 | 11.98 | 10.84 | 7.49 | 9.80 | 6.07 | 8.63 | 10.86 | 10.40 | 10.00 | 7.58 |
| $Na_2O$ | 1.56 | 2.15 | 3.34 | 1.01 | 2.68 | 3.70 | 3.55 | 4.63 | 3.20 | 2.30 | 2.87 | 3.01 | 3.69 |
| $K_20$ | 0.48 | 0.21 | 0.24 | 1.40 | 0.21 | 0.37 | 0.27 | 0.19 | 0.31 | 0.28 | 0.62 | 0.41 | 0.33 |
| MnO | 0.13 | 0.16 | 0.15 | 0.17 | 0.14 | 0.09 | 0.13 | 0.17 | 0.10 | 0.24 | 0.18 | 0.24 | 0.20 |
| $P_2O_5$ | 0.07 | 0.07 | 0.05 | 0.05 | 0.05 | 0.04 | 0.10 | 0.07 | 0.07 | 0.12 | 0.11 | 0.16 | 0.19 |
| $H_2O+$ | 2.58 | 2.98 | 1.56 | 2.07 | 1.51 | 0.96 | 3.02 | 2.97 | 2.56 | 1.50 | 1.16 | 2.46 | 1.78 |
| $H_2O-$ | 0.05 | 0.11 | 0.26 | 0.02 | 0.05 | 0.10 | 0.10 | 0.09 | 0.03 | 0.04 | 0.05 | 0.02 | 0.03 |
| $CO_2$ | 7.87 | 5.77 | 0.11 | 6.09 | 1.67 | 0.10 | 1.56 | 0.74 | 0.31 | 2.03 | 4.36 | 4.14 | 0.28 |
| Total | 101.78 | 101.34 | 99.73 | 100.14 | 98.96 | 98.93 | 101.56 | 100.05 | 99.20 | 98.90 | 99.05 | 106.99 | 99.89 |
| Mg # | 0.73 | 0.70 | 0.72 | 0.75 | 0.71 | 0.68 | 0.60 | 0.67 | 0.67 | 0.63 | 0.58 | 0.68 | 0.47 |
| Nb | <5 | 6 | <5 | 11 | 11 | 11 | <5 | 7 | 7 | 12 | 12 | <5 | 6 |
| Zr | 10 | 11 | 16 | 9 | 10 | 29 | 20 | 21 | 18 | 57 | 61 | 9 | 72 |
| Y | <5 | <5 | <5 | 9 | 6 | 8 | 7 | 12 | 14 | 25 | 23 | <5 | 27 |
| Sr | 139 | 167 | 150 | 76 | 146 | 210 | 226 | 110 | 149 | 221 | 90 | 47 | 127 |
| Rb | 11 | 8 | 5 | 5 | 5 | 10 | 8 | 7 | 5 | 5 | 19 | 8 | 8 |
| Cr | 1384 | 1639 | 503 | 1530 | 1525 | 378 | 177 | 315 | 216 | 393 | 422 | 1346 | 18 |
| Ni | 304 | 354 | 121 | 336 | 339 | 82 | 69 | 97 | 72 | 170 | 123 | 289 | 9 |
| V | 200 | 217 | 155 | 174 | 196 | 165 | 297 | 260 | 271 | 216 | 276 | 183 | 429 |
| Sc | 33 | 28 | 34 | 32 | 31 | 35 | 37 | 39 | 45 | 35 | 38 | 33 | 42 |
| Ba | 35 | 33 | 29 | 28 | 14 | 41 | 27 | <10 | 13 | 49 | 57 | 26 | 55 |
| Zn | 60 | 59 | 64 | 37 | 61 | 54 | 85 | 75 | 84 | 99 | 114 | 62 | 117 |
| Cu | 9 | 25 | <5 | 5 | 62 | 207 | 13 | 9 | 5 | <5 | 5 | <5 | 13 |
| Yb | <10 | <10 | <10 | <10 | <10 | <10 | <10 | <10 | <10 | <10 | <10 | 12 | <10 |
| Co | 47 | 42 | 38 | 45 | 45 | 27 | 38 | 35 | 40 | 43 | 46 | 47 | 35 |
| Ce | <10 | <10 | 13 | <10 | <10 | <10 | 22 | 13 | <10 | <10 | <10 | 13 | 24 |

NOTES: Major elements given as wt. %, trace elements in ppm. Chemical analyses are by XRF, except FeO by titration, and $H_2O+$, $H_2O-$, and $CO_2$ by ?.

$Fe_2O_3$ calculated as stoichiometric difference between FeO and total Fe as $Fe_2O_3$. Mg# calculated as $Mg/(Mg + Fe^{2+})$.

*BAS—Bangardsvola "anomalous" sample (see text).

Table III-1, continued

| | Lomsjødalen Complex | | | | | | | | | Fundsjø Group | | | |
|---|---|---|---|---|---|---|---|---|---|---|---|---|---|
| Sample | Lomsjø-1 | Lomsjø-2 | Lomsjø-3 | Lomsjø-4 | Lomsjø-5 | Lomsjø-6 | A1457 | A1463 | A1698 | Sivil-2 | Sivil-4 | Sivil-5 | Sivil-6 |
| $SiO_2$ | 50.06 | 50.61 | 49.41 | 49.27 | 48.31 | 48.10 | 52.00 | 49.31 | 47.74 | 50.99 | 57.97 | 48.93 | 55.56 |
| $Al_2O_3$ | 13.47 | 13.94 | 13.85 | 14.42 | 14.08 | 13.99 | 15.72 | 13.11 | 15.59 | 13.81 | 14.55 | 14.37 | 14.06 |
| $Fe_2O_3$ | 1.77 | 1.68 | 1.36 | 2.08 | 1.33 | 2.53 | 0.59 | 1.17 | 2.96 | 3.21 | 1.74 | 3.37 | 2.23 |
| FeO | 8.10 | 7.90 | 6.82 | 6.06 | 7.88 | 7.71 | 6.32 | 7.57 | 7.86 | 7.46 | 6.91 | 8.45 | 7.19 |
| $TiO_2$ | 0.87 | 0.84 | 0.76 | 0.73 | 1.07 | 1.00 | 0.70 | 1.03 | 1.19 | 1.23 | 1.40 | 1.56 | 1.46 |
| MgO | 9.67 | 9.51 | 11.55 | 9.02 | 9.47 | 11.31 | 9.37 | 10.04 | 8.10 | 5.97 | 4.22 | 5.08 | 4.36 |
| CaO | 9.02 | 8.90 | 9.59 | 10.92 | 9.64 | 10.02 | 6.21 | 11.80 | 9.83 | 4.65 | 2.27 | 6.10 | 3.70 |
| $Na_2O$ | 3.45 | 3.62 | 2.64 | 3.11 | 3.31 | 2.51 | 4.79 | 2.35 | 3.19 | 3.98 | 5.54 | 5.05 | 5.02 |
| $K_20$ | 0.18 | 0.18 | 0.12 | 0.15 | 0.14 | 0.12 | 0.07 | 0.14 | 0.43 | 0.05 | 0.04 | 0.08 | 0.32 |
| MnO | 0.14 | 0.13 | 0.12 | 0.10 | 0.15 | 0.15 | 0.09 | 0.14 | 0.20 | 0.23 | 0.22 | 0.26 | 0.13 |
| $P_2O_5$ | 0.07 | 0.07 | 0.07 | 0.09 | 0.14 | 0.14 | 0.06 | 0.11 | 0.12 | 0.16 | 0.16 | 0.17 | 0.30 |
| $H_2O+$ | 2.29 | 2.24 | 3.33 | 2.64 | 2.94 | 3.27 | 2.82 | 1.65 | 1.39 | 4.70 | 3.48 | 3.73 | 3.38 |
| $H_2O-$ | 0.06 | 0.05 | 0.04 | 0.06 | 0.12 | 0.06 | 0.04 | 0.00 | 0.40 | 0.06 | 0.02 | 0.10 | 0.03 |
| $CO_2$ | 0.11 | 0.66 | 0.06 | 0.90 | 0.73 | 0.07 | 0.10 | 0.10 | 0.10 | 3.59 | 1.75 | 1.63 | 2.79 |
| Total | 99.26 | 100.33 | 99.72 | 99.55 | 99.31 | 100.98 | 98.88 | 98.52 | 99.10 | 100.09 | 100.27 | 98.88 | 100.53 |
| Mg # | 0.68 | 0.68 | 0.75 | 0.73 | 0.68 | 0.62 | 0.73 | 0.70 | 0.65 | 0.59 | 0.52 | 0.52 | 0.52 |
| Nb | 5 | <5 | <5 | 6 | 12 | 9 | 9 | 15 | 12 | <5 | 8 | 5 | 6 |
| Zr | 33 | 33 | 27 | 28 | 58 | 56 | 30 | 58 | 62 | 87 | 106 | 102 | 109 |
| Y | 18 | 17 | 18 | 17 | 21 | 21 | 16 | 19 | 26 | 27 | 34 | 32 | 33 |
| Sr | 107 | 124 | 128 | 170 | 89 | 139 | 88 | 146 | 97 | 69 | 46 | 67 | 99 |
| Rb | 5 | 6 | 8 | 7 | 7 | 8 | 5 | 5 | 7 | <5 | 7 | <5 | 9 |
| Cr | 882 | 869 | 1039 | 812 | 1443 | 690 | 681 | 683 | 413 | 52 | 5 | 21 | <5 |
| Ni | 379 | 363 | 432 | 347 | 299 | 228 | 262 | 217 | 130 | 12 | <5 | 9 | <5 |
| V | 175 | 166 | 192 | 177 | 235 | 227 | 176 | 225 | 273 | 273 | 219 | 349 | 205 |
| Sc | 31 | 29 | 27 | 28 | 34 | 34 | 35 | 29 | 46 | 35 | 21 | 42 | 18 |
| Ba | 12 | 14 | 27 | 31 | 31 | 33 | 14 | 19 | 50 | 21 | <10 | 14 | 69 |
| Zn | 82 | 80 | 58 | 63 | 87 | 72 | 58 | 68 | 94 | 145 | 430 | 84 | 101 |
| Cu | <5 | <5 | 95 | 65 | 41 | 6 | 5 | 19 | 5 | 21 | 45 | 53 | <5 |
| Yb | 13 | 13 | 10 | 12 | <10 | <10 | <10 | <10 | <10 | <10 | <10 | <10 | <10 |
| Co | 57 | 52 | 47 | 45 | 51 | 42 | 40 | 38 | 47 | 19 | 18 | 30 | 19 |
| Ce | 13 | 15 | 11 | 12 | 22 | 17 | <10 | <10 | <10 | 17 | 20 | 23 | 38 |

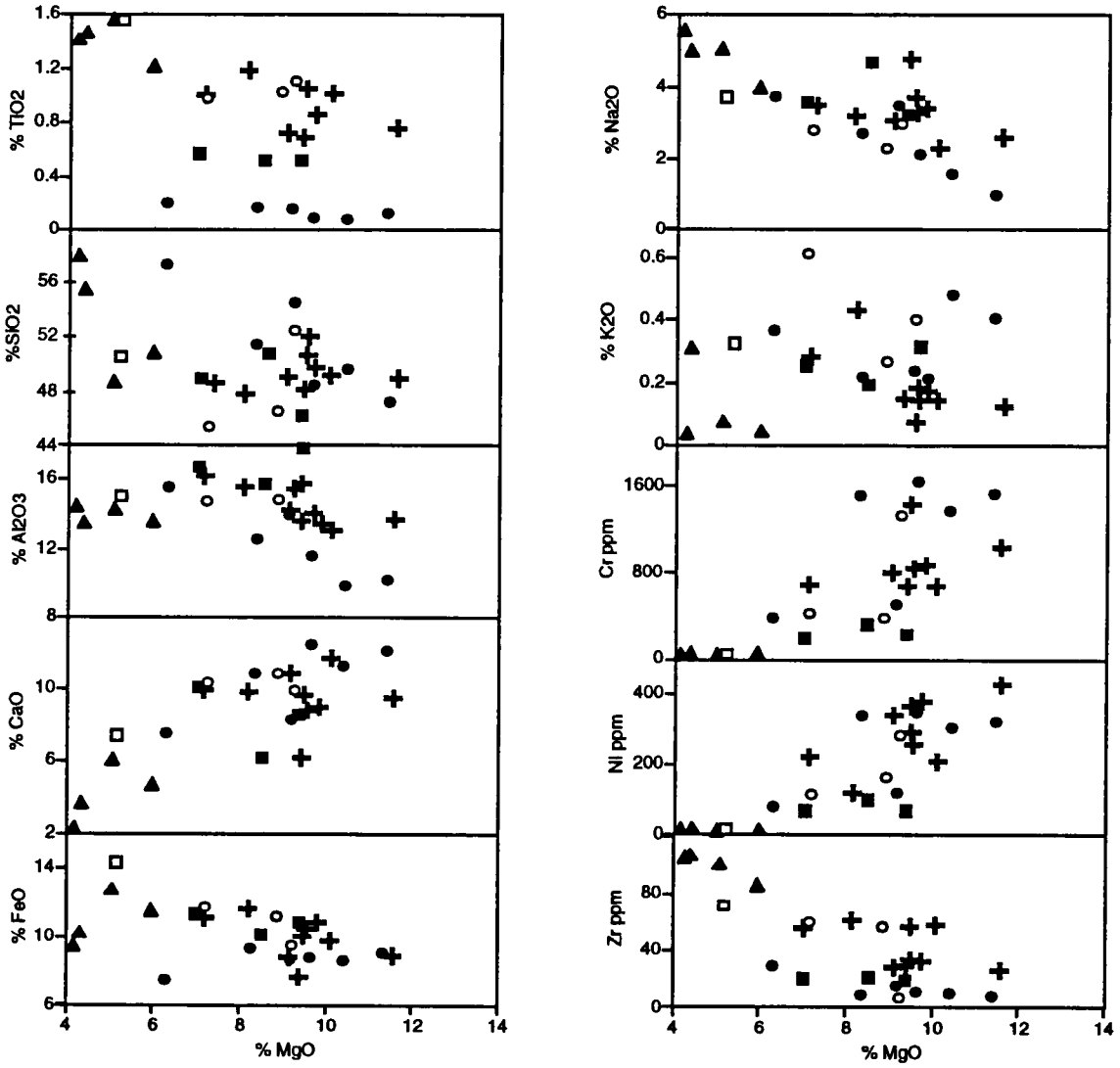



Figure III-4
Variation diagrams of major and trace elements versus wt. % MgO. Filled circles—Bangardsvola Group I; filled boxes—Bangardsvola Group II; open box—"anomalous" Bangardsvola sample; crosses—Lomsjødalen complex; open circles—dike (?) samples; triangles—Fundsjø Group.

ocean floor alteration and greenschist facies metamorphism (Pearce, 1975), although $K_2O$ values are somewhat scattered, probably reflecting element mobility. $TiO_2$ and Zr behavior is especially interesting, and provides a good method for distinguishing between units. Based on the absolute abundances of $TiO_2$, the Bangardsvola samples can be divided into two distinct geochemical groups (Fig. III-4). Group I is strongly depleted in $TiO_2$, and shows only a slight decrease with increasing MgO, while Group II is less depleted than Group I, but more so than samples from the Lomsjødalen complex or Fundsjø Group. The distinction between Groups I and II is less obvious with respect to Zr, although both are highly depleted in this element relative to the other units. The two groups can also be distinguished with respect to Cr and Ni, as most of the Group I samples are highly enriched in both elements in comparison with Group II.

Samples from the Lomsjødalen complex show consistent trends of decreasing $TiO_2$ and increasing Cr and Ni with increasing MgO, and the absolute abundances of Cr and Ni are relatively high. When Zr is plotted against MgO, the trend is flat and the samples appear to fall into two groups, although the less Mg-rich samples have the highest Zr values. The dike samples show trends similar to the Lomsjødalen metabasalts, and tend to plot with the most evolved of that group, suggesting a possible comagmatic relationship. The Fundsjø Group samples are all characterized by high $TiO_2$ and Zr, and extremely low Cr and Ni. Interestingly, one Bangardsvola sample (K2201) is quite anomalous, and generally plots with the Fundsjø analyses.

*Tectonic Discrimination Diagrams*

The elements Ti, Zr, and Y are considered to be relatively immobile during weathering and greenschist facies metamorphism (Cann, 1970; Pearce and Cann, 1971), and several variation diagrams involving these elements have been shown to be useful in discriminating the tectonic setting of altered basic volcanic rocks (Pearce and Cann, 1971, 1973; Pearce and Norry, 1979; Pearce, 1980). Pearce and Cann (1973) restricted the use of the Ti-Zr-Y diagram to basaltic rocks in which CaO + MgO falls between 12 and 20%. In addition, the Ti-Zr (Pearce and Cann, 1973) and Zr/Y-Zr (Pearce and Norry, 1979) diagrams should not be used for lavas containing cumulate crystals, although the Ti-Zr-Y diagram can be applicable because it considers the relative proportions of these elements (Pearce and Cann, 1973). Because the samples of this study are, in general, totally recrystallized, it is impossible to determine petrographically whether cumulate crystals were originally present. Geochemically, however, the Bangardsvola Group I samples tend to follow accumulation trends on the $Al_2O_3/TiO_2$ vs. Ti and Cr/Ti vs. Ti

diagrams (Pearce and Flower, 1977) (not shown), similar to the Troodos upper pillow lavas, and the absolute abundances of Ti, Zr, Mgo, Cr, and Ni suggest cumulate olivine may have been present in the original rock (Pearce and Cann, 1973). Nevertheless, Bangardsvola samples are shown on the following diagrams in order to highlight their distinctive character relative to the more "ordinary" behavior of the other units.

On the $TiO_2$ vs. Zr, Zr/Y vs. Zr, and Ti-Zr-Y diagrams (Figs. III-5, III-6, & III-7), Lomsjødalen metabasalts plot almost exclusively in the island-arc tholeiite field. A few samples with relatively high absolute values of $TiO_2$ and Zr fall within the overlapping IAT-MORB fields, but lie along a trend suggesting they are comagmatic with the others. Again, the dike (?) rocks plot consistently with the Lomsjødalen samples in the overlapping field, with the exception of Fiskt-4 which falls well outside any field because of very low abundances of Zr and Y. In contrast, Fundsjø Group samples (and the anomalous Bangardsvola sample) show no indication of island-arc affinity, but appear to most closely resemble MORB, although their relatively high $TiO_2$ values place them in the "within-plate" field on the $TiO_2$ vs. Zr diagram (Fig. III-5).

As discussed previously, Bangardsvola metabasalts are characterized by extreme depletion in Ti and Zr. Consequently, the typical discrimination diagrams are virtually useless for these rocks, particularly for Group I samples. Group II rocks, however, do lie in or peripheral to the IAT field in each case. A more useful discriminator, perhaps, is the Ti-V diagram of Shervais (1982) (Fig. III-8). Due to the varying valence states of V as a function of oxygen fugacity during partial melting and fractional crystallization, the covariation of these two relatively immobile elements can be a useful indicator of tectonic setting of various volcanic rock associations. MORB basalts have Ti/V ratios of 20–50 (Fig. IV-8), whereas the ratios for alkaline rocks are generally greater than 50. With the exception of calc-alkaline basalts, most modern island-arc related volcanic basalts have Ti/V less than 20. The ratios for calc-alkaline basalts are more variable due to the effects of magnetite fractionation (Shervais, 1982); this should not be a problem for the present study, however, because there are no field, petrologic, or geochemical indications that any true calc-alkaline rocks are present among the units sampled.

Also shown on Figure III-8 are fields for several volcanic suites considered to comprise lavas of the "boninite series" (Meijer, 1980; Crawford *et al.*, 1989). Ti/V ratios of these suites are generally $\leq$10, implying a subduction-related setting, either within an island arc or a small marginal basin (Shervais, 1982). Bangardsvola Group I samples all have Ti/V less than 10, and fall in or peripheral to these fields, suggesting a similar tectonic setting. The Bangardsvola

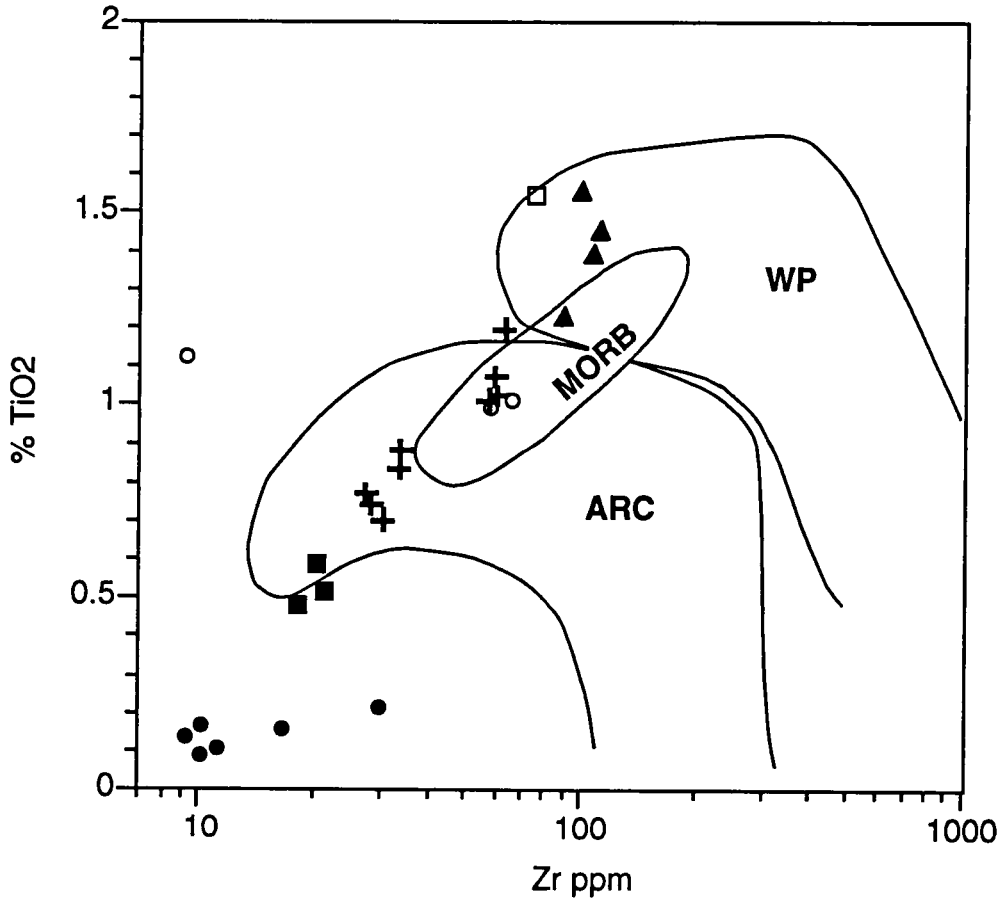



Figure III-5
TiO2 vs. Zr plot. (Pearce and Cann, 1973.) Symbols same as in Figure III-4.

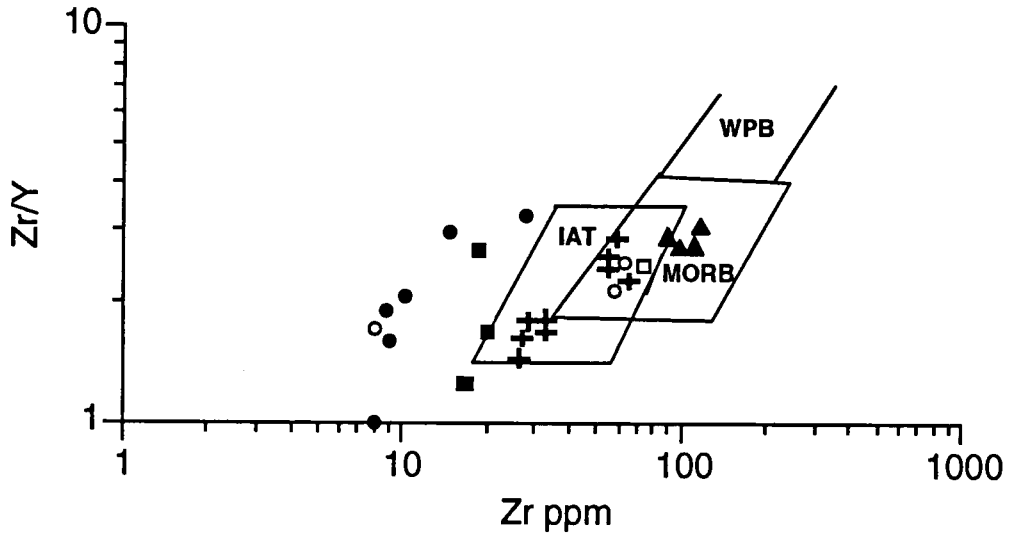



Figure III-6
Zr/Y vs. Zr plot. (Pearce and Norry, 1979.) Symbols same as in Figure III-4.

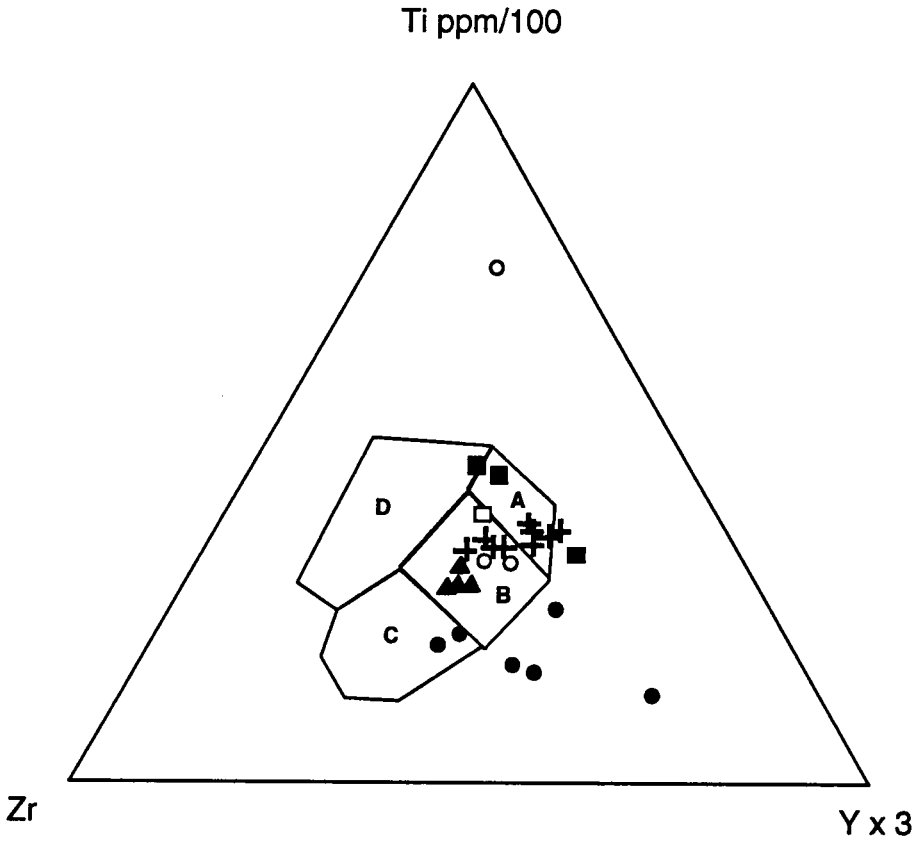



Figure III-7
Ti–Zr–Y plot. (Pearce and Cann, 1973.) Fields are: A &B—island arc tholeiite; B—ocean floor basalts; C—calc–alkaline basalts; D—"within–plate" basalts. Symbols same as in Figure III-4.

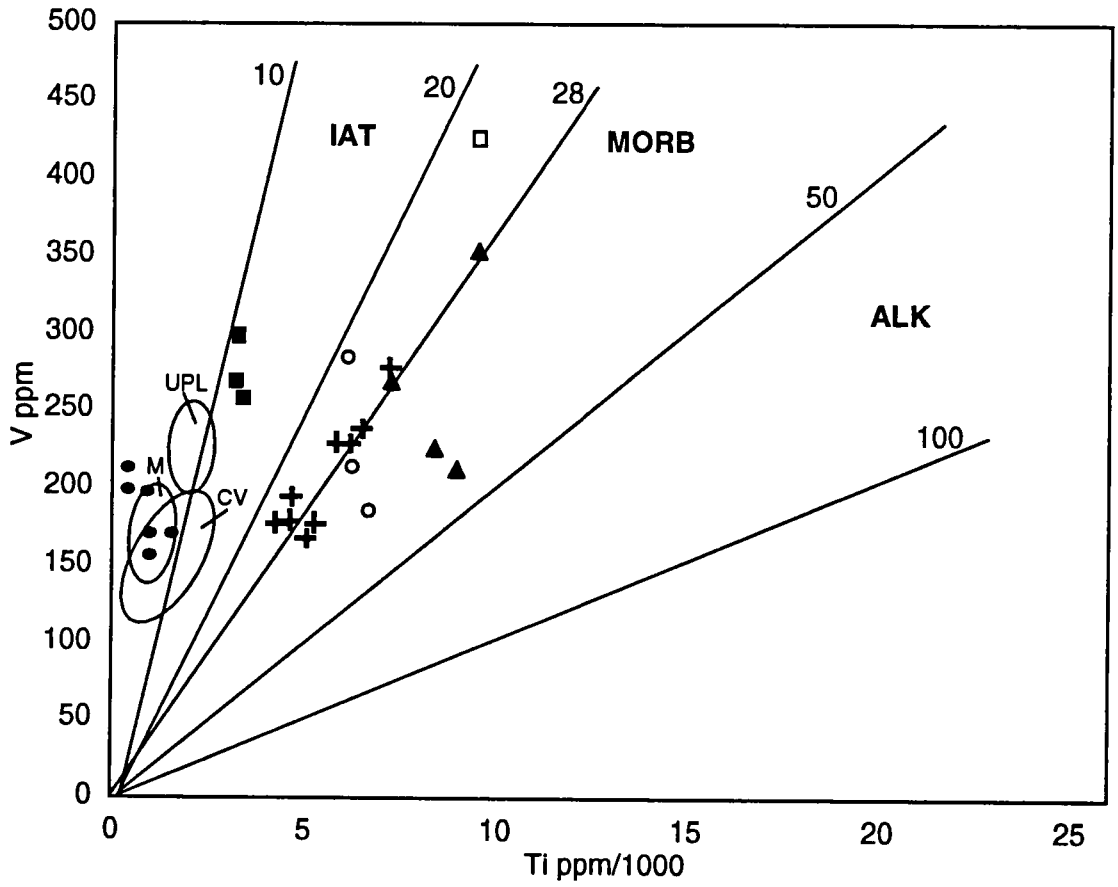



Figure III-8
Ti–V plot. (Shervais, 1982.) Fields are: UPL—Troodos upper pillow lavas; M—Mariana forearc boninites; CV—Cape Vogel high-Mg andesites. Symbols same as in Figure III-4.

Group II ratios fall between 10 and 15, compatible with the resemblance to IAT in the previous diagrams.

Despite the consistent IAT affinity of Lomsjødalen rocks in the previous diagrams, all of the samples plot in the MORB field on the Ti/V diagram. There can be some overlap, however, in IAT and MORB ratios (between 20 and 27) at V<350 ppm (Shervais, 1982). It must be noted, also, that ratios from backarc basins basalts overlap both IAT and MORB fields, and these rocks tend to be less highly enriched in both Ti and V than typical island arc or MORB basalts.

*Boninite vs. Komatiitic Basalt*

Boninite is an unusual and relatively rare rock type identified from Mesozoic and Tertiary forearc and/or backarc settings, and from some older ophiolites. Cameron *et al.* (1979) defined boninite as a glassy lava containing one or more types of pyroxene, with accessory magnesiochromite. Olivine is a common minor constituent, although plagioclase is rare. Meijer (1980) included related rocks in a "boninite series," characterized by silica saturation, enrichment in Mg, Cr, and Ni, and depletion in the high field strength elements (Ti, Zr, and Y) and rare earth elements relative to the tholeiitic series. Crawford *et al.* (1989) divided boninitic magmas into high-Ca and low-Ca suites, based on major element compositions; low-Ca boninites are characterized by $SiO_2$>55% and $CaO/Al_2O_3 \leq 0.75$, whereas high-Ca boninites have $SiO_2$<56% and $CaO/Al_2O_3$>0.75, more closely resembling the Bangardsvola Group I samples. Magnesium numbers ($Mg/Mg + Fe^{2+}$) are generally >0.6. The low-Ca suite, subdivided into three types, includes lavas from the Mariana forearc and trench, Cape Vogel (Papua New Guinea), the Setouchi area in southwest Japan, and the type locality of Chichi-jima, in the Japanese Bonin arc. The reference suite for high-Ca boninites is the Troodos upper pillow lavas (UPL); other high-Ca suites include late Tertiary lavas from the Tongan forearc, and Proterozoic dikes from Antarctica and Greenland. There appears to be a transition between low-Ca and high-Ca types, and between high-Ca boninites and low-Ti arc lavas (Crawford *et al.*, 1989).

Komatiitic basalts ($SiO_2$<50%) and siliceous high-Mg basalts ($SiO_2$=51–55%) are geochemically and petrographically similar to boninites (Cameron *et al.*, 1979; Sun *et al.*, 1989). Given the similarities, the possible "boninitic" affinity of the Bangardsvola metabasalts, and "komatiitic" affinity of the Gula greenstone (Nilsen, 1974), it is important to ask how these rock types can be distinguished from one another, and how the Bangardsvola and Lomsjødalen samples compare with either boninites or komatiitic basalts. Some key element concentrations and ratios are given in Table III-2. Whereas there is a wide overlap in most of the major

Table III-2: Comparison of element concentrations and ratios between silicious high-magnesian basalts (SHMB), komatiitic basalts, boninites, Bangardsvola Group I, and Lomsjødalen metavolcanic rocks.

| | SHMB[a] | Komatiitic basalts[b] (average of 4 analyses) | Bonin Island boninites[c] | Troodos high-Ca boninites[d] | Northern Appalachian boninites[e] | Bangardsvola Group I metavolcanics[f] | Lomsjødalen metavolcanics[f] |
|---|---|---|---|---|---|---|---|
| % $SiO_2$ | 51–55 | 48.3 | 57–60 | 50–55 | 43–60 | 47–57 | 48–52 |
| % MgO | 6–16 | 14.7 | 5.7–12.3 | 11.1–16.3 | 6.5–15.6 | 6.4–11.5 | 7–11.5 |
| % $TiO_2$ | 0.39–1.0 | 0.6 | 0.1–0.3 | 0.22–0.36 | 0.11–0.27 | 0.08–0.21 | 0.7–1.19 |
| % FeO* | 9.6–12.8 | 13.3 | 8.3–8.8 | 7.6–9.7 | 5.6–11.4 | 7.4–9.9 | 7.7–11.8 |
| $Al_2O_3/TiO_2$ | 20–27 | 19 | 50–134 | 27–56 | 57–103 | 74–122 | 13–29 |
| $CaO/TiO_2$ | ≈18 | 16 | 30–81 | 24–47 | 33–83 | 36–144 | 8–17 |
| Sc/Y | 2–3 | — | 4.5–22.5 | 4.4–5.8 | 3.3–34 | 3.5–13.6 | 1.5–2.1 |
| Ti/Zr | 50–75 | 128 | 24–65 | 56–239 | 29–102 | 43–96 | 106–169 |
| Ti/Sc | ≈74 | — | 16–48 | 32–49 | 14–45 | 14–36 | 120–213 |
| Ti/V | ≈15.5 | 16 | 3.5–5.5 | 6.0–9.5 | — | 2.7–7.6 | 24–30 |

Data sources: [a] Sun et al., 1989 (Archaean—W. Australia and early Proterozoic—Antarctica); [b] Arnt and Nesbitt, 1982 (in Schaefer and Morton, 1991) (Munro Township, Ontario); [c] Hickey and Frey (in Wilson, 1989); [d] Cameron, 1985 (in Crawford et al., 1989); [e] Coish, 1989 (Ordovician—Betts Cove); [f] Present investigations.

element concentrations, the variations in the high field strength elements (Ti, Zr, Y) are noticably different between komatiitic basalt or SHMB and boninite (Coish, 1989). Boninites are characterized by $TiO_2$ contents generally less than 0.3%, regardless of $SiO_2$ or MgO content (Fig. III-9), and the various ratios involving Ti consequently reflect its extreme depletion. Likewise, the Sc/Y ratio is higher for boninites than for komatiitic basalts or SHMB, due to depletion of Y in boninitic rocks. The Bangardsvola Group I samples compare well with boninites in the very low $TiO_2$ content (0.08–0.21%), and also in the comparable Sc/Y ratios. Bangardsvola Group II samples (not shown in Table III-2) are more similar to SHMB because of their higher $TiO_2$ content, and appear to be geochemically transitional between these rocks and boninites (Fig. III-9).

Lomsjødalen metabasalts do not show boninitic affinities, and are more similar, although not identical to komatiitic basalt or SHMB (Table III-2). Most of the samples fall within the SHMB or komatiitic basalt fields on the $TiO_2$ vs. MgO diagram (Fig. III-9). These samples compare favorably with other Gula greenstone samples of similar $SiO_2$ content (Nilsen, 1974), thus supporting Nilsen's suggestion that they are of "komatiitic affinity".

*Trace Element Patterns*

A useful way of comparing the trace element characteristics of basalts from different tectonic settings is by use of the MORB-normalized spiderdiagram (Pearce, 1982) (Fig. III-10). Average compositions of different types of basaltic lavas show various patterns of enrichment or depletion relative to MORB (Fig. III-10a). In particular, the broad concave-upward, U-shaped pattern of Tertiary boninites reflects the extreme depletion in the incompatible elements of high ionic potential, and enrichment in Cr (and to a lesser extent, Ni) relative to MORB. This pattern appears to be unique among basaltic lavas—although komatiitic basalt has a similarly shaped pattern (Coish, 1989), the extent of depletion in the incompatible elements is not nearly so great.

Shown in Figure III-10b are average compositions of the Troodos upper pillow lavas (UPL), which are divided into three geochemical groups (Cameron, 1985), and lavas from the adjacent Arakapas fault belt (AFB). The most highly depleted of the UPL, Group III, comprise the reference suite for the high-Ca boninites of Crawford *et al.* (1989). In addition, boninite from the Ordovician Betts Cove ophiolite, Newfoundland (Coish, 1989), is included for comparison. Note the similarity of Betts Cove, Group III UPL, and AFB lavas to Tertiary boninites (Fig. III-10a). With the exception of the elements Nb, Ce, and P, the pattern for the average Bangardsvola Group I composition (Fig. III-10c) is nearly identical to that of the boninites (Figs. IV-10a & b). Surprisingly, even the low field strength element pattern is consistent, despite the

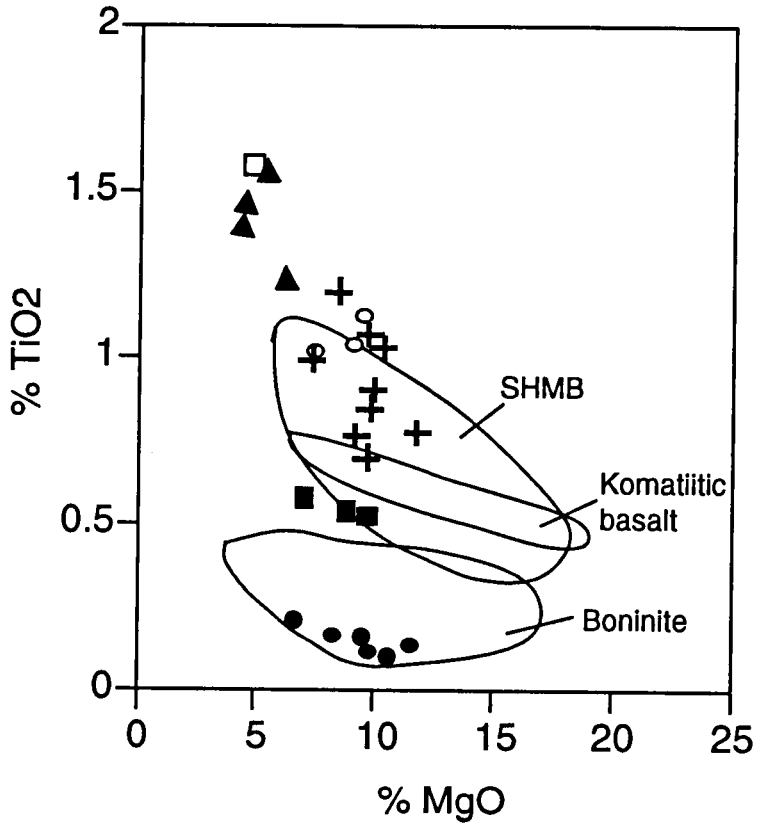
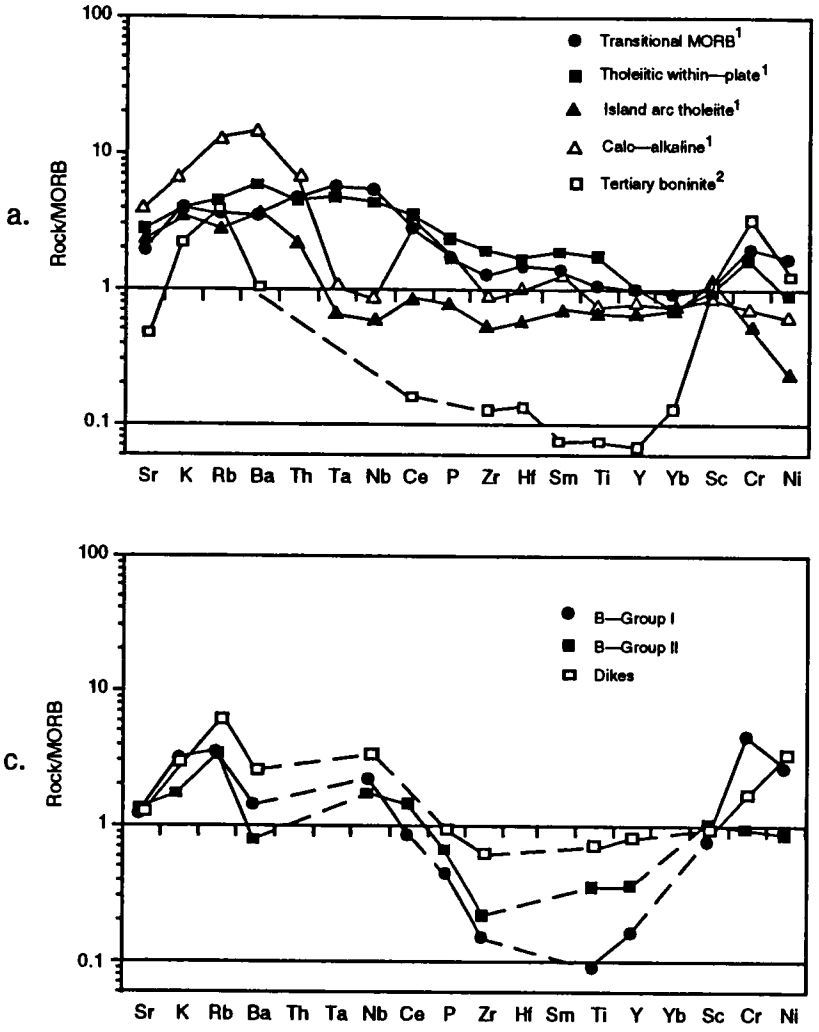
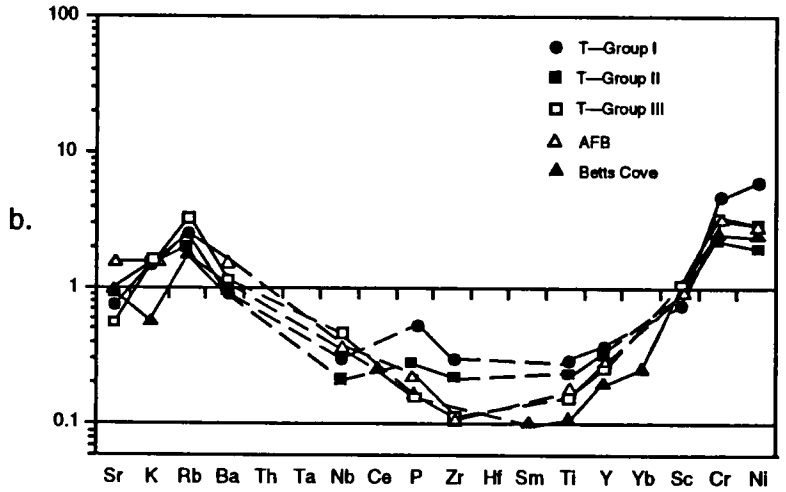


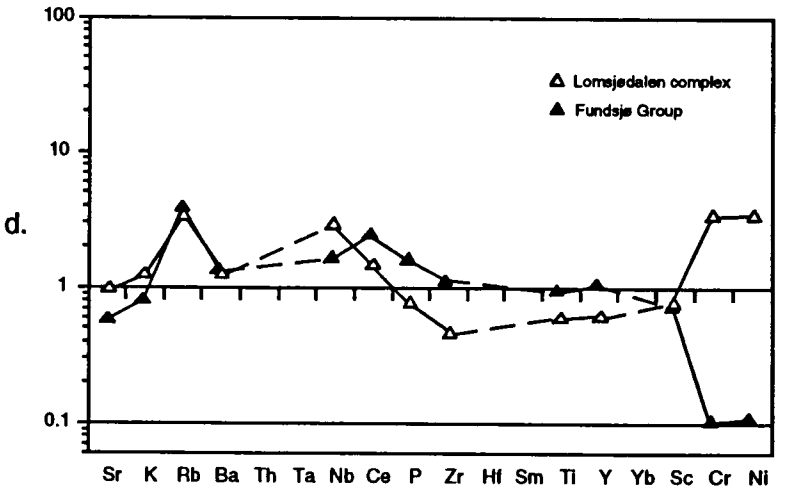

Figure III-9
TiO2 vs MgO plot. SHMB—siliceous high-Mg basalt. Fields for boninite and komatiitic basalt from Coish (1989); field for SHMB from data in Sun et al. (1989). Symbols same as in Figure III-4.

Figure III-10
MORB-normalized trace element diagrams. A) Trace element patterns for typical volcanic rock types. Sources: [1]Pearce (1982); [2]Hickey and Frey (1982). B) Average values for Troodos upper pillow lavas (Gps. I, II, and III) and volcanics from Arakapas fault belt (AFB), Cyprus (Cameron, 1985), and boninitic rocks from Betts Cove ophiolite, Newfoundland (Coish, 1989). Average values for metavolcanic rocks in this study: C) Bangardsvola Groups I and II, and dike rocks (note that sample Fiskt-4 was not utilitzed to calculate average of dikes, because it differs drastically in trace element abundances). D) Lomsjødalen complex and Fundsjø Group. Normalizing values from Pearce (1982). Dashed lines indicate elements not analyzed.


a.
Rock/MORB
100
10
1
0.1
Transitional MORB[1]
Tholeiitic within—plate[1]
Island arc tholeiite[1]
Calc—alkaline[1]
Tertiary boninite[2]
Sr K Rb Ba Th Ta Nb Ce P Zr Hf Sm Ti Y Yb Sc Cr Ni


b.
100
10
1
0.1
T—Group I
T—Group II
T—Group III
AFB
Betts Cove
Sr K Rb Ba Th Ta Nb Ce P Zr Hf Sm Ti Y Yb Sc Cr Ni


c.
Rock/MORB
100
10
1
0.1
B—Group I
B—Group II
Dikes
Sr K Rb Ba Th Ta Nb Ce P Zr Hf Sm Ti Y Yb Sc Cr Ni


d.
100
10
1
0.1
Lomsjødalen complex
Fundsjø Group
Sr K Rb Ba Th Ta Nb Ce P Zr Hf Sm Ti Y Yb Sc Cr Ni

tendency for these elements to be highly mobile during weathering and metamorphism. The Bangardsvola Group II pattern nearly parallels that of Group I from Sr through Zr, but differs in the less extreme depletion in Ti and Y, and in much lower Cr and Ni values. Although the Group II pattern differs from the typical IAT in some respects, IAT is characterized by a similar low abundance of the incompatible elements Ta–Yb, and low Cr (Pearce, 1982).

The trace-element pattern of the Lomsjødalen complex (Fig. III-10d) resembles that of IAT with respect to the incompatible elements, but the high concentrations of Cr and Ni are uncharacteristic of typical IAT (Fig. III-10a). This enrichment in the compatible elements, along with the rather high magnesium numbers (Table III-1), indicates the primitive nature of the Lomsjødalen metabasalts. The Fundsjø Group samples are also characterized by somewhat transitional compositions (Fig. III-10d)—whereas the incompatible elements show a flat pattern, near unity relative to MORB, the rocks are extremely depleted in Cr and Ni, similar to island-arc tholeiite.

In summary, on the basis of incompatible trace elements the Lomsjødalen complex appears to have an IAT affinity, in agreement with the results of Rainey (1980). The high concentrations of the compatible elements Cr and Ni, and the relatively high MgO content, however, are indicative of the primitive nature of these rocks. Of the Bangardsvola complex samples, three also have an IAT affinity, although rather depleted in incompatible elements, whereas the remainder are highly depleted and show a strong resemblance to subduction-related boninites. The Fundsjø Group samples, on the other hand, are geochemically similar to MORB. Although this study admittedly contains a small sampling of Fundsjø rocks, the MORB geochemical signature contrasts highly with that of rocks from the Bangardsvola complex, which was previously correlated with the Fundsjø Group (Mosson *et al.*, 1972; Nilsen and Wolff, 1989). Previous studies of the Fundsjø and correlative (?) Hersjø rocks (Grenne and Lagerblad, 1985; Grenne, 1988; Skyseth and Reitan, in preparation), however, have shown both along-strike and across-strike geochemical variations that range from IAT (Skyseth and Reitan, in preparation, Grimsdalen area), to MORB and transitional types, including HFSE-depleted types (Grenne and Lagerblad, 1985, Meråker area; and Grenne, 1988, Røros area). The latter type resembles the Lomsjødalen and Bangardsvola Group II rocks, although it does not show the extreme depletion characteristic of the "boninitic" Bangardsvola Group I metabasalts.

## *Discussion*

### *Paleotectonic Setting*

The resemblance of the primitive IAT of the Lomsjødalen complex to one variant of metabasalt in the eastern Trondheim district (ETD) sequence [Fundsjø Group Type I (Grenne and Lagerblad, 1985) and Hersjø Formation Type A (Grenne, 1988)] suggests that the Gula metavolcanic rocks may represent a tectonic setting comparable to that of the ETD. Based on the geochemical complexity of the Fundsjø/Hersjø sequence, the ETD metavolcanites were interpreted to have formed in either an immature ensimatic arc (Grenne and Lagerblad, 1985), or a marginal basin above a subduction zone (Grenne, 1988). Back-arc basin basalts (BABB) are commonly transitional between N-type MORB and island arc basalts (Saunders and Tarney, 1984). A comparison of the Lomsjødalen samples with basalts from the Lau basin behind the Tonga-Kermadec ridge (Hawkins, 1976; Gill, 1976; Hawkins and Melchior, 1985), shows similarities particularly in $TiO_2$, MgO (and Mg#), Cr, and Ni abundances. Lau basin basalts (LBB) are divided into two main geochemical groups (Hawkins and Melchior, 1985). N-type LBB, occurring in the central part of the basin, were suggested to be akin to N-MORB, while T-type LBB, found on the margins of the basin, resemble basalts from an analogous tectonic setting in the Mariana Trough (Hawkins and Melchior, 1985). The MORB-normalized trace element pattern (Fig. III-11) for average abundances in N-type LBB with comparable magnesium numbers to Lomsjødalen metabasalts shows a strong resemblance to that of the Lomsjødalen samples (Fig. III-10d) for the elements P through Ni. Disparities exist in the strong depletion of LIL elements in the N-type LBB, although this pattern is uncharacteristic of back-arc basin basalts (Saunders and Tarney, 1984) and could be partially due to mobility of these elements during alteration. The overall pattern of the T-type LBB also resembles that of the Lomsjødalen samples, and even more so of the dike (?) samples (Fig. III-10c).

Field relationships may provide some insight into the derivation of the Lomsjødalen complex. The association of thick sequences of quartzose and calcareous metasedimentary rocks and volcaniclastics (Volengsvola/Svartlia units) with the Lomsjødalen complex suggests proximity of either an island or a continental margin (Nilsen, 1978). In contrast, the thinly layered metachert, coticule, sulfidic black phyllite, and metalliferous sedimentary rocks that directly overlie the pillow lavas appear to be analogous to pelagic muds and hydrothermal deposits that blanket oceanic crust at modern-day spreading ridges. Indeed, the pods of iron formation and sulfide mineralization may represent "fossil" black smokers, loci of hydrothermal vents where circulating metalliferous brines are exhaled. The abundance of

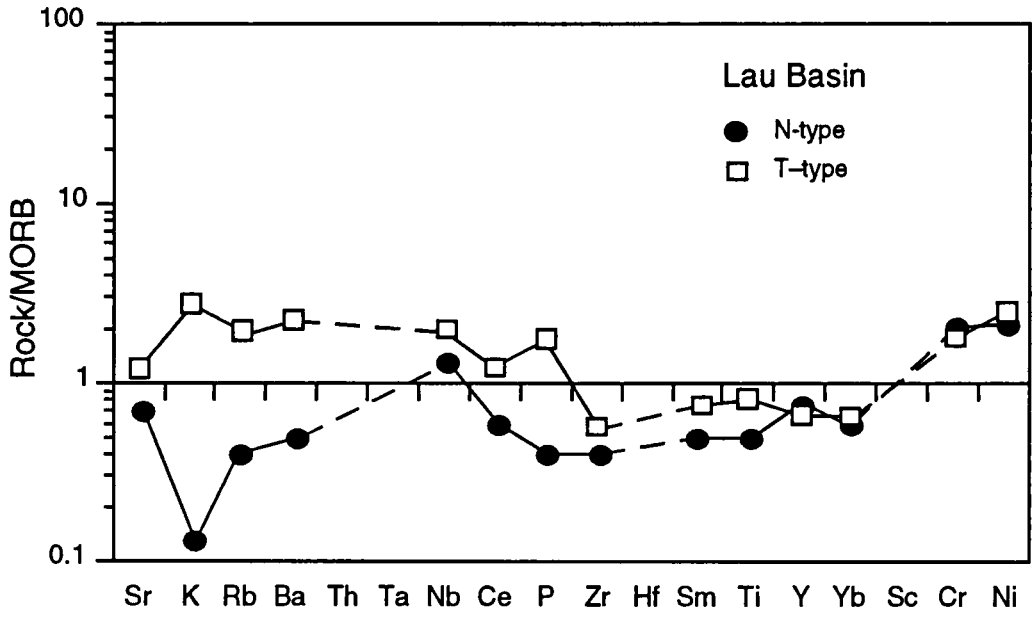



Figure III-11
MORB-normalized trace element diagram for Lau basin basalts. (Hawkins and Melchior, 1985.) Dashed lines indicate elements not analyzed.

high-Mn coticule horizons is greatest in rocks surrounding the mineralized zones, and decreases gradually away from the zones. This pattern is predictable from modern-day hydrothermal vents, where the readily oxidized Fe-rich phases are precipitated at the vent, while the Mn-rich phases (less easily oxidized) are carried farther from the exhalation site (Bonatti, 1975; Jenkyns, 1986). In a comparison of sedimentation in marginal basins vs. volcanic arcs, Carey and Sigurdsson (1984) noted that Fe- and Mn-rich hydrothermal deposits have been documented at back-arc spreading centers (for instance, Bonatti *et al.*, 1979; Cronan *et al.*, 1984), but indicated that these types of deposits are not characteristic of volcanic arc sediments. In fact, the discovery of high Fe and Mn concentrations in sediment from the Lau basin led Cronan *et al.* (1984) to suggest the presence of hydrothermal vents in the vicinity of the axial rift of the basin.

The combined sedimentological and geochemical evidence from the Lomsjødalen complex in this study and from the correlative Gula greenstone in previous works (Nilsen, 1974, 1978; Rainey, 1980) clearly points to derivation of the volcanic complex in a subduction-related setting, but one that was characterized at least locally by an extensional regime. A back-arc spreading center such as the Lau basin example discussed above may provide the most likely analogy. The characteristics of the earliest stages of arc volcanism are still relatively unknown, however, because the roots of most modern-day arcs are covered by subsequent volcanic material and sediment. Stern and Bloomer (1992) based a model for the early evolutionary stages of subduction-zone development on observations from the Izu-Bonin-Mariana arc system, the characteristics of which include formation of tholeiitic and boninitic magmas in an extensional environment prior to stabilization of the volcanic-arc axis. Therefore, it cannot be ruled out that the Lomsjødalen complex represents the incipient stages of arc formation, particularly when the association with the Bangardsvola complex is taken into consideration.

Metabasalts of the Bangardsvola complex comprise a combination of primitive island-arc tholeiites and basalts having boninitic affinities. Although the latter are generally lower in $SiO_2$ than most Tertiary boninites, they are essentially identical to the "high-Ca" boninite suite of Crawford *et al.* (1989). The possible mobility of $SiO_2$ during sea-floor alteration and low-grade metamorphism must be taken into account when considering ancient metabasalts, and it should be noted that a relatively low $SiO_2$ content, averaging approximately 52%, is characteristic of Early Paleozoic northern Appalachian boninitic rocks of the Betts Cove ophiolite and Pacquet Harbour Group, Newfoundland, and the Thetford Mines ophiolite, Quebec (Coish, 1989). Various models have been proposed for the generation of boninitic lavas (Cameron *et al.*, 1979; Meijer, 1980; Crawford *et al.*, 1981; Hickey and Frey, 1982; Crawford *et al.*, 1989), but there is a general consensus that they form by partial melting of a depleted mantle

source in a subduction zone setting. Boninites are generally associated with tholeiitic basalts of island-arc, or less commonly, MORB to BABB affinity, and the spatial and temporal relationships are important to the petrogenetic models. In the western Pacific Mariana-Bonin arc systems, boninites occur in the forearc regions and have been interpreted to represent the earliest stages of island arc volcanism (Hickey and Frey, 1982; Hawkins *et al.*, 1984; Bloomer and Hawkins, 1987). However, boninitic lavas commonly overlie arc tholeiites, for instance, in DSDP Hole 458 in the Mariana forearc (Meijer, 1980), the Thetford Mines ophiolite, Quebec (Coish, 1989), and the Troodos ophiolite (Cameron, 1985), or are interlayered with arc tholeiites on Guam (Reagan and Meijer, 1984), and in the Betts Cove ophiolite, Newfoundland (Coish *et al.*, 1982; Coish, 1989). In addition, at Betts Cove, the boninites are overlain by lavas similar to MORB or BAB basalts. These observations suggest that boninites are also generated during arc rifting and initiation of back-arc spreading (Crawford *et al.*, 1981).

The Lomsjødalen and Bangardsvola complexes are interpreted to have been emplaced onto the continental margin as a composite thrust nappe (Chapter II). Stratigraphic relationships between the complexes remain unresolved, however, because of internal deformation within the thrust sheet and lack of age constraints. Although the uncertainties preclude a comprehensive model that ties together the formation of both complexes, several observations suggest that the mafic complexes may have been associated both spatially and temporally. Geochemically, both complexes show a clear suprasubduction-zone signature, and can be considered as part of the common boninite/tholeiite association. In the study area, the Lomsjødalen and Bangardsvola complexes are in contact with quartzose or calcareous schist that locally contains dike-like mafic layers bearing similar geochemical signatures to that of the Lomsjødalen basalts, and may be slightly more evolved products of the same magmatic event. Fuchsite-bearing marble and quartzite that comprise the highest unit in the Savalen thrust sheet are locally in contact with both mafic complexes; the nature of the contact suggests either an early fault or an unconformity that developed prior to emplacement of the Savalen thrust sheet. The presence of fuchsite indicates the proximity of a high-Cr source, possibly derived from erosion of the boninitic lavas or an unknown ultramafic source.

A possible analogy for the Bangardsvola and Lomsjødalen complexes is the upper part of the Late Cretaceous Troodos ophiolite, Cyprus, in which a sequence of higher-Ti "lower pillow lavas" is overlain by low-Ti "upper pillow lavas", including the type high-Ca boninites of Crawford *et al.* (1989). Massive sulfide deposits are intercalated with, or overlie the lower pillow lavas, and are in turn overlain by Fe-rich metalliferous sediments (ochres) (Constantinou, 1980; Hamelin *et al.*, 1988), while sediments rich in both Fe and Mn (umbers) overlie the upper pillow lavas (Robertson and Hudson, 1974). Fragments of hydrothermal

vents, or black smokers, have also been identified from massive sulfide deposits intercalated between the lower and upper pillow lavas (Oudin and Constantinou, 1984). Although Troodos is one of the most well-studied ophiolites in the world, its tectonic setting is still highly debated. Early workers recognized the complex as a section of oceanic crust (Gass, 1968; Moores and Vine, 1971; Gass and Smewing, 1973), and the presence of an extensive sequence of sheeted dikes is indicative of formation in a spreading environment. Early geochemical studies, however, showed island-arc affinities for the complex (Miyashiro, 1973; Pearce, 1975). The necessity of reconciling the spreading center field characteristics with the arc geochemistry has led to numerous hypotheses concerning the tectonic setting, including formation in an interarc basin (Pearce, 1975; Gass, 1980), in a suprasubduction-zone environment with no arc development (Pearce *et al.*, 1984), or as the earliest stages of an island arc (Rautenschlein *et al.*, 1985). Moores *et al.* (1984) suggested that an actualistic model for the Troodos and related Mideast ophiolites may be the Andaman Sea region of the Indian Ocean, where short spreading segments formed above an oblique subduction zone, and are separated by transform faults. The region is characterized by an active ridge-transform system rather than development of a continuous, mature arc. This model was later modified to include the possibility of splitting of an immature, submarine arc prior to back-arc spreading (Flower and Levine, 1987; Thy and Moores, 1988).

*Regional Comparisons*

Although a complete ophiolite stratigraphy has not been recognized in the Einunnfjellet-Savalen area, the complexes can be reasonably compared with the higher volcanic/sedimentary parts of more complete ophiolite sequences. Norwegian ophiolites can be divided into two main groups (Pedersen *et al.*, 1988; Sturt and Roberts, 1991): Early Ordovician complexes that developed mainly in a suprasubduction-zone setting; and Late Ordovician to Early Silurian complexes that probably represent small, spreading-related marginal basins. Isotopic dating is not yet available for metaigneous rocks in the Einunnfjellet-Savalen area, but they are lithologically and geochemically most similar to the former group of Early Ordovician ophiolites. For example, they compare well with those in southwestern Norway, including the extensively studied Karmøy ophiolite (Sturt and Thon, 1978b; Sturt *et al.*, 1979) and ophiolite fragments in the Major and Minor Bergen Arcs. Pillow lavas in the Karmøy ophiolite are capped by a well-developed pelagic sequence, the Torvastad Group (Sturt *et al.*, 1979; Solli, 1981), that contains Mn-rich chert and various metalliferous sediments similar to those associated with the Lomsjødalen complex. Comparable Mn-rich metasedimentary rocks and

metachert are also associated with mafic rocks in the Samnanger Complex, Major Bergen Arc (Thon, 1985) and in the correlative but more strongly deformed Nordåsvatn Complex, Minor Bergen Arc (Fossen, 1989). The Karmøy igneous complex, which formed between 493 and 470 Ma (Dunning and Pedersen, 1988), consists of an axis sequence of gabbro and sheeted dikes formed from IAT and MORB-like magmas, that was subsequently intruded by magmas with boninitic affinities (Pedersen and Hertogen, 1990). Later intrusions graded from boninitic back into IAT- and MORB-like compositions, whereas the youngest intrusions and extrusions were calc-alkaline to alkalic. Similarly, a succession of MORB-like basalts followed by low-Ti tholeiitic and calc-alkaline magmatism has been reported from fragmented ophiolites in the Major Bergen Arc (Furnes *et al.*, 1980).

Pedersen and Hertogen (1990) explained the variety and sequence of development of magma compositions in the Karmøy ophiolite, and particularly the presence of boninitic magmas, by a model involving rifting of an island arc and subsequent development of a marginal basin. Similarly, a rifted arc or marginal basin model was proposed for the Fundsjø Group/Hersjø Formation sequence (Grenne and Lagerblad, 1985; Grenne, 1988) to explain the association of a diverse group of basalt types, ranging from MORB and IAT to transitional calc-alkaline and within-plate affinities. In the study area, the Einunnfjellet-Savalen complexes are in fault contact with metavolcanic rocks of the Fundsjø Group, although the amount of displacement on the fault is unknown (Chapter IV). Geochemical similarities between the Hersjø Type A basalts in the Røros area (Grenne, 1988) and the primitive arc tholeiites of this study, discussed earlier, suggest that these rocks either formed in comparable tectonic environments, or are tectonically disrupted elements of a more extensive sequence.

Stephens and Gee (1985) also proposed a rifted arc model for possible Fundsjø correlative rocks in the Gjersvik nappe. In this model, the Gula nappe was interpreted as a fore-arc basin developed in front of an arc in the Gjersvik terrane, which formed near the Laurentian margin. The features of the Einunnfjellet-Savalen area (Chapter II), however, show greater resemblance to their Virisen terrane, formed near the Baltoscandian margin; characteristics of this terrane include lack of a significant tectonic break between the Köli and Seve nappes, presence of solitary ultramafic bodies or detrital serpentinites, and the presence of an overlying sequence of clastic rocks that were apparently derived from an eastern platformal or cratonic source. In addition, the Einunnfjellet-Savalen area is tentatively correlated (Chapter II) with the Otta nappe, including the Early Ordovician or older Vågåmo ophiolite (Sturt *et al.*, 1991), which Stephens and Gee (1985) considered to be part of the Virisen terrane. Therefore, it appears that the Virisen and Gjersvik terranes share some elements, and were not entirely separated by a segment of the Iapetus Ocean, as in their model. Perhaps these and other Scandinavian

ophiolitic sequences are best explained in the context of a complex, rapidly evolving subduction-zone environment such as the modern-day examples of arc systems described by Hamilton (1988), or as segments of oceanic crust separated by a system of transform faults above a subduction zone (Sturt and Roberts, 1991), similar to the Andaman Sea example discussed previously.

## *Conclusions*

The paleotectonic setting of the Gula nappe is a critical element in attempts to model the development of the Trondheim nappe complex. Studies of mafic metavolcanic rocks that occur throughout the Gula nappe may hold the most promise for determining the environment of formation, and relationship of the Gula rocks to other tectonic units within the Trondheim nappe complex. Geochemistry and field relationships of Gula greenstone-equivalent metavolcanic rocks in the Einunnfjellet-Savalen area indicate that these rocks, informally referred to as the Lomsjødalen complex, formed in a suprasubduction-zone setting. Despite the IAT chemistry of the metabasalts, overlying metalliferous sediments and possible remnants of black smokers suggest some type of spreading-ridge environment, probably either an opening marginal basin or an incipient arc that underwent rifting prior to back-arc spreading. Significantly, the Lomsjødalen complex is associated with a bimodal metavolcanic sequence, the Bangardsvola complex, in which the mafic rocks have boninitic affinities uniquely characteristic of subduction-related settings. The association of primitive arc tholeiites, boninites, and Fe- and Mn-rich metalliferous sediments is strongly analogous to the upper parts of the Troodos ophiolite, Cyprus. Although the tectonic setting of Troodos is still highly debated, a suggested actualistic model is the Andaman Sea region of the Indian Ocean, where short spreading segments form above an oblique subduction zone (Moores *et al.*, 1984; Flower and Levine, 1987; Thy and Moores, 1988).

The Bangardsvola complex was previously correlated in part with the Fundsjø Group (Köli nappes) and in part with the Essandsjø nappe (Seve nappes) (Nilsen and Wolff, 1989). Results of this study show, however, that Bangardsvola rocks of boninitic affinity are geochemically distinct from metabasalts of the Fundsjø Group or the correlative (?) Hersjø Formation (Grenne and Lagerblad, 1985; Grenne, 1988; Skyseth and Reitan, in preparation), although it cannot be ruled out that these represent time-transgressive elements in the same or a related sequence. The latter correlation, with rocks equivalent to the Seve nappes, suggests that the Seve is a composite unit, consisting not only of Baltoscandian miogeoclinal rocks (Stephens and Gee, 1985), but also containing higher-grade equivalents of the Köli oceanic terranes.

Metaigneous rocks of the Einunnfjellet-Savalen area are lithologically and geochemically similar to dated Early Ordovician Norwegian ophiolites that formed in a suprasubduction-zone environment. Although the Gula nappe may have formed in a fore-arc setting as suggested by Stephens and Gee (1985), the resemblance of the Einunnfjellet-Savalen area to their Virisen terrane could indicate that the subduction zone lay in closer proximity to Baltoscandia rather than to Laurentia, as in their model.

# CHAPTER IV

## Deformational and Metamorphic History of the Einunnfjellet-Savalen Area, Southeastern Trondheim Nappe Complex

### *Introduction*

The central Scandinavian Caledonides comprise a historic area for the study of thrust and nappe tectonics and metamorphic petrology. The nappe theory as traditionally applied to the Caledonides was first proposed by Törnebohm (1888) at Åreskutan, in Sweden near the border with Norway, and the orogen has subsequently been found to be built of thrust nappes, stacked from west to east across the Baltic Shield. One of the classic works of the early days of metamorphic petrology, Goldschmidt's metamorphic map of the central Caledonides (1915, in Miyashiro, 1973b), portrays the remarkable symmetry of the Trondheim region, in which a relatively high-grade thermal axis parallel to the trend of the orogen gives way to belts of decreasing metamorphic grade on either side. Despite the comparatively uncomplicated appearance of the orogen on this scale, detailed work over the past two decades has uncovered evidence for multiple phases of deformation involving varied strain histories (e.g., Roberts, 1971, 1979), multiple metamorphic phases, and inverted metamorphic gradients both between nappes and within single nappes (Andréasson and Gorbatschev, 1980).

It is now known that at least two major events comprise the Caledonian orogeny in Scandinavia. During the Siluro-Devonian Scandian phase (Gee, 1975), closing of the Iapetus ocean basin and collision between the Baltoscandian and Laurentian continents produced intense deformation, metamorphism, and major nappe transport. An earlier event in the central and southwestern Caledonides involved emplacement of fragments of the Iapetus ocean basin (Furnes *et al.*, 1980) during Early Ordovician time (the "Trondheim disturbance" of Holtedal, 1920). This event was probably diachronous, and is possibly correlative with the Finnmarkian orogeny in northern Norway (Ramsay and Sturt, 1976; Sturt *et al.*, 1978). Although the effects of this event have been largely obscured by the pervasive Scandian deformation, some evidence exists for the presence of pre-Scandian metamorphism and/or deformation (Vogt, 1945; Kvale, 1960; Sturt and Thon, 1976; Naterstad, 1976; Guezou, 1978).

In general, it appears that final nappe stacking postdated peak metamorphism and development of the regional foliation (Andréasson and Gorbatschev, 1980; Andréasson and Lagerblad, 1980; Roberts and Wolff, 1981). This relationship is not resolved in every case, however, and, while some nappe boundaries consistently juxtapose rocks of contrasting metamorphic grade, others have uncertain or ambiguous histories. Therefore, key questions

that must be asked in any one area are: 1) what is the sequence of deformational events; 2) what is the relationship and relative timing of deformation and metamorphism; and 3) does evidence exist for deformation and/or metamorphism related to the Ordovician event? Studies of deformation and metamorphism are of continuing importance in order to resolve these and related problems throughout the Caledonides, and particularly in the upper allochthon, the subject of this study.

## *Regional Structural Relationships*

The stratigraphy of the upper allochthon and the Trondheim nappe complex was described in Chapter I (pp. 7–11). Most of the early structural studies of the Trondheim nappe complex were concentrated in the northern Trondheim region (Peacy, 1964; Roberts 1967, 1971, 1979). Four deformational episodes, all related to Mid-Silurian orogenesis, were recognized in low- to middle-greenschist facies Köli-equivalent rocks (Roberts, 1971; 1979). $D_1$ involved tight to isoclinal folding and development of an axial-planar regional schistosity ($S_1$), creation of fold nappes with inversion of stratigraphy in some areas, and dissection of the nappe pile by progressive simple shear. Shear deformation was accompanied and followed by a component of flattening and stretching that produced the lensoid outcrop pattern commonly observed throughout the Trondheim region. $D_2$ was generally coaxial with $D_1$, and produced open, upright folds with a locally developed axial-planar cleavage. A pervasive set of folds having flat-lying axial surfaces and a well-developed crenulation cleavage was produced during $D_3$. These folds, which are generally asymmetric and overturned down dip, were interpreted to represent gravitational collapse of the nappe pile (Ramberg, 1967; Ramberg and Ghosh, 1968; Roberts, 1971, 1979). The final deformation episode, $D_4$, involved minor kink bands and kink folds.

Complications to the relatively simple sequence described above arise when the Gula and Seve nappes in the Trondheim area are considered. In the Tømmerås area of the northern Trondheim region, the penetrative regional foliation is Scandian ($S_1$, above), but transposed an earlier foliation in the rocks of the Seve nappe that is represented by aggregates of partly retrogressed kyanite + staurolite + almandine (Andréasson and Gorbatschev, 1980; Andréasson and Lagerblad, 1980). Pre- or early Scandian foliations were also observed in ore quartzite and calcareous schist of the Gula nappe (Andréasson and Gorbatschev, 1980). Similarly, Guezou (1978) found evidence for early, relatively high-T metamorphism and deformation confined to Gula rocks in the Dombås area, southwestern Trondheim nappe complex. This lends support to the idea that the Gula nappe is, at least in part, a Seve-equivalent unit (Roberts and Wolff,

1981). Clearly, the history of Gula nappe is crucial to knowledge of the tectonic evolution of the Trondheim nappe complex. More studies of the Gula nappe and possibly equivalent rocks elsewhere are necessary in order to determine if it is a composite nappe, composed of units with different deformational and metamorphic histories, and whether or not it is structurally and/or lithologically equivalent to all or parts of the Seve nappe. Rocks of the Gula nappe comprise a significant part of the Einunnfjellet-Savalen map area, so it is an excellent location to try to shed some light on the Gula nappe problem.

## *Einunnfjellet-Savalen Area*

The stratigraphy of the Einunnfjellet-Savalen map area (Fig. II-1 & Plate I) was described in detail in Chapter II. The geologic map of the study area (Plate I), which is dominated by the Einunnfjellet dome to the west, and a ductile shear zone at the eastern boundary, can be divided into three main tectonostratigraphic units, all of which have experienced multiple phases of deformation and were metamorphosed from greenschist to lower amphibolite faces: 1) The Einunnfjellet dome is cored by a quartzite-schist sequence correlated with the Hummelfjell Formation (Rui, 1972). These rocks are considered as a higher-grade tectonic unit equivalent to Late Proterozoic sandstone and quartzite of the Särv nappe that represents the Baltoscandian continental margin. 2) The quartzite-schist sequence was overthrust by the Savalen thrust complex (STC), that contains fragments of oceanic crust, along with pelagic, volcaniclastic and turbiditic sediments, and carbonate. 3) An unconformable sequence of polymict conglomerate (containing clasts of mafic and felsic volcanic rocks, carbonate, and quartzite) and finer-grained clastic sediment is interpreted to have been deposited upon both the continental margin rocks and the thrust complex. Based on lithologic similarities and tectonostratigraphic position, I suggested in Chapter II a correlation of the Einunnfjellet-Savalen area with the Otta nappe (Strand, 1961; Sturt *et al.*, 1991a, 1991b) at the southern termination of the Trondheim nappe complex (Fig. I-2). There, a quartzite/schist sequence, the Heidal Series, was overthrust by the Vågåmo ophiolite (Sturt *et al.*, 1991b); subsequently, both units were overstepped by the fossiliferous Otta conglomerate. This relationship implies emplacement of the STC onto the edge of the continental margin (or a microcontinent rifted from Baltica) and early deformation in the pre-unconformity rocks prior to or during earliest Ordovician time, probably correlative with Trondheim or Finnmarkian orogenic phases elsewhere in the Caledonides. On the Røros 1:250,000 map sheet (Nilsen and Wolff, 1989), the basal thrust below the quartzite/schist sequence (base of the upper allochthon) crops out approximately 15 km east of the Einunnfjellet-Savalen area. The quartzite is thrust upon arkosic

sandstone of the middle allochthon, or locally, a slice of Proterozoic augen gneiss, and the thrust contact appears relatively flat and unfolded or only gently folded. This relationship suggests that the basal thrust is a relatively late feature, and cuts earlier Scandian and pre-Scandian structures, as shown in the cross sections through the study area (Plate II).

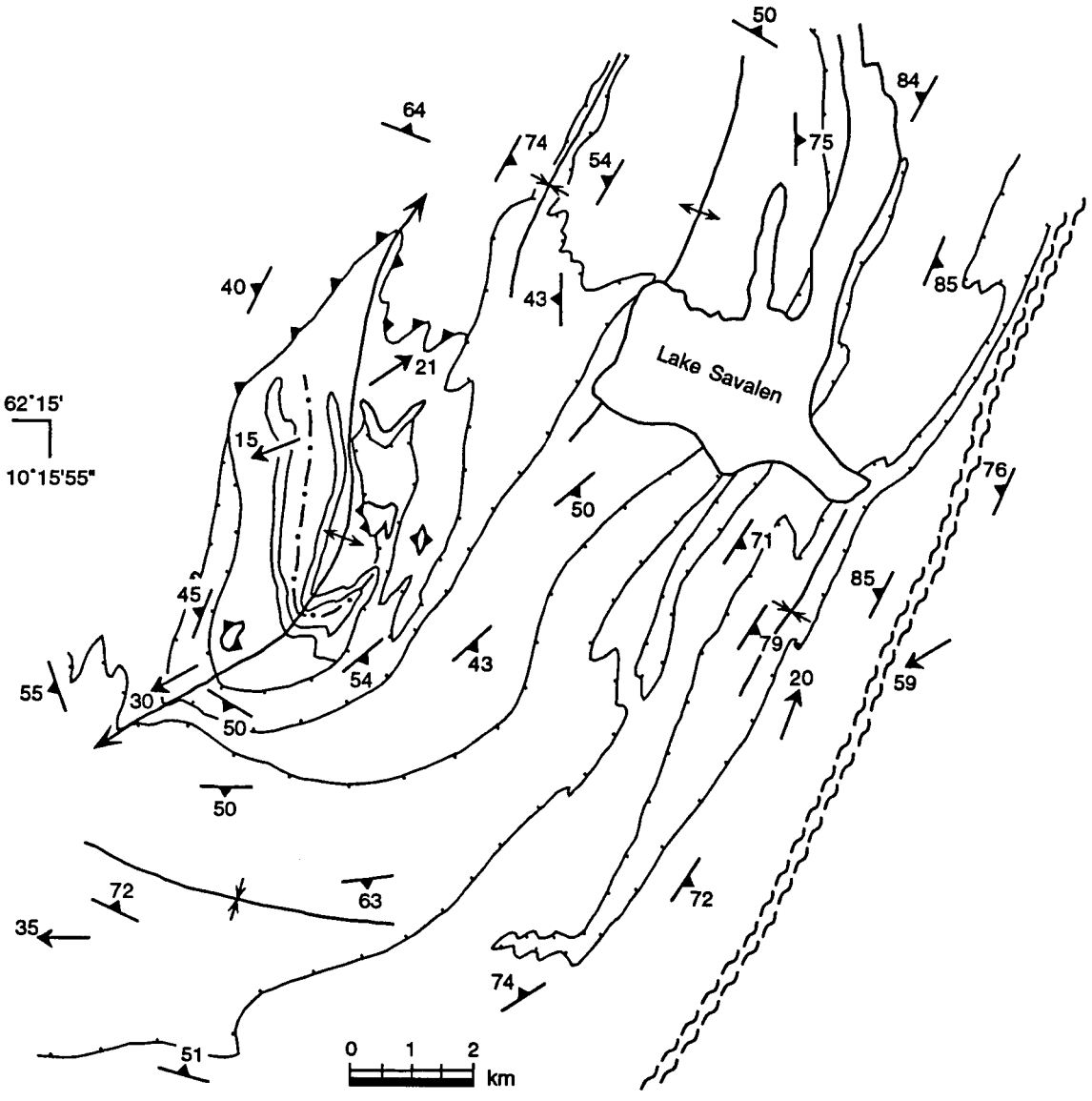
The Savalen thrust complex, an internally deformed sheet of oceanic crustal rocks and associated sediments, includes units previously correlated with the upper Seve nappes as well as much of the Gula nappe (Fig. II-5). Although the extent of internal thrusting within the STC is not clear because of lack of facing criteria or age dates, mafic metavolcanic rocks in both the Gula and Seve-equivalent units were shown to be a related sequence of boninitic and primitive island-arc rocks of suprasubduction-zone origin (Chapter III), and therefore must have been closely linked in space and time. A fault is required to explain the juxtaposition of rocks of oceanic crustal origin with a miogeoclinal quartzite sequence, although the contact between the STC and the underlying quartzite-schist sequence is presently concordant and no fault-related fabrics are specifically localized along it (Chapter II). In contrast, the eastern boundary of the STC with rocks of the Fundsjø Group (Meråker nappe) is characterized by pervasive mylonitic fabrics and shear-related structures.

In this chapter, I attempt to document the sequence of deformational events in the Einunnfjellet-Savalen area, to characterize the P-T conditions of metamorphism, and to delineate the timing of deformation relative to metamorphism. As a corollary, I will discuss the evidence that the STC was emplaced prior to pervasive Scandian deformation and metamorphism, as well as evidence for the relative timing of ductile shearing between the STC and the Fundsjø Group.

## *Meso- and Macroscopic Structure*

The Einunnfjellet-Savalen area can be divided into two major domains on the basis of orientations of foliations, folds, and lineations: 1) the area encompassed by the Einunnfjellet dome; and 2) the Savalen area, south and east of lake Savalen. A simplified structural map of the entire study area is shown in Figure IV-1. In the following discussion, the earliest structures in the Einunnfjellet-Savalen area are interpreted to represent pre-Scandian deformation, which I designate $D_1$ (Table IV-1). These structures, mostly evident on the meso- and macroscopic scale, are collectively grouped, although the early history of all units may not have been identical. $D_1$ structures have only been observed in rocks of the Hummelfjell Formation and in the STC, and therefore are interpreted to have formed before these rocks were eroded and the upper unconformable sequence was deposited. I suggest that $D_1$

Figure IV-1
Simplified structural map of the Einunnfjellet-Savalen area, showing representative orientations of the dominant foliation and lineation, and trend of major structures. Two major domains are discussed in the text: 1) the area to the west, where foliation dips away from the axis of the Einunnfjellet dome; and 2) the area of steeply dipping foliation, south and east of lake Savalen.




## Explanation

- strike and dip of foliation
- trend and plunge of mineral lineation
- major axis of Einunnfjellet dome
- axial trace of antiform
- axial trace of synform
- axial trace of pre-Scandian (?) fold
- pre-Scandian (?) thrust fault
- lithologic contact
- unconformable contact
- ductile shear zone

Table IV-1: Sequence of deformation in the Einunnfjellet-Savalen area

| Deformation phase | *Time of deformation | Folds | Foliations | Faults |
|---|---|---|---|---|
| $D_3$ | Siluro-Devonian (late Scandian) | open and kink folds | none | basal thrust of Trondheim nappe complex |
| $D_2$ | Silurian (Scandian) | | | |
| $D_{2b}$ | | tight, asymmetric folds and crenulations | crenulation cleavage (composite of $S_{2a}$ + $S_{2b}$ locally) | Stei-Langsætra shear zone |
| $D_{2a}$ | | isoclinal folds | axial planar foliation | none recognized |
| $D_1$ | Early Ordovician? (pre-Arenig) | isoclinal | none or equivocal | emplacement of Savalen thrust complex |

*Based on correlations with other areas where age control exists.

deformation was related to initial emplacement of the STC onto the miogeoclinal quartzites, prior to the main (Scandian) orogenic phase. Two phases of clearly Scandian deformation, designated $D_{2a}$ and $D_{2b}$ (Table IV-1), were dominantly responsible for the outcrop patterns and regional foliation in the Einunnfjellet-Savalen area. The latest structures formed during brittle deformation, $D_3$, of younger but uncertain age.

*Folds and Lineations*

*Einunnfjellet Dome Area*: The Einunnfjellet dome is defined by a major NE-SW doubly plunging antiformal axis, and a minor axis that plunges gently NW-SE (Fig. IV-1). Several phases of deformation affected the dome, suggesting that it is complex interference structure. The first phase, $D_1$, involved isoclinal, recumbent folds, indicated by a type 2 refold pattern (Ramsay, 1967) of the Bjørnkletten quartzite in the core of the dome (Figs. II-1 & IV-1). Mesoscopic refolded $F_1$ folds occur in pelitic and amphibolitic rocks in the Savalen thrust complex (Fig. IV-2), and locally in pelitic schist, an early foliation defined by mica growth parallel to the compositional layering is folded by $F_{2a}$ isoclinal folds having an axial-planar schistosity (e.g., UTM 669 974).

On the macroscopic scale, the second phase, $D_2$, produced the NNE-striking antiformal structure (Fig. IV-1). Second-order folds on the limbs of the antiform are large-scale tight to isoclinal folds with steep axial surfaces, that are generally overturned and verge with normal asymmetry (Hanson, 1971) toward the central antiformal axis (Plate II). The earliest mesoscopic $F_{2a}$ folds are inclined isoclinal folds with an axial planar schistosity. Most commonly, $F_{2a}$ axial planes strike WNW and dip gently to moderately NW, and axes plunge toward the west (Fig. IV-3). $F_{2a}$ folds were overprinted by pervasive $D_{2b}$ deformation that produced tight flexural-flow buckle folds in quartzite and other competent rocks, and crenulations in schist. Mineral lineations, present generally as quartz rods, consistently parallel $F_{2b}$ fold axes. The Einunnfjellet dome area can be divided into five subdomains (Figs. IV-4 & 5), in which the orientation of $D_{2b}$ structures depends upon their position with respect to the dome axes (Fig. IV-1). Axial planes of $F_{2b}$ tight folds (Fig. IV-4) strike NE and dip steeply nearest the core of the dome (Domains 1, 3, and 4), whereas they flatten in Domain 2, perhaps in response to the open NW-trending synform in that area (Fig. IV-1). An exception to the general NE strike of folds occurs in Domain 1, where poles to the axial surfaces describe a great circle yielding a β-axis (55°, S68W) that corresponds closely to the mean orientation of the fold axes (44°, S82W). Domain analysis shows a swing from a SW plunge of all $D_{2b}$ linear features on the southern flank on the dome, to NE on the northern flank (Figs. IV-4 & 5). The sense of

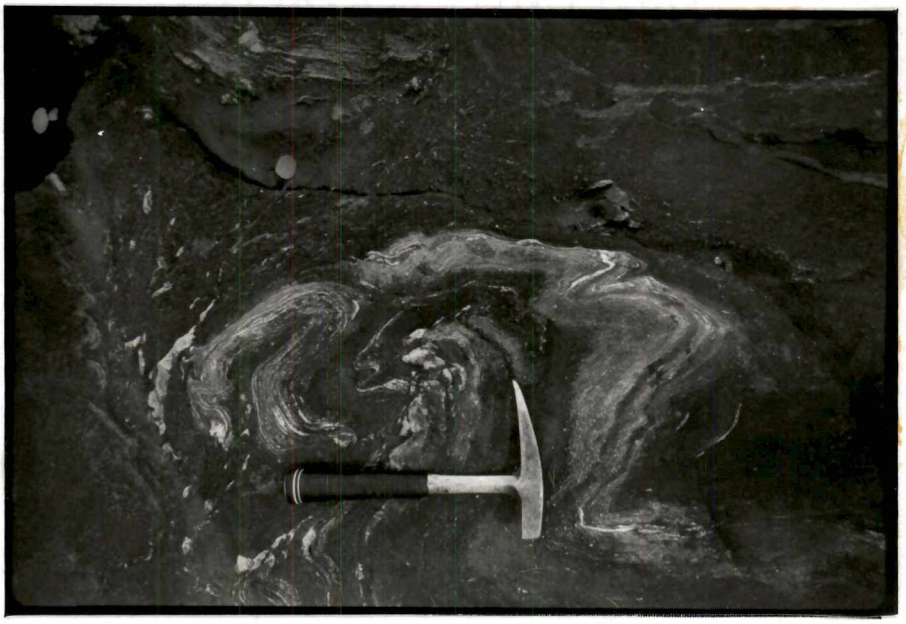


Figure IV-2
Boudinage and refolded folds in amphibole schist of the Savalen thrust sheet (Einunna mafic complex, UTM 701 005).

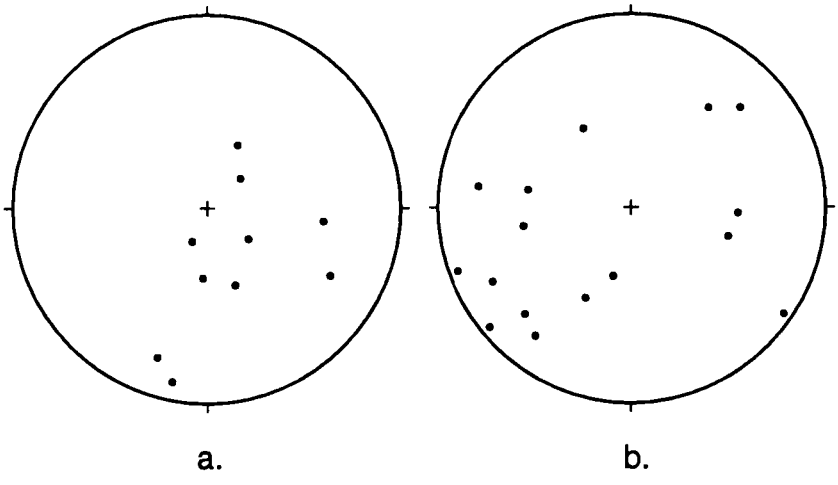



Figure IV-3
Lower hemisphere equal area projection of isoclinal folds, Einunnfjellet dome area.
a) Poles to axial surfaces (n = 10). b) Fold axes (n = 16).

Figure IV-4
Lower hemisphere equal area projection of a) poles to axial surfaces, and b) fold axes of tight folds in 5 subdomains in the Einunnfjellet dome area. Domain 1: $n_a = 25$, $n_b = 17$. Domain 2: $n_a = 10$, $n_b = 8$. Domain 3: $n_a = 28$, $n_b = 21$. Domain 4: $n_a = 10$, $n_b = 28$. Domain 5: $n_a = 10$, $n_b = 11$.

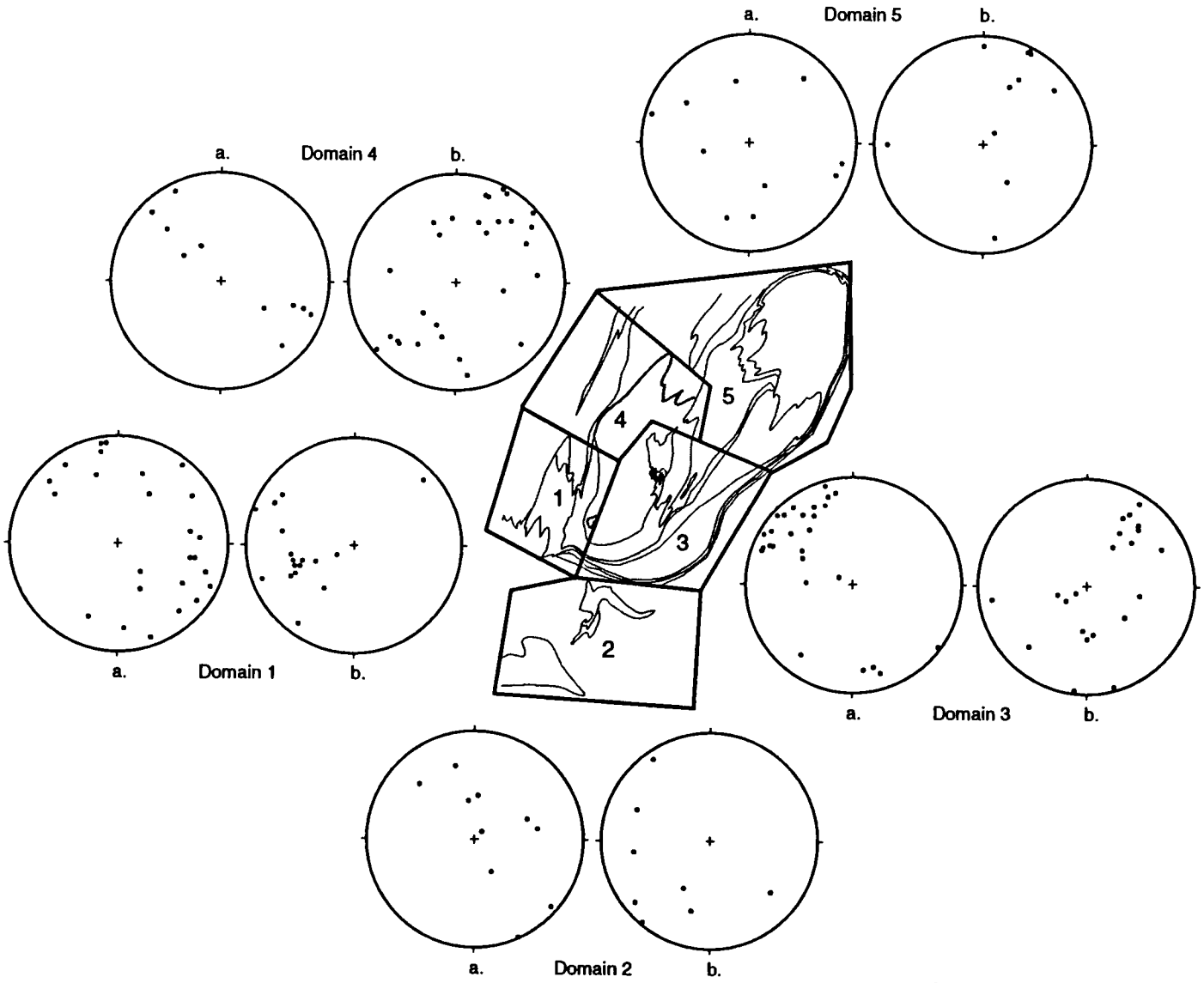
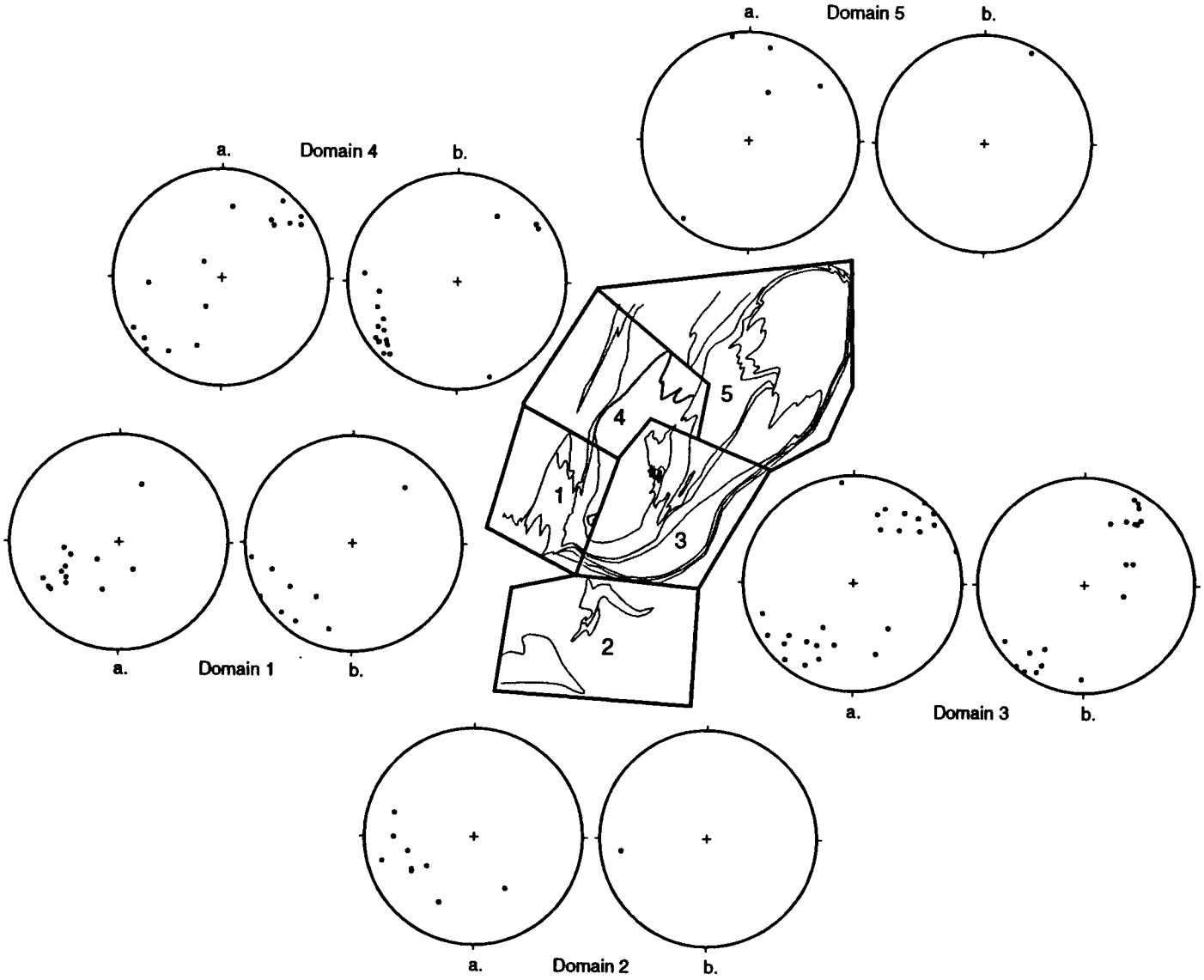

a.
Domain 5
b.
a.
Domain 4
b.
1
2
3
4
5
a.
Domain 1
b.
a.
Domain 3
b.
a.
Domain 2
b.

Figure IV-5
Lower hemisphere equal area projection of a) crenulation axes, and b) mineral lineations in 5 subdomains in the Einunnfjellet dome area. Domain 1: $n_a = 13$, $n_b = 9$. Domain 2: $n_a = 9$, $n_b = 1$. Domain 3: $n_a = 25$, $n_b = 19$. Domain 4: $n_a = 15$, $n_b = 16$. Domain 5: $n_a = 5$, $n_b = 1$.

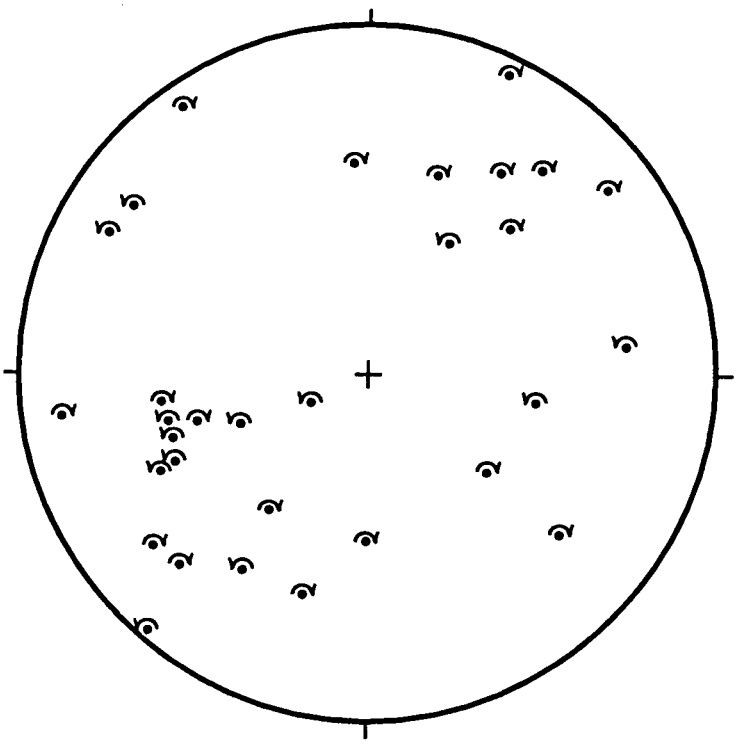

a.
Domain 5
b.
a.
Domain 4
b.
5
4
1
3
2
a.
Domain 1
b.
a.
Domain 3
b.
a.
Domain 2
b.

vergence of tight $F_{2b}$ folds with clear "Z" or "S" asymmetry (Fig. IV-6) is away from the domal axis, that is, dominantly westward for those folds having a SW plunge, and eastward for those with a NE plunge. Relative to the major dome axis, this constitutes reverse asymmetry (Hanson, 1971), opposite to that of the large-scale folds discussed above. Alternative explanations for reverse fold asymmetry include formation of folds as parasitic structures on the limbs of a mushroom-shaped antiformal structure (Hanson, 1971), or as a consequence of gravitational collapse after initial doming (Ramberg, 1967; Roberts, 1979). The most likely explanation for $F_{2b}$ folds in the area of this study, however, is that they formed subsequent to the development of the major axis of the dome (Fig. IV-1), and the variation in plunge is due to the overprinting of $F_{2b}$ folds on the limbs of a preexisting structure (Ramsay and Huber, 1987). Alternatively, or in addition, the relationship may be an indication that the minor NW-SE warping of the dome occurred later, reorienting structures on opposite limbs of the minor axis. A similar relationship was described from a fold arch in Vermont by White and Jahns (1950), and discussed by Ramsay (1967) as an example of type 2 fold interference.

The latest stage of deformation, $D_3$, includes minor brittle structures that formed after the main deformational and metamorphic event. Open, upright flexural-slip folds generally strike NE and dip steeply NW or SE, and most plunge gently to moderately SW (Fig. IV-7). The gentle warping of the Einunnfjellet antiform about a NW-SE axis, that accentuated the elongate dome structure, may also represent a $D_3$ structure. As discussed above, it may have occurred later than the main folding of the antiform, causing the reorientation of $F_{2b}$ structures to a NE plunge in the northern part of the dome (Figs. IV-4 & 5).

*Savalen Area*: The deformation sequence in the Savalen area is similar to the Einunnfjellet dome area, but $D_{2b}$ structures are most prominent. Intrafolial $F_{2a}$ isoclinal folds have steeply dipping axial surfaces, and generally plunge NNE. The Savalen area is dominated by tight, upright to overturned $F_{2b}$ folds. From field observation, large-scale folds are commonly doubly plunging, producing a lenticular outcrop pattern (Fig. II-1, Plate I). Mesoscopic tight, commonly asymmetric $F_{2b}$ folds occur in layered lithologies, while crenulations are almost ubiquitous in phyllite and slate. Axial surfaces of tight folds generally strike NE, with moderate to steep dips, and axes plunge dominantly SW (Fig. IV-8). $F_{2b}$ crenulations plunge consistently SW (Fig. IV-9a & b), as do mineral lineations (Fig. IV-9c).

Late brittle structures in the Savalen area, collectively grouped as $D_3$, include open upright folds and kink bands. Mesoscopic kink folds with fractured hinges occur as single south-plunging folds or as conjugate sets. The kink folds are especially common in the Nausterdalen



↷ = "z"-shaped (clockwise rotation)

↶ = "s"-shaped (counterclockwise rotation)

Figure IV-6
Lower hemisphere equal area projection of 31 asymmetric fold axes, Einunnfjellet dome area. Sense of asymmetry shown.

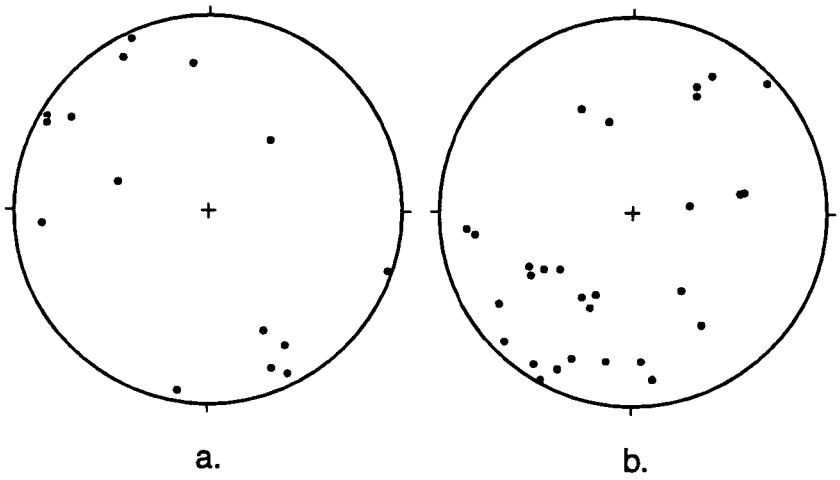



Figure IV-7
Lower hemisphere equal area projection of open folds, Einunnfjellet dome area.
a) Poles to axial surfaces (n = 15. b) fold axes (n = 29).

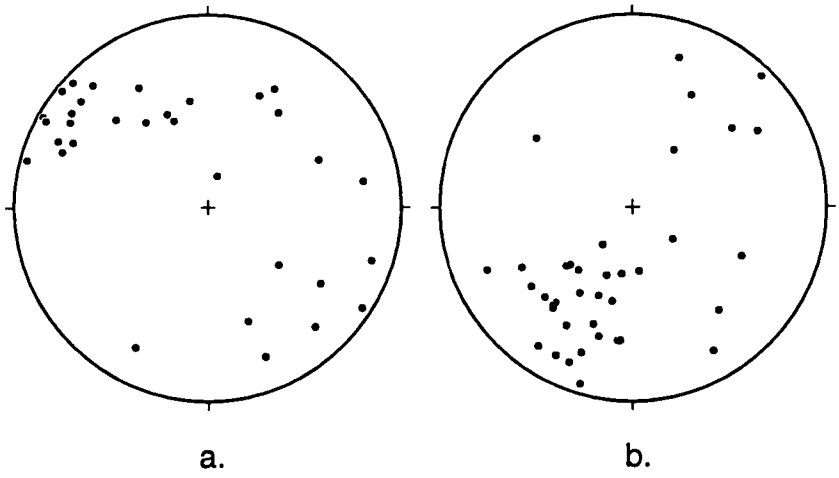



Figure IV-8
Lower hemisphere equal area projection of tight folds, Savalen area.
a) Poles to axial surfaces (n = 32). b) Fold axes (n =40).

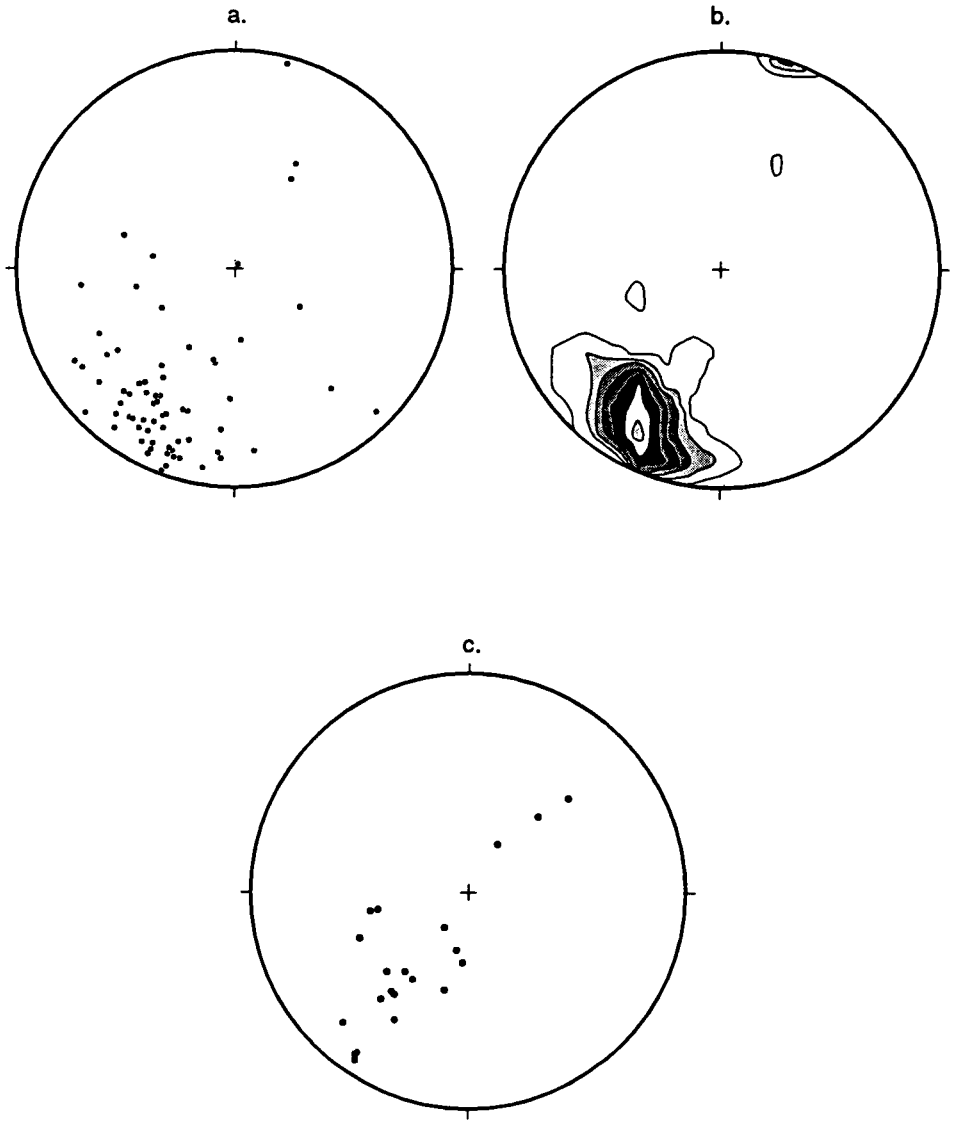



Figure IV-9
Crenulation axes and mineral lineations in the Savalen area: a) Scatter plot, and b) contoured plot of crenulation axes (n = 68); c) mineral lineations (n = 21). C. I. = 2%/% area.

area (Plate I), where they fold the regional foliation into an E-W striking orientation, approximately perpendicular to the consistent NE strike elsewhere in the area.

*Stei-Langsætra Shear Zone*: The eastern contact of phyllite of the STC with bimodal volcanic rocks of the Fundsjø Group (Meråker nappe) is a steep, northwest-dipping $D_{2b}$ ductile shear zone, that is well-exposed near Stei-Langsætra, southeast of lake Savalen (Plate I). The shear zone is characterized by widespread mylonitic textures in quartz keratophyre and greenstone of the Fundsjø Group (described in a later section), and to a lesser degree, in STC phyllite. Boudins of felsic rock in the shear zone footwall (Fundsjø Group) have a consistent top-to-SSW geometry (Fig. IV-10a), although this evidence for shear sense is contradicted by the presence of some tight folds that verge NE, and of ductile faults having an apparent top-to-N sense of movement (Fig. IV-10b).

Because the shear-sense indicators are ambiguous, a separate method of kinematic analysis is necessary to determine movement sense in the zone. Hinge lines of minor folds in a ductile shear zone commonly lie in a plane that is subparallel to the mean mylonitic foliation, and the relationship between these two planes can be used to determine the sense of shear (Mies, 1991). For this method it is assumed that: 1) during progressive simple shear, axes of contemporary folds rotate variably toward the extension direction (e.g., Carreras *et al.*, 1977); and 2) the mylonitic foliation is either the flattening plane of finite strain (Ramsay and Graham, 1970), or a shear-plane foliation (Berthé *et al.*, 1979), in either case containing the intermediate strain axis. The sense of shear can be determined from the incomplete rotation of the hinge-line girdles toward the mean mylonitic foliation, which generally leaves a small separation angle (4–9°) between the two planes (Mies, 1991). In the Savalen area, mylonitic foliations in the shear zone are steeply dipping, generally to the northwest. For kinematic analysis, mylonitic foliations and contemporary $F_{2b}$ folds were utilized from STC rocks in the hanging wall of the shear zone and from Fundsjø Group rocks in the footwall. The mean mylonitic foliation was determined by the Fisher vector distribution method, and the best-fit plane to fold hinges by the Bingham axial distribution method, both in the "Stereonet 4.3" program of Allmendinger (1991). In the hanging wall, the best-fit plane is incompletely rotated toward the mylonitic foliation in a top-to-NE sense (Fig. IV-11a), whereas the footwall exhibits top-to-SW sense (Fig. IV-11b), both indicating clockwise (dextral) rotation in the shear zone. The separation angle between the hinge-line girdle and mylonitic foliation is much smaller in the footwall rocks (8°) than in the STC rocks (30°). The smaller angle probably indicates higher shear strain (Mies, 1991), in this case in the footwall rocks.

a.



b.



Figure IV-10
Outcrop photos of Stei-Langsætra shear zone. a) Outcrop photo of mylonite in ductile shear zone, showing boudins having top-to-SW sense of asymmetry (UTM 791961). b) Outcrop photo of small ductile fault with top-to-N sense of movement, from same outcrop.

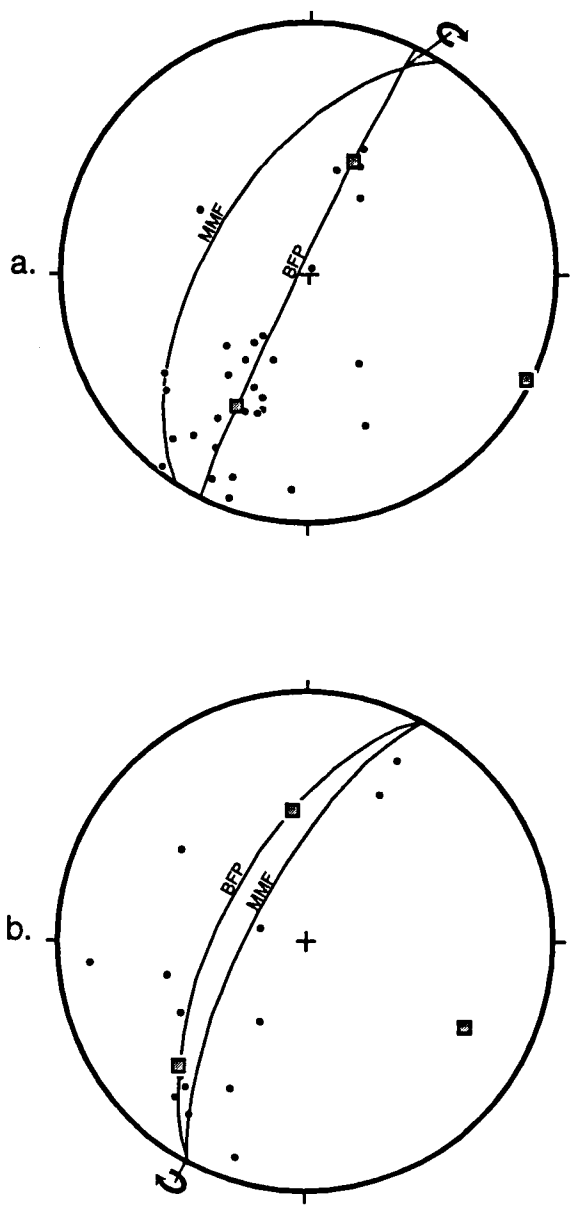



Figure IV-11
Kinematic analysis of sense of movement in shear zone (Mies, 1991). a) Relationship of mean mylonitic foliation plane (MMF) to best-fit plane to fold hinges (BFP) in shear zone hangingwall indicates top-to-NE, clockwise rotation. Angle between planes = 30°. b) Same relationships in footwall indicate top-to-SW, clockwise rotation. Angle between planes = 8°. Dots: fold hinges; box: β-axis to BFP. MMF is mean of a) 66 measurements; and b) 54 measurements.

The amount of displacement between rocks of the STC and the Fundsjø Group produced by the shear zone is unknown, but several lines of evidence suggest that the displacement is not major. Unconformable conglomerate and slaty phyllite horizons that stratigraphically overlie the Fundsjø Group (Plate I) are similar to the upper Savalen sequence, and indicate that rocks of the STC and the Fundsjø Group may have experienced comparable pre-Scandian histories. In addition, rocks correlative with the parts of the STC (Gudå Formation) are in apparent stratigraphic continuity with the Fundsjø Group in the Færen (Wolff, 1967) and Inndalen (Lagerblad, 1984a) areas (Fig. I-2). Finally, in Chapter III, I discussed the geochemical similarity between STC metavolcanic rocks and certain variants of the Fundsjø Group in the Røros area (Grenne, 1988), and surmised that the rocks either formed in similar tectonic environments, or are tectonically disrupted elements of a related sequence.

*Mesoscopic Foliations*

Lower hemisphere projection of poles to the dominant foliation in the Einunnfjellet dome area (Fig. IV-12a) indicates a variety of attitudes around the dome, but with maxima having both NW and SE dips. The poles lie on a great circle yielding a β-axis of 15°, S29W. The distribution of poles along the great circle suggests later subcylindrical folding of the foliation in which the SE limb is dominant. In contrast, a steep NE-striking regional foliation (Figs. IV-1 & IV-12b) is pervasive in the Savalen area. Poles to foliation also lie on a great circle, but the distribution indicates that the folds are limb-dominated. The β-axis to the great circle (16°, S31W) is, however, approximately parallel to that in the Einunnfjellet dome area.

In many outcrops throughout the Einunnfjellet-Savalen area, only one foliation is distinguishable. Compositional layering, which may represent bedding ($S_0$) in rocks such as laminated phyllite or alternating quartzite and schist, is generally transposed into the regional foliation. Locally, however, $S_0$ is preserved in the hinges of mesoscopic folds and crosscut at a high angle by the regional foliation. This relationship is most commonly observed in the southern part of the area, in the vicinity of Volengsvola (Plate I), indicating that this area represents a macroscopic fold hinge. On a lower hemisphere projection (Fig. IV-13), poles to $S_0$ have a planar distribution yielding a β-axis plunging 7°, N51E, possibly marking the orientation of early folds. In the same outcrops, the cross-cutting foliation strikes consistently N20E to N40E, and dips steeply.

Elsewhere in the Einunnfjellet-Savalen area, it is sometimes possible to differentiate the dominant schistosity that transposed compositional layering ($S_{2a}$) from a spaced crenulation cleavage ($S_{2b}$) in the same outcrop. Around the Einunnfjellet dome, poles to the crenulation

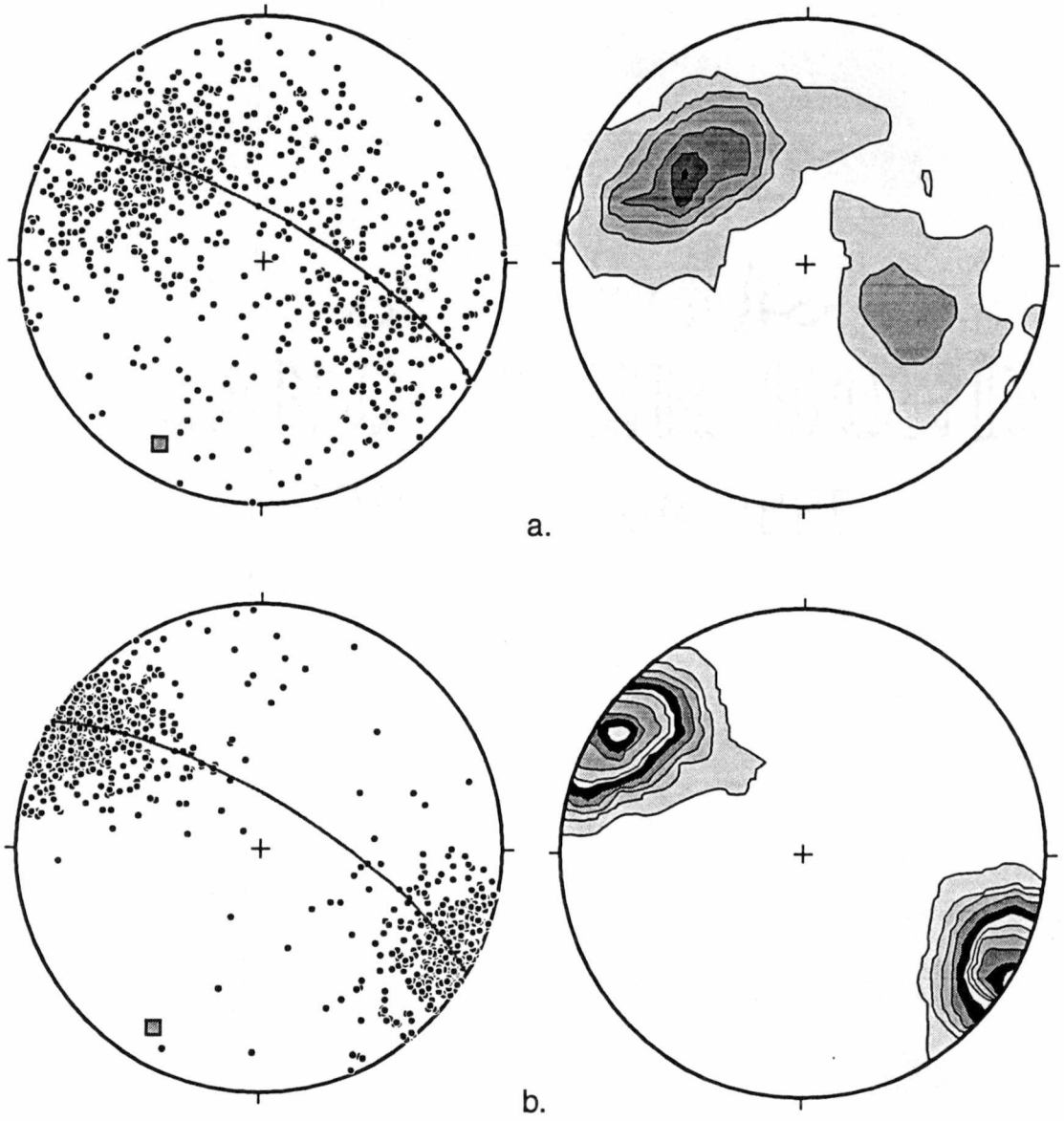



Figure IV-12
Dominant foliations. a) Scatter plot (left) and contoured plot (right) of poles to dominant foliation, Eininnfjellet dome area (n = 825). Best-fit plane to poles yields a β-axis of 15°, S29W. b) Scatter plot (left) and contoured plot (right) of poles to dominant foliation, Savalen area (n = 888). Best-fit plane to poles yields a β-axis of 16°, S31W. C. I. = 1%/% area.

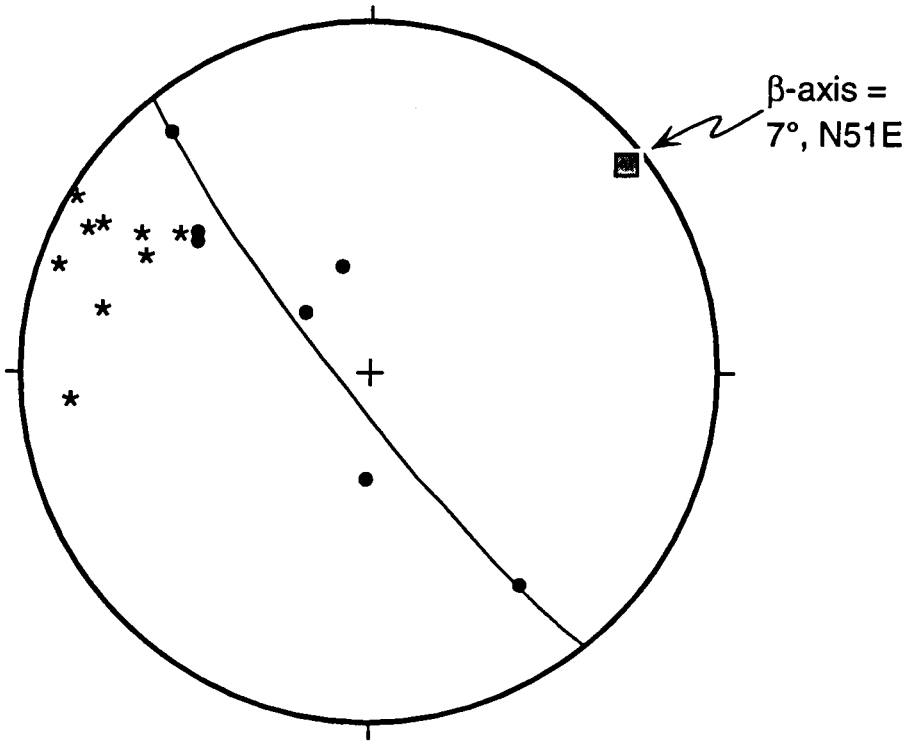



Figure IV-13
Poles to compositional layering, or bedding (?), compared to dominant schistosity in same outcrops. Compositional layering–dots, schistosity–stars. Best-fit plane to compositional layering yields a β-axis of 7°, N51E.

cleavage have a planar distribution with similar orientation to $S_{2a}$ (Fig. IV-14a & b). Poles to both surfaces lie in a plane yielding a β-axis plunging approximately 20°, S50W, and indicating cylindrical folding of both surfaces, similar to the overall regional foliation (Fig. IV-12a). In the Savalen area, however, $S_{2a}$ appears to rotate toward a more northerly strike, and the $S_{2b}$ cleavage strikes consistently due north, dipping steeply to the west, or less commonly, to the east (Fig. IV-14c & d). In proximity of the Stei-Langsætra shear zone, the foliations merge into a composite, strongly oriented mylonitic foliation, suggesting that as the shear zone is approached, $S_{2b}$ becomes more dominant, and the earlier foliation is rotated toward the shear direction. Rotation of foliation can occur during progressive shearing deformation through a continuous process of transposition by developing meso- and microscale folds, accompanied by dynamic recrystallization (Mawer and Williams, 1991). This process is likely to account for the relationships described above and in Figure IV-14, since, as noted in an earlier section, F2b folds and crenulations are pervasive in the Savalen area. The associated microscopic foliations and structures are discussed in the following section.

## *Microscopic Structures*

$D_1$ structures are rarely observed on the microscopic scale, although some quartz-rich layers in STC phyllites contain a bedding-parallel foliation consisting of fine-grained muscovite and chlorite that is folded around $F_2$ fold hinges. This uncommon foliation may represent recrystallization associated with $D_1$ deformation, or alternatively, a very early stage of Scandian deformation.

On the basis of overprinting relationships, particularly on the microstructural scale, the Scandian ($D_2$) event appears to be a progressive deformation in the sense of Tobisch and Paterson (1988) and can be divided into two principal phases. A flattening phase, $D_{2a}$, produced tight to isoclinal folds with an axial planar foliation, accompanied by recrystallization of the assemblage chlorite + muscovite + biotite ± graphite ± garnet. $D_{2b}$ was overprinted by a second pervasive phase that involved a strong component of simple shear, demonstrated by the asymmetry of folds, crenulations, and individual mineral grains, rotation of opaque porphyroblasts and development of pressure shadows (Fig. IV-15a), and synkinematic growth and rotation of garnet. Asymmetric crenulations (Fig. IV-15b) commonly have a strong differentiated crenulation cleavage ($S_{2b}$) resulting from recrystallization in short limbs of the folds. Where crenulations are fairly open, the cleavage is oblique to, and easily distinguished from, $S_{2a}$. With further flattening and tightening of the crenulations, especially in the vicinity of the Stei-Langsætra shear zone, the foliations are subparallel and form a composite foliation

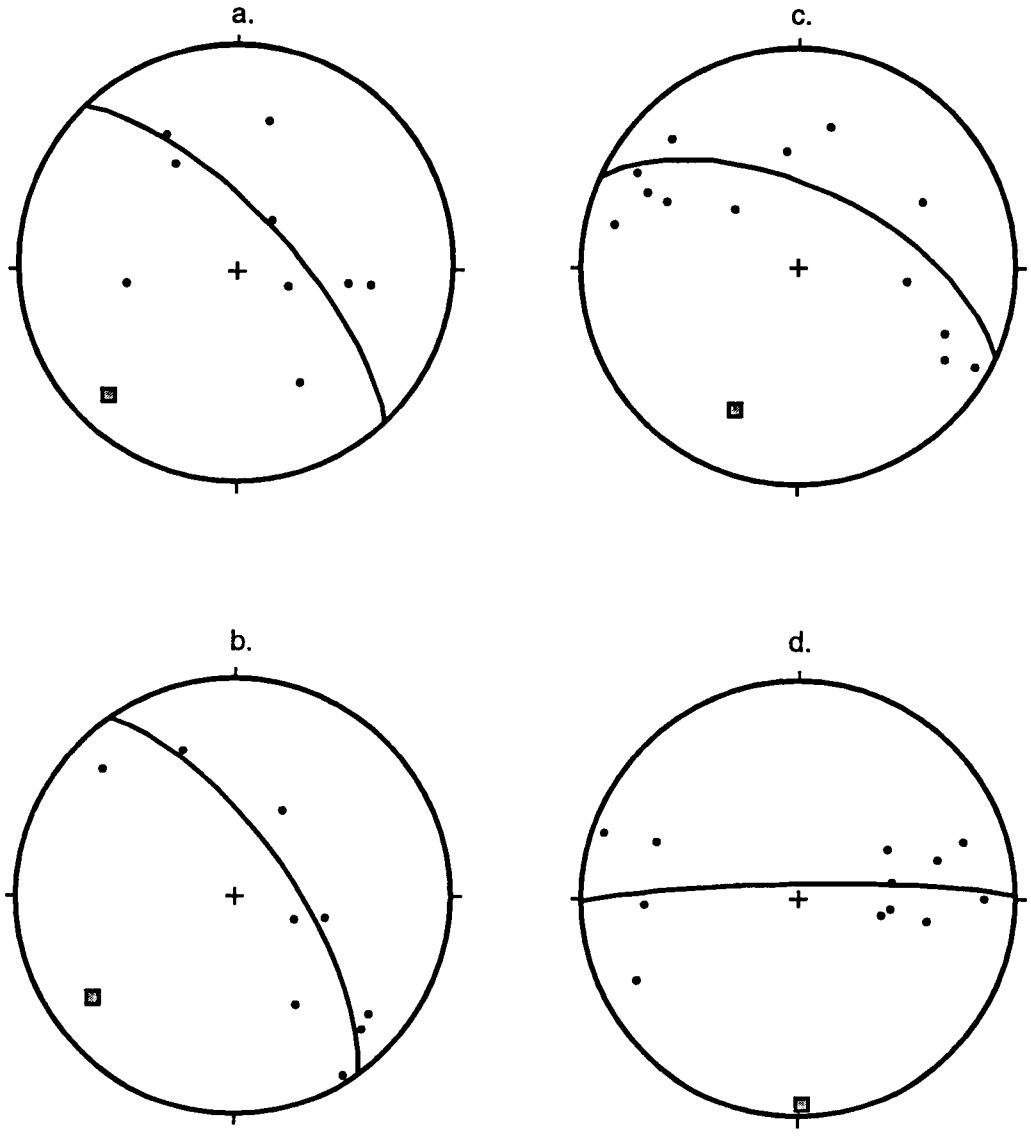
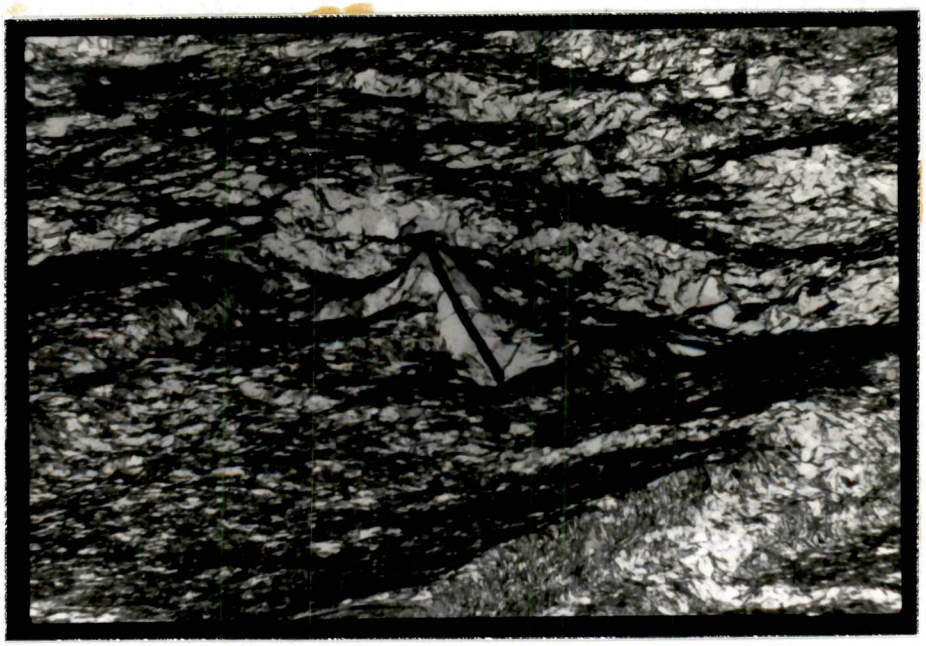



Figure IV-14
Dominant schsistosity vs. crenulation cleavage. a) Poles to dominant schistosity; and b) poles to crenulation cleavage in same outcrops, Einunnfjellet dome area (n=9). c) Poles to dominant schistosity; and d) poles to crenulation cleavage in same outcrops, Savalen area (n=12). Great circles are best-fit planes to poles, and boxes represent b-axes to planes.

a.



b.

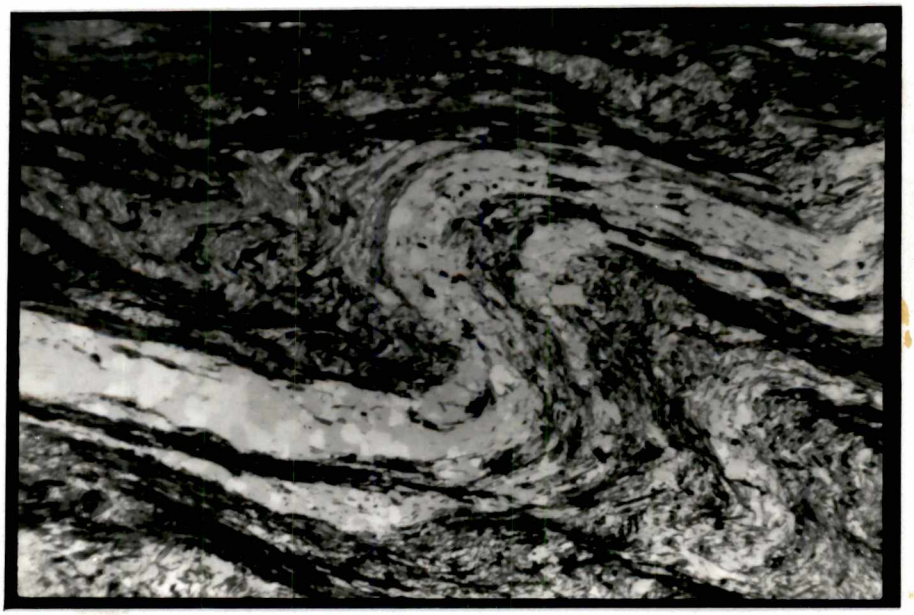


Figure IV-15
Photomicrographs of features of $D_{2b}$ deformation. a) Rotated opaque porphyroblast in crenulated schist. Long dimension of photograph 2.8 mm. b) Asymmetric crenulations and associated crenulation cleavage ($S_{2b}$) overprinting $S_{2a}$ in schist. Long dimension of photograph 10 mm.

(Tobisch and Paterson, 1988) (Fig. IV-16), a relationship similar to that described by Williams and Zwart (1977) from the Seve nappe in Sweden.

Microstructural fabrics related to the Stei-Langsætra ductile shear zone are most spectacular in the felsic rocks, and grade from a mortar texture of fine-grained recrystallized material along grain boundaries and internal deformation zones in plagioclase porphyroclasts (Fig. IV-17a), indicating the initial stages of dynamic recrystallization of the feldspar grains (Tullis and Yund, 1985), to a strongly oriented mylonitic foliation consisting of quartz ribbons in a fine-grained, partly to mostly recrystallized quartzofeldspathic groundmass (Fig. IV-17b). The mylonitic foliation anastomoses around asymmetric feldspar porphyroclasts, some of which display strained twins and recrystallization around the edge of the grains. Polycrystalline wing-like appendages attached to the porphyroclasts typically show a subtle stair-step geometry, as defined by Hanmer and Passchier (1991). Using the criteria of Simpson (1985), the extent of recovery and recrystallization in the quartz-rich matrix, and the presence of kinked twins and some recrystallization in plagioclase, suggest that deformation took place at middle to upper greenschist facies conditions.

$D_3$ microscopic structures are generally confined to quartz-rich rocks in or near the core of Einunnfjellet dome, and are characterized by undulose extinction and deformation lamellae in quartz grains. Where late kink folds occur, the hinges are commonly fractured and infilled by quartz. More rarely, pervasive fractures and veins that offset mineral grains occur at a high angle to the foliation.

## *Garnet Zoning*

### *Textural Zoning*

Inclusions in porphyroblastic metamorphic minerals provide valuable clues to the crystallization history, and in many cases, to the relationship of metamorphism and deformation. Preserved inclusions and inclusion trails traditionally have been utilized as indicators of mineral phases and fabrics that have since been obliterated or modified in the matrix of the rock. Textural zoning of garnets in pelitic rocks from the Einunnfjellet-Savalen area indicates that crystallization of garnet occurred both synkinematically and interkinematically, reflecting changing stress regimes during mineral growth. As many as three distinct zones can be defined by the presence or absence of inclusions, and orientation of inclusion trails ($S_i$) relative to the external foliation ($S_e$). The most common included phase is

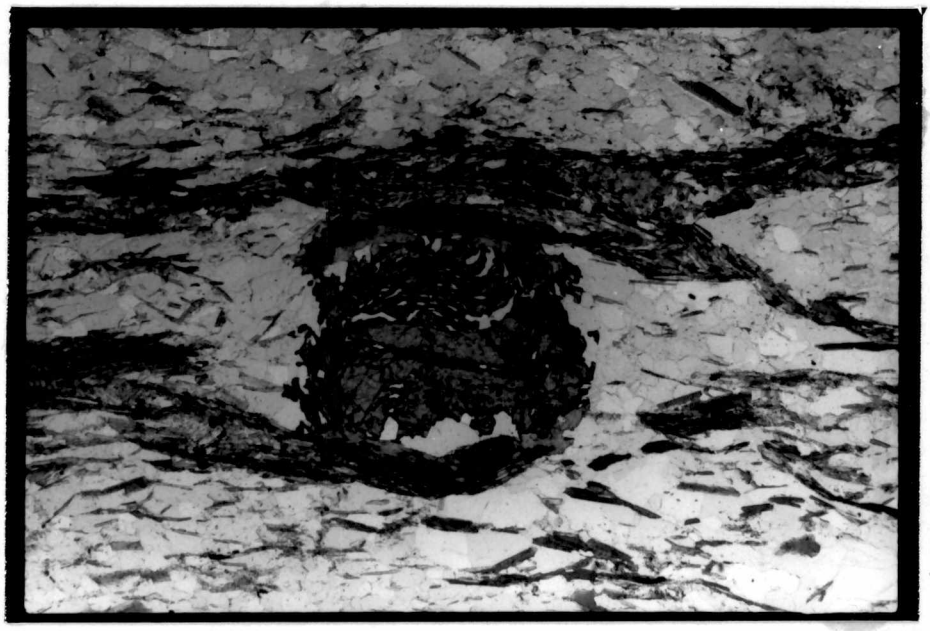
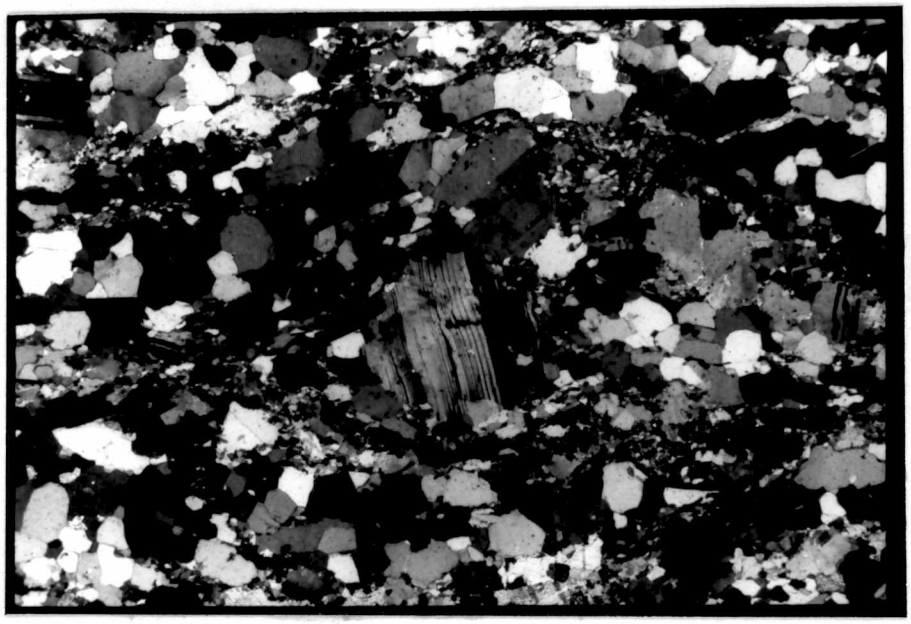


Figure IV-16
Photomicrograph of composite foliation. Tight crenulations, $F_{2b}$, with associated cleavage, fold $S_{2a}$ (above garnet) but are coplanar with it. Garnet is interpreted as having synkinematic rims that overgrew crenulations at an early, more open stage (see text for discussion). Long dimension of photograph 4.5 mm.

a.



b.

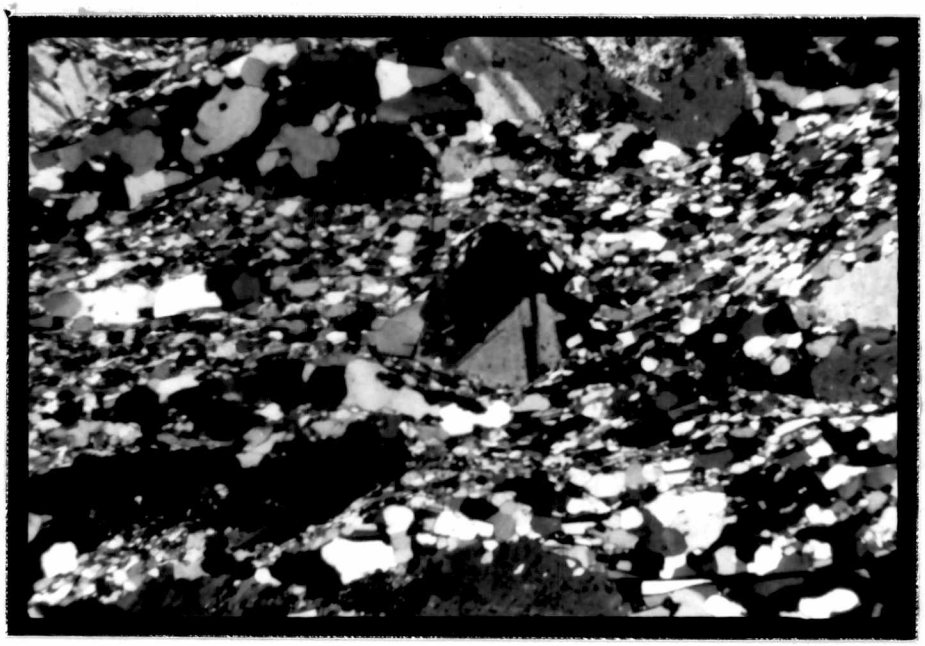


Figure IV-17
Photomicrographs of mylonitic foliation. a) Deformed feldspar porphyroclast, in mylonitic matrix having mortar texture. Long dimension of photograph 2.8 mm. b) Strongly oriented mylonitic foliation. Feldspar porphyroclast has quartzofeldspathic "wings" with stair-step geometry. Long dimension of photograph 2.8 mm.

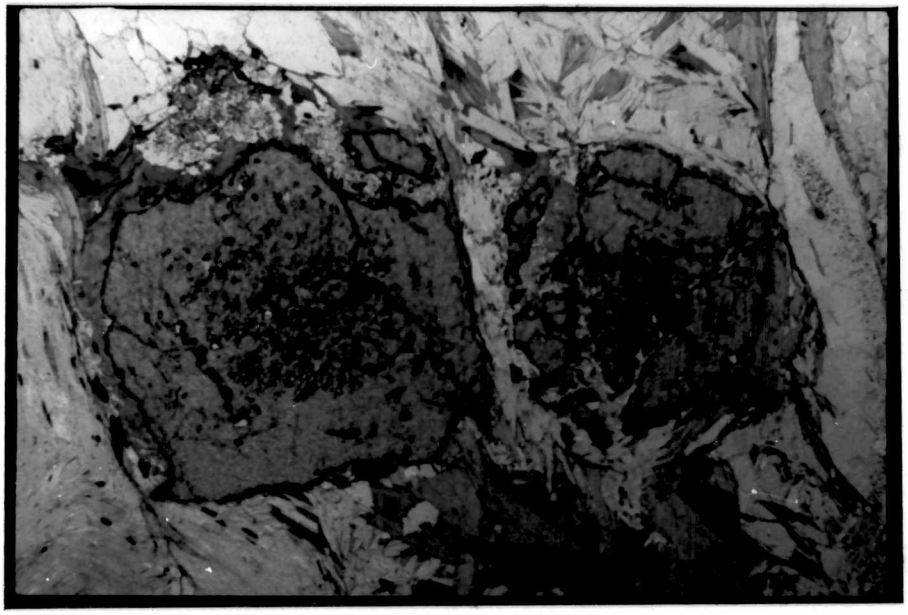
quartz, although opaque minerals (ilmenite, graphite), epidote, plagioclase, and micas also occur.

Garnet cores representing the earliest stage of garnet growth are interpreted to have formed during the $D_{2a}$ deformation phase. Distinct cores are not present in all samples, nor are the inclusion patterns identical in all rocks that contain them. Near the garnet isograd, cores of garnets in STC rocks typically contain very fine-grained, quartz-rich inclusions that are randomly oriented relative to $S_e$. In correlative rocks farther to the west from the isograd, $S_i$ is more strongly oriented and makes a high angle with $S_e$ (Fig. IV-18a). Generally, only clear, inclusion-free garnet cores are present in schists from the Hummellfjell Formation. Formation of anhedral poikiloblasts containing numerous inclusions is considered to reflect rapid growth and relative instability, compared to slower growth of euhedral, inclusion-free grains (Barker, 1990). Thus, the variation in core fabrics could be a function of: 1) structural position within the deforming nappe pile, suggesting slower and more consistent heating for longer periods of time may occur for those rocks at depth, leading to formation of inclusion-free grains; 2) higher Mn- and Ca-content, which stabilizes garnet at lower temperature, possibly leading to more rapid growth in poikiloblastic grains (Crawford, 1977); or 3) some combination of the two factors above.

The second stage of garnet growth took place syn- to late-kinematically with respect to $D_{2b}$ deformation, and garnets of this type occur with remarkable consistency in all units. This stage is characterized by fairly coarse-grained inclusions, a rotational fabric of $S_i$ relative to $S_e$, and development of pressure shadows adjacent to garnet grains. The rotational fabric typically consists of curved or sigmoidal inclusion trails that may be oblique to (Fig. IV-16) or continuous with (Fig. IV-18b) the crenulated matrix, or more rarely have the classic spiral or "snowball" texture (Fig. IV-19a). Garnets in which the inclusions are of the same composition but somewhat finer-grained than mineral grains in the matrix, and $S_i$ is at a high angle to $S_e$ (Fig. IV-19b), are interpreted to have grown early during the crenulation phase, and rotated up to 90° relative to the matrix during subsequent deformation. Others appear to have overgrown open crenulations in the foliation and preserved them while the matrix was flattened and transposed into the composite regional foliation (Fig. IV-16). Porphyroblasts in which the sigmoidal inclusion trails are completely continuous with $S_e$ ( Fig. IV-18b) could be interpreted as post-kinematic overgrowth of preexisting crenulations that are present throughout the matrix; the deflection of the matrix around the porphyroblast and the presence of asymmetric pressure shadows adjacent to the grains, however, suggests growth during shear deformation.

Clear, inclusion-free rims are common, although not ubiquitous, in garnets throughout the Einunnfjellet-Savalen area. These typically occur as either thin, continuous rims around

a.



b.

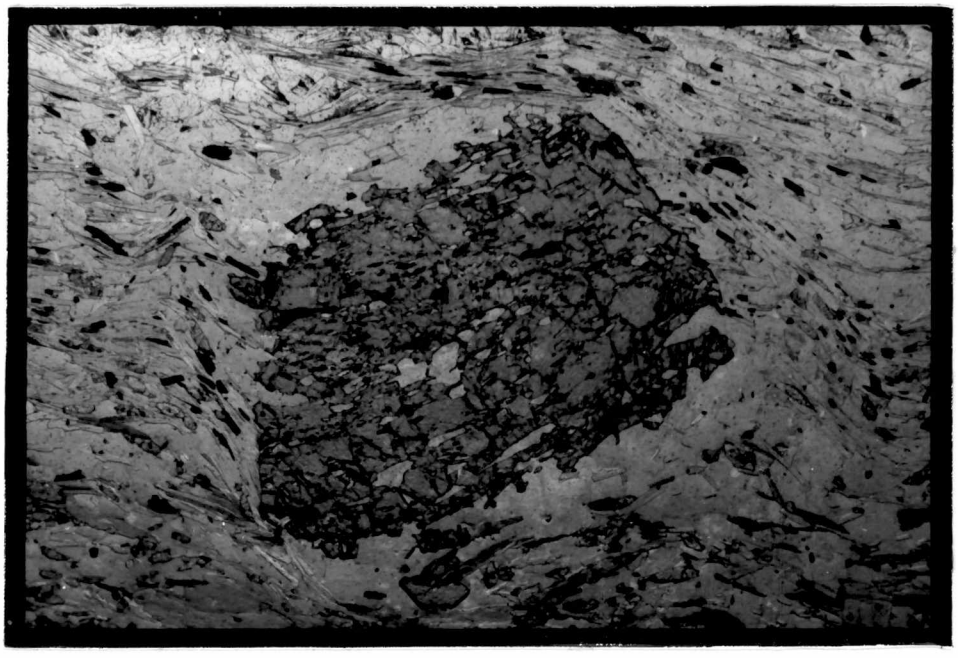
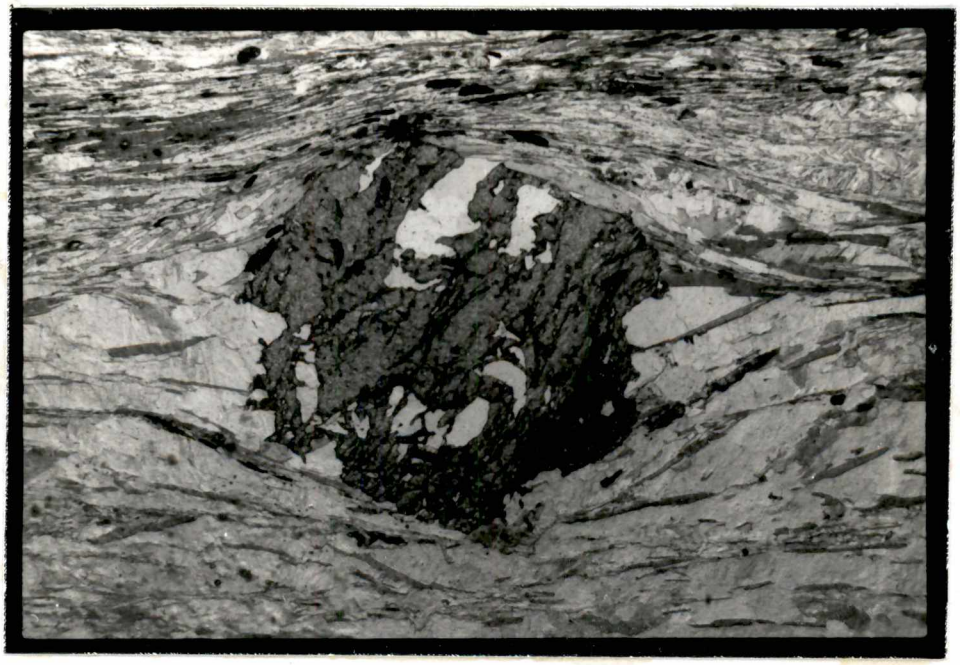


Figure IV-18
Photomicrographs of garnets with inclusions. a) Garnet with fine-grained inclusions in core. Long dimension of photograph 4.5 mm. b) Garnet with inclusion trails; $S_i$ is continuous with $S_e$. Long dimension of photograph 4.5 mm.

a.



b.

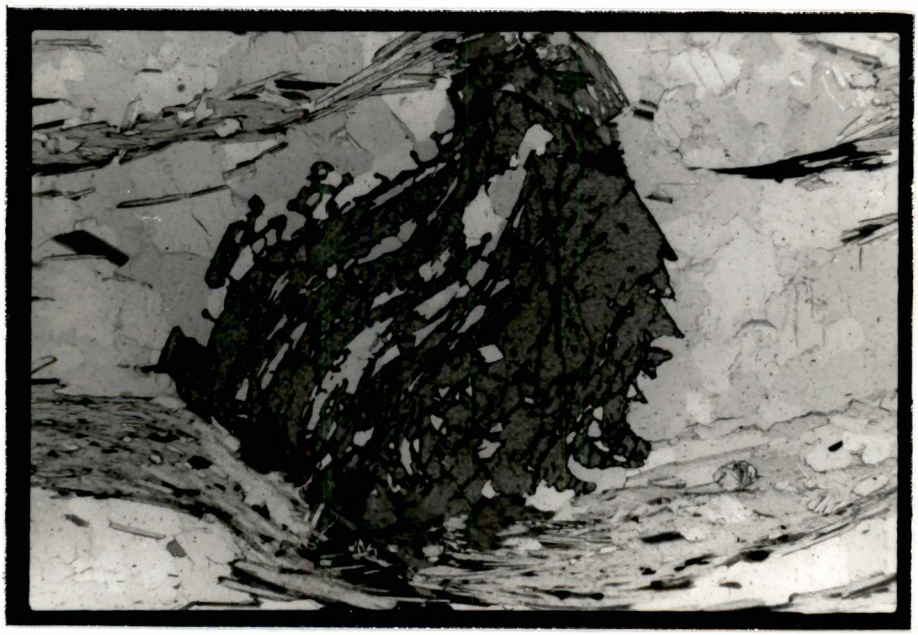


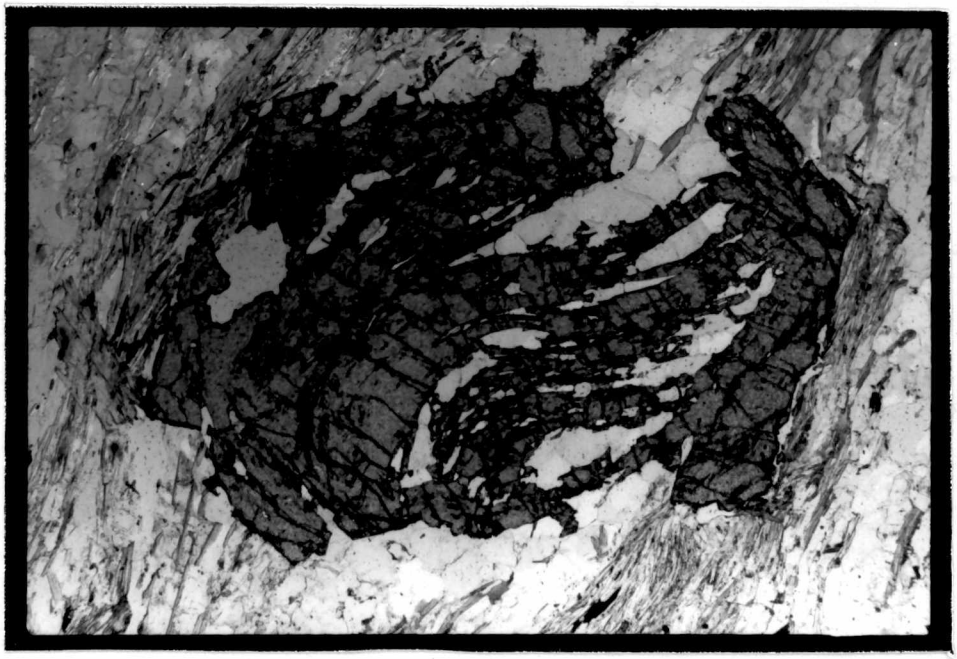
Figure IV-19
Photomicrographs of garnets with inclusion trails, various orientations. a) "Snowball" garnet with spiral inclusion trails. Long dimension of photograph 4.5 mm. b) Garnet with $S_i$ nearly perpendicular to $S_e$. Rim of garnet curves into $S_e$ on lower right side. Long dimension of photograph 4.5 mm.

garnets displaying one or both of the stages discussed above, or as discontinuous rims on cores having a rotational fabric (Fig. IV-20a). In the latter case, rims developed adjacent to mica-rich regions in the foliation. Because of the lack of inclusions, it is unclear if these rims are late- or post-kinematic to $D_{2b}$. A third type of rim texture in which the garnet completely overgrew the $F_{2b}$ crenulations (Fig. IV-20b) appears to have grown statically after $D_{2b}$, indicating temperatures remained elevated for some time after deformation ceased.

*The Rotation Controversy*: Sigmoidal and spiral inclusion fabrics in porphyroblasts, and particularly in garnet, have traditionally been interpreted to indicate synkinematic rotation of the rigid porphyroblast during growth (e.g., Spry, 1963; Rosenfeld, 1968, 1970; Schoneveld, 1977; Powell and Vernon, 1979; Meneilly and Storey, 1986). During the past decade, however, an alternative opinion was offered by Bell and Rubenach (1983), and developed in numerous subsequent publications by Bell and various co-workers (e.g., Bell, 1985; Bell *et al.*, 1986; Bell and Johnson, 1989; Bell and Hayward, 1991; Bell *et al.*, 1992a, 1992b). To summarize their model, they proposed that porphyroblasts do not rotate relative to geographic coordinates, and that the inclusion trails result from incremental porphyroblast growth during multiple cycles of uplift and collapse (Bell and Johnson, 1989). In this scenario, horizontal shortening associated with formation of a steeply dipping foliation is followed by gravitational spreading with associated flat-lying foliation. The porphyroblasts grow discontinuously, preserving the near-orthogonal foliations, and what appear to be smooth, curving trails are actually truncated by horizontal and vertical surfaces. The uplift-collapse cycle must be repeated many times to form a truly spiral-shaped inclusion trail; four repetitions of the cycle would be required for an apparent rotation of 270°, and many more for garnets that have "rotated" as much as 800°, as observed by Schoneveld (1977). This interpretation has been challenged by others (Passchier et al., 1992; Lister, 1993), who note that many of the relationships seen by Bell and co-workers can easily be explained by more conventional ideas. Although both uplift and collapse may be important elements of orogenesis, numerous cycles of orthogonal deformation phases are not necessarily required; indeed, there is a general lack of evidence that these cycles existed outside of the porphyroblasts (Lister, 1993). Consequently, while Bell and coworkers have done a service by cautioning that not all oblique or sigmoidal inclusion trails signify porphyroblast rotation (for example, in post-kinematic garnets that overgrew a folded foliation) (Hanmer and Passchier, 1991; Passchier et al., 1992), their model of orogenesis remains an "alternative hypothesis" in the minds of many geologists at this time.

In relation to this study, close inspection of inclusion trails in garnets from the study areashows that the trails are generally smoothly curving, with no evidence for orthogonal

a.



b.

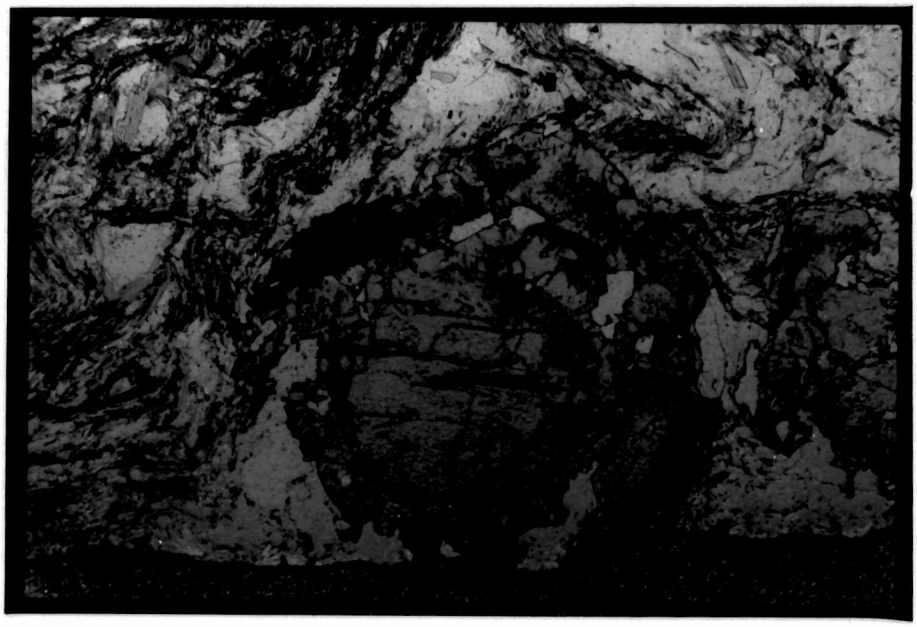


Figure IV-20
Photomicrographs of rimmed garnets. a) Garnet with clear rims. Long dimension of photograph 4.5 mm. b) Garnet with late- or postkinematic rim that includes folded foliation ($F_{1b}$ crenulations). Long dimension of photograph 10 mm.

truncation surfaces as would be expected in the Bell model. On the larger scale, synmetamorphic deformation (D2) in the area is interpreted as a continuous deformation in which earlier flattening foliations are rotated by subsequent shearing. Where more than one foliation exists in an outcrop, the surfaces are rarely, if ever, orthogonal to each other (Fig. IV-14). Perhaps the strongest evidence for porphyroblast rotation in these rocks is from the crenulated schist shown in Figure IV-15a. In this sample, where elongate opaque grains are oblique to the $S_{2b}$ crenulation cleavage, the terminal edges of the crystals curve smoothly into the cleavage. This type of relationship is difficult to explain as resulting from discontinuous growth during near-othogonal deformation events.

*Compositional Zoning*

Garnets in pelitic schists from across the Einunnfjellet-Savalen area (Fig. IV-21) were analyzed for compositional variation, and representative profiles are shown in Figure IV-22. Analytical techniques and complete electron microprobe analyses of garnet, as well as amphibole, plagioclase, micas, and epidote, are given in Appendix 1. The garnets typically display moderate to strong compositional zonation, characterized by systematic decrease in Mn from cores to rims, coupled with an inverse rise in Fe. Mg generally is slightly enriched toward the rims, whereas Ca varies from sample to sample. Several samples (A1435, A933, A1337) show a slight "reverse zoning" at or near the rim, in which a decrease in Fe is coupled with an increase in Mn and/or Ca. Compositional variation appears to be independent of pre- and syn-$D_{2b}$ textural zonation, but the post-kinematic rims, particularly evident in samples A1718 and A933 (Fig. IV-20b), coincide with a significant increase in Fe. In these samples, the rims overgrew a narrow area of reverse zoning (Fig. IV-22).

One anomalous sample (A2061, Fig. IV-18b) from on the SE flank of Einunnfjellet dome (Fig. IV-21), a calcareous pelitic schist, contains the assemblage quartz + muscovite + biotite + epidote + garnet + chlorite + albite + ilmenite. Some epidote grains surround allanite cores. Garnet in this sample contains numerous inclusions of quartz, epidote, and ilmenite, particularly in the cores. Because of the abundant inclusions, analyses in the cores of the grains were difficult to obtain. From midway to the rim, however, garnet composition is very symmetric (Fig. IV-22). Mg and Ca patterns are similar to those above, relatively flat with a decrease in Ca and increase in Mg at the rim. Garnet is very spessartine-rich, however, having up to 19% MnO , and displays strong reverse zoning of Fe and Mn at the rim, as illustrated in the ternary Fe-Mg-Mn diagram (Fig. IV-23).

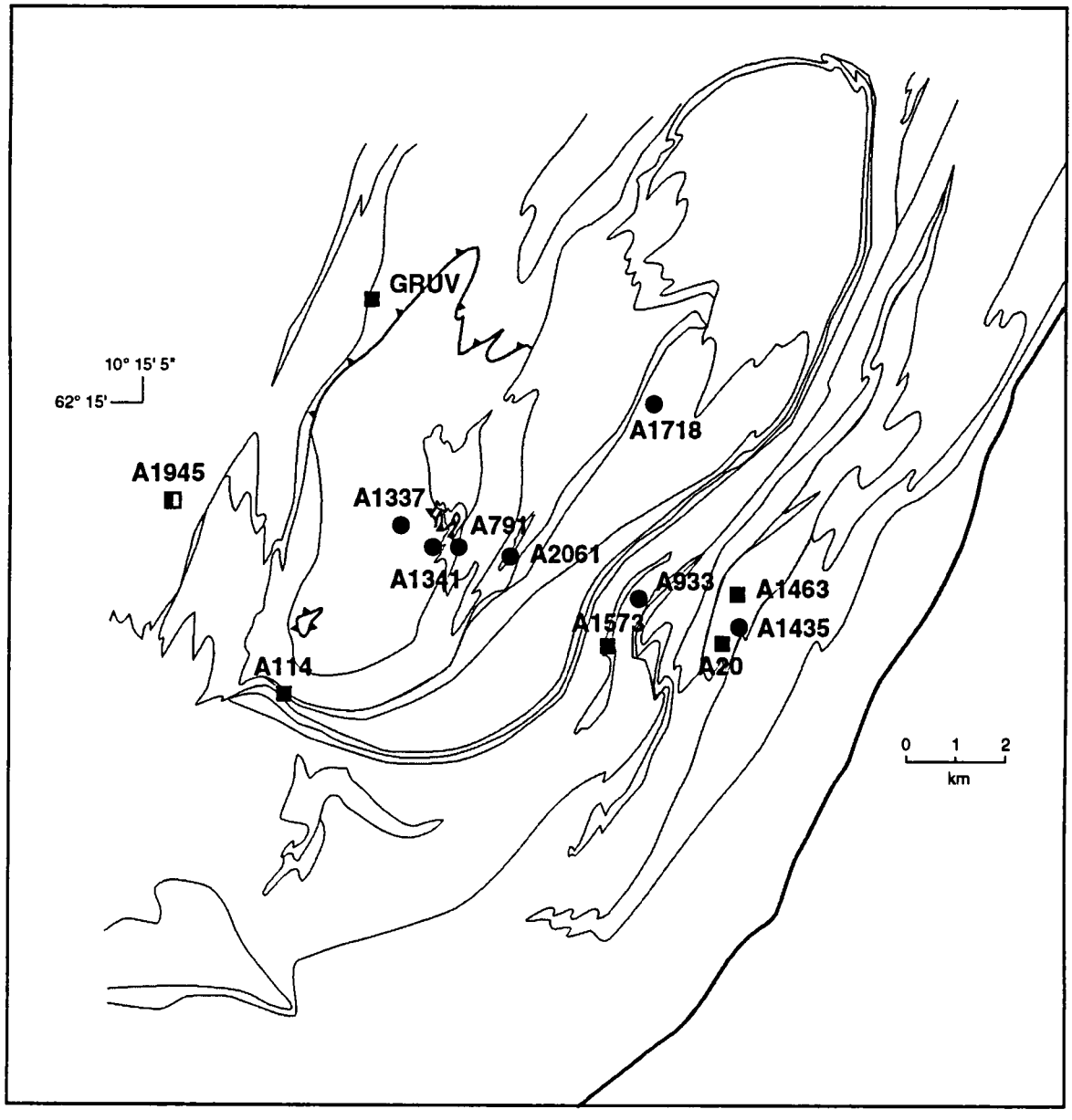



Figure IV-21
Sample location map. Garnet-mica schists (dots), greenschists or amphibolites (solid squares), and amphibole-bearing garnet schist (two-toned square).

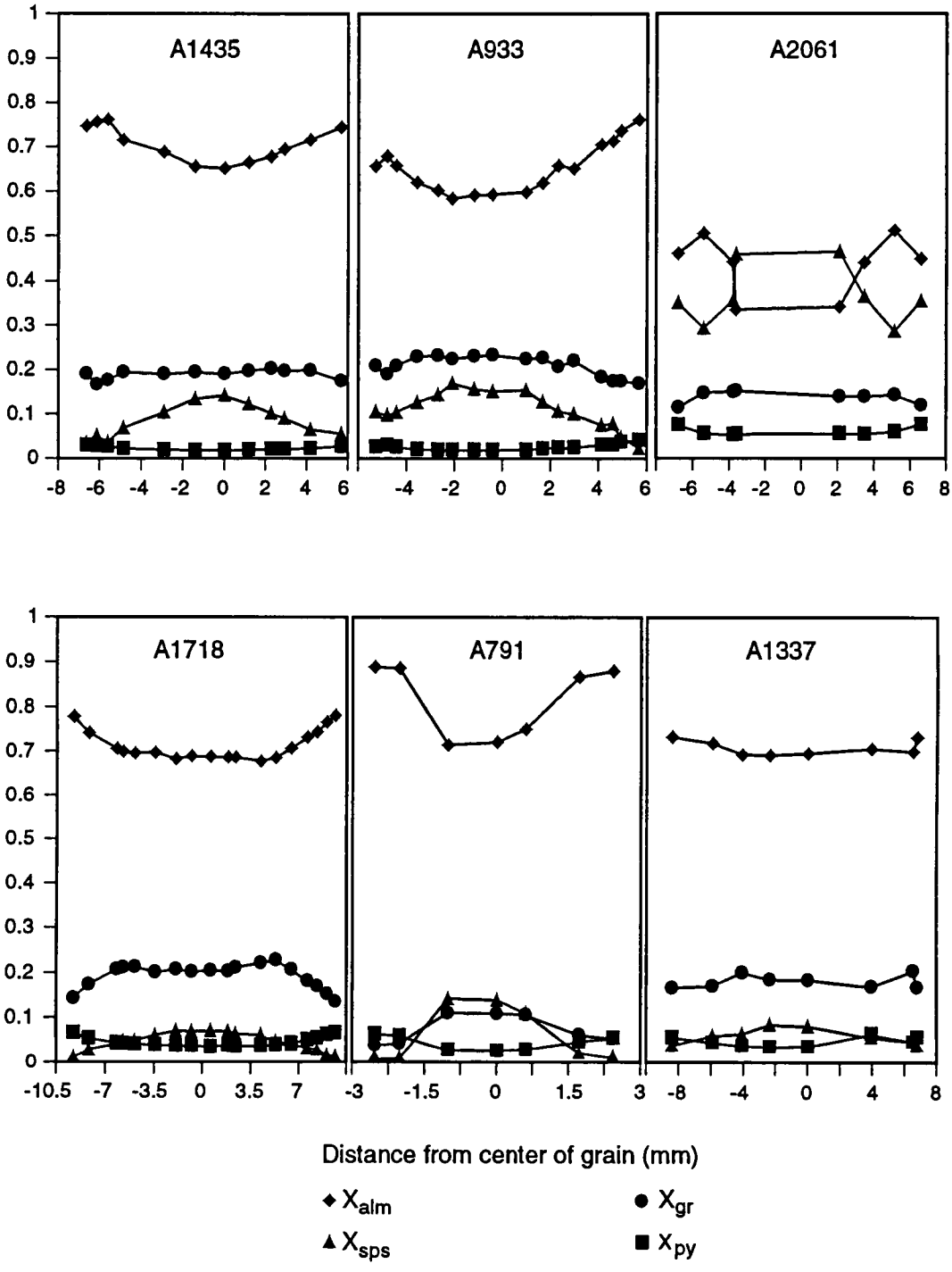



Figure IV-22
Zoning profiles of garnets from the Einunnfjellet-Savalen area. Almandine, spessartine, grossular, and pyrope components shown.

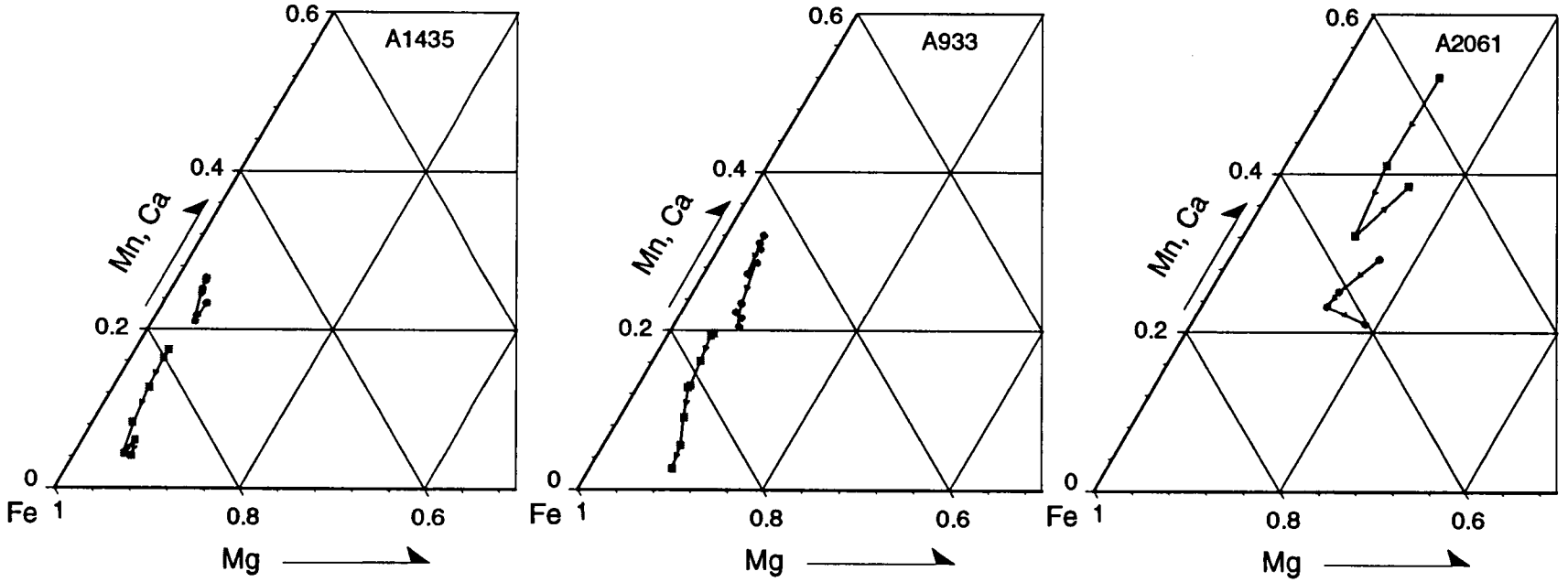



Figure IV-23
Fe-Mg-Mn (squares) and Fe-Mg-Ca (dots) ternary diagrams of garnet composition. Compare with Figure 22 for true distance along garnet.

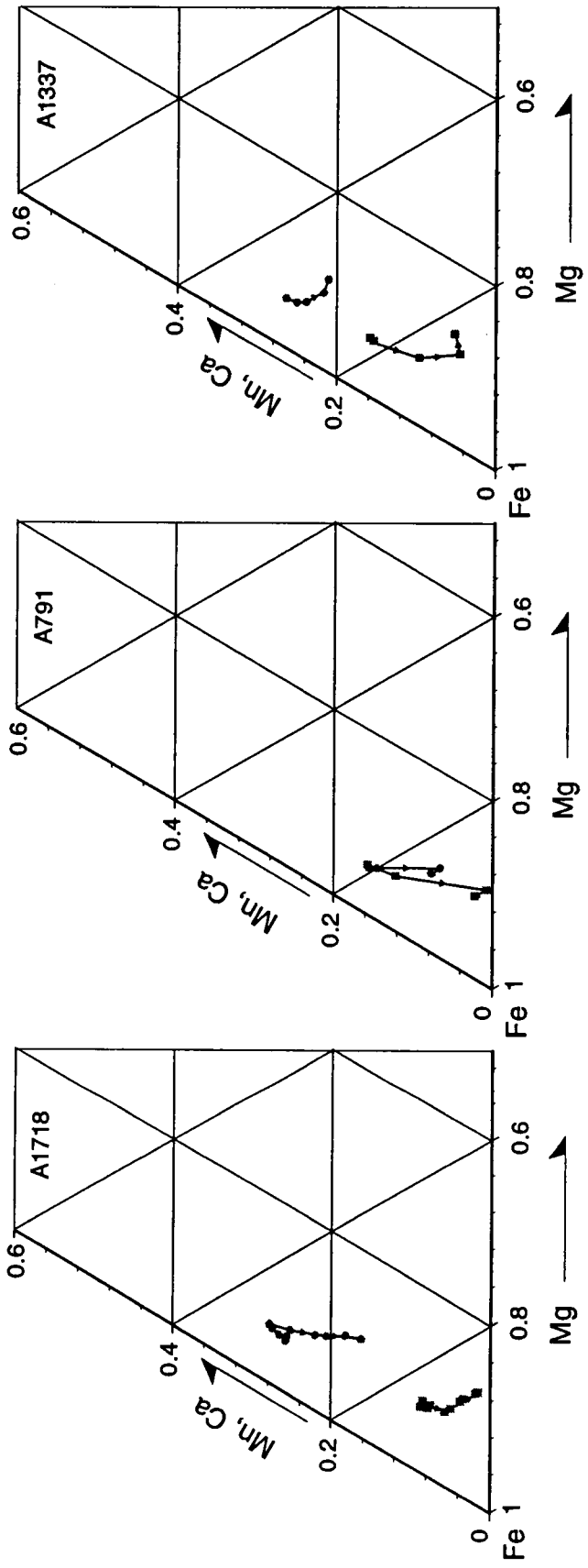



Figure IV-23, continued

Bell-shaped profiles of Mn, coupled with inverse Fe profiles, are typical of progressive growth zoning in garnets from medium-grade metamorphic rocks (Tracy, 1982). Growth zoning occurs as the composition of material available to the growing surface of the crystal changes continuously or discontinuously, generally during a reaction involving the breakdown of chlorite (Kretz, 1973; Miyashiro, 1973b; Winkler, 1979; Barker, 1990). Slow volume diffusion is required such that the core of the grain becomes isolated from the rest of the rock as the grain continues to grow (Tracy, 1982). Garnet will strongly fractionate Mn relative to other minerals, such as biotite and chlorite, and the matrix will become depleted in Mn as it is concentrated in the early garnet nuclei. Subsequent additions to the growing mineral, having less Mn available, will become progressively less enriched in the spessartine component (Chinner, 1965; Harte and Henley, 1966; Tracy, 1982). The core-to-rim decrease in Mn and Ca is evident on the ternary Fe-Mg-Mn and Fe-Mg-Ca diagrams (Fig. IV-23) (Tracy *et al.*, 1976; Tracy, 1982). Most of the samples yield a smooth, continuous path, indicative of garnet growth during a single reaction (Tracy, 1982). By comparison with Figure IV-22, the kinks that occur in some paths (for example, A1435 and A791) are only present at the very edge of the grains, and represent the reverse zoning noted earlier. The slight curvature of some paths toward higher Mg at the rims (i.e., A1337) is consistent with a reaction in which Mg is increasingly available to the garnet growth surface at higher temperature.

Although the behavior of Ca may be generally similar to Mn (Tracy, 1982), the mechanisms that produce zoning of Ca in garnets are independent of those that produce Fe, Mn, or Mg zoning (Crawford, 1977). The presence of calcic phases such as epidote or plagioclase in the rock may produce complex variations in the Ca profile. The Ca profiles for samples of this study are quite variable, although the general trend is toward decreasing Ca toward the rims. The latter relationship may be explained by a continuous reaction with rising temperature, in which plagioclase becomes more calcic and garnet less Ca-rich (Crawford, 1977). This is supported by plagioclase analyses in sample A1337 in which matrix plagioclase is $An_{14-17}$ (Appendix 1E, analyses 3&7), whereas feldspar inclusions in garnet are $An_6$ (Appendix 1E, analyses 1&2).

Various hypotheses have been offered to explain reverse zoning of Mn and Fe at the rim in lower-grade garnets, including: 1) minor retrogression (Woodsworth, 1977), 2) continued chlorite consumption that eventually leads to breakdown of Mn-rich chlorite cores (Kretz, 1973; Tracy, 1982), and 3) diffusion (Anderson and Olimpio, 1977). The latter hypothesis cannot be evaluated here, although diffusion in garnet may not become significant until sillimanite-grade metamorphic conditions have been reached (Tracy, 1982). Breakdown of chlorite cores may have been a factor in producing the reverse zoning in sample A2061, in which the decrease in

Fe and increase in Mn is accompanied by an increase in Mg (Fig. IV-22; IV-23), since chlorite in this sample is significantly more Mg- and Mn-rich than other chlorites throughout the area (Appendix 1F, analysis 11). Retrogression, indicated by late chlorite in the matrix and as partial pseudomorphs after garnet, is evident in some rocks from this area, particularly in graphite-bearing schists such as samples A1718 and A791. These samples, however, contain little or no reverse zoning, whereas the samples that have the strongest reverse zoning (i.e. A1435, A2061) display little or no evidence of retrogression. In addition, as noted above, post-kinematic rims overgrew the area of reverse zoning in some samples, including A1718, indicating that reverse zoning developed prior to the latest garnet growth, and certainly prior to retrograde conditions.

## *Conditions of Metamorphism*

Progressive regional metamorphism is most easily characterized by study of pelitic rocks, in which discontinuous reactions with rising temperature and pressure produce successive metamorphic zones based on the first appearance of particular minerals (e.g., Barrow, 1893). In contrast, metamorphic reactions in mafic rocks are continuous, and mineral phases may coexist over a range of temperature and pressure. Therefore, although mineral equilibria in mafic rocks have been used to characterize the general conditions of metamorphism from some of the earliest studies of metamorphism (Eskola, 1920), the continous variations in mineral composition and abundance with increasing temperature and pressure are still insufficiently correlated with specific P-T conditions. In the following study, the metamorphic conditions in the Einunnfjellet-Savalen area are deduced from both pelitic and mafic rocks, and the results compared.

### *Garnet-biotite Thermometry*

The most reliable and widely used geothermometer for medium-grade pelitic rocks (Essene, 1982) is based on the exchange reaction involving garnet and biotite:

$$KMg_3AlSi_3O_{10}(OH)_2 + Fe_3Al_2Si_3O_{12} = KFe_3AlSi_3O_{10}(OH)_2 + Mg_3Al_2Si_3O_{12}$$

and the distribution coefficient $K_D$:

$$K_D = (Fe/Mg)_{biotite} / (Fe/Mg)_{garnet}.$$

The geothermometer has been calibrated both experimentally (Ferry and Spear, 1978; Perchuk and Lavrent'eva, 1981) and empirically (Thompson, 1976; Goldman and Albee, 1977). Ferry and Spear (1978) incorporated a model of ideal Fe-Mg mixing, and indicated that the geothermometer should be used with caution for natural systems in which significant amounts of Ca or Mn are present in garnet, or Ti and $Al^{VI}$ in biotite. Hodges and Spear (1982) refined the Ferry and Spear calibration, correcting for non-ideal mixing for Ca in garnet, whereas Ganguly and Saxena (1984) incorporated non-ideal mixing terms for Ca, Mn, and Fe-Mg solution in garnet.

Compositions of garnet rims and adjacent biotite grains were analyzed in seven pelitic schists from an east-to-west traverse across the study area (Fig. IV-21). Temperatures were calculated by the Thermobarometry program of Spear and Peacock (1989), and the results, using the calibrations of Ferry and Spear (1978), Hodges and Spear (1982), and Ganguly and Saxena (1984), were compared (Table IV-2). The three calibrations differ in absolute temperature, but all yield similar patterns—a general increase from east to west with temperatures peaking near the core of the dome (samples A1337 and A791), then dropping slightly on the western flank of the dome (A1945).

Particularly in the lowest-grade samples, the Ferry and Spear (1978) calibration appears to yield unreasonably low temperatures for rocks containing garnet with a significant almandine component. The problem may arise from the calcareous nature of several of the pelitic schists, indicated by the presence of epidote, and in the case of A1945, calcic amphibole. Garnet rim compositions from four of the samples contain $(Ca + Mn)/(Ca + Mn + Mg + Fe) > 0.2$, exceeding the suggested limit for the use of the Ferry and Spear (1978) calibration. Although the Ganguly and Saxena (1984) calibration corrects for Ca, the additional corrections for Mn and Fe-Mg may not be justified because of the high correlation between MnO and Fe/Mg (Spear and Peacock, 1989). Therefore, the Hodges and Spear (1982) calibration was chosen to graphically illustrate the temperature variation across the area (Fig. IV-24).

*Amphibole Chemistry*

Laird and Albee (1981) compared mineral chemistry in natural mafic assemblages in Vermont to metamorphic grade deduced from interlayered pelitic rocks. Utilizing mafic rocks with the *common assemblage* amphibole + chlorite + epidote + plagioclase + quartz + Ti-phase ± carbonate ± K-mica ± $Fe^{3+}$, they characterized the compositional and modal variations in the various phases from biotite to sillimanite grade conditions by a series of formula proportion

Table IV-2: Comparison of garnet-biotite thermometry of pelitic schists from the Einunnfjellet-Savalen area.

| | | Temperature, °C (± 50°) | | |
|---|---|---|---|---|
| *Sample | $K_D$ | Ferry and Spear (1978) | Hodges and Spear (1982) | Ganguly and Saxena (1984) |
| A1435 | 0.090 | 396 | 465 | 460 |
| A933 | 0.108 | 437 | 507 | 497 |
| A1718 | 0.137 | 498 | 557 | 509 |
| A791 | 0.168 | 559 | 578 | 558 |
| A1341 | 0.110 | 491 | 525 | 504 |
| A1337 | 0.138 | 500 | 567 | 530 |
| A1945 | 0.124 | 472 | 540 | 483 |

*Samples arranged from east (A1435) to west (A1945).

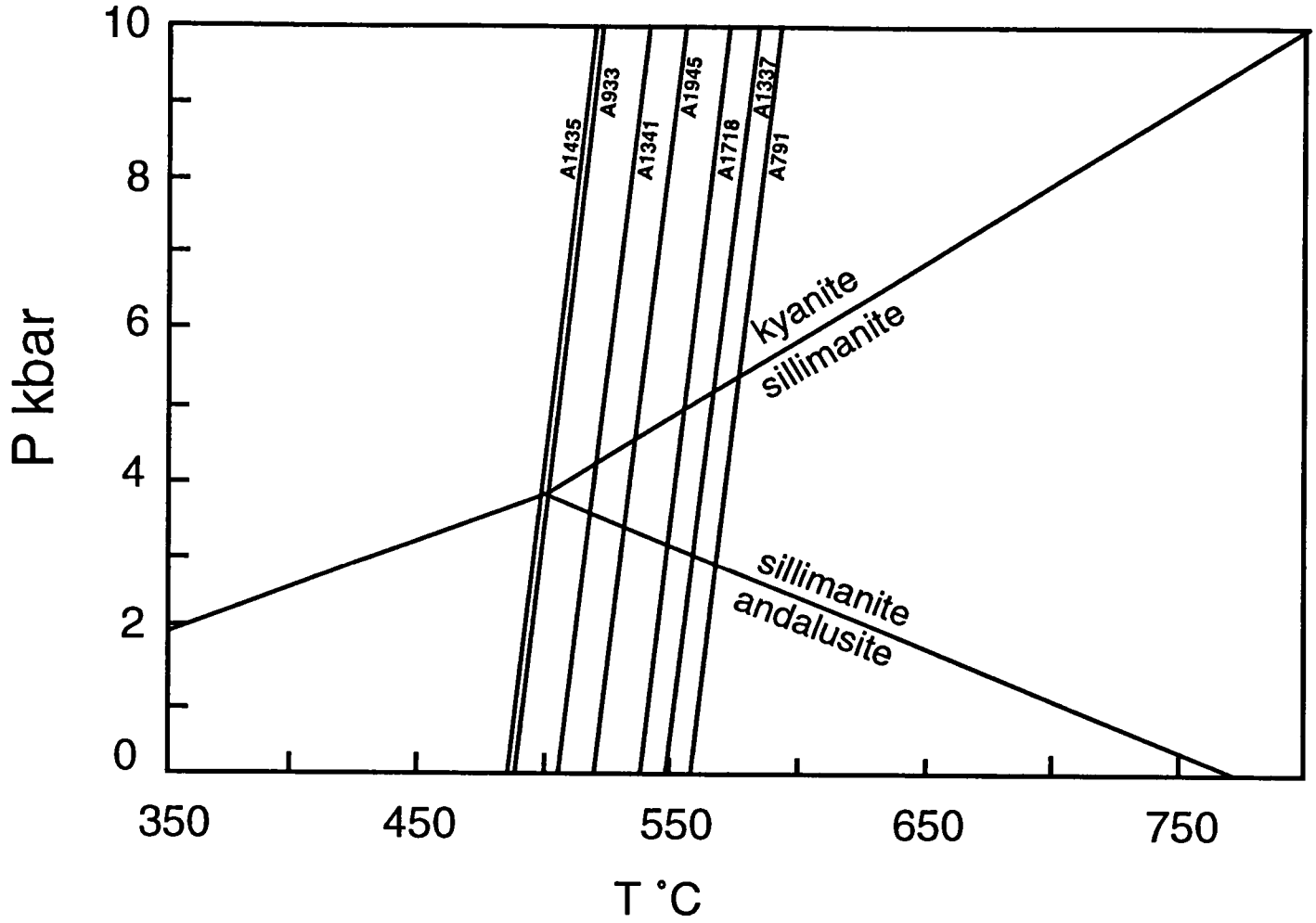



Figure IV-24
Garnet-biotite temperatures, at various pressures, calculated using Hodges and Spear (1982) calibration. $Al_2SiO_5$ phase boundaries shown for reference.

diagrams (for example, Fig. IV-25). Their results, especially for medium pressure conditions, are supported by experimental studies (Apted and Liou, 1983), and clearly demonstrate that the *tschermak*, $(Al^{VI} + Fe^{3+} + Ti + Cr)$, $Al^{IV} \leftrightarrow (Fe^{2+} + Mg + Mn)$, Si, and *glaucophane*, $Na^{M4}$, $(Al^{VI} + Fe^{3+} + Ti + Cr) \leftrightarrow Ca$, $(Fe^{2+} + Mg + Mn)$, substitutions increase continuously with metamorphic grade, whereas the *edenite*, $(Na^{A} + K)$, $Al^{IV} \leftrightarrow \square$, Si, substitution increases through garnet grade, then decreases ($\square$ indicates a vacancy in the A-site). It should be noted that although most of the parameters plotted on the diagrams depend on the normalization method used to transform amphibole analyses into mineral formulas, the ratios plotted in Figure IV-25a are independent of technique (Laird and Albee, 1981).

Six amphibole-bearing samples from an east-to-west traverse across the Einunnfjellet-Savalen area (Fig. IV-21) were chosen for electron microprobe analyses. Five of the samples (A1463, A20, A1573, A114A, and GRUV) contain the *common assemblage*, and are interpreted to represent basaltic protoliths. One sample (A1945) is a calcarous metapelite (quartz + plagioclase + mica + amphibole + garnet + calcite + epidote + Ti-phase), and is included here as a comparison. It must be noted, however, that amphiboles in garnet-bearing mafic rocks metamorphosed at medium pressure tend to be more aluminous than those from garnet-free rocks (Laird and Albee, 1981), and it might be expected that those from pelitic rocks would be even more Al-rich. Amphibole analyses were normalized following the method of Leake (1978), based on 23 oxygens (Appendix 1). All analyses are calcic amphiboles, having $(Ca + Na)M4 > 1.34$, $NaM4 < 0.67$, $(Na + K)A < 0.5$, and $Ti < 0.5$, and consequently can be named according to the terminology of Leake (1978) for calcic amphiboles, based on Si vs. $Mg/(Mg + Fe^{2+})$ (Fig. IV-26). The amphiboles analyzed cover virtually the entire range of calcic amphiboles, from actinolite to tschermakite, although most plot toward the tschermakitic end (Fig. IV-26).

Samples A1463, A20, and A1573 occur to the east of Einunnfjellet dome (Fig. IV-21). Both A1463 and A20 are fine-grained greenstones, containing aggregates of randomly oriented light green amphibole (Fig. IV-27). The acicular amphibole grains, generally less than 0.25 mm in length, are dominantly magnesiohornblende, although discrete grains of actinolite to actinolitic hornblende are present (Fig. IV-26). Analyses of cores vs. rims were difficult to obtain because of the fine grain size, although some grains in A20 are optically zoned. In the diagrams of Laird and Albee (1981), the two samples exhibit a range of amphibole compositions that span the biotite zone and the low garnet zone (Fig. IV-28). Toward the west, sample A1573 is a slightly coarser-grained greenschist, and contains approximately 2 mm long, gray-green amphiboles in a fine-grained matrix of acicular, randomly oriented grains (Fig. IV-29a). Amphibole composition is dominantly tschermakitic hornblende (Fig. IV-26), although larger

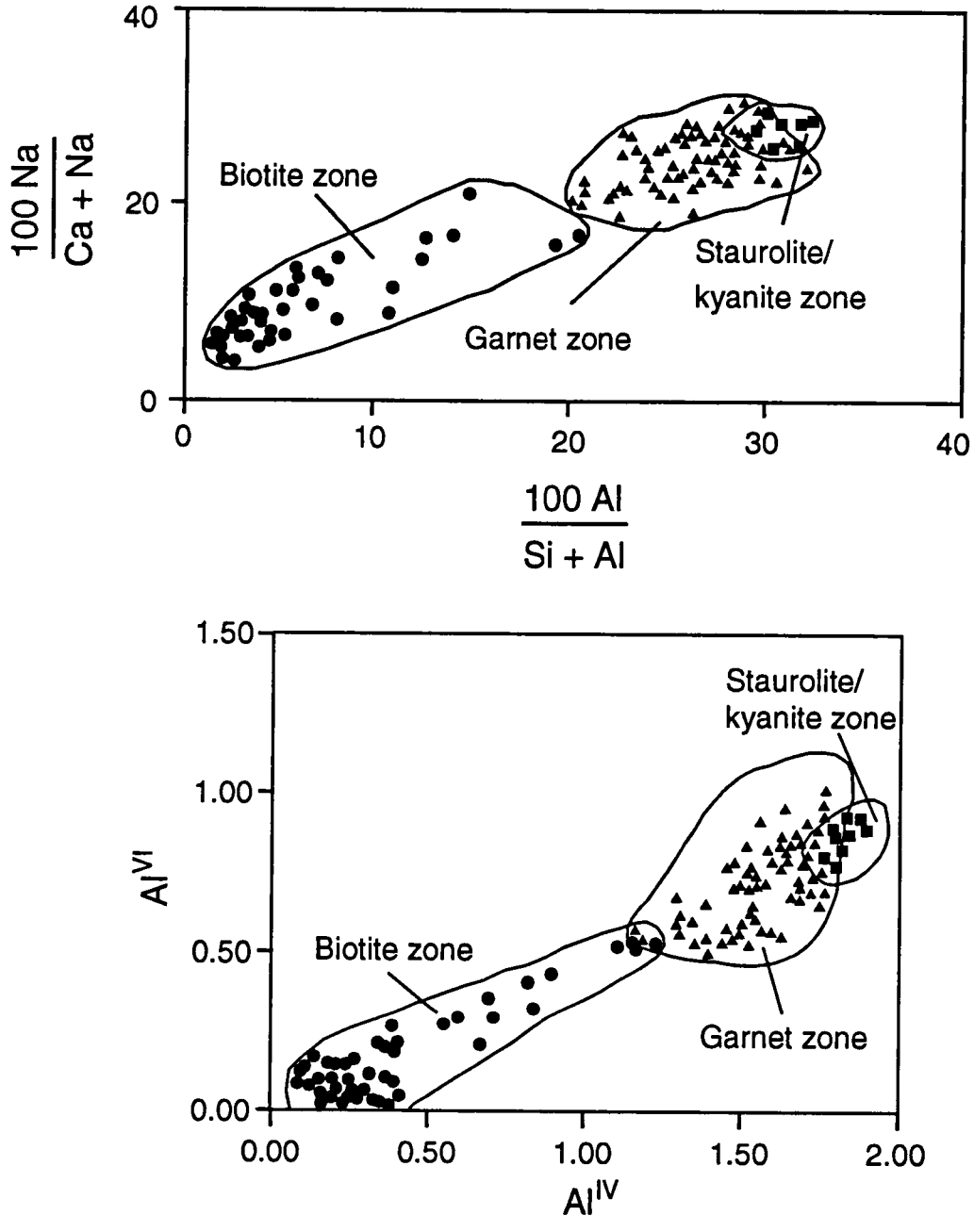



Figure IV-25
Examples of amphibole formula proportion diagrams developed by Laird and Albee (1981). Metamorphic zones determined from pelitic schist interlayered with amphibolite.

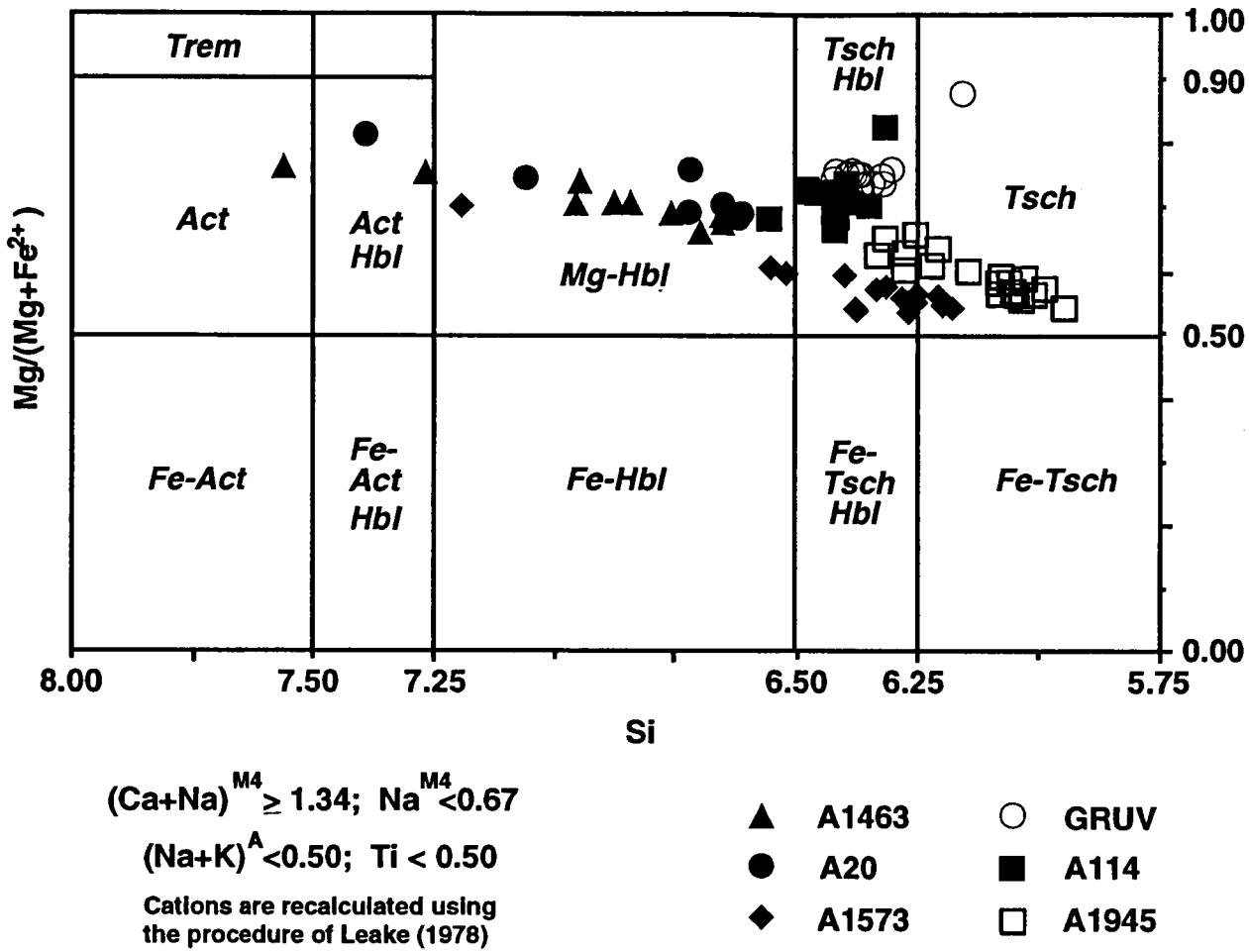



Figure IV-26
Leake (1978) classification for calcic amphiboles.

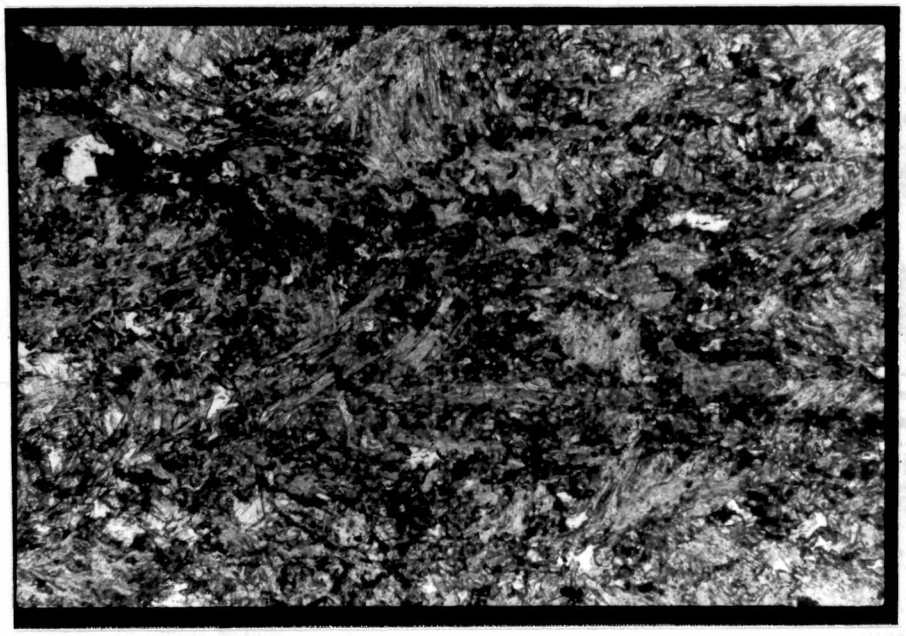


Figure IV-27
Photomicrograph of fine-grained greenstone, sample A1463. Felted mass of elongate grains is amphibole; small, round high-relief grains are epidote. Long dimension of photograph 1.7 mm.

a.

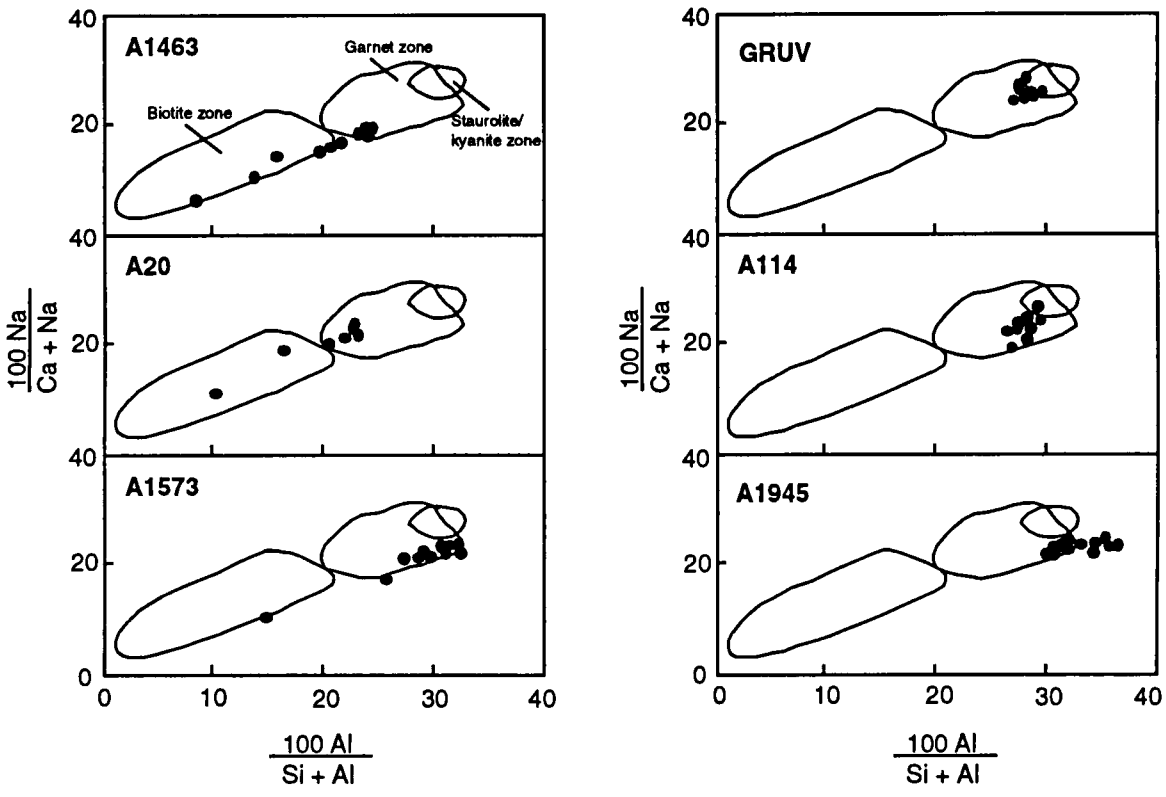



Figure IV-28
Formula proportion diagrams for amphibolites, Einunnfjellet-Savalen area. a) (100 Na)/(Ca + Na) vs. (100 Al)/(Si + Al) diagram for amphibolites. b) $Al^{IV}$ vs. $Al^{VI}$ diagram for amphibolites. After Laird and Albee (1981).

b.

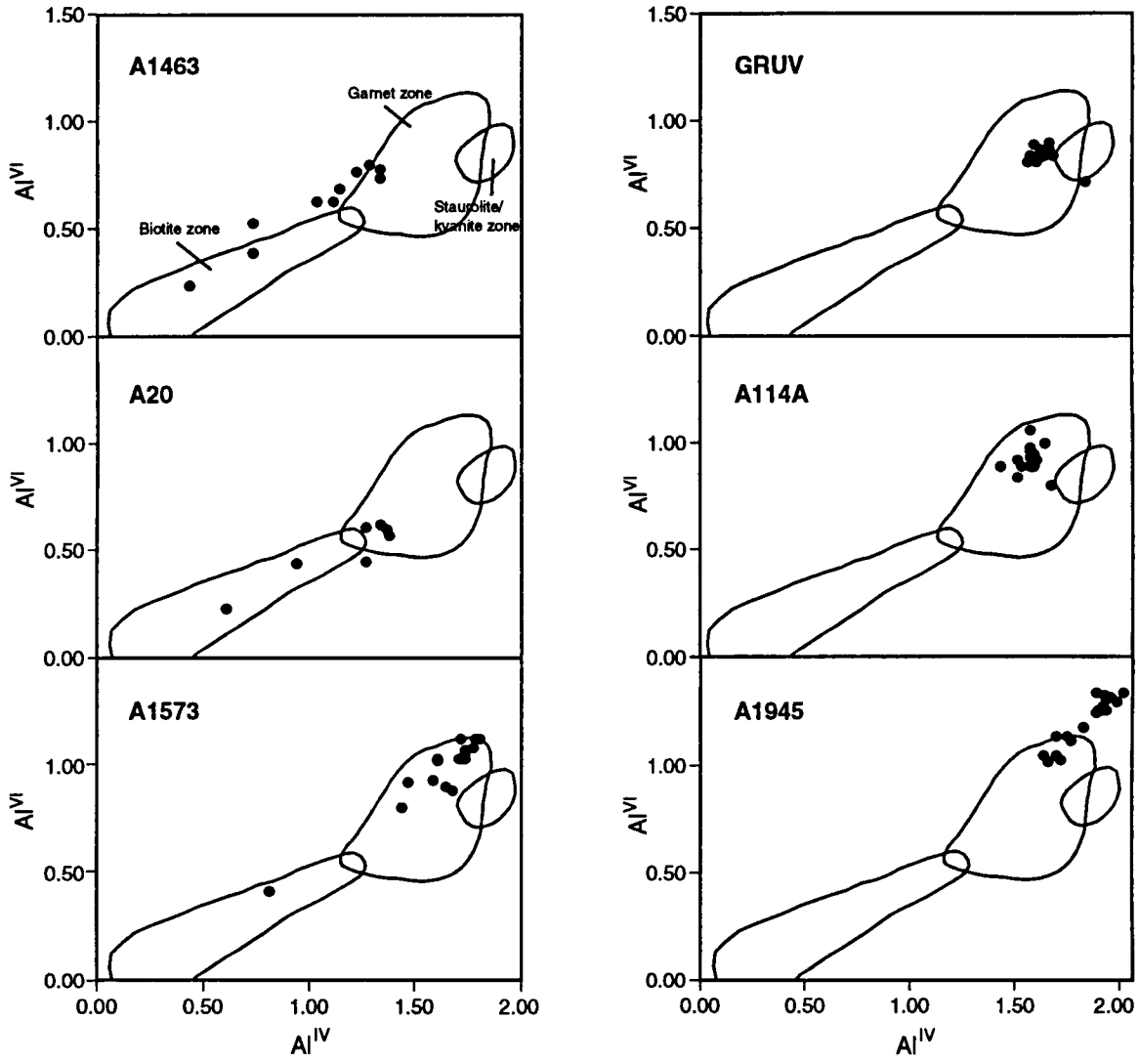
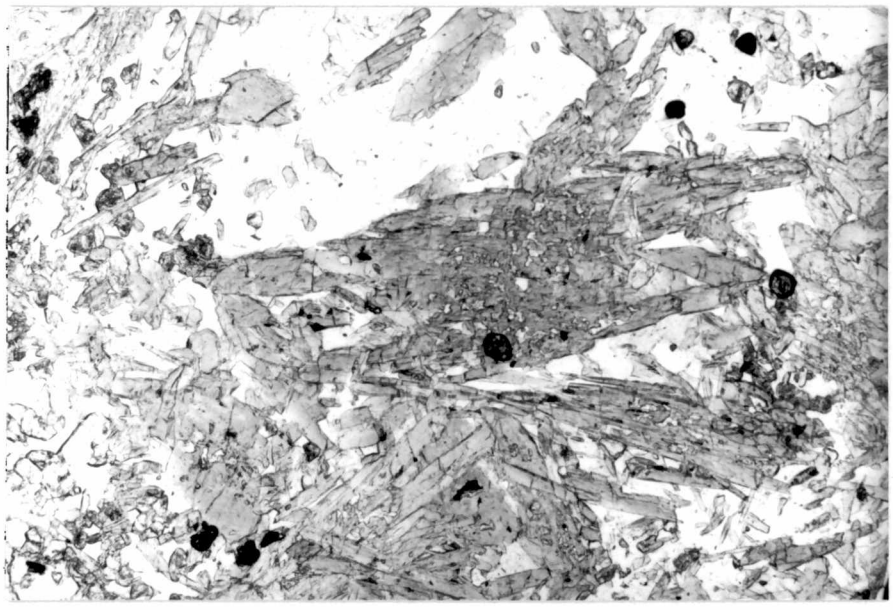



Figure IV-28, continued

a.



b.



Figure IV-29
Photomicrographs of amphibolite. a) Sample A1573; large amphiboles in fine-grained matrix of amphibole, epidote, and feldspar. Large amphibole in center of photograph is compositionally zoned, from magnesiohornblende (core) to tschermakitic hornblende (rim). Long dimension of photograph 4.5 mm. b) Sample A114. Amphibole grain-size is bimodally distributed. Long dimension of photograph 4.5 mm.

grains are distinctly zoned. Similar to the samples above, the compositions create a spread of points on the formula proportion diagrams, although all but one fall in the garnet zone (Fig. IV-28).

In contrast to the samples described above, amphibolite closer to the core of Einunnfjellet dome (samples GRUV and A114) is relatively coarse-grained, strongly foliated, and dark-colored. In thin section, amphiboles are bluish-green, and have a bimodal grain-size distribution. GRUV contains prismatic grains that range from 0.25 to 2 mm, whereas A114 contains small acicular grains that are generally overgrown by larger anhedral to prismatic grains up to 4 mm long (Fig. IV-29b). Despite the overprinting relationships, both the matrix grains and larger amphiboles in both samples form a tight cluster in the tschermakitic hornblende field of the Leake diagram (Fig. IV-26), suggesting that the amphiboles do not represent growth under significantly different metamorphic conditions. Only two analyses deviate from this composition; one, a rim of a large amphibole from GRUV, is a Mg-rich tschermakite, while the other is a core of magnesiohornblende from a prismatic grain in A114. The amphiboles cluster in the high garnet zone, adjacent to or slightly overlapping the staurolite/kyanite field (Fig. IV-28).

Sample A1945 (Fig. IV-21) is a garnet- and amphibole-bearing calcareous schist. Poikiloblastic amphibole grains, up to 3 mm long, contain abundant fine-grained inclusions of epidote and quartz. Amphiboles are either homogenous tschermakite, or tschermakite rimmed by tschermakitic hornblende (Fig. IV-26). From Figure IV-28, the amphibole composition appears to indicate high garnet-grade conditions. As noted earlier, however, the conditions indicated by this sample should be viewed with caution, because the amphibole composition is not buffered by the *common assemblage*. Other formula proportion diagrams, not shown here, yield results consistent with those in Figure IV-28 for all samples.

*Barometry*

Pelitic schists from the Einunnfjellet-Savalen area lack mineral phases that give some indication of pressure conditions (in particular, $Al_2SiO_5$ polymorphs) and, consequently, in the assemblages most commonly used for barometry in metapelites (for example, the garnet-plagioclase-$Al_2SiO_5$-quartz barometer, or GASP). Ghent and Stout (1981) introduced a geobarometer utilizing the assemblage garnet + muscovite + plagioclase + biotite, which is common in garnet to sillimanite grade metasedimentary rocks. Potential problems with the geobarometer, discussed by Ghent and Stout (1981) and by Essene (1989), include dependence on the resolution of the garnet-biotite thermometer, uncertainties of mixing models for garnet,

plagioclase, and biotite, presence of additional high-Al phases, and substitutions in muscovite solid solutions. Keeping these in mind, the barometer was applied to sample A933 from the Einunnfjellet–Savalen area. Calculations were again made by the Thermobarometry program (Spear and Peacock, 1989), utilizing modifications of the barometer by Hodges and Crowley (1985) and Powell and Hodges (1988). These intersect the Hodges and Spear (1982) temperature at 8.25 and 9.75 kbar, respectively ($\pm$ 0.8 kbar).

The relatively high pressures are in agreement with pressure estimates for the central Trondheim nappe complex (Lagerblad, 1984b). They are not, however, consistent with field, petrologic, and chemical observations from the Einunnfjellet-Savalen area. The mineral assemblages in both pelitic and mafic rocks from this area appear to represent medium-pressure regional metamorphism, and this is particularly supported by amphibole compositions, which fall entirely within the medium-pressure fields of Laird and Albee (1981) (Fig. IV-30). Therefore, the pressure estimate must remain equivocal until further study can be made.

*Greenschist-Amphibolite Facies Transition*

The transition from greenschist to amphibolite facies is interpreted to occur over a 2.5 km-wide zone in the Lomsjødalen area (Fig. IV-31). In the field, this is indicated by a change from phyllite and greenstone to coarser-grained schist and amphibolite. Within this zone, actinolitic amphibole coexists with more hornblendic varieties in mafic rocks (Fig. IV-26), and garnet in pelitic rocks is strongly zoned. Plagioclase composition increases abruptly from almost pure albite in sample A20 to $An_{17-22}$ in sample A1463, and the oligoclase isograd in mafic rocks appears to correspond closely to the formation of almandine-rich rims on garnet in pelitic rocks (Fig. IV-31). All of these characteristics correspond to the epidote-amphibolite facies, which represents a transition zone, over a narrow range in temperature, between the greenschist facies and full-blown amphibolite facies in medium-pressure metamorphic rocks (Turner, 1981). The absolute P-T conditions of this complex, multiphase transition are difficult to quantify (Apted and Liou, 1983), and depending upon the criteria used to define it, the boundary may vary between 450 and 550° C (Essene, 1989). Based on experiments involving basaltic compositions, Apted and Liou (1983) attempted to quantify the P-T conditions of this transition as a function of oxygen fugacity, and suggested that it occurs over a temperature range of 500–575° C. Using either the calibration of Hodges and Spear (1982), or Ganguly and Saxena (1984), metamorphic temperatures for the pelitic schists A1435 and A933 (Table IV-2), which occur in the transition zone, reasonably correlate with the interpreted transition.

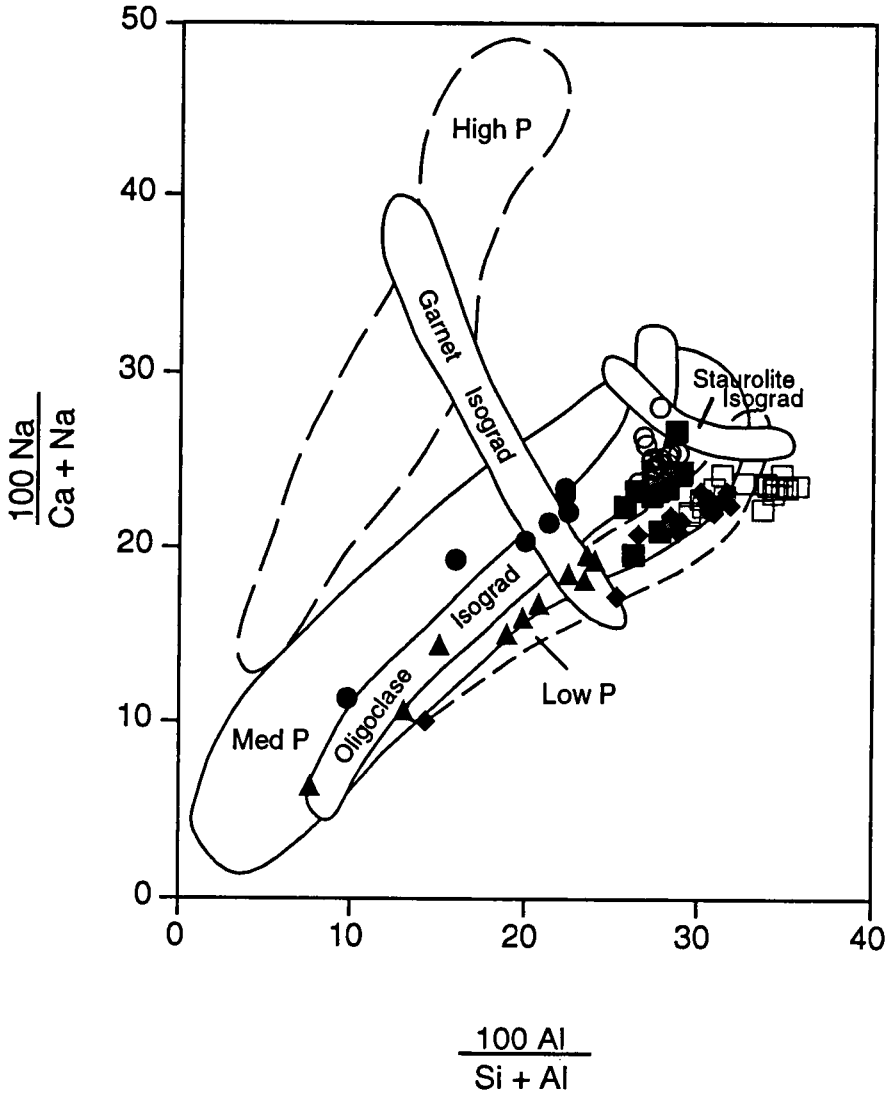



Figure IV-30
(100 Na)/(Ca + Na) vs. (100 Al)/(Si + Al) diagram for amphibolites. Fields for high, medium, and low pressure conditions are shown; also oligoclase, garnet, and staurolite isograds. Symbols same as in Figure IV-26.

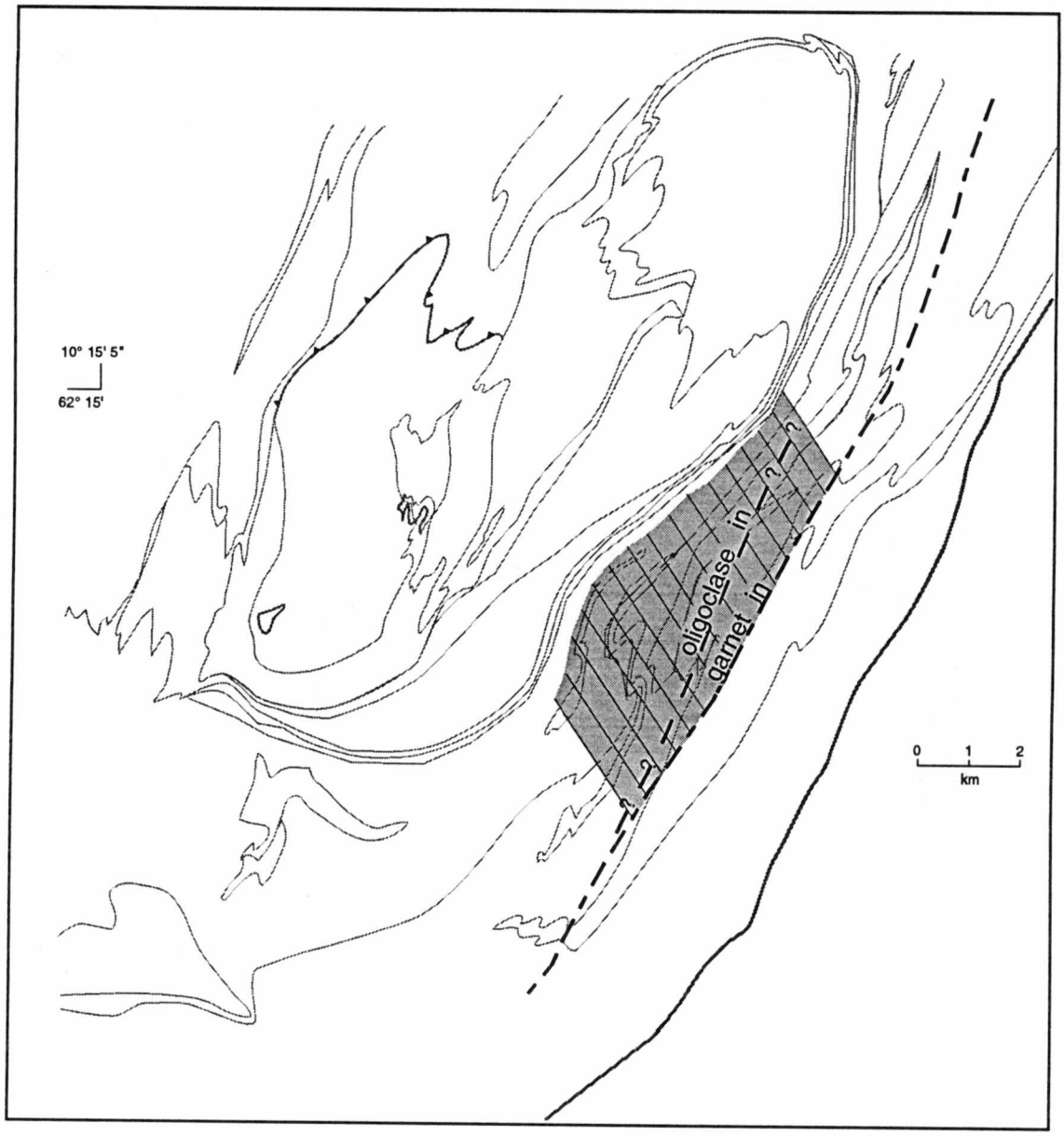



Figure IV-31
Metamorphic map of Einunnfjellet-Savalen area. Location of almandine garnet and oligoclase isograds are shown, and shaded area of greenschist-to-amphibolite transition zone (i.e., epidote-amphibolite facies).

Westward from the transition zone, both amphibole chemistry and geothermometry indicate that the metamorphic grade increases continually (Figs. IV-24 & IV-28). The highest temperatures (approximately 575° C) appear to have occurred close to the core of the dome, peaking near conditions at which staurolite would begin to form in rocks of appropriate composition (Figs. IV-28 & IV-30), although the calcareous nature of pelitic schists from this area would most likely preclude formation of this phase (Boyle and Westhead, 1992). Finer-grained lithologies that occur within the higher-grade rocks generally contain a significant amount of graphite, giving the rock a more "slaty" appearance; garnet-biotite thermometry does not, however, indicate that these rocks are lower grade than the surrounding rocks (for example, samples A933, A791, and A1718). The presence of graphite reduces $a_{H_2O}$ of the metamorphic fluid, and, as a result, dehydration reactions occur at lower temperatures than in rocks without graphite (Labotka, 1991). By the same reasoning, it would seem that the growth of hydrous phases (micas) would be inhibited in graphite-bearing rocks, resulting in a finer-grained appearance when compared to the surrounding coarse-grained, graphite-free mica schists. The anomalously low temperature recorded by the clear garnet rim in sample A1341 (Table IV-2; Fig. IV-24), from near the core of the dome, could indicate that the rim grew relatively late, and does not represent peak metamorphic conditions.

## *Regional Implications*

The sequence of Scandian deformation ($D_2$ of this study) is broadly equivalent to the $D_1$ and $D_2$ phases recognized by Roberts (1971, 1979) in the northern Trondheim region. His $F_3$ folds having flat-lying axial surfaces and associated crenulation cleavage do not appear to be well-developed in the Einunnfjellet-Savalen area, however, unless crenulations that are overturned down-dip on the flanks of Einunnfjellet dome can be attributed to a phase equivalent to his $D_3$ deformation.

In the Einunnfjellet-Savalen area, it appears that Gula rocks in the Savalen thrust complex are lithologically and structurally equivalent to the upper subunit of the Seve nappe, which Andréasson and Gorbatchev (1980) considered transitional to the overlying Köli nappe. The absence in this area of the earlier, high-grade metamorphism of Gula-equivalent rocks elsewhere (Guezou, 1978; Andréasson and Lagerblad, 1980; Andréasson and Gorbatchev, 1980) indicates that the entire Gula nappe may be a composite unit, and supports a correlation with the Seve nappe, as suggested by Roberts and Wolff (1981). Alternatively, or in conjunction with this interpretation, the Early Ordovician thrusting of oceanic crust throughout the Scandinavian Caledonides may have been similar to the situation in present-day Oman, where

the effects of Late Cretaceous obduction of the Semail ophiolite were not subsequently overprinted by continent-continent collision. Deformation of the basement and shelf units was widespread, but high-grade metamorphism was confined to either the sole thrust beneath the ophiolite, or related to localized A-type subduction of the basement and shelf units (high P/T assemblages) (El-Shazly and Coleman, 1990; Métour *et al.*, 1990).

## *Summary*

The sequence of tectonic events in the Einunnfjellet-Savalen area began with emplacement of an oceanic thrust complex eastward onto continental-margin quartzite, probably in the Early Ordovician, followed by erosion of both the quartzite and oceanic rocks and subsequent deposition of coarse to fine-grained clastic sediments. During Scandian orogenesis, in approximately Mid-Silurian time, the entire sequence was thrust eastward, imbricated, folded, and metamorphosed. Thrusting of the Savalen thrust complex onto the Hummelfjell Formation is interpreted to have occurred prior to the Scandian orogeny based on the presence of early ($D_1$) structures that occur only in rocks stratigraphically below the unconformity, as well as the age relationships in the probably correlative Otta nappe to the south (Chapter II). Detailed petrologic study of the rocks in the Einunnfjellet-Savalen area, however, does not reveal evidence of metamorphism related to this event, other than a rare, weak foliation of muscovite and chlorite in some rocks that may be attributed to $D_1$. If it did occur, the conditions must have been low grade enough to have been completely overprinted by Scandian metamorphism.

Scandian orogenesis ($D_2$) was a progressive deformation that can be divided into two main phases: a flattening phase ($D_{2a}$) followed by a phase of pervasive shearing ($D_{2b}$). In some rocks two distinct foliations related to these phases can be distinguished, although locally the regional foliation is a composite of the two. In pelitic rocks, the mineral assemblage associated with both $S_{2a}$ and $S_{2b}$ is muscovite + biotite + chlorite + graphite + garnet; therefore, it appears that the transition from two separate S-surfaces to one composite foliation represents a continuum during a single metamorphic event. Textural zoning in garnet indicates that garnet growth began late during $D_{2a}$ in some samples, although the dominant period of growth was synkinematic with respect to $D_{2b}$, suggesting that metamorphism peaked after the transition from flattening to a simple shear regime. Temperatures remained high after deformation ceased, however, as indicated by garnet rims that overgrew the crenulated foliation. Based on compositional zoning patterns, garnet appears to have grown during a single reaction, with the exception of slight reverse zoning at or near the rims in some samples. Garnet-biotite thermometry and amphibole composition indicate a progressive metamorphic increase from

greenschist to amphibolite facies across the area. A rather sudden change in the field appearance of both pelitic and mafic rocks corresponds to the transition zone between the two facies (i.e., the epidote-amphibolite facies), and is characterized by a change from albite to oligoclase and presence of coexisting calcic amphiboles in mafic rocks, and strong compositional zoning of garnet in pelitic rocks. Mineral assemblages and compositions are consistent with medium-pressure regional metamorphism.

The thrust contact between the Savalen thrust complex and rocks of the Hummelfjell Formation is entirely overprinted by the Scandian deformation—no metamorphic break occurs at the contact and $D_2$ structures occur in both the hanging wall and footwall rocks—consistent with the STC having been emplaced prior to Scandian orogenesis. In contrast, the eastern contact of the STC with the Meråker nappe is a prograde $D_{2b}$ shear zone that developed at greenschist facies conditions. Kinematic analysis indicates a clockwise (dextral) sense of movement on the shear zone, although the amount of displacement may be relatively minor.

Post-metamorphic brittle deformation ($D_3$) is characterized by open folding and warping, and locally common kink folds with fractured hinges. Although a minor component of the tectonic history, deformation associated with this phase may have been locally important in accentuating the structure of the Einunnfjellet dome, and in reorienting fold axes and mineral lineations to a NE plunge on the north side of the dome.

# CONCLUSIONS

1) The Einunnfjellet-Savalen area, southeastern Trondheim nappe complex, Norway, contains a polydeformed continental margin quartzite-schist sequence in the core of the Einunnfjellet dome. These rocks, which can be linked to the Baltoscandian miogeocline, were overthrust by the Savalen thrust complex, containing fragments of oceanic crust and associated sediments, then eroded and unconformably succeeded by polymict conglomerate and fine-grained clastic sediment.

2) The Einunnfjellet-Savalen area can be correlated with the Otta nappe to the south, where conglomerate overlying the Vågåmo ophiolite and Heidal quartzite contains an Arenig to Llanvirn faunal assemblage. This correlation implies that emplacement of the Savalen thrust complex onto the continental margin occurred prior to the Siluro-Devonian Scandian orogeny. Subsequent to deposition of the unconformable sequence, the entire package was thrust eastward, imbricated, folded, and metamorphosed during Scandian orogenesis.

3) Tectonostratigraphic relationships similar to the Einunnfjellet-Savalen area are widespread in the Trondheim nappe complex and throughout the upper allochthon of Norway and Sweden. The interpretations for the study area support the idea that the upper allochthon is a composite terrain, and that at least the outermost parts of the Baltoscandian margin experienced deformation both prior to and during the Scandian orogeny.

4) Field and geochemical evidence from two metaigneous complexes that occur in the Einunnfjellet-Savalen area indicates that both complexes formed in a suprasubduction-zone setting. Although isotopic dating is not yet available for the metaigneous rocks of the Einunnfjellet-Savalen area, they are lithologically and geochemically similar to dated Early Ordovician Norwegian ophiolites that formed in a suprasubduction-zone environment.

5) Metabasalts of the Lomsjødalen complex, directly correlative with the Gula greenstone, are primitive arc tholeiites. Overlying Fe- and Mn-rich metalliferous sediments and possible remnants of black smokers suggest a spreading ridge environment, probably either an opening marginal basin or the earliest stage of island arc development.

6) Mafic rocks of the Bangardsvola complex, previously correlated with either the Fundsjø Group or with rocks equivalent to the structurally lower Seve nappe, have boninitic affinities uniquely characteristic of subduction-related settings.

7) The association of primitive IAT, boninite, and Fe- and Mn-rich metalliferous sediments is strongly analogous to the upper parts of the Troodos Ophiolite, Cyprus, which may have formed as short spreading segments above an oblique subduction zone, similar to the Andaman Sea region of the Indian Ocean (Moores *et al.*, 1984).

8) The Einunnfjellet dome resulted from several phases of deformation: a pre-Scandian phase ($D_1$); the dominant Scandian phase ($D_2$); and late brittle deformation ($D_3$). The dome is defined by a major NE-SW doubly plunging antiformal axis, and a minor axis that plunges gently NW-SE.

9) $D_1$ involved structures present only in rocks stratigraphically below the unconformity. $F_1$ isoclinal, recumbent folds are indicated by a type-2 refold pattern in the core of the dome, and mesoscopic refolded $F_1$ folds occur in the Savalen thrust complex. Detailed petrologic study does not reveal firm evidence of metamorphism related to this event.

10) $D_2$ produced the NNE-striking antiformal structure of the dome, and was a progressive deformation that can be divided into: a flattening phase ($D_{2a}$); followed by a phase of pervasive shearing ($D_{2b}$). The earliest mesoscopic $F_{2a}$ folds are inclined isoclinal folds, that were overprinted by pervasive $D_{2b}$ deformation which produced tight flexural flow buckle folds in quartzite and other competent rocks, and crenulations in schist.

11) In some rocks two distinct foliations related to these phases can be distinguished, although both formed during a single metamorphic event. Toward the eastern boundary of the Savalen thrust, which is defined by a NNE-striking ductile shear zone, the regional foliation is composite. Geometric relationships indicate that the composite foliation formed from rotation of the earlier fabric ($S_{2a}$) into the plane of shearing during development of $S_{2b}$.

12) Late gentle warping of the Einunnfjellet antiform about a NW-SE axis accentuated the elongate dome structure, and reoriented fold axes and mineral lineations to a NE plunge on the north side of the dome.

13) Textural zoning in garnet indicates that garnet growth began late during $D_{2a}$ in some samples, although the dominant period of growth was synkinematic with respect to $D_{2b}$, suggesting that metamorphism peaked after the transition from flattening to a simple shear regime. Temperatures remained high after deformation ceased, however, as indicated by garnet rims that overgrew the crenulated foliation.

14) Garnet-biotite thermometry and amphibole composition indicate a progressive metamorphic increase from greenschist to amphibolite facies across the Einunnfjellet-Savalen area. The transition zone between the two facies (i.e., the epidote-amphibolite facies) is characterized by a change from albite to oligoclase and presence of coexisting calcic amphiboles in mafic rocks, and strong compositional zoning of garnet in pelitic rocks. Mineral assemblages and compositions are consistent with medium-pressure regional metamorphism.

15) The thrust contact between the Savalen thrust complex and the underlying quartzite-schist sequence is entirely overprinted by Scandian deformation—no metamorphic break occurs at the contact and $D_2$ structures occur in both the hangingwall and footwall rocks—consistent with the thrust complex having been emplaced prior to Scandian orogenesis. In contrast, the eastern contact of the Savalen thrust complex with the Fundsjø Group (Meråker nappe) is a prograde $D_{2b}$ shear zone that developed at greenschist facies conditions. Kinematic analysis indicates a clockwise (dextral) sense of movement on the shear zone, although the amount of displacement may be relatively minor.

# REFERENCES CITED

# REFERENCES CITED

Anderson, D. E., and Olimpio, J. C., 1977, Progressive homogenization of metamorphic garnets, South Morar, Scotland: evidence for volume diffusion: Canadian Mineralogist, v. 15, p. 205-216.

Andréasson, P. G., and Gorbatschev, R., 1980, Metamorphism in extensive nappe terrains: a study of the central Scandinavian Caledonides: Geologiska Föreningens i Stockholm Förhandlingar, v. 102, p. 335–357.

Andréasson, P. G., and Lagerblad, B., 1980, Occurrence and significance of inverted metamorphic gradients in the western Scandinavian Caledonides: Journal of the Geological Society of London, v. 137, p. 219–230.

Apted, M. J., and Liou, J. G., 1983, Phase relations among greenschist, epidote-amphibolite, and amphibolite in a basaltic system: American Journal of Science, v. 283-A, p. 328–354.

Arndt, N. T., and Nesbitt, R. W., 1982, Geochemistry of Munro Township basalts, *in* Arndt, N. T., and Nisbet, E. G. Nisbet, eds., Komatiites: London, George Allen and Unwin, p. 309–329.

Barker, A. J., 1990, Introduction to metamorphic textures and microstructures: New York, Chapman and Hall, 162 p.

Barrow, G., 1893, On an intrusion of muscovite-biotite gneiss on the southeastern Highlands of Scotland, and its accompanying metamorphism: Quarterly Journal of the Geological Society of London, v. 49, p. 330–356.

Bell, T. H., 1985, Deformation partitioning and porphyroblast rotation in metamorphic rocks: a radical reinterpretation: Journal of Metamorphic Geology, v. 3, p. 109–118.

Bell, T. H., and Hayward, N., 1991, Episodic metamorphic reactions during orogenesis: the control of deformation partitioning on reaction sites and reaction duration: Journal of Metamorphic Geology, v. 9, p. 619–640.

Bell, T. H., and Johnson, S. E., 1989, Porphyroblast inclusion trails: the key to orogenesis: Journal of Metamorphic Geology, v. 7, p. 279–310.

Bell, T. H., and Rubenach, M. J., 1983, Sequential porphyroblast growth and crenulation cleavage development during progressive deformation: Tectonophysics, v. 92, p. 171–194.

Bell, T. H., Fleming, P. D., and Rubenach, M. J., 1986, Porphyroblast nucleation, growth, and dissolution in regional metamorphic rocks as a function of deformation partitioning during foliation development: Journal of Metamorphic Geology, v. 4, p. 37–67.

Bell, T. H., Forde, A., and Hayward, N., 1992a, Do smoothly curving, spiral-shaped inclusion trails signify porphyroblast rotation?: Geology, v. 20, p. 59–62.

Bell, T. H., Johnson, S. E., Davis, B., Forde, A., Hayward, N., and Wilkins, C., 1992b, Porphyroblast inclusion-trail orientation data: eppure non son girate!: Journal of Metamorphic Geology, v. 10, p. 295–307.

Bergman, S., 1987, A possible ophiolite at Handöl, Swedish Caledonides: Geologiska Föreningens i Stockholm Förhandlingar, v. 109, p. 340–343.

Berthe, D., Choukroune, P., and Jegouzo, P., 1979, Orthogneiss, mylonite, and noncoaxial deformation of granites: the example of the South Armorican shear zone: Journal of Structural Geology, v. 1, p. 31–42.

Berthomier, C., Maillot, J., Mosson, P., Quesnel, G., and Rollet, M., 1970, Aperçu géologique sur la région orientale et septentrionale de Folldal (Sud du Trondheim–Norvege): Bulletin de la Federation des Societes d'Histoire Naturelle de Franche–Comte, v. 72, p. 1–10.

Bloomer, S. H., and Hawkins, J. W., 1987, Petrology and geochemistry of boninite series volcanic rocks from the Mariana trench: Contributions to Mineralogy and Petrology, v. 97, p. 361–377.

Bonatti, E., 1975, Metallogenesis at oceanic spreading centers, *in* Donath, F., Stehli, F. G., and Wetherhill, G. W., eds., Annual Reviews in Earth and Planetary Sciences, v. 3, p. 401–431.

Bonatti, E., Kolla, V., Moore, W. S., and Stern, C., 1979, Metallogenesis in marginal basins: Fe-rich basal deposits from the Philippine Sea: Marine Geology, v. 32, p. 21–37.

Boyle, A. P., and Westhead, R. K., 1992, Metamorphic peak geothermometry in the Furulund Group, Sulitjelma, Scandinavian Caledonides: implications for uplift: Journal of Metamorphic Geology, v. 10, p. 615–626.

Bruton, D. L., and Bockelie, J. F., 1980, Geology and palaeontology of the Hølonda area, western Norway—a fragment of North America, *in* Wones, D.R., ed., The Caledonides in the U.S.A.: Virginia Polytechnical Institute and State University Memoir 2, p. 41–47.

Bruton, D. L. and Harper, D. A. T., 1981, Brachiopods and trilobites of the early Ordovician serpentine Otta conglomerate, south central Norway: Norsk Geologisk Tidsskrift, v. 61, p. 153–181.

Bruton, D. L. and Harper, D. A. T., 1988, Arenig–Llandovery stratigraphy and faunas across the Scandinavian Caledonides, *in* Harris, A. L., and Fettes, D. J., eds., The Caledonian–Appalachian orogen: Geological Society Special Publication 38, p. 247–268.

Bruton, D. L., Lindström, M., and Owen, A. W., 1985, The Ordovician of Scandinavia, *in* Gee, D. G., and Sturt, B. A., eds., The Caledonide orogen—Scandinavia and related areas: Chichester, John Wiley and Sons, p. 273–282.

Bryhni, I., 1983, Regional overview of metamorphism in the Scandinavian Caledonides, *in* Schenck, P. E., ed., Regional Trends in the geology of the Appalachian–Caledonian–Hercynian–Mauritanide orogen: Dordrecht, Reidel, p. 193–204.

Bryhni, I., 1988, Early Palaeozoic metamorphism in the Scandinavian Caledonides, *in* Harris, A. L., and Fettes, D. J., eds., The Caledonian–Appalachian orogen: Geological Society Special Publication 38, p. 135–140.

Bryhni, I., and Andréasson, P. G., 1985, Metamorphism in the Scandinanvian Caledonides, *in* Gee, D. G., and Sturt, B. A., eds., The Caledonide orogen—Scandinavia and related areas: Chichester, John Wiley and Sons, p. 763–781.

Bugge, C., 1910, Rennebu: Fjeldbygningen inden rektangel-kartet Rennebus omraade: Norges Geologiske Undersøkelse, v. 56, 42 p.

Cameron, W. E., 1985, Petrology and origin of primitive lavas from the Troodos ophiolite, Cyprus: Contributions to Mineralogy and Petrology, v. 89, p. 256–262.

Cameron, W. E., Nisbet, E. G., and Dietrich, V. J., 1979, Bonintes, komatiites, and ophiolitic basalts: Nature, v. 280, p. 550–553.

Cann, J. R., 1970, Rb, Sr, Y, Zr, Nb in some ocean-floor basaltic rocks: Earth and Planetary Science Letters, v. 10, p. 7–11.

Carey, S., and Sigurdsson, H., 1984, A model of volcanogenic sedimentation in marginal basins, *in* Kokelaar, B. P., and Howell, M. F., eds., Marginal basin geology: Geological Society Special Publication 16, p. 37–58.

Carreras, J., Estrada, A., and White, S., 1977, The effects of folding on the c-axis fabrics of a quartz mylonite: Tectonophysics, v. 39, p. 3–24.

Chaloupsky, J., 1970, Geology of the Hølonda-Hulsjøn area, Trondheim region: Norges Geologiske Undersøkelse, v. 266, p. 277–304.

Chaloupsky, J. and Fediuk, F., 1967, Geology of the western and north–eastern part of the Meråker area: Norges Geologiske Undersøkelse, v. 245, p. 9–21.

Chinner, G. A., 1965, The kyanite isograd in Glen Clova, Angus, Scotland: Mineralogical Magazine, v. 34, p. 132-143.

Claesson, S. and Roddick, J. C., 1983, $^{40}Ar/^{39}Ar$ data on the age and metamorphism of the Ottjället dolerites, Särv Nappe, Swedish Caledonides: Lithos, v. 16 p. 61-73.

Coish, R. A., 1989, Boninitic lavas in Appalachian ophiolites: a review, *in* Crawford, A. J., ed., Boninites: London, Unwin Hyman, p. 264–288.

Coish, R. A., Hickey, R., and Frey, F. A., 1982, Rare earth element geochemistry of the Betts Cove ophiolite, Newfoundland: complexities in ophiolite formation: Geochimica et Cosmochimica Acta, v. 46, p. 2117–2134.

Constantinou, G., 1980, Metallogenesis associated with Troodos ophiolite, *in* Panayiotou, A., ed., Proceedings of the International Ophiolite Symposium, Cyprus 1979, p. 663–674.

Crawford, M. L., 1977, Calcium zoning in almandine garnet, Wissahickon Formation, Philadelphia, Pennsylvania: Canadian Mineralogist, v. 15, p. 243-249.

Crawford, A. J., Beccaluva, L., and Serri, G., 1981, Tectonomagmatic evolution of the West Philippine-Mariana Region and the origin of boninites: Earth and Planetary Science Letters, v. 54, p. 346–356.

Crawford, A. J., Falloon, T. J., and Green, D. H., 1989, Classification, petrogenesis and tectonic setting of boninites, *in* Crawford, A. J., ed., Boninites: London, Unwin Hyman, p. 2–49.

Cronan, D. S., Moorby, S. A., Glasby, G. P., Knedler, K., Thomson, J., and Hodkinson, R., 1984, Hydrothermal and volcaniclastic sedimentation on the Tonga–Kermadec Ridge and in its adjacent marginal basins, *in* Kokelaar, B. P., and Howell, M. F., eds., Marginal basin geology: Geological Society Special Publication 16, p. 137–149.

Dunning, G. R. and Pedersen, R. B., 1988, U/Pb ages of ophiolites and arc–related plutons of the Norwegian Caledonides: Implications for the development of Iapetus: Contributions to Mineralogy and Petrology, v. 98, p. 13–23.

El-Shazly, A. K, and Coleman, R. G., 1990, Metamorphism in the Oman Mountains in relation to the Semail ophiolite emplacement, *in* Robertson, A. H. F., Searle, M. P., and Ries, A. C., eds., The geology and tectonics of Oman: Geological Society Special Publication 49, p. 473–493.

Eskola, P., 1920, The mineral facies of rocks. Norsk Geologisk Tidsskrift, v. 6, p. 143–194.

Essene, E. J., 1982, Geologic thermometry and barometry, *in* Ferry, J. M., ed., Characterization of metamorphism through mineral equilibria: Reviews in Mineralogy, v. 10, p.153–206.

Essene, E. J., 1989, The current status of thermobarometry in metamorphic rocks, *in* Daly, J. S., Cliff, R. A., and Yardley, W. D., eds., Evolution of metamorphic rocks: Geological Society of London Special Publication 43, p. 1–44.

Ferry, J. M., and Spear, F. S., 1978, Experimental calibration of the partitioning of Fe and Mg between biotite and garnet: Contributions to Mineralogy and Petrology, v. 66, p. 113–117.

Flower, M. F. J., and Levine, H. M., 1987, Petrogenesis of a tholeiite-boninite sequence from Ayios Mams, Troodos ophiolite: evidence for splitting of a volcanic arc?: Contributions to Mineralogy and Petrology, v. 97, p. 509–524.

Fossen, H., 1989, Geology of the Minor Bergen Arc, west Norway: Norges Geologisk Undersøkelse, v. 416, p. 47–62.

Furnes, H., and Færseth, R. B., 1975, Interpretation of preliminary trace element data from the Lower Paleozoic greenstone sequences on Stord, west Norway: Norsk Geologisk Tidsskrift, v. 55, p. 157–169.

Furnes, H., Roberts, D., Sturt, B. A., Thon, A., and Gale, G. H., 1980, Ophiolite fragments in the Scandinavian Caledonides, *in* Panayiotou, A., ed., Proceedings of the International Ophiolite Symposium, Cyprus 1979, p. 582–600.

Furnes, H., Thon, A., Nordås, J., and Garmann, L. B., 1982, Geochemistry of Caledonian metabasalts from some Norwegian ophiolite fragments: Contributions to Mineralogy and Petrology, v. 79, p. 295-307.

Furnes, H., Ryan, P. D., Grenne, T., Roberts, D., Sturt, B. A., and Prestvik, T., 1985, Geological and geochemical classification of the ophiolitic fragments in the Scandinavian Caledonides, *in* Gee, D. G., and Sturt, B. A., eds., The Caledonide orogen—Scandinavia and related areas: Chichester, John Wiley and Sons, p. 657–669.

Færseth, R. B., Thon, A., Larsen, S. G., Sivertsen, A., and Elvestad, L., 1977, Geology of the Lower Paleozoic rocks in the Samnanger–Osterøy area, Major Bergen Arc, western Norway: Norges Geologiske Undersøkelse, v. 334, p. 19–58.

Gale, G. H., 1975, Ocean floor–type basalts from the Grimeli Formation, Stavenes Group, Sunnfjord: Norges Geologiske Undersøkelse, v. 319, p. 47–58.

Gale, G. H. and Roberts, D., 1972, Paleogeographical implications of greenstone petrochemistry in the southern Norwegian Caledonides: Nature, v. 238, p. 60-61.

Gale, G. H. and Roberts, D., 1974, Trace element geochemistry of Norwegian lower Paleozoic basic volcanics and its tectonic implications: Earth and Planetary Science Letters, v. 22, p. 380–390.

Ganguly, J., and Saxena, S. K., 1984, Mixing properties of aluminosilicate garnets: constraints from natural and experimental data, and applications to geothermo-barometry: American Mineralogist, v. 69, p. 88–97.

Gass, I. G., 1968, Is the Troodos Massif of Cyprus a fragment of Mesozoic ocean floor?: Nature, v. 220, p. 39–42.

Gass, I. G., 1980, The Troodos massif: Its role in the unravelling of the ophiolite problem and its significance in the understanding of constructive plate margin processes, *in* Panayiotou, A., ed., Ophiolites: Proceedings of the International Ophiolite Symposium, Cyprus 1979, p. 23–35.

Gass, I. G., and Smewing, J. D., 1973, Intrusion, extrusion and metamorphism at constructive margins: evidence from the Troodos Massif, Cyprus: Nature, v. 243, p. 26-29.

Gee, D. G., 1975, A tectonic model for the central part of the Scandinavian Caledonides: American Journal of Science, v. 275–A, p. 468–515.

Gee, D. G., 1978, The Swedish Caledonides—A short synthesis, *in* Caledonian–Appalachian orogen of the North Atlantic Region: Geological Survey of Canada Paper 78–13, p. 63–72.

Gee, D. G., 1981, The Dictyonema-bearing phyllites at Nordaunevoll, eastern Trøndelag, Norway: Norsk Geologisk Tidsskrift, v. 61, p. 93–95.

Gee, D. G., 1987, Early Caledonian tectonothermal activity in the Scandes—the Finnmarkian and Trondheimian episodes: Geologiska Föreningens i Stockholm Förhandlingar, v. 109, p. 343–345.

Gee, D. G., and Wilson, M. R., 1974, The age of orogenic deformation in the Swedish Caledonides: American Journal of Science, v. 274, p. 1–9.

Gee, D. G., and Zachrisson, E., 1974, Comments on the stratigraphy, faunal provinces, and structure of the metamorphic allochthon, central Scandinavian Caledonides: Geologiska Föreningens i Stockholm Förhandlingar, v. 96, p. 61–66.

Gee, D. G., and Zachrisson, E., 1979, The Caledonides in Sweden: Sverige Geologiske Undersökelse, C769, 48 p.

Gee, D. G., Guezou, J.C., Roberts, D., and Wolff, F. C., 1985, The central–southern part of the Scandinavian Caledonides, *in* Gee, D. G., and Sturt, B. A., eds., The Caledonide orogen—Scandinavia and related areas: Chichester, John Wiley and Sons, p. 109–133.

Ghent, E. D., and Stout, M. Z., 1981, Geobarometry and geothermometry of plagioclase-biotite-garnet-muscovite assemblages: Contributions to Mineralogy and Petrology, v. 76, p. 92–97.

Gill, J. B., 1976, Composition and age of Lau Basin and Ridge volcanic rocks: Implications for evolution of an interarc basin and remnant arc: Geological Society of America Bulletin, v. 87, p. 1384–1395.

Gilotti, J. A., and Kumpulainen, R., 1986, Strain softening induced ductile flow in the Särv thrust sheet, Scandinavian Caledonides: Journal of Structural Geology, v. 8, p. 441–455.

Gjelsvik, T., 1946, Anorthosittkomplekset i Heidal: Norsk Geologisk Tidsskrift, v. 26, p. 1.

Goldman, D. S., and Albee, A. L., 1977, Correlation of Mg/Fe partitioning between garnet and biotite with $O^{18}/O^{16}$ partitioning between quartz and magnetite: American Journal of Science, v. 277, p. 750–761.

Gorbatschev, R., 1985, Precambrian basement of the Scandinavian Caledonides, *in* Gee, D. G., and Sturt, B. A., eds., The Caledonide orogen—Scandinavia and related areas: Chichester, John Wiley and Sons, p. 197–212.

Grenne, T., 1988, Marginal basin type metavolcanics of the Hersjø Formation, eastern Trondheim district, central Norwegian Caledonides: Norges Geologiske Undersøkelse, v. 412, p. 29–42.

Grenne, T., and Lagerblad, B., 1985, The Fundsjø Group, central Norway—a Lower Paleozoic island arc sequence: geochemistry and regional implications, *in* Gee, D. G., and Sturt, B. A., eds., The Caledonide orogen—Scandinavia and related areas: Chichester, John Wiley and Sons, p. 745–760.

Grenne, T., and Roberts, D., 1980, Geochemistry and volcanic setting of the Ordovician Forbordfjell and Jonsvatn greenstones, central Norwegian Caledonides: Contributions to Mineralogy and Petrology, v. 74, p. 374–386.

Guezou, J. C., 1978, Geology and structure of the Dombås–Lesja area, southern Trondheim region, south-central Norway: Norges Geologiske Undersøkelse, v. 340, p. 1–34.

Hamelin, B., Dupré, B., Brévart, O., and Allègre. C. J., 1988, Metallogenesis at paleo–spreading centers: Lead isotopes in sulfides, rocks and sediments from the Troodos ophiolite (Cyprus): Chemical Geology, v. 68, p. 229–238.

Hamilton, W. B., 1988, Plate tectonics and island arcs: Geological Society of America Bulletin, v. 100, p. 1503–1527.

Hanmer, S., and Passchier, C., 1991, Shear-sense indicators: a review: Geological Society of Canada Paper 90-17, 72 p.

Hanson, E., 1971, Strain facies: New York, Springer-Verlag, 207 p.

Harland, W. B. and Gayer, R. A., 1972, The Arctic Caledonides and earlier oceans: Geological Magazine, v. 109, p. 289–314.

Harte, B., and Henley, K. J., 1966, Occurrence of compositionally zoned almanditic garnets in regionally metamorphosed rocks: Nature, v. 210, p. 689.

Hatcher, R. D., Sturt, B. A., and Ramsay, D. M., 1991, The central and southern Norway thrust stacks, I—Crustal contrasts along the Precambrian Baltic margin, or in source and transport mechanisms: Geological Society of America Abstracts with Programs, v. 23, p. A311.

Hawkins, J. W., 1976, Petrology and geochemistry of basaltic rocks of the Lau Basin: Earth and Planetary Science Letters, v. 28, p. 283–297.

Hawkins, J. W., and Melchior, J. T., 1985, Petrology of Mariana Trough and Lau Basin basalts: Journal of Geophysical Research, v. 90, p. 11431–11468.

Hawkins, J. W., Bloomer, S. H., Evans, C. A., and Melchior, J. T., 1984, Evolution of intra-oceanic arc-trench systems: Tectonophysics, v. 102, p. 174–205.

Hedström, H., 1930, Om Ordoviciska fossil fran Ottadalen i det centrala Norge: Avhandlinger Utgitt av det Norske Vitenskaps–Academi i Oslo, Matematisk–Naturvidenskapelig Klasse, v. 10, p. 1–10.

Heinriksen, H., 1981, A major unconformity within metamorphic Lower Paleozoic sequence of the Major Bergen Arc, Osterøy, western Norway: Norges Geologiske Undersøkelse, v. 367, p. 65–75.

Hickey, R. L., and Frey, F. A., 1982, Geochemical characteristics of boninite series volcanics: implications for their source: Geochimica et Cosmochimica Acta, v. 46, p. 2099–2115.

Hodges, K. V., and Crowley, P. D., 1985, Error estimation and empirical geothermobarometry for pelitic systems: American Mineralogist, v. 70, p. 702–709.

Hodges, K. V., and Spear, F. S., 1982, Geothermometry, geobarometry and the $Al_2SiO_5$ triple point at Mt. Moosilauke, New Hampshire: American Mineralogist, v. 67, p. 1118–1134.

Holtedahl, O., 1920, Paleogeography and diastrophism in the Atlantic–Arctic region during Paleozoic time: American Journal of Science, v. 49, p. 1–25.

Horne, G. S., 1979, Mélange in the Trondheim Nappe suggests a new tectonic model for central Norwegian Caledonides: Nature, v. 281, p. 267–270.

Hossack, J. R., 1985, The role of thrusting in the Scandinavian Caledonides, *in* Gayer, R. A., ed., The tectonic evolution of the Caledonide-Appalachian orogen: Wiesbaden, Braunschweig, p. 97–116.

Ingdahl, S. E., 1989, The Upper Ordovician–Lower Silurian rocks in the Os area, Major Bergen Arc, western Norway: Norsk Geologisk Tidsskrift, v. 69, p. 163–175.

Jenkyns, H. C., 1986, Pelagic environments, *in* Reading, H. G., ed., Sedimentary environments and facies, p. 343–397.

Kleine–Hering, R., 1969, Die Geologie des Alvdal–Gebietes: Unpublished thesis, Mainz, 89 p.

Klingspor, I., and Gee, D. G., 1981, Isotopic age-determination studies of the Trøndelag trondhjemites: Terra cognita, v. 1, p. 55.

Kollung, S., 1990, The Surna, Rinna, and Orkla nappes of the Surnadal–Orkdal district, southwestern Trondheim region: Norges Geologiske Undersøkelse, v. 418, p. 9–17.

Kretz, R., 1973, Kinetics of the crystallization of garnet at two localities near Yellowknife: Canadian Mineralogist, v. 12, p. 1–20.

Krill, A. G., 1980, Tectonics of the Oppdal area, central Norway: Geologiska Föreningens i Stockholm Förhandlingar, v. 102, p. 523–530.

Kumpulainen, R., 1980, Upper Proterozoic stratigraphy and depositional environments of the Tossåsfjället Group, Särv Nappe, southern Swedish Caledonides: Geologiska Föreningens i Stockholm Förhandlingar, v. 102, p. 531–550.

Kvale, A., 1960, The nappe area of the Caledonides in western Norway: International Geological Congress, XXI Session Norden. Guide to excursions no. A7 and no. C4, 43 p.

Labotka, T. C., 1991, Chemical and physical properties of fluids, *in* Kerrick, D. M., ed., Contact metamorphism: Reviews in Mineralogy, v. 26, p. 43–104.

Lagerblad, B., 1984a, Tectono-metamorphic relationships of the Gula–Fundsjø Group contact zone in the Inndalen–Faeren area, Trøndelag, central Norwegian Caledonides: Geologiska Föreningens i Stockholm Förhandlingar, v. 105, p. 131–153.

Lagerblad, B., 1984b, Geology, mineral reactions and mineral chemistry in the rocks of the northern part of the Trondheim nappe complex, central Scandinavian Caledonides: Unpublished thesis, University of Lund, Sweden, 152 p.

Laird, J., and Albee, A. L., 1981, Pressure, temperature, and time indicators in mafic schist: their application in reconstructing the polymetamorphic history of Vermon: American Journal of Science, v. 281, p. 127–143.

Leake, B. E., 1978, Nomenclature of amphiboles: American Mineralogist, v. 63, p. 1023–1052.

Lieungh, B., 1970, Map sheet Alvdal 1:50,000 (unpublished): Rørosprosjektet, University of Oslo, Norway.

Lisle, R. J., 1984, Strain discontinuities within the Seve–Köli nappes complex, Scandinavian Caledonides: Journal of Structural Geology, v. 6, p. 101–110.

Lister, G. S., 1993, Comment on "Do smoothly curving, spiral-shaped inclusion trails signify porphyroblast rotation" by T. H. Bell, A. Forde, and N. Hayward: Geology, v. 21, p. 479–480.

Mawer, C. K., and Williams, P. F., 1991, Progressive folding and foliation development in a sheared, coticule-bearing phyllite: Journal of Structural Geology, v. 13, p. 539–555.

Meijer, A., 1980, Primitive arc volcanism and a boninite series: Examples from western Pacific island arcs, *in* Hayes, D. E., ed., Tectonic and geologic evolution of southwest Asian seas and islands: American Geophysical Union Monograph 3, p. 269–282.

Meneilly, A. W., and Storey, B. C., 1986, Ductile thrusting within subduction complex rocks on Signy Island, South Orkney Islands: Journal of Structural Geology, v. 8, p. 457–472.

Métour, D. R., Tegyey, M., Béchennec, F., Beurrier, M., and Villey, M., 1990, Subduction and obduction: two stages in the Eo-Alpine tectonometamorphic evolution of the Oman Mountains, *in* Robertson, A. H. F., Searle, M. P., and Ries, A. C., eds., The geology and tectonics of Oman: Geological Society Special Publication Number 49, p. 327–339.

Mies, J. W., 1991, Planar dispersion of folds in ductile shear zones and kinematic interpretation of fold-hinge girdles: Journal of Structural Geology, v. 13, p. 281–297.

Miyashiro, A., 1973a, The Troodos ophiolite complex was probably formed in an island arc: Earth and Planetary Science Letters, v. 19, p. 218–224.

Miyashiro, A., 1973b, Metamorphism and metamorphic belts: New York, John Wiley and Sons, 492 p.

Moores, E. M., and Vine, F. J., 1971, The Troodos Massif, Cyprus, and other ophiolites as oceanic crust: evaluation and implications: Philosophical Transactions of the Royal Society of London, Serial A, v. 268, p. 443–466.

Moores, E. M., Robinson, P. T., Malpas, J., and Xenophonotos, C., 1984, Model for the origin of the Troodos massif, Cyprus, and other mideast ophiolites; Geology, v. 12, p. 500–503.

Mosson, P., Quenardel, J. M., and Quesnel, G, 1972, Essais de corrélations lithostratigraphiques dans le Sud du Bassin de Trondheim, région de l'Einunnfjell: Sciences de la Terre, v. 17, p. 289–302.

Naterstad, J., 1976, Comment on the Lower Paleozoic unconformity in west Norway: American Journal of Science, v. 276, p. 394–397.

Nicholson, R., 1966, On the relations between volcanic and other rocks in the fossiliferous east Lomivann area of Norwegian Sulitjelma: Norges Geologiske Undersøkelse, v. 242, p. 143–156.

Nilsen, O., 1971, Sulphide mineralization and wall rock alteration at Rødhammeren mine, Sør-Trøndelag, Norway: Norsk Geologisk Tidsskrift, v. 54, p. 329–354.

Nilsen, O., 1974, Mafic and ultramafic inclusions from the initial (Cambrian?) volcanism in the central Trondheim region, Norway: Norsk Geologisk Tidsskrift, v. 54, p. 337–359.

Nilsen, O., 1978, Caledonian sulphide deposits and minor iron–formations from the southern Trondheim region, Norway: Norges Geologiske Undersøkelse, v. 340, p. 35–85.

Nilsen, O., 1988, The tectonostratigraphic setting of stratabound sulphide deposits in the southern Trondheim region, central Norwegian Caledonides: Norges Geologiske Undersøkelse, v. 412, p. 55–66.

Nilsen, O., and Mukherjee, A. D., 1972, Geology of the Kvikne mines with special reference to the sulphide ore mineralization: Norsk Geologisk Tidsskrift, v. 52, p. 151–192.

Nilsen, O., and Wolff, F. C., 1989, Geologisk kart over Norge, berggrunnskart Røros og Sveg, 1:250,000: Norges Geologiske Undersøkelse.

Oudin, E., and Constantinou, G., 1984, Black smoker chimney fragments in Cyprus sulphide deposits: Nature, v. 308, p. 349–353.

Passchier, C. W., Trouw, R. A. J., Zwart, H. J., and Vissers, R. L. M., 1992, Porphyroblast rotation: eppur si muove?: Journal of Metamorphic Geology, v. 10, p. 283–294.

Peacy, J. S., 1964, Reconnaissance of the Tømmerås anticline: Norges Geologiske Undersøkelse, v. 227, p. 13–84.

Pearce, J. A., 1975, Basalt chemistry used to investigate past tectonic environments on Cyprus: Tectonophysics, v. 25, p. 41–67.

Pearce, J. A., 1980, Geochemical evidence for the genesis and eruptive setting of lavas from Tethyan ophiolites, *in* Panayiotou, A., ed., Ophiolites: Proceedings of the International Ophiolite Symposium, Cyprus, 1979, p. 261–272.

Pearce, J. A., 1982, Trace element characteristics of lavas from destructive plate margins, in Thorpe, R.S., ed., Andesites: Orogenic andesites and related rocks: Chichester, John Wiley and Sons, p. 526–548.

Pearce, J. A., and Cann, J. R., 1971, Ophiolite origin investigated by discriminant analysis using Ti, Zr and Y: Earth and Planetary Science Letters, v. 12, p. 339–349.

Pearce, J. A., and Cann, J. R., 1973, Tectonic setting of basic volcanic rocks determined using trace element analysis: Earth and Planetary Science Letters, v. 19, p. 290–300.

Pearce, J. A., and Flower, M. F. J., 1977, The relative importance of petrogenetic variables in magma genesis at accreting plate margins: a preliminary investigation: Journal of the Geological Society of London, v. 134, p. 103–127.

Pearce, J. A., and Norry, M. J., 1979, Petrogenetic implications of Ti, Zr, Y, and Nb variations in volcanic rocks: Contributions to Mineralogy and Petrology, v. 69, p. 33-47.

Pearce, J. A., Lippard, S. J., and Roberts, S., 1984, Characteristics and tectonic significance of supra–subduction zone ophiolites, *in* Kokelaar, B. P., and Howell, M. F., eds., Marginal basin geology: Geological Society Special Publication 16, p. 77–94.

Pedersen, R. B., and Hertogen, J., 1990, Magmatic evolution of the Karmøy Ophiolite Complex, SW Norway: Relationships between MORB-IAT–boninitic–calc-alkaline and alkaline magmatism: Contributions to Mineralogy and Petrology, v. 104, p. 277–293.

Pedersen, R. B., Furnes, H., and Dunning, G., 1988, Some Norwegian ophiolite complexes revisited, *in* Kristoffersen, Y., ed., Progress in studies of the lithosphere in Norway: Norges Geologiske Undersøkelse Special Publication 3, p. 80–85.

Perchuk, L. L., and Lavrent'eva, I. V., 1983, Experimental investigation of exchange equilibria in the system cordierite-garnet-biotite, *in* Saxenea, S.K., ed., Kinetics and equilibrium in mineral reactions: Advances in Physical Chemistry, v. 3, p. 199–239.

Powell, R., and Hodges, T. J. B., 1988, An internally consistent dataset with uncertainties and correlations: 3. applications to geobarometry, worked examples and a computer program: Journal of Metamorphic Geology, v. 6, p. 173–204.

Powell, C. McA., and Vernon, R. H., 1979, Growth and rotation history of garnet porphyroblasts with inclusion spirals in a Karakoram schist: Tectonophysics, v. 54, p. 25–43.

Quenardel, J. M., 1972, Un exemple de niveau repere dans les formations métamorphiques: les minéralisations a sulfures et a oxydes a l'Ouest du lac Savalen: Sciences de la Terre, v. 17, p. 303–313.

Rainey, D. I., 1980, The structure and petrology of the Gula Group, central Norwegian Caledonides, with special reference to sulfide mineralisation—Implications to the geology of the Trondheim Nappe: Unpublished Ph.D. thesis, University of Edinburgh, 322 p.

Ramberg, H., 1967, The Scandinavian Caledonide as studied by centrifuged dynamic models: Bulletin of the Geologic Institute of Uppsala, v. 43, p. 1–72.

Ramberg, H., and Ghosh, S. K., 1968, Deformation structures in the Hovin Group schists in the Hommelvik–Hell region (Norway): Tectonophysics, v. 6, p. 311–330.

Ramsay, D. M., and Sturt, B. A., 1976, The syn–metamorphic emplacement of the Magerøy nappe: Norsk Geologisk Tidsskrift, v. 56, p. 291–307.

Ramsay, J. G., 1967, Folding and fracturing of rocks: New York, McGraw–Hill, 568 p.

Ramsay, J. G., and Graham, R. H., 1970, Strain variation in shear belts: Canadian Journal of Earth Sciences, v. 7, p. 786–813.

Ramsay, J. G., and Huber, M. I., 1987, The techniques of modern structural geology, Volume 2: Folds and fractures: London, Academic Press, p. 309–700.

Rautenschlein, M., Jenner, G. A., Hertogen, J., Hofman, A. W., Kerrich, R., Schmincke, H. U., and White, W. M., 1985, Isotopic and trace element composition of volcanic glasses from the Akaki Canyon, Cyprus: implications for the origin of the Troodos ophiolite: Earth and Planetary Science Letters, v. 75, p. 369-383.

Reagan, M. K., and Meijer, A., 1984, Geology and geochemistry of early arc-volcanic rocks from Guam: Geological Society of America Bulletin, v. 95, p. 701–713.

Reymer, A. P. S., Boelrijk, N. A. I. M., Hebeda, E. H., Priem, H. N. A., Verdurmen, E. A. T., and Verschure, R. H., 1980, A note on Rb–Sr whole–rock ages in the Seve nappe of the central Scandinavian Caledonides: Norsk Geologisk Tidsskrift, v. 60, p. 139–147.

Roberts, D., 1967, Structural observations from the Kopperå–Riksgrense area and discussion of the tectonics of Stjørdalen and the N.E. of Trondheim region: Norges Geologiske Undersøkelse, v. 245, p. 64–122.

Roberts, D., 1971, Stress regime and distribution of a conjugate fold system from the Trondheim region, central Norway: Tectonophysics, v. 12, p. 155–165.

Roberts, D., 1979, Structural sequence in the Limingen–Tunnsjøen area of the Grong district, Nord-Trøndelag: Norges Geologiske Undersøkelse, v. 354, p. 101–114.

Roberts, D. and Sturt, B. A., 1980, Caledonian deformation in Norway: Journal of the Geological Society of London, v. 137, p. 241–250.

Roberts, D. and Wolff, F. C., 1981, Tectonostratigraphic development of the Trondheim region Caledonides, central Norway: Journal of Structural Geology, v. 3, p. 487–494.

Roberts, D. and Gee, D. G., 1985, An introduction to the structure of the Scandinavian Caledonides, *in* Gee, D. G., and Sturt, B.A., eds., The Caledonide orogen—Scandinavia and related areas: Chichester, John Wiley and Sons, p. 55–68.

Roberts, D., Springer, J., and Wolff, F. C., 1970, Evolution of the Caledonides in the northern Trondheim region, central Norway: a review: Geological Magazine, v. 107, p. 133–145.

Roberts, D., Grenne, T., and Ryan, P. D., 1984, Ordovician marginal basin development in the central Norwegian Caledonides, *in* Kokelaar, B. P., and Howell, M. F., eds., Marginal basin geology: Geological Society Special Publication 16, p. 233–244.

Roberts, D., Sturt, B. A., and Furnes, H., 1985, Volcanite assemblages and environments in the Scandinavian Caledonides and the sequential development history of the mountain belt, *in* Gee, D. G., and Sturt, B. A., eds., The Caledonide orogen—Scandinavia and related areas: Chichester, John Wiley and Sons, p. 919–930.

Robertson, A. H. F., and Hudson, J. D., 1974, Pelagic sediments in the Cretaceous and Tertiary history of the Troodos massif, Cyprus, *in* Hsü, K. J., and Jenkyns, H. C., eds., Pelagic sediments: on land and under the sea: Oxford, Blackwell Scientific Publications, Osney Mead, p. 403–436.

Robinson, P., Spear, F. S., Schumacher, J. C., Laird, J., Klein, C., Evans, B. W., and Doolan, B. L., Phase relations of metamorphic amphiboles: natural occurrence and theory, in Veblen, D. R., and Ribble, P. H., eds., Amphiboles: petrology and experimental phase relations: Review in Mineralogy, v. 9B: pp. 1–227.

Rosenfeld, J. L., 1968, Garnet rotations due to major Paleozoic deformations in southeast Vermont, *in* Zen, E. A., White, W.S., Hadley, J. B., and Thompson, J. B., Jr., eds., Studies of Appalachian geology: northern and maritime: New York, John Wiley and Sons, p. 185–202.

Rosenfeld, J. L., 1970, Rotated garnets in metamorphic rocks: Geological Society of America Special Paper 129, 105 p.

Rui, I. J., 1972, Geology of the Røros district, south-eastern Trondheim region, with a special study of the Kjøliskarvene–Holtsjøen area: Norsk Geologisk Tidsskrift, v. 52, p. 1–21.

Rui, I. J., 1973, Geology and structures of the Røstvangen sulphide deposit in the Kvikne district, central Norwegian Caledonides: Norsk Geologisk Tidsskrift, v. 53, p. 433–442.

Rui, I. J., and Nilsen, O., 1988, Geological map of the Einunnfjell anticline (map sheet Alvdal and Kvikneskogen), 1:50,000 (unpublished).

Ryan, P. D., Williams, D. M., and Skevington, D., 1980, A revised interpretation of the Løkken-Meldal area, Sør Trøndelag, Norway, *in* Wones, D. R., ed., The Caledonides in the U.S.A.: Virginia Polytechnic Institute Department of Geological Sciences Memoir 2, p. 99–103.

Saunders, A. D., and Tarney, J., 1984, Geochemical characteristics of basaltic volcanism within back-arc basins, *in* Kokelaar, B. P., and Howell, M. F., eds., Marginal basin geology: Geological Society Special Publication 16, p. 59–76.

Schaefer, S. J., and Morton, P., 1991, Two komatiitic pyroclastic units, Superior Province, northwestern Ontario: their geology, petrography, and correlation: Canadian Journal of Earth Science, v. 28, p. 1455–1470.

Shervais, J. W., 1982, Ti–V plots and the petrogenesis of modern and ophiolitic lavas: Earth and Planetary Science Letters, v. 59, p. 101–118.

Schoneveld, C., 1977, A study of some typical inclusion patterns in strongly paracrystalline rotated garnets: Tectonophysics, v. 39, p. 453–471.

Simpson, C., 1985, Deformation of granitic rocks across the ductile-brittle transition: Journal of Stuctural Geology, v. 7, p. 503–507.

Sjöstrom, H., 1983, The Seve–Köli nappe complex of the Handöl–Storlien–Essandsjøen area, Scandinavian Caledonides: Geologiska Föreningens i Stockholm Förhandlingar, v. 105, p. 93–118.

Solli, T., 1981, The geology of the Torvastad Group, the cap rocks to the Karmøy ophiolite: Unpublished cand. real. thesis, University of Bergen, Norway, 272 p.

Solyom, Z., Andréasson, P. G., and Johansson, I., 1979, Geochemistry of amphibolites from Mt. Sylarna, Central Scandinavian Caledonides: Geologiska Föreningens i Stockholm Förhandlingar, v. 101, p. 17–25.

Spear, F. S., and Peacock, S. M., 1989, Metamorphic pressure-temperature-time paths: International Geological Congress Short Course in Geology 7. American Geophysical Union, Washington, D.C.

Spry, A., 1963, The origin and significance of snowball structure in garnet: Journal of Petrology, v. 4, p. 211–222.

Steltenpohl, M. G., Andresen, A., and Tull, J. F., 1990, Lithostratigraphic correlation of the Salangen (Ofoten) and Balsfjord (Troms) Groups: evidence for the post–Finnmarkian unconformity, north Norwegian Caledonides: Norges Geologiske Undersøkelse, v. 418, p. 61–77.

Stephens, M. B., and Gee, D. G., 1985, A tectonic model for the evolution of the eugeoclinal terranes in the central Scandinavian Caledonides, *in* Gee, D. G., and Sturt, B. A., eds., The Caledonide orogen—Scandinavia and related areas: Chichester, John Wiley and Sons, p. 953–978.

Stephens, M. B., Gustavson, M., Ramberg, I. B., and Zachrisson, E., 1985, The Caledonides of central–north Scandinavia—a tectonostratigraphic review, *in* Gee, D. G., and Sturt, B. A., eds., The Caledonide orogen—Scandinavia and related areas. Chichester, John Wiley and Sons, p. 135–162.

Stern, R. J., and Bloomer, S. H., 1992, Subduction zone infancy: Examples from the Eocene Izu-Bonin-Mariana and Jurassic California arcs: Geological Society of America Bulletin, v. 104, p. 1621–1636.

Strand, T., 1951, The Sel and Vågå map areas: Norges Geologiske Undersøkelse, v. 178, 117 p.

Strand, T., 1961, The Scandinavian Caledonides, a review: American Journal of Science, v. 259, p. 161–172.

Strand, T. and Kulling, O., 1972, Scandinavian Caledonides: New York, John Wiley and Sons, 302 p.

Sturt, B. A., 1984, The accretion of ophiolitic terranes in the Scandinavian Caledonides: Geologie en Mijnbouw, v. 63, p. 201–212.

Sturt, B. A. and Thon, A., 1976, Discussion: The age of orogenic deformation in the Swedish Caledonides: American Journal of Science, v. 276, p. 385–390.

Sturt, B. A., and Thon, A., 1978a, A major early Caledonian igneous complex and a profound unconformity in the Lower Paleozoic sequence of Karmøy, southwest Norway: Norsk Geologisk Tidsskrift, v. 58, p. 221–228.

Sturt, B. A. and Thon, A., 1978b, An ophiolite complex of probable early Caledonian age discovered on Karmøy: Nature, v. 275, p. 538–539.

Sturt, B. A., and Roberts, D., 1991, Tectonostratigraphic relationships and obduction histories of Scandinavian ophiolitic terranes, *in* Peters, Tj., Nicolas, A., and Coleman, R.G., eds., Ophiolite genesis and evolution of the oceanic lithosphere: Proceedings of the Ophiolite Conference, 1990, Ministry of Petroleum and Minerals, Sultanate of Oman, p. 745–769.

Sturt, B. A., Miller, J. A., and Fitch, F. J., 1967, The age of alkaline rocks from west Finnmark, northern Norway, and their bearing on the dating of the Caledonian orogeny: Norsk Geologisk Tidsskrift, v. 47, p. 255–273.

Sturt, B. A., Pringle, I. R., and Ramsay, D. M., 1978, The Finnmarkian phase of the Caledonian orogeny: Journal of the Geological Society of London, v. 135, p. 597–610.

Sturt, B. A., Thon, A., and Furnes, H., 1979, The Karmøy ophiolite, southwest Norway: Geology, v. 7, p. 316–320.

Sturt, B. A., Ramsay, D. M., and Bøe, R., 1991a, The Otta nappe—Significance for Scandinavian Caledonide reconstruction: Terra Abstracts, v. 3, p. 215–216.

Sturt, B. A., Ramsay, D. M., and Neuman, R. B., 1991b, The Otta Conglomerate, the Vågåmo Ophiolite—further indications of early Ordovician orogenesis in the Scandinavian Caledonides: Norsk Geologisk Tidsskrift, v. 71, p. 107–115.

Sun, S. S., Nesbitt, R. W., and McCulloch, M. T., 1989, Geochemistry and petrogenesis of Archaean and early Proterozoic siliceous high-magnesian basalts, *in* Crawford, A. J., ed., Boninites: London, Unwin Hyman, p. 149–173.

Thompson, A. B., 1976, Mineral reactions in pelitic rocks II: calculations of some P-T-X (Fe-Mg) phase relations: American Journal of Science, v. 276, p. 425–454.

Thon, A., 1980, Steep shear zones in the basement and associated deformation of the cover sequence on Karmøy, SW Norwegian Caledonides: Journal of Structural Geology, v.2, p. 75–80.

Thon, A., 1985a, Late Ordovician and Early Silurian cover sequences to the west Norwegian ophiolite fragments: stratigraphy and structural evolution, *in* Gee, D. G., and Sturt, B. A., eds., The Caledonide orogen—Scandinavia and related areas: Chichester, John Wiley and Sons, p. 407-415.

Thon, A., 1985b, The Gullfjellet ophiolite complex and the structural evolution of the major Bergen arc, west Norwegian Caledonides, *in* Gee, D. G., and Sturt, B. A., The Caledonide orogen—Scandinavia and related areas: Chichester, John Wiley and Sons, p. 671–677.

Thy, P., and Moores, E. M., 1988, Crustal accretion and tectonic setting of the Troodos ophiolite, Cyprus: Tectonophysics, v. 147, p. 221–245.

Tobisch, O. T., and Paterson, S. R., 1988, Analysis and interpretation of composite foliations in areas of progressive deformation: Journal of Structural Geology, v. 10, p. 745–754.

Townsend, C., and Gayer, R. A., 1989, The timing of orogenesis in northern Norway: did the Finnmarkian Orogeny occur?, *in* Gayer, R. A., ed., The Caledonide geology of Scandinavia, p. 63–65.

Tracy, R. J., 1982, Compositional zoning and inclusions in metamorphic minerals, *in* Ferry, J. M., ed., Characterization of metamorphism through mineral equilibria: Reviews in Mineralogy , v. 10, p. 355–397.

Tracy, R. J., Robinson, P., and Thompson, A. B., 1976, Garnet composition and zoning in the determination of temperature and pressure metamorphism, central Massachusetts: American Mineralogist, v. 61, p. 762-775.

Tullis, J., and Yund, R. A., 1985, Dynamic recrystallization of feldspar: a mechanism for ductile shear zone formation: Geology, v. 13, p. 238–241.

Turner, F. J., 1981, Metamorphic petrology, 2nd edition: New York, McGraw-Hill, 524 p.

Törnebohm, A. E., 1888, Om fjällproblemet: Geologiska Föreningens i Stockholm Förhandlingar, v. 10, p. 328-336.

Vogt, T., 1941, Geological notes on the Dictyonema locality and the upper Guldal district in the Trondheim area: Norsk Geologisk Tidsskrift, v. 20, p. 171–192.

Vogt, T., 1945, The geology of part of the Hølonda–Horg district, a type area in the Trondheim region: Norsk Geologisk Tidsskrift, v. 25, p. 449–536.

White, W. S., and Jahns, R. H., 1950, The structure of central and east-central Vermont: Journal of Geology, v. 58, p. 179–220.

Williams, P. F., and Schoneveld, C., 1981, Garnet rotations and the development of axial plane crenulation cleavage: Tectonophysics, v. 78, p. 307–334.

Williams, P. F., and Zwart, H. J., 1977, A model for the development of the Seve–Köli Caledonian nappe complex, *in* Saxena, S. K., and Bhattacharji , S., eds., Energetics of geological processes: New York, Springer-Verlag, p. 169–187.

Wilson, M., 1989, Igneous petrogenesis: London, Unwin Hyman, 466 p.

Winkler, H. G. F., 1979, Petrogenesis of metamorphic rocks, 5th edition: New York, Springer-Verlag, 348 p.

Wolff, F. C., 1964, Stratigraphical position of the Gudå conglomerate zone: Norges Geologiske Undersøkelse, v. 227, p. 85–93.

Wolff, F. C., 1967, Geology of the Meråker area as a key to the eastern part of the Trondheim region: Norges Geologiske Undersøkelse, v. 245, p. 123–146.

Wolff, F. C., 1973, Meråker og Faeren: Beskrivelse til de berggrunnsgeologiske kart—1:50,000: Norges Geologiske Undersøkelse, Skrifter 5, v. 295, 42 p.

Wolff, F. C., 1976, Geologisk kart over Norge, berggrunnskart Trondheim, 1:250,000. Norges Geologiske Undersøkelse.

Woodsworth, G. J., 1977, Homogenization of zoned garnets from pelitic schists: Canadian Mineralogist, v. 15, p. 230–242.

Yochelson. E. L., 1963, Gastropods from the Otta conglomerate: Norsk Geologisk Tidsskrift, v. 43, p. 75–81.

# APPENDICES

# APPENDIX 1
## Electron Microprobe Analyses

# APPENDIX 1

## Electron Microprobe Analyses

### *Analytical Techniques*

Analyses of garnet, amphibole, biotite, muscovite, feldspar, chlorite, and epidote were run on the CAMECA SX-50 (wavelength-dispersive) electron microprobe at the University of Tennessee, Knoxville. Polished thin sections were photographed, mapped, and carbon-coated prior to analysis. All analyses were run at an accelerating voltage of 15 Kv. A beam current of 30 nA was used for garnet, chlorite, and epidote, and 20 nA for phases containing the volatile elements Na or K (micas, amphibole, feldspar). Beam diameter was dependent on grain size and elements analyzed; generally 5 mm for garnet, and 10 mm for feldspar and micas. Natural mineral standards included the range of compositions of the elements analyzed. Matrix corrections were made by the ZAF procedure.

The electron microprobe cannot distinguish between $Fe^{2+}$ and $Fe^{3+}$, or between O and (OH) in hydrous phases. The routines used for micas, chlorite, epidote, and amphibole, however, automatically calculate a certain amount of O in order to bring the analysis to an acceptable total. Total Fe is reported as FeO. Cations are reported on the following basis:

| | |
|---|---|
| Garnet | 12 (O) |
| Biotite, muscovite | 12 (O, OH, F, Cl) |
| Feldspar | 8 (O) |
| Chlorite | 18 (O, OH) |
| Epidote | 26 (O, OH) |

Amphibole cations were calculated using the standard formula from Leake (1978), and site terminology from Robinson *et al.* (1982):

$$A_{0\text{-}1}(M4)_2(M1, 2, 3)_5{}^{VI}(T1)_4(T2)_4{}^{IV}O_{22}\,(OH, F, Cl)_2$$

Amphibole formulae were then derived by recalculating total cations to 13 exclusive of K, Na, Ca, using the reasonable crystal-chemical limits set forth by Leake (1978) and Robinson *et al.* (1982).

Appendix 1A: Garnet Analyses

Sample A1718

| Analysis #: | 304 | 305 | 306 | 307 | 308 | 309 | 310 | 311 | 312 | 313 | 314 | 315 | 316 | 317 | 318 | 319 | 320 | 321 | 322 |
|---|---|---|---|---|---|---|---|---|---|---|---|---|---|---|---|---|---|---|---|
| SiO2 | 36.63 | 36.97 | 37.04 | 37.00 | 36.75 | 36.89 | 36.16 | 36.80 | 36.74 | 36.55 | 36.89 | 36.40 | 36.60 | 36.67 | 36.52 | 36.99 | 36.49 | 36.79 | 37.10 |
| TiO2 | 0.07 | 0.06 | 0.08 | 0.06 | 0.14 | 0.16 | 0.14 | 0.12 | 0.12 | 0.15 | 0.15 | 0.13 | 0.13 | 0.14 | 0.13 | 0.13 | 0.03 | 0.04 | 0.06 |
| Al2O3 | 20.73 | 21.30 | 21.36 | 21.20 | 20.94 | 21.03 | 20.84 | 21.10 | 20.87 | 20.92 | 21.09 | 20.72 | 20.96 | 20.95 | 21.19 | 21.06 | 20.84 | 21.05 | 21.25 |
| Cr2O3 | 0.00 | 0.03 | 0.02 | 0.01 | 0.03 | 0.00 | 0.00 | 0.03 | 0.05 | 0.00 | 0.00 | 0.00 | 0.02 | 0.01 | 0.00 | 0.03 | 0.02 | 0.01 | 0.03 |
| MgO | 2.70 | 2.59 | 2.25 | 2.13 | 1.80 | 1.63 | 1.57 | 1.53 | 1.63 | 1.52 | 1.59 | 1.61 | 1.65 | 1.73 | 1.74 | 1.80 | 2.21 | 2.70 | 2.82 |
| CaO | 5.54 | 6.29 | 6.97 | 7.47 | 8.51 | 9.32 | 8.99 | 8.68 | 8.45 | 8.53 | 8.44 | 8.62 | 8.31 | 8.83 | 8.66 | 8.53 | 7.01 | 5.90 | 5.46 |
| MnO | 0.59 | 0.71 | 1.25 | 1.39 | 1.72 | 1.93 | 2.50 | 2.68 | 2.94 | 2.96 | 2.95 | 2.96 | 2.54 | 2.03 | 1.94 | 1.74 | 1.18 | 0.51 | 0.63 |
| FeO | 31.58 | 31.44 | 30.43 | 30.08 | 29.07 | 28.09 | 27.56 | 28.21 | 28.64 | 28.63 | 28.85 | 28.51 | 28.84 | 28.89 | 28.75 | 29.11 | 29.97 | 31.92 | 32.06 |
| total | 97.83 | 99.39 | 99.40 | 99.33 | 98.95 | 99.05 | 97.77 | 99.14 | 99.45 | 99.25 | 99.95 | 98.95 | 99.05 | 99.25 | 98.93 | 99.39 | 97.75 | 98.91 | 99.40 |
| Si | 2.993 | 2.973 | 2.977 | 2.978 | 2.973 | 2.976 | 2.962 | 2.973 | 2.968 | 2.961 | 2.965 | 2.959 | 2.965 | 2.963 | 2.956 | 2.977 | 2.984 | 2.976 | 2.982 |
| Ti | 0.004 | 0.004 | 0.005 | 0.003 | 0.008 | 0.010 | 0.009 | 0.007 | 0.007 | 0.009 | 0.009 | 0.008 | 0.008 | 0.008 | 0.008 | 0.008 | 0.002 | 0.003 | 0.004 |
| Al | 1.996 | 2.019 | 2.023 | 2.011 | 1.997 | 1.999 | 2.011 | 2.009 | 1.987 | 1.997 | 1.997 | 1.985 | 2.002 | 1.995 | 2.022 | 1.998 | 2.008 | 2.007 | 2.013 |
| Cr | 0.000 | 0.002 | 0.001 | 0.000 | 0.002 | 0.000 | 0.000 | 0.002 | 0.003 | 0.000 | 0.000 | 0.000 | 0.002 | 0.000 | 0.000 | 0.002 | 0.001 | 0.001 | 0.002 |
| Mg | 0.328 | 0.311 | 0.270 | 0.256 | 0.217 | 0.196 | 0.192 | 0.184 | 0.196 | 0.184 | 0.190 | 0.195 | 0.199 | 0.209 | 0.210 | 0.215 | 0.269 | 0.325 | 0.338 |
| Ca | 0.485 | 0.542 | 0.600 | 0.644 | 0.737 | 0.806 | 0.789 | 0.751 | 0.732 | 0.740 | 0.726 | 0.751 | 0.721 | 0.764 | 0.751 | 0.736 | 0.614 | 0.511 | 0.470 |
| Mn | 0.041 | 0.048 | 0.085 | 0.095 | 0.118 | 0.132 | 0.173 | 0.183 | 0.201 | 0.203 | 0.201 | 0.204 | 0.174 | 0.139 | 0.133 | 0.119 | 0.082 | 0.035 | 0.043 |
| Fe | 2.158 | 2.114 | 2.045 | 2.025 | 1.967 | 1.895 | 1.888 | 1.906 | 1.935 | 1.939 | 1.939 | 1.938 | 1.954 | 1.952 | 1.946 | 1.960 | 2.049 | 2.160 | 2.155 |
| total | 8.005 | 8.013 | 8.006 | 8.012 | 8.019 | 8.014 | 8.024 | 8.015 | 8.029 | 8.033 | 8.027 | 8.040 | 8.025 | 8.030 | 8.026 | 8.015 | 8.009 | 8.018 | 8.007 |

Appendix 1A: Garnet Analyses

Sample A933, Location 2 Traverse across large garnet (optically zoned)

| Analysis #: | 170 | 171 | 172 | 173 | 174 | 175 | 176 | 177 | 178 | 179 | 180 | 181 | 182 | 183 | 184 | 185 | 186 | 187 | 188 | 189 | 190 |
|---|---|---|---|---|---|---|---|---|---|---|---|---|---|---|---|---|---|---|---|---|---|
| SiO2 | 36.80 | 36.86 | 36.88 | 36.55 | 36.33 | 36.74 | 35.49 | 36.60 | 36.51 | 36.55 | 36.70 | 36.79 | 36.76 | 36.83 | 36.45 | 36.87 | 36.85 | 36.47 | 36.60 | 35.41 | 36.80 |
| TiO2 | 0.14 | 0.15 | 0.14 | 0.14 | 0.10 | 0.12 | 0.06 | 0.09 | 0.06 | 0.08 | 0.16 | 0.12 | 0.11 | 0.10 | 0.10 | 0.11 | 0.10 | 0.08 | 0.08 | 0.08 | 0.05 |
| Al2O3 | 20.63 | 20.68 | 20.75 | 20.57 | 20.70 | 20.90 | 20.00 | 20.77 | 20.78 | 20.90 | 20.62 | 20.55 | 20.62 | 20.78 | 20.25 | 20.63 | 20.62 | 20.51 | 20.73 | 19.69 | 20.97 |
| Cr2O3 | 0.02 | 0.06 | 0.02 | 0.05 | 0.03 | 0.06 | 0.01 | 0.01 | 0.03 | 0.03 | 0.01 | 0.01 | 0.02 | 0.01 | 0.04 | 0.03 | 0.04 | 0.00 | 0.01 | 0.02 | 0.00 |
| MgO | 0.81 | 0.81 | 0.83 | 0.95 | 1.02 | 1.02 | 1.27 | 1.33 | 1.59 | 1.72 | 0.81 | 0.83 | 0.88 | 1.07 | 1.24 | 1.10 | 1.10 | 1.17 | 1.28 | 1.36 | 1.80 |
| CaO | 9.49 | 9.63 | 9.25 | 9.42 | 8.52 | 9.14 | 7.33 | 7.29 | 7.26 | 7.02 | 9.36 | 9.59 | 9.48 | 8.66 | 7.67 | 8.49 | 8.57 | 7.61 | 7.85 | 7.25 | 6.88 |
| MnO | 6.45 | 6.26 | 6.37 | 5.32 | 4.39 | 4.17 | 3.04 | 3.26 | 2.05 | 1.01 | 7.06 | 5.91 | 5.24 | 4.32 | 3.94 | 4.30 | 4.34 | 4.38 | 3.53 | 2.41 | 1.00 |
| FeO | 24.31 | 24.44 | 24.61 | 25.64 | 26.98 | 26.98 | 28.08 | 29.71 | 30.52 | 31.40 | 24.22 | 24.79 | 25.54 | 27.17 | 27.30 | 26.74 | 27.24 | 27.62 | 28.28 | 27.88 | 31.46 |
| total | 98.65 | 98.89 | 98.83 | 98.64 | 98.07 | 99.13 | 95.27 | 99.06 | 98.79 | 98.71 | 98.93 | 98.60 | 98.66 | 98.94 | 97.00 | 98.28 | 98.86 | 97.83 | 98.35 | 94.11 | 98.95 |
| Si | 2.995 | 2.992 | 2.995 | 2.980 | 2.979 | 2.977 | 2.994 | 2.978 | 2.975 | 2.976 | 2.985 | 2.995 | 2.992 | 2.990 | 3.014 | 3.006 | 2.996 | 2.997 | 2.989 | 3.015 | 2.985 |
| Ti | 0.009 | 0.009 | 0.008 | 0.009 | 0.006 | 0.007 | 0.004 | 0.006 | 0.004 | 0.005 | 0.010 | 0.008 | 0.007 | 0.006 | 0.006 | 0.007 | 0.006 | 0.005 | 0.005 | 0.005 | 0.003 |
| Al | 1.979 | 1.978 | 1.986 | 1.976 | 2.000 | 1.996 | 1.989 | 1.992 | 1.995 | 2.005 | 1.976 | 1.972 | 1.978 | 1.988 | 1.973 | 1.983 | 1.975 | 1.986 | 1.995 | 1.976 | 2.005 |
| Cr | 0.001 | 0.004 | 0.001 | 0.003 | 0.002 | 0.004 | 0.001 | 0.001 | 0.002 | 0.002 | 0.001 | 0.001 | 0.001 | 0.001 | 0.280 | 0.002 | 0.003 | 0.000 | 0.000 | 0.002 | 0.000 |
| Mg | 0.098 | 0.098 | 0.101 | 0.116 | 0.124 | 0.123 | 0.160 | 0.161 | 0.193 | 0.209 | 0.098 | 0.101 | 0.107 | 0.130 | 0.152 | 0.134 | 0.133 | 0.144 | 0.156 | 0.173 | 0.218 |
| Ca | 0.828 | 0.837 | 0.805 | 0.823 | 0.749 | 0.794 | 0.663 | 0.636 | 0.633 | 0.612 | 0.815 | 0.837 | 0.827 | 0.753 | 0.680 | 0.742 | 0.747 | 0.670 | 0.687 | 0.662 | 0.598 |
| Mn | 0.444 | 0.431 | 0.438 | 0.367 | 0.305 | 0.286 | 0.217 | 0.225 | 0.141 | 0.070 | 0.486 | 0.408 | 0.361 | 0.297 | 0.276 | 0.297 | 0.299 | 0.305 | 0.244 | 0.174 | 0.068 |
| Fe | 1.654 | 1.659 | 1.671 | 1.748 | 1.850 | 1.828 | 1.981 | 2.022 | 2.080 | 2.138 | 1.647 | 1.689 | 1.739 | 1.845 | 1.888 | 1.823 | 1.852 | 1.898 | 1.932 | 1.985 | 2.134 |
| total | 8.007 | 8.008 | 8.004 | 8.022 | 8.014 | 8.016 | 8.007 | 8.020 | 8.023 | 8.016 | 8.018 | 8.010 | 8.012 | 8.009 | 7.992 | 7.994 | 8.010 | 8.005 | 8.008 | 7.991 | 8.010 |

Appendix 1A: Garnet Analyses

| | Sample 1337, Location 1 (Traverse, single garnet) | | | | | | | | | | | Sample 1337, Location 2 (Traverse, single garnet) | | | | |
|---|---|---|---|---|---|---|---|---|---|---|---|---|---|---|---|---|
| Analysis #: | 8 | 9 | 10 | 11 | 12 | 13 | 14 | 15 | 16 | 17 | 18 | 28 | 29 | 30 | 31 | 32 |
| SiO2 | 37.28 | 37.11 | 37.08 | 36.86 | 36.99 | 36.85 | 37.01 | 37.14 | 37.32 | 37.19 | 37.27 | 37.08 | 37.14 | 37.03 | 36.95 | 37.17 |
| TiO2 | 0.07 | 0.06 | 0.15 | 0.19 | 0.17 | 0.08 | 0.10 | 0.09 | 0.10 | 0.04 | 0.07 | 0.09 | 0.12 | 0.09 | 0.09 | 0.09 |
| Al2O3 | 21.11 | 21.11 | 20.92 | 20.83 | 20.87 | 20.99 | 20.95 | 21.15 | 21.21 | 21.17 | 20.92 | 21.02 | 20.99 | 21.14 | 20.91 | 21.13 |
| Cr2O3 | 0.04 | 0.08 | 0.10 | 0.05 | 0.02 | 0.02 | 0.01 | 0.00 | 0.05 | 0.02 | 0.04 | 0.00 | 0.09 | 0.03 | 0.04 | 0.03 |
| MgO | 2.57 | 2.00 | 1.73 | 1.26 | 1.22 | 1.27 | 1.51 | 2.07 | 2.48 | 2.55 | 2.11 | 1.77 | 1.98 | 2.43 | 2.43 | 2.68 |
| CaO | 6.81 | 7.95 | 8.32 | 8.00 | 8.15 | 7.70 | 7.78 | 7.30 | 7.04 | 6.71 | 7.42 | 8.03 | 8.49 | 7.04 | 6.38 | 6.96 |
| MnO | 1.66 | 1.73 | 2.29 | 5.39 | 5.24 | 5.49 | 3.34 | 1.56 | 1.78 | 1.66 | 1.57 | 2.66 | 1.95 | 1.62 | 1.81 | 2.37 |
| FeO | 30.61 | 30.02 | 29.36 | 27.38 | 27.31 | 27.80 | 29.53 | 30.55 | 29.78 | 30.64 | 30.79 | 28.98 | 28.94 | 30.47 | 31.13 | 28.92 |
| total | 100.15 | 100.05 | 99.94 | 99.95 | 99.97 | 100.20 | 100.23 | 99.86 | 99.76 | 99.98 | 100.18 | 99.64 | 99.69 | 99.86 | 99.74 | 99.35 |
| Si | 2.979 | 2.973 | 2.977 | 2.973 | 2.979 | 2.968 | 2.974 | 2.980 | 2.986 | 2.977 | 2.984 | 2.982 | 2.980 | 2.969 | 2.974 | 2.983 |
| Ti | 0.004 | 0.003 | 0.009 | 0.011 | 0.010 | 0.005 | 0.006 | 0.005 | 0.006 | 0.002 | 0.004 | 0.006 | 0.007 | 0.006 | 0.005 | 0.005 |
| Al | 1.988 | 1.993 | 1.979 | 1.980 | 1.981 | 1.992 | 1.984 | 1.999 | 2.000 | 1.997 | 1.974 | 1.992 | 1.984 | 1.998 | 1.984 | 1.999 |
| Cr | 0.002 | 0.005 | 0.006 | 0.003 | 0.002 | 0.001 | 0.001 | 0.000 | 0.003 | 0.002 | 0.003 | 0.000 | 0.006 | 0.002 | 0.003 | 0.002 |
| Mg | 0.307 | 0.238 | 0.207 | 0.151 | 0.147 | 0.153 | 0.181 | 0.248 | 0.295 | 0.304 | 0.252 | 0.213 | 0.236 | 0.291 | 0.291 | 0.320 |
| Ca | 0.583 | 0.682 | 0.716 | 0.691 | 0.703 | 0.664 | 0.669 | 0.627 | 0.603 | 0.576 | 0.636 | 0.692 | 0.730 | 0.605 | 0.550 | 0.598 |
| Mn | 0.113 | 0.117 | 0.155 | 0.368 | 0.357 | 0.375 | 0.227 | 0.106 | 0.121 | 0.113 | 0.107 | 0.181 | 0.132 | 0.110 | 0.124 | 0.161 |
| Fe | 2.045 | 2.012 | 1.971 | 1.847 | 1.840 | 1.872 | 1.984 | 2.049 | 1.992 | 2.051 | 2.062 | 1.950 | 1.942 | 2.044 | 2.096 | 1.941 |
| total | 8.021 | 8.023 | 8.020 | 8.024 | 8.019 | 8.030 | 8.026 | 8.014 | 8.006 | 8.022 | 8.022 | 8.016 | 8.017 | 8.025 | 8.027 | 8.009 |

Appendix 1A: Garnet Analyses

| | Sample 1337, Location 2, continued | | | | | | | | | | Sample 1341, Location 2 | | | | | |
|---|---|---|---|---|---|---|---|---|---|---|---|---|---|---|---|---|
| Analysis #: | 33 | 34 | 35 | 36 | 37 | 38 | 39 | 40 | 41 | 42 | 75 | 76 | 77 | 78 | 79 | 80 |
| SiO2 | 37.08 | 37.14 | 36.63 | 36.97 | 36.93 | 37.09 | 36.87 | 37.13 | 37.32 | 37.22 | 36.05 | 36.14 | 35.96 | 35.73 | 36.27 | 36.32 |
| TiO2 | 0.11 | 0.07 | 0.10 | 0.10 | 0.09 | 0.11 | 0.03 | 0.08 | 0.06 | 0.10 | 0.05 | 0.06 | 0.05 | 0.09 | 0.07 | 0.06 |
| Al2O3 | 20.99 | 21.05 | 21.05 | 20.97 | 20.88 | 20.90 | 20.97 | 20.89 | 20.86 | 20.83 | 20.61 | 20.58 | 20.56 | 20.48 | 20.71 | 20.62 |
| Cr2O3 | 0.04 | 0.00 | 0.03 | 0.04 | 0.00 | 0.00 | 0.03 | 0.03 | 0.02 | 0.03 | 0.03 | 0.00 | 0.00 | 0.05 | 0.00 | 0.00 |
| MgO | 2.11 | 1.83 | 2.43 | 1.50 | 1.46 | 1.57 | 1.93 | 2.49 | 2.41 | 2.31 | 2.01 | 1.66 | 1.64 | 1.66 | 2.13 | 2.07 |
| CaO | 7.32 | 7.82 | 6.32 | 7.68 | 7.70 | 8.36 | 7.14 | 6.88 | 6.93 | 6.60 | 3.32 | 2.86 | 2.36 | 2.18 | 3.12 | 2.68 |
| MnO | 1.79 | 2.74 | 1.81 | 3.44 | 3.57 | 2.72 | 2.56 | 1.66 | 1.63 | 1.67 | 0.04 | 0.05 | 0.23 | 0.13 | 0.62 | 0.52 |
| FeO | 30.14 | 29.11 | 30.69 | 28.91 | 28.65 | 28.66 | 29.92 | 30.42 | 30.23 | 30.25 | 36.68 | 37.95 | 38.33 | 38.61 | 35.83 | 36.76 |
| total | 99.57 | 99.77 | 99.05 | 99.62 | 99.28 | 99.41 | 99.44 | 99.58 | 99.46 | 99.00 | 98.77 | 99.30 | 99.13 | 98.94 | 98.75 | 99.02 |
| Si | 2.983 | 2.983 | 2.965 | 2.982 | 2.988 | 2.990 | 2.977 | 2.985 | 3.000 | 3.004 | 2.965 | 2.969 | 2.965 | 2.956 | 2.976 | 2.979 |
| Ti | 0.007 | 0.004 | 0.006 | 0.006 | 0.005 | 0.007 | 0.002 | 0.005 | 0.003 | 0.006 | 0.003 | 0.004 | 0.003 | 0.005 | 0.004 | 0.004 |
| Al | 1.990 | 1.993 | 2.008 | 1.994 | 1.991 | 1.986 | 1.996 | 1.979 | 1.976 | 1.982 | 1.998 | 1.992 | 1.997 | 1.996 | 2.002 | 1.993 |
| Cr | 0.003 | 0.000 | 0.002 | 0.003 | 0.000 | 0.000 | 0.002 | 0.002 | 0.001 | 0.002 | 0.002 | 0.000 | 0.000 | 0.003 | 0.000 | 0.000 |
| Mg | 0.253 | 0.219 | 0.293 | 0.180 | 0.176 | 0.189 | 0.232 | 0.298 | 0.289 | 0.278 | 0.246 | 0.203 | 0.201 | 0.205 | 0.261 | 0.253 |
| Ca | 0.631 | 0.673 | 0.548 | 0.664 | 0.668 | 0.722 | 0.618 | 0.592 | 0.596 | 0.571 | 0.292 | 0.252 | 0.208 | 0.193 | 0.274 | 0.235 |
| Mn | 0.122 | 0.187 | 0.124 | 0.235 | 0.245 | 0.186 | 0.175 | 0.113 | 0.111 | 0.114 | 0.003 | 0.004 | 0.016 | 0.009 | 0.043 | 0.036 |
| Fe | 2.028 | 1.956 | 2.077 | 1.950 | 1.938 | 1.932 | 2.020 | 2.045 | 2.031 | 2.042 | 2.523 | 2.607 | 2.643 | 2.671 | 2.459 | 2.521 |
| total | 8.017 | 8.015 | 8.023 | 8.014 | 8.011 | 8.012 | 8.022 | 8.019 | 8.007 | 7.999 | 8.032 | 8.031 | 8.033 | 8.038 | 8.019 | 8.021 |

Appendix 1A: Garnet Analyses

| | Sample 1341, Location 3 continued | | | Sample 1435, Location 1 (Traverse across single garnet) | | | | | | | |
|---|---|---|---|---|---|---|---|---|---|---|---|
| Analysis #: | 60 | 61 | 62 | 130 | 131 | 132 | 133 | 134 | 135 | 136 | 137 |
| SiO2 | 36.78 | 36.50 | 36.62 | 36.60 | 36.56 | 36.78 | 36.83 | 36.61 | 36.65 | 36.75 | 36.72 |
| TiO2 | 0.05 | 0.05 | 0.03 | 0.08 | 0.07 | 0.07 | 0.08 | 0.06 | 0.06 | 0.09 | 0.10 |
| Al2O3 | 21.10 | 20.85 | 20.94 | 20.68 | 20.59 | 20.67 | 20.62 | 20.68 | 20.56 | 20.69 | 20.51 |
| Cr2O3 | 0.02 | 0.02 | 0.00 | 0.00 | 0.01 | 0.00 | 0.00 | 0.01 | 0.01 | 0.00 | 0.03 |
| MgO | 2.54 | 1.90 | 2.03 | 1.16 | 1.09 | 1.03 | 0.93 | 0.92 | 1.03 | 0.99 | 1.11 |
| CaO | 3.63 | 3.02 | 3.27 | 7.99 | 7.01 | 7.72 | 7.82 | 8.01 | 7.64 | 7.74 | 7.51 |
| MnO | 0.03 | 0.01 | 0.01 | 1.76 | 2.15 | 2.03 | 2.25 | 2.72 | 2.01 | 2.32 | 1.59 |
| FeO | 35.80 | 38.06 | 37.06 | 31.13 | 31.58 | 31.42 | 30.61 | 30.39 | 31.28 | 30.98 | 31.56 |
| total | 99.95 | 100.41 | 99.96 | 99.40 | 99.06 | 99.72 | 99.13 | 99.40 | 99.25 | 99.56 | 99.12 |
| Si | 2.970 | 2.962 | 2.973 | 2.974 | 2.984 | 2.982 | 2.997 | 2.978 | 2.985 | 2.983 | 2.991 |
| Ti | 0.003 | 0.003 | 0.002 | 0.005 | 0.004 | 0.004 | 0.005 | 0.004 | 0.004 | 0.005 | 0.006 |
| Al | 2.008 | 1.994 | 2.003 | 1.980 | 1.981 | 1.975 | 1.977 | 1.982 | 1.974 | 1.979 | 1.969 |
| Cr | 0.001 | 0.001 | 0.000 | 0.000 | 0.001 | 0.000 | 0.000 | 0.001 | 0.000 | 0.000 | 0.002 |
| Mg | 0.306 | 0.229 | 0.246 | 0.141 | 0.133 | 0.125 | 0.113 | 0.111 | 0.125 | 0.120 | 0.135 |
| Ca | 0.314 | 0.263 | 0.284 | 0.696 | 0.613 | 0.670 | 0.681 | 0.698 | 0.667 | 0.673 | 0.655 |
| Mn | 0.002 | 0.001 | 0.001 | 0.121 | 0.148 | 0.139 | 0.155 | 0.187 | 0.138 | 0.160 | 0.109 |
| Fe | 2.417 | 2.583 | 2.515 | 2.115 | 2.156 | 2.130 | 2.083 | 2.067 | 2.131 | 2.103 | 2.150 |
| total | 8.021 | 8.036 | 8.024 | 8.032 | 8.020 | 8.025 | 8.011 | 8.028 | 8.024 | 8.023 | 8.017 |

| | Sample 1341, Location 2, continued | | | | | | Sample 1341, Location 3 | | | | | | | | | |
|---|---|---|---|---|---|---|---|---|---|---|---|---|---|---|---|---|
| Analysis #: | 81 | 82 | 85 | 86 | 87 | 88 | 43 | 44 | 45 | 46 | 47 | 54 | 55 | 56 | 57 | 58 |
| SiO2 | 36.33 | 36.18 | 36.48 | 36.23 | 36.21 | 36.66 | 36.70 | 36.30 | 35.98 | 36.36 | 36.25 | 35.97 | 36.01 | 36.37 | 36.32 | 36.70 |
| TiO2 | 0.05 | 0.07 | 0.05 | 0.06 | 0.04 | 0.05 | 0.02 | 0.02 | 0.07 | 0.03 | 0.06 | 0.05 | 0.08 | 0.02 | 0.03 | 0.11 |
| Al2O3 | 20.70 | 20.87 | 20.84 | 20.69 | 20.70 | 20.81 | 21.07 | 20.84 | 20.78 | 20.94 | 20.96 | 20.68 | 20.70 | 21.00 | 20.95 | 21.10 |
| Cr2O3 | 0.02 | 0.01 | 0.00 | 0.02 | 0.00 | 0.00 | 0.00 | 0.00 | 0.02 | 0.04 | 0.02 | 0.01 | 0.00 | 0.00 | 0.04 | 0.00 |
| MgO | 2.36 | 2.46 | 2.53 | 1.91 | 1.89 | 2.31 | 2.33 | 1.63 | 0.81 | 1.27 | 0.92 | 2.06 | 1.98 | 1.78 | 1.89 | 2.40 |
| CaO | 2.92 | 3.11 | 2.95 | 3.28 | 2.65 | 2.88 | 2.87 | 3.40 | 5.94 | 5.04 | 5.29 | 2.95 | 2.33 | 4.08 | 2.38 | 3.36 |
| MnO | 0.04 | 0.01 | 0.06 | 0.01 | 0.01 | 0.04 | 0.04 | 0.04 | 1.79 | 0.62 | 0.96 | 0.01 | 0.07 | 0.16 | 0.06 | 0.03 |
| FeO | 36.57 | 36.30 | 36.12 | 37.28 | 37.75 | 36.99 | 36.88 | 37.19 | 33.45 | 35.00 | 35.36 | 37.23 | 38.37 | 36.53 | 38.10 | 36.17 |
| total | 98.98 | 99.01 | 99.03 | 99.49 | 99.24 | 99.73 | 99.91 | 99.41 | 98.85 | 99.30 | 99.82 | 98.95 | 99.53 | 99.94 | 99.77 | 99.87 |
| Si | 2.973 | 2.959 | 2.976 | 2.964 | 2.970 | 2.979 | 2.973 | 2.970 | 2.960 | 2.970 | 2.957 | 2.957 | 2.953 | 2.957 | 2.964 | 2.969 |
| Ti | 0.003 | 0.004 | 0.003 | 0.004 | 0.002 | 0.003 | 0.001 | 0.001 | 0.004 | 0.002 | 0.004 | 0.003 | 0.005 | 0.001 | 0.002 | 0.007 |
| Al | 1.997 | 2.011 | 2.004 | 1.995 | 2.001 | 1.993 | 2.012 | 2.009 | 2.014 | 2.016 | 2.015 | 2.004 | 2.001 | 2.012 | 2.014 | 2.012 |
| Cr | 0.001 | 0.001 | 0.000 | 0.001 | 0.000 | 0.000 | 0.000 | 0.000 | 0.001 | 0.002 | 0.001 | 0.001 | 0.000 | 0.000 | 0.002 | 0.000 |
| Mg | 0.288 | 0.300 | 0.308 | 0.233 | 0.231 | 0.280 | 0.282 | 0.198 | 0.099 | 0.154 | 0.112 | 0.252 | 0.242 | 0.215 | 0.230 | 0.289 |
| Ca | 0.256 | 0.272 | 0.258 | 0.288 | 0.233 | 0.251 | 0.249 | 0.298 | 0.524 | 0.441 | 0.463 | 0.260 | 0.205 | 0.356 | 0.208 | 0.291 |
| Mn | 0.002 | 0.001 | 0.004 | 0.001 | 0.001 | 0.002 | 0.003 | 0.002 | 0.125 | 0.043 | 0.067 | 0.000 | 0.005 | 0.011 | 0.004 | 0.002 |
| Fe | 2.503 | 2.483 | 2.465 | 2.550 | 2.589 | 2.514 | 2.499 | 2.545 | 2.301 | 2.391 | 2.412 | 2.560 | 2.632 | 2.483 | 2.600 | 2.447 |
| total | 8.023 | 8.031 | 8.018 | 8.036 | 8.027 | 8.022 | 8.019 | 8.023 | 8.028 | 8.019 | 8.031 | 8.037 | 8.043 | 8.035 | 8.024 | 8.017 |

Appendix 1A: Garnet Analyses

Sample 1435, Location 3

| | Garnet #1 | | | | | | | | Garnet #2 | | | | | | | | |
|---|---|---|---|---|---|---|---|---|---|---|---|---|---|---|---|---|---|
| Analysis #: | 138 | 139 | 140 | 141 | 142 | 143 | 144 | 145 | 146 | 147 | 148 | 149 | 150 | 151 | 152 | 153 | 154 |
| SiO2 | 36.43 | 36.69 | 36.38 | 36.69 | 36.63 | 36.67 | 36.64 | 36.72 | 36.74 | 36.73 | 36.77 | 36.58 | 36.58 | 36.59 | 36.65 | 36.62 | 36.65 |
| TiO2 | 0.12 | 0.14 | 0.14 | 0.15 | 0.12 | 0.09 | 0.11 | 0.11 | 0.09 | 0.07 | 0.08 | 0.08 | 0.07 | 0.12 | 0.12 | 0.15 | 0.08 |
| Al2O3 | 20.53 | 20.61 | 20.27 | 20.45 | 20.48 | 20.53 | 20.51 | 20.56 | 20.61 | 20.70 | 20.74 | 20.67 | 20.78 | 20.68 | 20.65 | 20.58 | 20.75 |
| Cr2O3 | 0.00 | 0.01 | 0.05 | 0.02 | 0.03 | 0.01 | 0.03 | 0.01 | 0.06 | 0.02 | 0.01 | 0.00 | 0.00 | 0.05 | 0.00 | 0.07 | 0.05 |
| MgO | 0.95 | 0.74 | 0.73 | 0.72 | 0.75 | 0.78 | 0.89 | 0.95 | 1.02 | 1.15 | 1.23 | 1.21 | 1.07 | 0.86 | 0.79 | 0.82 | 1.09 |
| CaO | 8.49 | 8.47 | 7.80 | 8.49 | 8.21 | 8.12 | 8.24 | 7.99 | 8.58 | 7.82 | 6.89 | 7.52 | 7.62 | 8.35 | 8.37 | 8.03 | 7.46 |
| MnO | 3.11 | 5.41 | 5.98 | 5.82 | 5.87 | 4.91 | 3.13 | 2.54 | 1.60 | 2.21 | 1.77 | 1.79 | 1.77 | 3.74 | 4.77 | 4.36 | 1.92 |
| FeO | 28.83 | 27.27 | 27.21 | 26.72 | 27.57 | 28.08 | 29.70 | 30.25 | 31.11 | 30.72 | 31.81 | 31.59 | 31.89 | 28.70 | 28.10 | 28.51 | 31.37 |
| total | 98.45 | 99.34 | 98.55 | 99.05 | 99.64 | 99.19 | 99.24 | 99.15 | 99.79 | 99.41 | 99.29 | 99.43 | 99.78 | 99.08 | 99.45 | 99.15 | 99.37 |
| Si | 2.982 | 2.983 | 2.987 | 2.991 | 2.978 | 2.987 | 2.983 | 2.989 | 2.975 | 2.982 | 2.989 | 2.974 | 2.967 | 2.980 | 2.978 | 2.983 | 2.979 |
| Ti | 0.007 | 0.008 | 0.008 | 0.009 | 0.007 | 0.006 | 0.006 | 0.007 | 0.005 | 0.004 | 0.005 | 0.005 | 0.005 | 0.007 | 0.007 | 0.009 | 0.005 |
| Al | 1.980 | 1.974 | 1.962 | 1.965 | 1.962 | 1.972 | 1.968 | 1.973 | 1.967 | 1.980 | 1.986 | 1.981 | 1.987 | 1.984 | 1.977 | 1.976 | 1.988 |
| Cr | 0.000 | 0.000 | 0.003 | 0.001 | 0.002 | 0.001 | 0.002 | 0.001 | 0.004 | 0.001 | 0.001 | 0.000 | 0.000 | 0.003 | 0.000 | 0.005 | 0.003 |
| Mg | 0.116 | 0.090 | 0.089 | 0.087 | 0.090 | 0.095 | 0.108 | 0.116 | 0.123 | 0.140 | 0.149 | 0.146 | 0.129 | 0.104 | 0.096 | 0.100 | 0.133 |
| Ca | 0.745 | 0.738 | 0.686 | 0.741 | 0.715 | 0.709 | 0.719 | 0.697 | 0.744 | 0.680 | 0.600 | 0.655 | 0.662 | 0.728 | 0.729 | 0.701 | 0.649 |
| Mn | 0.216 | 0.373 | 0.416 | 0.402 | 0.404 | 0.339 | 0.216 | 0.175 | 0.110 | 0.152 | 0.122 | 0.123 | 0.122 | 0.258 | 0.328 | 0.301 | 0.132 |
| Fe | 1.974 | 1.854 | 1.869 | 1.821 | 1.874 | 1.913 | 2.023 | 2.059 | 2.107 | 2.085 | 2.162 | 2.147 | 2.164 | 1.955 | 1.909 | 1.942 | 2.132 |
| total | 8.020 | 8.020 | 8.020 | 8.017 | 8.032 | 8.022 | 8.025 | 8.017 | 8.035 | 8.024 | 8.014 | 8.031 | 8.036 | 8.019 | 8.024 | 8.017 | 8.021 |

Appendix 1A: Garnet Analyses

| Sample A1945, Location 1 | | | | | | Sample A1945, Location 2 | | | | | | | | | |
|---|---|---|---|---|---|---|---|---|---|---|---|---|---|---|---|
| Analysis #: | 256 | 257 | 258 | 259 | 260 | 246 | 247 | 248 | 249 | 250 | 251 | 252 | 253 | 254 | 255 |
| SiO2 | 37.11 | 37.08 | 37.09 | 37.23 | 37.28 | 37.07 | 37.22 | 37.08 | 37.85 | 36.93 | 37.16 | 37.05 | 37.08 | 37.03 | 37.17 |
| TiO2 | 0.13 | 0.08 | 0.09 | 0.06 | 0.08 | 0.17 | 0.11 | 0.10 | 0.15 | 0.14 | 0.15 | 0.18 | 0.11 | 0.10 | 0.12 |
| Al2O3 | 20.95 | 20.99 | 21.19 | 21.29 | 21.06 | 20.99 | 21.03 | 21.08 | 20.92 | 20.91 | 21.03 | 21.02 | 21.11 | 21.13 | 21.13 |
| Cr2O3 | 0.04 | 0.00 | 0.00 | 0.00 | 0.02 | 0.07 | 0.00 | 0.04 | 0.00 | 0.03 | 0.04 | 0.00 | 0.04 | 0.06 | 0.00 |
| MgO | 3.02 | 2.87 | 3.00 | 3.05 | 3.14 | 3.08 | 3.07 | 3.07 | 3.02 | 3.10 | 2.96 | 3.00 | 3.02 | 3.01 | 2.89 |
| CaO | 6.29 | 6.22 | 6.69 | 7.09 | 6.76 | 6.22 | 6.46 | 6.98 | 6.20 | 5.67 | 6.55 | 7.03 | 6.58 | 6.44 | 6.71 |
| MnO | 2.75 | 3.10 | 2.86 | 2.89 | 2.31 | 2.77 | 2.82 | 1.95 | 3.10 | 3.27 | 2.59 | 2.04 | 2.53 | 2.65 | 2.31 |
| FeO | 29.05 | 29.09 | 28.31 | 28.52 | 28.78 | 29.22 | 28.96 | 28.92 | 28.59 | 28.81 | 28.91 | 28.72 | 29.12 | 28.74 | 28.57 |
| total | 99.33 | 99.43 | 99.22 | 100.14 | 99.41 | 99.58 | 99.67 | 99.21 | 99.84 | 98.86 | 99.39 | 99.03 | 99.59 | 99.16 | 98.89 |
| Si | 2.981 | 2.980 | 2.977 | 2.966 | 2.985 | 2.974 | 2.980 | 2.976 | 3.016 | 2.982 | 2.981 | 2.979 | 2.971 | 2.976 | 2.990 |
| Ti | 0.008 | 0.005 | 0.005 | 0.004 | 0.005 | 0.010 | 0.007 | 0.006 | 0.009 | 0.008 | 0.009 | 0.011 | 0.007 | 0.006 | 0.007 |
| Al | 1.983 | 1.989 | 2.004 | 1.999 | 1.987 | 1.984 | 1.985 | 1.994 | 1.965 | 1.989 | 1.989 | 1.991 | 1.994 | 2.002 | 2.003 |
| Cr | 0.002 | 0.000 | 0.000 | 0.000 | 0.001 | 0.004 | 0.000 | 0.003 | 0.000 | 0.002 | 0.002 | 0.000 | 0.002 | 0.004 | 0.000 |
| Mg | 0.362 | 0.344 | 0.358 | 0.363 | 0.375 | 0.368 | 0.366 | 0.367 | 0.358 | 0.374 | 0.354 | 0.359 | 0.361 | 0.361 | 0.346 |
| Ca | 0.542 | 0.535 | 0.575 | 0.605 | 0.580 | 0.534 | 0.554 | 0.600 | 0.530 | 0.491 | 0.563 | 0.606 | 0.565 | 0.555 | 0.578 |
| Mn | 0.187 | 0.211 | 0.194 | 0.195 | 0.156 | 0.188 | 0.191 | 0.133 | 0.209 | 0.224 | 0.176 | 0.139 | 0.172 | 0.180 | 0.157 |
| Fe | 1.952 | 1.955 | 1.900 | 1.900 | 1.927 | 1.960 | 1.939 | 1.942 | 1.905 | 1.945 | 1.940 | 1.931 | 1.952 | 1.932 | 1.921 |
| total | 8.017 | 8.019 | 8.013 | 8.032 | 8.016 | 8.022 | 8.021 | 8.020 | 7.992 | 8.015 | 8.014 | 8.016 | 8.024 | 8.016 | 8.002 |

Appendix 1A: Garnet Analyses

Sample A2061A, Location 1

| Analysis #: | 191 | 192 | 193 | 194 | 195 | 196 | 197 | 198 |
|---|---|---|---|---|---|---|---|---|
| SiO2 | 36.71 | 36.72 | 36.31 | 36.69 | 36.41 | 39.69 | 36.56 | 36.82 |
| TiO2 | 0.03 | 0.16 | 0.14 | 0.22 | 0.25 | 0.21 | 0.17 | 0.07 |
| Al2O3 | 20.80 | 20.59 | 20.56 | 20.33 | 19.91 | 20.27 | 20.44 | 20.94 |
| Cr2O3 | 0.00 | 0.00 | 0.01 | 0.02 | 0.02 | 0.02 | 0.00 | 0.01 |
| MgO | 3.09 | 2.46 | 2.23 | 2.25 | 2.22 | 2.20 | 2.27 | 3.05 |
| CaO | 4.85 | 5.91 | 5.74 | 5.72 | 6.27 | 6.29 | 6.09 | 4.63 |
| MnO | 14.38 | 11.85 | 15.05 | 19.09 | 18.99 | 14.89 | 12.11 | 14.29 |
| FeO | 18.22 | 21.18 | 18.21 | 14.02 | 13.89 | 18.49 | 20.83 | 18.78 |
| total | 98.08 | 98.87 | 98.25 | 98.33 | 97.95 | 99.06 | 98.46 | 98.60 |
| | | | | | | | | |
| Si | 2.988 | 2.981 | 2.971 | 2.994 | 2.990 | 2.982 | 2.983 | 2.983 |
| Ti | 0.002 | 0.010 | 0.009 | 0.013 | 0.015 | 0.013 | 0.010 | 0.004 |
| Al | 1.995 | 1.970 | 1.983 | 1.956 | 1.926 | 1.941 | 1.965 | 2.000 |
| Cr | 0.000 | 0.000 | 0.001 | 0.001 | 0.001 | 0.001 | 0.000 | 0.001 |
| Mg | 0.375 | 0.298 | 0.273 | 0.274 | 0.272 | 0.267 | 0.276 | 0.369 |
| Ca | 0.423 | 0.514 | 0.503 | 0.500 | 0.552 | 0.547 | 0.532 | 0.402 |
| Mn | 0.991 | 0.814 | 1.043 | 1.319 | 1.321 | 1.025 | 0.837 | 0.981 |
| Fe | 1.240 | 1.438 | 1.246 | 0.957 | 0.954 | 1.257 | 1.421 | 1.273 |
| total | 8.013 | 8.025 | 8.028 | 8.014 | 8.031 | 8.034 | 8.024 | 8.012 |

Sample A2061A, Location 2

| Analysis #: | 199 | 200 | 201 | 202 | 203 | 204 | 205 | 206 |
|---|---|---|---|---|---|---|---|---|
| SiO2 | 36.35 | 36.16 | 36.69 | 36.58 | 36.00 | 36.07 | 36.66 | 36.36 |
| TiO2 | 0.30 | 0.18 | 0.08 | 0.08 | 0.31 | 0.22 | 0.22 | 0.11 |
| Al2O3 | 20.31 | 20.52 | 20.83 | 20.89 | 20.19 | 20.44 | 20.18 | 20.81 |
| Cr2O3 | 0.02 | 0.00 | 0.00 | 0.00 | 0.02 | 0.03 | 0.00 | 0.04 |
| MgO | 2.17 | 2.19 | 3.01 | 3.02 | 2.36 | 2.23 | 2.17 | 2.97 |
| CaO | 6.16 | 5.57 | 4.71 | 4.74 | 5.94 | 6.17 | 6.17 | 5.02 |
| MnO | 19.63 | 20.28 | 14.56 | 15.19 | 18.47 | 16.49 | 14.99 | 14.50 |
| FeO | 13.55 | 13.64 | 18.54 | 18.09 | 14.98 | 16.71 | 18.03 | 19.00 |
| total | 98.48 | 98.54 | 98.42 | 98.59 | 98.26 | 98.38 | 98.42 | 98.81 |
| | | | | | | | | |
| Si | 2.970 | 2.958 | 2.981 | 2.971 | 2.955 | 2.954 | 2.994 | 2.954 |
| Ti | 0.019 | 0.011 | 0.005 | 0.005 | 0.019 | 0.014 | 0.014 | 0.007 |
| Al | 1.956 | 1.979 | 1.995 | 1.999 | 1.953 | 1.973 | 1.943 | 1.993 |
| Cr | 0.001 | 0.000 | 0.000 | 0.000 | 0.001 | 0.002 | 0.000 | 0.003 |
| Mg | 0.264 | 0.267 | 0.365 | 0.365 | 0.289 | 0.273 | 0.264 | 0.359 |
| Ca | 0.540 | 0.488 | 0.410 | 0.413 | 0.522 | 0.541 | 0.540 | 0.437 |
| Mn | 1.358 | 1.405 | 1.002 | 1.045 | 1.284 | 1.144 | 1.037 | 0.998 |
| Fe | 0.926 | 0.933 | 1.260 | 1.229 | 1.028 | 1.145 | 1.232 | 1.291 |
| total | 8.033 | 8.042 | 8.017 | 8.025 | 8.050 | 8.045 | 8.021 | 8.041 |

Appendix 1A: Garnet Analyses

| Sample 2079 | | | | | | | | Sample A933, Location 1 (Traverse-large inclusion–filled garnet) | | | | | | | |
|---|---|---|---|---|---|---|---|---|---|---|---|---|---|---|---|
| Analysis #: | 155 | 156 | 157 | 158 | 159 | 160 | 161 | 162 | 163 | 164 | 165 | 166 | 167 | 168 | 169 |
| SiO2 | 37.24 | 37.07 | 36.92 | 37.09 | 37.12 | 37.07 | 36.78 | 36.40 | 36.46 | 36.32 | 36.46 | 36.70 | 36.50 | 36.34 | 36.71 |
| TiO2 | 0.06 | 0.11 | 0.11 | 0.11 | 0.07 | 0.11 | 0.04 | 0.07 | 0.10 | 0.13 | 0.15 | 0.16 | 0.15 | 0.06 | 0.06 |
| Al2O3 | 20.93 | 20.96 | 20.84 | 20.85 | 20.98 | 20.93 | 20.99 | 20.96 | 20.83 | 20.80 | 20.69 | 20.59 | 20.62 | 21.01 | 21.03 |
| Cr2O3 | 0.03 | 0.08 | 0.05 | 0.05 | 0.06 | 0.06 | 0.03 | 0.00 | 0.02 | 0.00 | 0.02 | 0.00 | 0.03 | 0.00 | 0.01 |
| MgO | 2.76 | 2.51 | 2.26 | 2.26 | 2.64 | 2.25 | 2.40 | 1.81 | 1.19 | 0.87 | 0.75 | 0.75 | 0.83 | 1.69 | 1.90 |
| CaO | 6.71 | 6.73 | 7.09 | 6.83 | 6.52 | 7.49 | 6.43 | 6.94 | 7.70 | 9.21 | 9.20 | 9.42 | 9.38 | 6.87 | 6.44 |
| MnO | 3.09 | 4.51 | 5.41 | 5.48 | 2.98 | 5.56 | 5.42 | 0.98 | 4.11 | 5.72 | 7.90 | 7.72 | 6.25 | 1.71 | 0.90 |
| FeO | 28.80 | 28.11 | 26.75 | 27.22 | 29.02 | 26.05 | 27.16 | 31.97 | 28.60 | 25.55 | 23.30 | 23.34 | 24.47 | 30.98 | 32.37 |
| total | 99.62 | 100.07 | 99.43 | 99.88 | 99.36 | 99.51 | 99.24 | 99.14 | 99.01 | 98.61 | 98.48 | 98.68 | 98.22 | 98.61 | 99.43 |
| Si | 2.987 | 2.971 | 2.977 | 2.980 | 2.985 | 2.980 | 2.972 | 2.958 | 2.970 | 2.965 | 2.978 | 2.990 | 2.985 | 2.965 | 2.971 |
| Ti | 0.003 | 0.007 | 0.007 | 0.007 | 0.004 | 0.007 | 0.002 | 0.004 | 0.006 | 0.008 | 0.009 | 0.010 | 0.009 | 0.004 | 0.004 |
| Al | 1.979 | 1.980 | 1.981 | 1.975 | 1.988 | 1.983 | 1.999 | 2.007 | 1.999 | 2.002 | 1.992 | 1.977 | 1.987 | 2.020 | 2.006 |
| Cr | 0.002 | 0.005 | 0.003 | 0.003 | 0.004 | 0.004 | 0.002 | 0.000 | 0.002 | 0.000 | 0.002 | 0.000 | 0.002 | 0.000 | 0.001 |
| Mg | 0.329 | 0.300 | 0.271 | 0.271 | 0.317 | 0.269 | 0.289 | 0.220 | 0.144 | 0.107 | 0.092 | 0.091 | 0.101 | 0.206 | 0.229 |
| Ca | 0.577 | 0.578 | 0.613 | 0.588 | 0.562 | 0.645 | 0.556 | 0.604 | 0.672 | 0.806 | 0.805 | 0.822 | 0.821 | 0.601 | 0.559 |
| Mn | 0.210 | 0.306 | 0.369 | 0.373 | 0.203 | 0.379 | 0.371 | 0.067 | 0.283 | 0.395 | 0.546 | 0.533 | 0.433 | 0.118 | 0.062 |
| Fe | 1.932 | 1.884 | 1.804 | 1.829 | 1.952 | 1.752 | 1.835 | 2.173 | 1.948 | 1.745 | 1.592 | 1.590 | 1.673 | 2.109 | 2.191 |
| total | 8.019 | 8.030 | 8.024 | 8.025 | 8.015 | 8.019 | 8.026 | 8.034 | 8.024 | 8.026 | 8.016 | 8.012 | 8.012 | 8.022 | 8.022 |

Appendix 1A: Garnet Analyses

Sample A791, Location 1

| Analysis #: | 287 | 288 | 289 | 290 | 291 | 292 | 293 | 294 |
|---|---|---|---|---|---|---|---|---|
| SiO2 | 36.07 | 36.21 | 36.24 | 36.20 | 36.42 | 36.42 | 36.18 | 36.29 |
| TiO2 | 0.05 | 0.04 | 0.11 | 0.09 | 0.09 | 0.00 | 0.03 | 0.02 |
| Al2O3 | 20.79 | 20.85 | 20.40 | 20.44 | 20.51 | 20.80 | 20.70 | 20.69 |
| Cr2O3 | 0.03 | 0.02 | 0.00 | 0.00 | 0.03 | 0.00 | 0.02 | 0.00 |
| MgO | 2.01 | 2.34 | 1.24 | 1.14 | 1.19 | 2.37 | 2.54 | 2.69 |
| CaO | 2.64 | 2.29 | 4.47 | 4.64 | 4.66 | 1.86 | 1.85 | 1.65 |
| MnO | 0.91 | 0.35 | 4.62 | 5.90 | 5.98 | 0.64 | 0.34 | 0.27 |
| FeO | 36.30 | 36.68 | 31.20 | 30.25 | 29.83 | 36.26 | 37.02 | 36.87 |
| total | 98.81 | 98.77 | 98.29 | 98.65 | 98.72 | 98.34 | 98.68 | 98.48 |
| | | | | | | | | |
| Si | 2.966 | 2.971 | 2.992 | 2.983 | 2.992 | 2.993 | 2.973 | 2.982 |
| Ti | 0.003 | 0.003 | 0.007 | 0.006 | 0.006 | 0.000 | 0.002 | 0.001 |
| Al | 2.015 | 2.016 | 1.985 | 1.985 | 1.986 | 2.015 | 2.005 | 2.004 |
| Cr | 0.002 | 0.001 | 0.000 | 0.000 | 0.002 | 0.000 | 0.001 | 0.000 |
| Mg | 0.246 | 0.286 | 0.153 | 0.139 | 0.146 | 0.290 | 0.311 | 0.330 |
| Ca | 0.233 | 0.202 | 0.395 | 0.410 | 0.410 | 0.163 | 0.163 | 0.145 |
| Mn | 0.063 | 0.024 | 0.323 | 0.412 | 0.416 | 0.044 | 0.024 | 0.019 |
| Fe | 2.496 | 2.517 | 2.154 | 2.084 | 2.049 | 2.493 | 2.544 | 2.534 |
| total | 8.024 | 8.020 | 8.009 | 8.019 | 8.007 | 7.998 | 8.023 | 8.015 |

Sample A791, Location 2

| Analysis #: | 282 | 283 | 284 | 285 | 286 |
|---|---|---|---|---|---|
| SiO2 | 36.09 | 36.25 | 36.08 | 36.20 | 35.97 |
| TiO2 | 0.06 | 0.10 | 0.04 | 0.10 | 0.05 |
| Al2O3 | 20.75 | 20.81 | 20.69 | 20.68 | 20.82 |
| Cr2O3 | 0.05 | 0.00 | 0.05 | 0.00 | 0.01 |
| MgO | 1.91 | 1.06 | 1.03 | 1.24 | 2.35 |
| CaO | 3.70 | 4.99 | 4.04 | 4.59 | 2.07 |
| MnO | 1.78 | 6.84 | 7.82 | 4.87 | 0.65 |
| FeO | 34.92 | 29.01 | 28.37 | 31.47 | 36.70 |
| total | 99.27 | 99.05 | 98.11 | 99.14 | 98.62 |
| | | | | | |
| Si | 2.955 | 2.971 | 2.984 | 2.969 | 2.961 |
| Ti | 0.004 | 0.006 | 0.003 | 0.006 | 0.003 |
| Al | 2.003 | 2.010 | 2.018 | 1.999 | 2.020 |
| Cr | 0.003 | 0.000 | 0.003 | 0.000 | 0.001 |
| Mg | 0.233 | 0.129 | 0.127 | 0.151 | 0.288 |
| Ca | 0.325 | 0.438 | 0.358 | 0.403 | 0.182 |
| Mn | 0.123 | 0.475 | 0.548 | 0.339 | 0.045 |
| Fe | 2.392 | 1.989 | 1.962 | 2.159 | 2.526 |
| total | 8.038 | 8.018 | 8.003 | 8.026 | 8.026 |

Appendix 1A: Garnet Analyses

Sample 1435, Location 2 (Traverse across single garnet)

| Analysis #: | 115 | 116 | 117 | 118 | 119 | 120 | 121 | 122 | 123 | 124 | 125 | 126 | 127 | 128 | 129 |
|---|---|---|---|---|---|---|---|---|---|---|---|---|---|---|---|
| SiO2 | 36.52 | 36.69 | 36.84 | 36.70 | 36.52 | 36.64 | 43.85 | 36.67 | 36.25 | 36.74 | 36.51 | 36.56 | 36.61 | 36.35 | 36.43 |
| TiO2 | 0.08 | 0.08 | 0.12 | 0.14 | 0.20 | 0.14 | 0.12 | 0.11 | 0.16 | 0.08 | 0.09 | 0.10 | 0.11 | 0.09 | 0.11 |
| Al2O3 | 20.71 | 20.74 | 20.62 | 20.65 | 20.49 | 20.63 | 18.41 | 20.57 | 21.19 | 20.68 | 20.63 | 20.84 | 20.51 | 20.47 | 20.47 |
| Cr2O3 | 0.00 | 0.07 | 0.02 | 0.03 | 0.04 | 0.03 | 0.02 | 0.00 | 0.03 | 0.03 | 0.04 | 0.06 | 0.03 | 0.00 | 0.02 |
| MgO | 1.10 | 0.91 | 0.84 | 0.76 | 0.75 | 0.74 | 0.74 | 0.92 | 1.47 | 1.14 | 1.15 | 1.21 | 0.82 | 1.14 | 1.16 |
| CaO | 7.28 | 8.31 | 8.29 | 8.29 | 7.95 | 8.10 | 7.27 | 8.21 | 6.88 | 7.46 | 7.00 | 7.91 | 8.45 | 7.03 | 7.57 |
| MnO | 2.31 | 2.71 | 3.78 | 5.11 | 5.92 | 5.59 | 3.95 | 2.88 | 1.44 | 1.54 | 2.13 | 1.44 | 4.25 | 2.07 | 1.91 |
| FeO | 31.05 | 30.04 | 29.26 | 28.00 | 27.34 | 27.40 | 26.41 | 30.25 | 30.37 | 32.26 | 31.73 | 31.04 | 28.42 | 31.80 | 30.90 |
| total | 99.06 | 99.55 | 99.76 | 99.69 | 99.20 | 99.26 | 100.78 | 99.61 | 97.79 | 99.92 | 99.28 | 99.15 | 99.20 | 98.95 | 98.57 |
| | | | | | | | | | | | | | | | |
| Si | 2.978 | 2.976 | 2.984 | 2.977 | 2.979 | 2.983 | 3.400 | 2.978 | 2.971 | 2.976 | 2.976 | 2.972 | 2.982 | 2.975 | 2.984 |
| Ti | 0.005 | 0.005 | 0.007 | 0.009 | 0.012 | 0.009 | 0.007 | 0.006 | 0.010 | 0.005 | 0.005 | 0.006 | 0.007 | 0.006 | 0.007 |
| Al | 1.991 | 1.983 | 1.968 | 1.974 | 1.970 | 1.979 | 1.683 | 1.969 | 2.047 | 1.974 | 1.982 | 1.996 | 1.969 | 1.975 | 1.975 |
| Cr | 0.000 | 0.004 | 0.001 | 0.002 | 0.002 | 0.002 | 0.001 | 0.000 | 0.002 | 0.002 | 0.003 | 0.004 | 0.002 | 0.000 | 0.001 |
| Mg | 0.134 | 0.110 | 0.101 | 0.091 | 0.091 | 0.089 | 0.085 | 0.111 | 0.179 | 0.137 | 0.140 | 0.146 | 0.099 | 0.139 | 0.141 |
| Ca | 0.636 | 0.722 | 0.720 | 0.721 | 0.695 | 0.706 | 0.604 | 0.714 | 0.604 | 0.647 | 0.611 | 0.689 | 0.737 | 0.616 | 0.665 |
| Mn | 0.159 | 0.186 | 0.260 | 0.351 | 0.409 | 0.385 | 0.260 | 0.198 | 0.100 | 0.106 | 0.147 | 0.099 | 0.293 | 0.143 | 0.133 |
| Fe | 2.118 | 2.038 | 1.982 | 1.900 | 1.865 | 1.865 | 1.712 | 2.054 | 2.081 | 2.185 | 2.163 | 2.110 | 1.936 | 2.176 | 2.116 |
| total | 8.021 | 8.024 | 8.023 | 8.025 | 8.023 | 8.018 | 7.752 | 8.030 | 7.994 | 8.032 | 8.027 | 8.022 | 8.025 | 8.030 | 8.022 |

Appendix 1A: Garnet Analyses

| Sample K677 | | | | | | | | | | | Sample A321 | |
|---|---|---|---|---|---|---|---|---|---|---|---|---|
| Analysis #: | c28 | c29 | c30 | c31 | c32 | c33 | c34 | c35 | c36 | c37 | 323 | 324 |
| SiO2 | 36.74 | 36.46 | 36.2553 | 37.1208 | 36.8882 | 36.71 | 36.69 | 37.03 | 36.88 | 36.77 | 36.53 | 36.74 |
| TiO2 | 0.15 | 0.28 | 0.2809 | 0.28 | 0.0107 | 0.13 | 0.04 | 0.12 | 0.10 | 0.06 | 0.06 | 0.09 |
| Al2O3 | 20.24 | 19.62 | 19.3395 | 20.73 | 20.6204 | 19.99 | 20.50 | 20.78 | 20.09 | 20.24 | 20.97 | 21.00 |
| Cr2O3 | 0.03 | 0.03 | 0.0254 | 0.10 | 0.0308 | 0.02 | 0.01 | 0.01 | 0.00 | 0.02 | 0.02 | 0.04 |
| MgO | 0.79 | 0.95 | 0.5033 | 1.49 | 1.6262 | 0.69 | 1.70 | 1.72 | 1.03 | 1.19 | 1.74 | 1.50 |
| CaO | 7.39 | 6.09 | 6.2215 | 5.03 | 3.8718 | 7.27 | 3.83 | 3.94 | 7.57 | 6.54 | 6.99 | 7.53 |
| MnO | 15.05 | 17.99 | 20.2659 | 12.15 | 12.3745 | 16.77 | 11.66 | 11.51 | 12.38 | 11.86 | 1.31 | 1.82 |
| FeO | 19.95 | 18.51 | 16.6388 | 24.03 | 24.7055 | 18.61 | 25.89 | 25.89 | 21.78 | 23.39 | 31.40 | 30.60 |
| total | 100.34 | 99.94 | 99.5305 | 100.84 | 100.224 | 100.18 | 100.32 | 101.02 | 99.84 | 100.07 | 99.02 | 99.31 |
| Si | 2.978 | 2.982 | 2.987 | 2.983 | 2.988 | 2.985 | 2.978 | 2.978 | 2.995 | 2.985 | 2.968 | 2.974 |
| Ti | 0.009 | 0.018 | 0.017 | 0.017 | 0.007 | 0.008 | 0.002 | 0.007 | 0.006 | 0.004 | 0.004 | 0.005 |
| Al | 1.934 | 1.891 | 1.878 | 1.963 | 1.969 | 1.916 | 1.961 | 1.970 | 1.923 | 1.936 | 2.008 | 2.004 |
| Cr | 0.002 | 0.002 | 0.002 | 0.001 | 0.002 | 0.001 | 0.001 | 0.001 | 0.000 | 0.002 | 0.001 | 0.002 |
| Mg | 0.096 | 0.116 | 0.062 | 0.178 | 0.196 | 0.083 | 0.206 | 0.207 | 0.124 | 0.145 | 0.210 | 0.181 |
| Ca | 0.642 | 0.534 | 0.549 | 0.433 | 0.336 | 0.634 | 0.333 | 0.339 | 0.659 | 0.569 | 0.608 | 0.653 |
| Mn | 1.033 | 1.246 | 1.414 | 0.827 | 0.849 | 1.155 | 0.801 | 0.784 | 0.852 | 0.815 | 0.090 | 0.125 |
| Fe | 1.352 | 1.266 | 1.146 | 1.615 | 1.674 | 1.266 | 1.757 | 1.742 | 1.479 | 1.588 | 2.134 | 2.072 |
| total | 8.045 | 8.054 | 8.056 | 8.018 | 8.020 | 8.048 | 8.039 | 8.029 | 8.038 | 8.043 | 8.023 | 8.016 |

Appendix 1B: Amphibole Analyses

| Sample 1945, Location 1 | | | | | | | | | | | | Sample 1945, Location 3 | | | | | | | |
|---|---|---|---|---|---|---|---|---|---|---|---|---|---|---|---|---|---|---|---|
| Analysis # | 9 | 10 | 11 | 12 | 13 | 14 | 15 | 16 | 17 | 19 | 20 | 1 | 2 | 3 | 4 | 5 | 6 | 7 | 8 |
| SiO2 | 43.02 | 42.91 | 41.93 | 41.32 | 41.08 | 41.08 | 42.64 | 43.39 | 43.26 | 40.95 | 42.74 | 42.22 | 40.31 | 40.57 | 40.70 | 41.12 | 40.18 | 40.79 | 41.13 |
| TiO2 | 0.38 | 0.39 | 0.40 | 0.44 | 0.36 | 0.41 | 0.41 | 0.41 | 0.38 | 0.51 | 0.40 | 0.41 | 0.49 | 0.42 | 0.52 | 0.37 | 0.41 | 0.42 | 0.42 |
| Al2O3 | 15.87 | 16.33 | 17.31 | 18.10 | 18.07 | 18.64 | 16.65 | 15.47 | 15.46 | 18.23 | 15.85 | 16.53 | 19.14 | 18.67 | 18.45 | 18.41 | 18.56 | 18.21 | 17.87 |
| Cr2O3 | 0.00 | 0.05 | 0.03 | 0.00 | 0.00 | 0.00 | 0.02 | 0.01 | 0.00 | 0.03 | 0.03 | 0.01 | 0.05 | 0.11 | 0.03 | 0.04 | 0.04 | 0.04 | 0.06 |
| MgO | 9.79 | 9.45 | 9.04 | 8.73 | 8.61 | 8.35 | 9.45 | 10.05 | 9.95 | 8.49 | 9.84 | 9.53 | 7.78 | 8.06 | 8.17 | 8.34 | 8.12 | 8.51 | 8.55 |
| CaO | 11.02 | 11.08 | 11.03 | 11.01 | 11.06 | 11.13 | 11.02 | 10.94 | 11.16 | 11.14 | 10.84 | 10.84 | 11.05 | 10.91 | 11.01 | 10.99 | 10.88 | 10.94 | 11.06 |
| MnO | 0.08 | 0.12 | 0.11 | 0.16 | 0.08 | 0.11 | 0.07 | 0.15 | 0.11 | 0.07 | 0.17 | 0.13 | 0.18 | 0.12 | 0.16 | 0.13 | 0.15 | 0.12 | 0.15 |
| FeO | 14.43 | 14.14 | 14.46 | 14.20 | 14.58 | 14.39 | 14.35 | 14.23 | 14.06 | 14.37 | 14.28 | 14.00 | 15.06 | 14.70 | 14.51 | 14.15 | 14.61 | 14.57 | 14.44 |
| Na2O | 1.81 | 1.86 | 1.89 | 1.87 | 1.87 | 1.88 | 1.94 | 1.70 | 1.74 | 1.84 | 1.71 | 1.78 | 1.89 | 1.85 | 1.95 | 1.84 | 1.84 | 1.84 | 1.74 |
| K2O | 0.42 | 0.41 | 0.39 | 0.43 | 0.44 | 0.45 | 0.44 | 0.41 | 0.38 | 0.45 | 0.41 | 0.48 | 0.44 | 0.43 | 0.41 | 0.48 | 0.44 | 0.45 | 0.44 |
| H2O | 2.02 | 2.02 | 2.02 | 2.01 | 2.00 | 2.01 | 2.03 | 2.03 | 2.02 | 2.00 | 2.01 | 2.01 | 2.00 | 2.00 | 2.00 | 2.00 | 1.98 | 2.00 | 2.00 |
| total | 98.85 | 98.76 | 98.61 | 98.27 | 98.15 | 98.44 | 99.03 | 98.77 | 98.50 | 98.07 | 98.28 | 97.94 | 98.39 | 97.82 | 97.88 | 97.87 | 97.21 | 97.88 | 97.85 |
| Si | 6.302 | 6.303 | 6.171 | 6.104 | 6.087 | 6.073 | 6.246 | 6.341 | 6.359 | 6.079 | 6.278 | 6.233 | 5.980 | 6.035 | 6.061 | 6.109 | 6.014 | 6.056 | 6.110 |
| Al(IV) | 1.700 | 1.700 | 1.830 | 1.900 | 1.910 | 1.930 | 1.750 | 1.660 | 1.640 | 1.920 | 1.720 | 1.770 | 2.020 | 1.960 | 1.940 | 1.890 | 1.990 | 1.940 | 1.890 |
| Al(VI) | 1.040 | 1.130 | 1.170 | 1.250 | 1.250 | 1.320 | 1.130 | 1.010 | 1.040 | 1.270 | 1.020 | 1.110 | 1.330 | 1.310 | 1.300 | 1.330 | 1.290 | 1.250 | 1.240 |
| Ti | 0.042 | 0.043 | 0.045 | 0.049 | 0.040 | 0.046 | 0.045 | 0.045 | 0.041 | 0.056 | 0.044 | 0.045 | 0.055 | 0.047 | 0.058 | 0.042 | 0.046 | 0.047 | 0.047 |
| Fe3+ | 0.520 | 0.381 | 0.471 | 0.440 | 0.457 | 0.365 | 0.447 | 0.578 | 0.437 | 0.377 | 0.630 | 0.535 | 0.438 | 0.456 | 0.369 | 0.351 | 0.492 | 0.509 | 0.447 |
| Cr | 0.000 | 0.006 | 0.003 | 0.000 | 0.000 | 0.000 | 0.003 | 0.001 | 0.000 | 0.004 | 0.004 | 0.001 | 0.006 | 0.013 | 0.003 | 0.005 | 0.004 | 0.004 | 0.006 |
| Mg | 2.137 | 2.069 | 1.983 | 1.921 | 1.901 | 1.840 | 2.064 | 2.190 | 2.179 | 1.878 | 2.154 | 2.098 | 1.720 | 1.787 | 1.812 | 1.846 | 1.812 | 1.882 | 1.894 |
| Fe2+ | 1.248 | 1.356 | 1.309 | 1.314 | 1.349 | 1.415 | 1.311 | 1.161 | 1.291 | 1.407 | 1.125 | 1.194 | 1.431 | 1.372 | 1.438 | 1.407 | 1.337 | 1.300 | 1.347 |
| Mn | 0.010 | 0.015 | 0.014 | 0.020 | 0.010 | 0.013 | 0.009 | 0.019 | 0.013 | 0.008 | 0.021 | 0.016 | 0.022 | 0.015 | 0.020 | 0.016 | 0.019 | 0.015 | 0.019 |
| Ca | 1.729 | 1.744 | 1.740 | 1.740 | 1.756 | 1.762 | 1.730 | 1.713 | 1.758 | 1.772 | 1.706 | 1.715 | 1.756 | 1.739 | 1.756 | 1.749 | 1.745 | 1.740 | 1.760 |
| Na (M4) | 0.270 | 0.260 | 0.270 | 0.270 | 0.260 | 0.251 | 0.263 | 0.285 | 0.236 | 0.222 | 0.301 | 0.290 | 0.240 | 0.255 | 0.240 | 0.250 | 0.250 | 0.254 | 0.240 |
| Na (A) | 0.240 | 0.270 | 0.270 | 0.270 | 0.280 | 0.289 | 0.287 | 0.195 | 0.254 | 0.308 | 0.189 | 0.220 | 0.300 | 0.275 | 0.320 | 0.280 | 0.280 | 0.276 | 0.260 |
| K | 0.079 | 0.077 | 0.074 | 0.081 | 0.084 | 0.085 | 0.083 | 0.076 | 0.072 | 0.085 | 0.078 | 0.090 | 0.083 | 0.081 | 0.078 | 0.091 | 0.084 | 0.084 | 0.082 |
| total | 15.317 | 15.354 | 15.350 | 15.359 | 15.384 | 15.389 | 15.367 | 15.273 | 15.321 | 15.386 | 15.268 | 15.317 | 15.382 | 15.346 | 15.395 | 15.365 | 15.363 | 15.357 | 15.343 |

Appendix 1B: Amphibole Analyses

| | Sample GRUV, Location 1 | | | | Sample GRUV, Location 2 | | | | | | | | | | Sample A321 | | | |
|---|---|---|---|---|---|---|---|---|---|---|---|---|---|---|---|---|---|---|
| Analysis # | 21 | 22 | 23 | 24 | 25 | 26 | 27 | 28 | 29 | 30 | 31 | 32 | 33 | 34 | 89 | 90 | 91 | 92 |
| SiO2 | 42.64 | 44.31 | 44.58 | 44.12 | 43.82 | 43.95 | 43.19 | 44.47 | 43.61 | 44.14 | 43.53 | 43.43 | 43.99 | 43.50 | 39.29 | 39.70 | 39.27 | 39.73 |
| TiO2 | 0.31 | 0.36 | 0.33 | 0.37 | 0.35 | 0.35 | 0.34 | 0.31 | 0.39 | 0.31 | 0.39 | 0.32 | 0.33 | 0.36 | 0.41 | 0.37 | 0.37 | 0.39 |
| Al2O3 | 14.79 | 14.28 | 13.78 | 14.21 | 14.39 | 14.13 | 14.66 | 14.01 | 14.31 | 14.05 | 14.13 | 14.54 | 14.27 | 14.59 | 17.51 | 17.53 | 18.25 | 17.93 |
| Cr2O3 | 0.01 | 0.14 | 0.09 | 0.03 | 0.00 | 0.01 | 0.02 | 0.01 | 0.00 | 0.06 | 0.03 | 0.00 | 0.04 | 0.07 | 0.02 | 0.04 | 0.04 | 0.03 |
| MgO | 12.46 | 12.15 | 12.25 | 12.13 | 11.95 | 12.14 | 11.80 | 12.21 | 11.92 | 12.17 | 11.84 | 12.07 | 12.10 | 12.00 | 5.06 | 4.98 | 5.11 | 5.10 |
| CaO | 10.47 | 11.03 | 11.21 | 11.12 | 11.12 | 11.07 | 11.03 | 10.86 | 11.10 | 10.89 | 11.05 | 11.06 | 10.69 | 11.07 | 10.11 | 10.07 | 10.10 | 10.48 |
| MnO | 0.16 | 0.17 | 0.14 | 0.21 | 0.19 | 0.14 | 0.13 | 0.21 | 0.18 | 0.19 | 0.18 | 0.13 | 0.17 | 0.12 | 0.09 | 0.09 | 0.16 | 0.07 |
| FeO | 12.70 | 12.16 | 12.39 | 12.36 | 12.11 | 12.25 | 12.01 | 12.13 | 12.38 | 12.24 | 12.29 | 12.32 | 11.71 | 12.05 | 20.81 | 20.51 | 20.27 | 20.49 |
| Na2O | 1.94 | 2.05 | 1.94 | 2.00 | 2.04 | 2.03 | 2.06 | 2.13 | 2.03 | 2.11 | 1.98 | 2.05 | 2.29 | 2.03 | 2.03 | 2.07 | 2.20 | 2.03 |
| K2O | 0.36 | 0.30 | 0.31 | 0.31 | 0.34 | 0.31 | 0.37 | 0.31 | 0.35 | 0.35 | 0.37 | 0.35 | 0.34 | 0.36 | 0.55 | 0.54 | 0.59 | 0.59 |
| H2O | 2.02 | 2.05 | 2.05 | 2.04 | 2.03 | 2.03 | 2.02 | 2.04 | 2.03 | 2.04 | 2.02 | 2.03 | 2.03 | 2.03 | 1.93 | 1.94 | 1.95 | 1.96 |
| total | 97.86 | 99.00 | 99.05 | 98.89 | 98.35 | 98.40 | 97.63 | 98.67 | 98.29 | 98.53 | 97.83 | 98.30 | 97.96 | 98.17 | 97.81 | 97.83 | 98.30 | 98.78 |
| | | | | | | | | | | | | | | | | | | |
| Si | 6.183 | 6.404 | 6.448 | 6.389 | 6.390 | 6.396 | 6.346 | 6.442 | 6.367 | 6.410 | 6.388 | 6.329 | 6.420 | 6.348 | 5.989 | 6.048 | 5.950 | 6.007 |
| Al (IV) | 1.820 | 1.600 | 1.550 | 1.610 | 1.610 | 1.600 | 1.650 | 1.560 | 1.630 | 1.590 | 1.610 | 1.670 | 1.580 | 1.650 | 2.010 | 1.950 | 2.050 | 1.990 |
| Al (VI) | 0.710 | 0.830 | 0.800 | 0.820 | 0.860 | 0.820 | 0.890 | 0.830 | 0.830 | 0.800 | 0.830 | 0.830 | 0.880 | 0.860 | 1.140 | 1.200 | 1.210 | 1.210 |
| Ti | 0.034 | 0.039 | 0.035 | 0.040 | 0.038 | 0.038 | 0.037 | 0.033 | 0.043 | 0.034 | 0.043 | 0.036 | 0.037 | 0.040 | 0.047 | 0.043 | 0.043 | 0.044 |
| Fe3+ | 1.173 | 0.616 | 0.599 | 0.642 | 0.555 | 0.626 | 0.562 | 0.628 | 0.602 | 0.651 | 0.578 | 0.677 | 0.572 | 0.604 | 0.770 | 0.661 | 0.712 | 0.594 |
| Cr | 0.001 | 0.016 | 0.010 | 0.004 | 0.000 | 0.001 | 0.002 | 0.001 | 0.000 | 0.007 | 0.003 | 0.000 | 0.004 | 0.008 | 0.002 | 0.004 | 0.004 | 0.003 |
| Mg | 2.693 | 2.616 | 2.641 | 2.618 | 2.598 | 2.634 | 2.584 | 2.637 | 2.593 | 2.633 | 2.590 | 2.622 | 2.633 | 2.610 | 1.150 | 1.131 | 1.153 | 1.149 |
| Fe2+ | 0.368 | 0.854 | 0.899 | 0.855 | 0.921 | 0.865 | 0.914 | 0.841 | 0.909 | 0.836 | 0.929 | 0.824 | 0.858 | 0.866 | 1.883 | 1.952 | 1.857 | 1.998 |
| Mn | 0.020 | 0.020 | 0.017 | 0.026 | 0.024 | 0.017 | 0.016 | 0.026 | 0.023 | 0.023 | 0.023 | 0.016 | 0.021 | 0.014 | 0.011 | 0.011 | 0.021 | 0.009 |
| Ca | 1.626 | 1.708 | 1.737 | 1.725 | 1.737 | 1.726 | 1.737 | 1.686 | 1.737 | 1.695 | 1.738 | 1.727 | 1.671 | 1.731 | 1.651 | 1.643 | 1.639 | 1.697 |
| Na (M4) | 0.375 | 0.295 | 0.260 | 0.260 | 0.260 | 0.264 | 0.265 | 0.310 | 0.260 | 0.316 | 0.260 | 0.270 | 0.330 | 0.270 | 0.350 | 0.360 | 0.360 | 0.294 |
| Na (A) | 0.175 | 0.275 | 0.280 | 0.300 | 0.320 | 0.306 | 0.325 | 0.290 | 0.310 | 0.274 | 0.300 | 0.310 | 0.320 | 0.300 | 0.250 | 0.250 | 0.290 | 0.296 |
| K | 0.066 | 0.056 | 0.057 | 0.057 | 0.064 | 0.058 | 0.070 | 0.057 | 0.066 | 0.064 | 0.070 | 0.065 | 0.063 | 0.067 | 0.107 | 0.104 | 0.114 | 0.115 |
| total | 15.244 | 15.331 | 15.335 | 15.347 | 15.377 | 15.350 | 15.397 | 15.341 | 15.371 | 15.333 | 15.364 | 15.375 | 15.388 | 15.367 | 15.360 | 15.358 | 15.403 | 15.406 |

Appendix 1B: Amphibole Analyses

| | Sample A114A, Location 1 | | | | | | | | Sample A114A, Location 2 | | | | | | |
|---|---|---|---|---|---|---|---|---|---|---|---|---|---|---|---|
| Analysis # | 64 | 65 | 66 | 67 | 68 | 69 | 70 | 71 | 72 | 73 | 74 | 75 | 76 | 77 | 78 |
| SiO2 | 43.93 | 43.59 | 43.90 | 43.44 | 43.93 | 44.42 | 43.67 | 43.72 | 44.23 | 43.83 | 45.09 | 44.82 | 44.58 | 44.02 | 44.47 |
| TiO2 | 0.31 | 0.25 | 0.35 | 0.26 | 0.37 | 0.33 | 0.22 | 0.24 | 0.30 | 0.27 | 0.35 | 0.26 | 0.25 | 0.24 | 0.26 |
| Al2O3 | 14.53 | 14.28 | 14.51 | 15.18 | 15.11 | 13.52 | 14.54 | 14.57 | 14.37 | 14.32 | 13.37 | 14.07 | 14.01 | 14.34 | 14.30 |
| Cr2O3 | 0.18 | 0.16 | 0.13 | 0.05 | 0.20 | 0.14 | 0.18 | 0.19 | 0.03 | 0.06 | 0.09 | 0.09 | 0.09 | 0.02 | 0.15 |
| MgO | 11.40 | 12.18 | 11.25 | 11.29 | 10.75 | 11.94 | 11.39 | 11.66 | 12.03 | 11.79 | 11.49 | 12.12 | 12.07 | 11.59 | 11.85 |
| CaO | 11.08 | 10.73 | 11.07 | 11.15 | 10.74 | 11.40 | 11.37 | 11.30 | 11.17 | 11.05 | 11.17 | 11.20 | 11.33 | 11.04 | 11.35 |
| MnO | 0.19 | 0.21 | 0.16 | 0.25 | 0.17 | 0.18 | 0.14 | 0.17 | 0.19 | 0.14 | 0.16 | 0.13 | 0.15 | 0.21 | 0.17 |
| FeO | 12.59 | 12.37 | 12.31 | 12.01 | 12.32 | 12.25 | 11.93 | 11.68 | 12.05 | 11.78 | 12.78 | 11.71 | 11.94 | 12.60 | 12.35 |
| Na2O | 1.93 | 1.57 | 1.95 | 1.97 | 2.13 | 1.52 | 1.91 | 1.90 | 1.95 | 1.97 | 1.75 | 1.87 | 1.88 | 1.95 | 1.86 |
| K2O | 0.35 | 0.35 | 0.32 | 0.36 | 0.42 | 0.35 | 0.33 | 0.33 | 0.34 | 0.32 | 0.36 | 0.34 | 0.33 | 0.35 | 0.36 |
| H2O | 2.03 | 2.02 | 2.02 | 2.03 | 2.03 | 2.03 | 2.02 | 2.02 | 2.04 | 2.02 | 2.04 | 2.05 | 2.04 | 2.03 | 2.05 |
| total | 98.52 | 97.71 | 97.98 | 97.97 | 98.16 | 98.08 | 97.70 | 97.77 | 98.71 | 97.54 | 98.63 | 98.65 | 98.67 | 98.39 | 99.16 |
| Si | 6.407 | 6.337 | 6.443 | 6.370 | 6.442 | 6.496 | 6.437 | 6.422 | 6.418 | 6.439 | 6.576 | 6.500 | 6.478 | 6.421 | 6.439 |
| Al (IV) | 1.590 | 1.660 | 1.560 | 1.630 | 1.560 | 1.500 | 1.560 | 1.580 | 1.580 | 1.560 | 1.420 | 1.500 | 1.520 | 1.580 | 1.560 |
| Al (VI) | 0.910 | 0.790 | 0.950 | 0.990 | 1.050 | 0.830 | 0.970 | 0.940 | 0.880 | 0.920 | 0.880 | 0.910 | 0.880 | 0.890 | 0.880 |
| Ti | 0.034 | 0.028 | 0.039 | 0.028 | 0.040 | 0.037 | 0.025 | 0.027 | 0.033 | 0.029 | 0.038 | 0.028 | 0.028 | 0.026 | 0.028 |
| Fe3+ | 0.523 | 0.954 | 0.414 | 0.440 | 0.339 | 0.519 | 0.330 | 0.398 | 0.551 | 0.477 | 0.410 | 0.459 | 0.461 | 0.570 | 0.497 |
| Cr | 0.021 | 0.019 | 0.015 | 0.006 | 0.023 | 0.016 | 0.021 | 0.022 | 0.004 | 0.007 | 0.010 | 0.010 | 0.010 | 0.003 | 0.017 |
| Mg | 2.478 | 2.638 | 2.461 | 2.467 | 2.349 | 2.602 | 2.503 | 2.552 | 2.602 | 2.580 | 2.499 | 2.619 | 2.615 | 2.521 | 2.558 |
| Fe2+ | 1.013 | 0.550 | 1.097 | 1.033 | 1.172 | 0.979 | 1.140 | 1.036 | 0.911 | 0.970 | 1.148 | 0.962 | 0.990 | 0.967 | 0.998 |
| Mn | 0.024 | 0.026 | 0.020 | 0.030 | 0.021 | 0.022 | 0.017 | 0.021 | 0.023 | 0.017 | 0.020 | 0.016 | 0.019 | 0.026 | 0.021 |
| Ca | 1.732 | 1.671 | 1.741 | 1.753 | 1.687 | 1.787 | 1.796 | 1.779 | 1.737 | 1.739 | 1.745 | 1.740 | 1.764 | 1.725 | 1.761 |
| Na (M4) | 0.270 | 0.330 | 0.266 | 0.256 | 0.316 | 0.205 | 0.200 | 0.220 | 0.260 | 0.260 | 0.252 | 0.256 | 0.240 | 0.275 | 0.234 |
| Na (A) | 0.270 | 0.110 | 0.284 | 0.304 | 0.294 | 0.225 | 0.340 | 0.320 | 0.290 | 0.300 | 0.248 | 0.274 | 0.290 | 0.275 | 0.286 |
| K | 0.065 | 0.064 | 0.060 | 0.068 | 0.078 | 0.066 | 0.061 | 0.062 | 0.063 | 0.060 | 0.066 | 0.064 | 0.061 | 0.066 | 0.066 |
| total | 15.337 | 15.177 | 15.350 | 15.376 | 15.373 | 15.282 | 15.400 | 15.378 | 15.352 | 15.359 | 15.313 | 15.338 | 15.355 | 15.344 | 15.346 |

Appendix 1B: Amphibole Analyses

| Sample A20 | | | | | | | | Sample A1463 | | | | | | | | | |
|---|---|---|---|---|---|---|---|---|---|---|---|---|---|---|---|---|---|
| Analysis # | 80 | 81 | 82 | 83 | 84 | 85 | 87 | 52 | 53 | 55 | 56 | 57 | 58 | 59 | 60 | 61 | 62 |
| SiO2 | 44.42 | 46.32 | 51.92 | 44.88 | 48.82 | 45.56 | 46.05 | 52.89 | 45.74 | 47.70 | 45.73 | 47.10 | 47.57 | 46.56 | 50.65 | 45.66 | 48.11 |
| TiO2 | 0.37 | 0.24 | 0.13 | 0.36 | 0.23 | 0.40 | 0.35 | 0.08 | 0.29 | 0.26 | 0.31 | 0.27 | 0.25 | 0.27 | 0.14 | 0.30 | 0.25 |
| Al2O3 | 11.07 | 9.91 | 4.89 | 11.10 | 7.96 | 11.25 | 10.76 | 3.92 | 11.98 | 9.60 | 12.23 | 10.61 | 10.15 | 11.55 | 6.58 | 11.94 | 9.15 |
| Cr2O3 | 0.03 | 0.16 | 0.02 | 0.09 | 0.13 | 0.15 | 0.11 | 0.11 | 0.15 | 0.07 | 0.12 | 0.09 | 0.14 | 0.07 | 0.11 | 0.17 | 0.18 |
| MgO | 11.63 | 13.06 | 16.38 | 11.95 | 13.92 | 12.10 | 12.19 | 16.40 | 11.89 | 13.32 | 11.88 | 12.95 | 13.08 | 12.43 | 15.03 | 11.87 | 13.87 |
| CaO | 11.11 | 11.18 | 11.84 | 11.21 | 11.20 | 11.00 | 11.26 | 12.61 | 11.83 | 11.95 | 11.67 | 11.81 | 11.89 | 11.66 | 12.09 | 11.44 | 11.99 |
| MnO | 0.11 | 0.15 | 0.16 | 0.13 | 0.12 | 0.14 | 0.13 | 0.16 | 0.19 | 0.20 | 0.21 | 0.18 | 0.18 | 0.23 | 0.16 | 0.26 | 0.20 |
| FeO | 14.10 | 13.73 | 10.68 | 14.06 | 12.48 | 13.64 | 13.71 | 10.33 | 12.48 | 11.56 | 12.85 | 11.87 | 12.25 | 12.16 | 11.22 | 13.09 | 11.67 |
| Na2O | 1.72 | 1.56 | 0.85 | 1.88 | 1.48 | 1.81 | 1.69 | 0.46 | 1.45 | 1.17 | 1.51 | 1.31 | 1.23 | 1.46 | 0.80 | 1.51 | 1.09 |
| K2O | 0.26 | 0.28 | 0.12 | 0.29 | 0.23 | 0.39 | 0.28 | 0.08 | 0.29 | 0.22 | 0.28 | 0.22 | 0.21 | 0.30 | 0.18 | 0.33 | 0.21 |
| H2O | 1.98 | 2.03 | 2.08 | 2.00 | 2.05 | 2.02 | 2.03 | 2.09 | 2.03 | 2.04 | 2.04 | 2.05 | 2.05 | 2.05 | 2.07 | 2.03 | 2.06 |
| total | 96.80 | 98.63 | 99.06 | 97.94 | 98.62 | 98.46 | 98.53 | 99.13 | 98.32 | 98.10 | 98.83 | 98.44 | 99.00 | 98.73 | 99.03 | 98.60 | 98.78 |
| Si | 6.638 | 6.737 | 7.396 | 6.631 | 7.071 | 6.669 | 6.740 | 7.566 | 6.717 | 6.971 | 6.671 | 6.860 | 6.893 | 6.777 | 7.275 | 6.673 | 6.962 |
| Al (IV) | 1.360 | 1.260 | 0.600 | 1.370 | 0.930 | 1.330 | 1.260 | 0.430 | 1.280 | 1.030 | 1.330 | 1.140 | 1.110 | 1.220 | 0.730 | 1.330 | 0.730 |
| Al (VI) | 0.590 | 0.440 | 0.220 | 0.560 | 0.430 | 0.610 | 0.600 | 0.230 | 0.790 | 0.620 | 0.770 | 0.680 | 0.620 | 0.760 | 0.380 | 0.730 | 0.520 |
| Ti | 0.042 | 0.026 | 0.014 | 0.040 | 0.025 | 0.044 | 0.038 | 0.009 | 0.032 | 0.029 | 0.034 | 0.029 | 0.027 | 0.029 | 0.015 | 0.033 | 0.028 |
| Fe3+ | 0.578 | 0.779 | 0.486 | 0.574 | 0.501 | 0.576 | 0.513 | 0.168 | 0.219 | 0.224 | 0.344 | 0.297 | 0.333 | 0.293 | 0.316 | 0.436 | 0.377 |
| Cr | 0.004 | 0.018 | 0.002 | 0.010 | 0.014 | 0.018 | 0.012 | 0.013 | 0.017 | 0.008 | 0.014 | 0.010 | 0.016 | 0.009 | 0.013 | 0.020 | 0.020 |
| Mg | 2.590 | 2.831 | 3.476 | 2.631 | 3.004 | 2.641 | 2.659 | 3.496 | 2.603 | 2.901 | 2.583 | 2.811 | 2.824 | 2.696 | 3.216 | 2.585 | 2.992 |
| Fe2+ | 1.184 | 0.890 | 0.787 | 1.164 | 1.011 | 1.093 | 1.165 | 1.069 | 1.314 | 1.188 | 1.224 | 1.149 | 1.151 | 1.187 | 1.032 | 1.164 | 1.035 |
| Mn | 0.014 | 0.019 | 0.019 | 0.017 | 0.015 | 0.017 | 0.016 | 0.019 | 0.023 | 0.025 | 0.026 | 0.023 | 0.022 | 0.028 | 0.019 | 0.032 | 0.025 |
| Ca | 1.780 | 1.743 | 1.808 | 1.774 | 1.738 | 1.725 | 1.766 | 1.932 | 1.862 | 1.871 | 1.810 | 1.843 | 1.850 | 1.819 | 1.860 | 1.792 | 1.859 |
| Na (M4) | 0.220 | 0.257 | 0.175 | 0.243 | 0.266 | 0.270 | 0.224 | 0.070 | 0.140 | 0.130 | 0.190 | 0.160 | 0.160 | 0.180 | 0.150 | 0.210 | 0.140 |
| Na (A) | 0.280 | 0.183 | 0.055 | 0.297 | 0.144 | 0.240 | 0.256 | 0.060 | 0.270 | 0.200 | 0.240 | 0.210 | 0.190 | 0.230 | 0.070 | 0.220 | 0.170 |
| K | 0.049 | 0.053 | 0.022 | 0.055 | 0.042 | 0.072 | 0.052 | 0.015 | 0.055 | 0.041 | 0.052 | 0.040 | 0.039 | 0.055 | 0.033 | 0.062 | 0.039 |
| total | 15.329 | 15.236 | 15.060 | 15.366 | 15.192 | 15.306 | 15.301 | 15.077 | 15.321 | 15.238 | 15.288 | 15.251 | 15.234 | 15.282 | 15.109 | 15.286 | 14.897 |

Appendix 1B: Amphibole Analyses

| | Sample A1573, Location 1 | | | | | | | Sample A1573, Location 2 | | | | | | | | |
|---|---|---|---|---|---|---|---|---|---|---|---|---|---|---|---|---|
| Analysis # | 45 | 46 | 47 | 48 | 49 | 50 | 51 | 35 | 36 | 37 | 38 | 39 | 40 | 41 | 42 | 44 |
| SiO2 | 42.28 | 44.55 | 44.16 | 42.15 | 42.66 | 42.32 | 42.47 | 42.14 | 48.36 | 42.85 | 43.08 | 41.59 | 43.22 | 41.85 | 42.53 | 41.37 |
| TiO2 | 0.41 | 0.32 | 0.30 | 0.42 | 0.42 | 0.46 | 0.39 | 0.38 | 0.17 | 0.43 | 0.34 | 0.42 | 0.35 | 0.45 | 0.36 | 0.48 |
| Al2O3 | 16.00 | 12.82 | 13.61 | 15.90 | 14.44 | 15.81 | 14.52 | 16.10 | 6.90 | 14.94 | 15.00 | 16.15 | 14.36 | 16.56 | 15.65 | 16.51 |
| Cr2O3 | 0.04 | 0.00 | 0.05 | 0.01 | 0.03 | 0.04 | 0.01 | 0.01 | 0.02 | 0.01 | 0.00 | 0.00 | 0.00 | 0.00 | 0.01 | 0.00 |
| MgO | 8.62 | 10.25 | 9.76 | 8.77 | 8.96 | 8.87 | 9.10 | 8.35 | 13.37 | 8.79 | 8.68 | 8.72 | 9.54 | 8.59 | 8.74 | 8.25 |
| CaO | 11.08 | 11.63 | 11.08 | 11.32 | 11.01 | 11.21 | 11.22 | 11.08 | 11.81 | 11.20 | 11.25 | 11.15 | 11.12 | 11.27 | 11.06 | 11.02 |
| MnO | 0.11 | 0.16 | 0.21 | 0.13 | 0.18 | 0.26 | 0.24 | 0.19 | 0.21 | 0.15 | 0.22 | 0.11 | 0.16 | 0.15 | 0.23 | 0.16 |
| FeO | 15.74 | 15.31 | 15.02 | 15.49 | 16.42 | 15.48 | 16.13 | 15.64 | 12.63 | 15.59 | 16.06 | 15.27 | 15.25 | 15.34 | 15.84 | 15.70 |
| Na2O | 1.82 | 1.31 | 1.61 | 1.76 | 1.68 | 1.80 | 1.67 | 1.74 | 0.71 | 1.70 | 1.64 | 1.78 | 1.64 | 1.87 | 1.84 | 1.77 |
| K2O | 0.44 | 0.30 | 0.32 | 0.45 | 0.39 | 0.40 | 0.41 | 0.48 | 0.18 | 0.45 | 0.46 | 0.45 | 0.44 | 0.44 | 0.43 | 0.44 |
| H2O | 2.00 | 2.01 | 2.01 | 2.00 | 1.99 | 2.00 | 1.99 | 1.99 | 2.00 | 1.99 | 2.00 | 1.98 | 2.00 | 2.00 | 2.00 | 1.98 |
| total | 98.54 | 98.67 | 98.12 | 98.40 | 98.18 | 98.65 | 98.14 | 98.10 | 96.36 | 98.09 | 98.74 | 97.60 | 98.05 | 98.52 | 98.68 | 97.68 |
| | | | | | | | | | | | | | | | | |
| Si | 6.275 | 6.572 | 6.541 | 6.273 | 6.355 | 6.272 | 6.335 | 6.289 | 7.201 | 6.399 | 6.395 | 6.229 | 6.421 | 6.220 | 6.303 | 6.199 |
| Al (IV) | 1.730 | 1.430 | 1.460 | 1.730 | 1.640 | 1.730 | 1.670 | 1.710 | 0.800 | 1.600 | 1.600 | 1.770 | 1.580 | 1.780 | 1.700 | 1.800 |
| Al (VI) | 1.070 | 0.800 | 0.920 | 1.060 | 0.900 | 1.030 | 0.880 | 1.120 | 0.410 | 1.030 | 1.020 | 1.080 | 0.930 | 1.120 | 1.030 | 1.120 |
| Ti | 0.046 | 0.035 | 0.034 | 0.047 | 0.047 | 0.052 | 0.044 | 0.043 | 0.019 | 0.048 | 0.038 | 0.047 | 0.039 | 0.051 | 0.040 | 0.054 |
| Fe3+ | 0.422 | 0.447 | 0.429 | 0.368 | 0.579 | 0.433 | 0.540 | 0.364 | 0.336 | 0.312 | 0.372 | 0.416 | 0.471 | 0.347 | 0.457 | 0.438 |
| Cr | 0.005 | 0.000 | 0.006 | 0.001 | 0.004 | 0.005 | 0.001 | 0.002 | 0.002 | 0.001 | 0.000 | 0.000 | 0.000 | 0.000 | 0.001 | 0.000 |
| Mg | 1.907 | 2.254 | 2.154 | 1.946 | 1.988 | 1.959 | 2.022 | 1.858 | 2.967 | 1.956 | 1.921 | 1.946 | 2.112 | 1.903 | 1.930 | 1.843 |
| Fe2+ | 1.531 | 1.442 | 1.432 | 1.560 | 1.466 | 1.486 | 1.472 | 1.589 | 1.237 | 1.636 | 1.622 | 1.496 | 1.424 | 1.560 | 1.506 | 1.530 |
| Mn | 0.013 | 0.020 | 0.027 | 0.017 | 0.023 | 0.032 | 0.031 | 0.023 | 0.027 | 0.019 | 0.028 | 0.013 | 0.020 | 0.019 | 0.029 | 0.020 |
| Ca | 1.763 | 1.838 | 1.758 | 1.804 | 1.758 | 1.781 | 1.793 | 1.772 | 1.885 | 1.793 | 1.789 | 1.789 | 1.770 | 1.794 | 1.757 | 1.770 |
| Na (M4) | 0.246 | 0.165 | 0.243 | 0.195 | 0.226 | 0.220 | 0.224 | 0.230 | 0.102 | 0.201 | 0.214 | 0.200 | 0.241 | 0.210 | 0.240 | 0.226 |
| Na (A) | 0.274 | 0.215 | 0.217 | 0.315 | 0.264 | 0.300 | 0.256 | 0.270 | 0.108 | 0.289 | 0.256 | 0.320 | 0.229 | 0.330 | 0.290 | 0.284 |
| K | 0.083 | 0.057 | 0.060 | 0.086 | 0.073 | 0.075 | 0.078 | 0.091 | 0.035 | 0.086 | 0.087 | 0.086 | 0.083 | 0.083 | 0.080 | 0.085 |
| total | 15.365 | 15.276 | 15.281 | 15.400 | 15.324 | 15.374 | 15.346 | 15.360 | 15.128 | 15.368 | 15.342 | 15.392 | 15.319 | 15.417 | 15.362 | 15.368 |

Appendix 1C: Biotite Analyses

| Sample: | A791 | | A1718 | | A1945 | | | | |
|---|---|---|---|---|---|---|---|---|---|
| Analysis #: | 25 | 26 | 27 | 28 | 17 | 18 | 20 | 14 | 21 |
| SiO2 | 35.11 | 35.04 | 35.62 | 35.63 | 36.80 | 36.50 | 36.38 | 36.44 | 36.76 |
| TiO2 | 1.38 | 1.65 | 1.24 | 1.79 | 1.77 | 1.81 | 1.75 | 1.53 | 1.50 |
| Al2O3 | 18.33 | 18.18 | 18.19 | 17.71 | 17.87 | 17.88 | 18.18 | 17.64 | 17.80 |
| Cr2O3 | 0.04 | 0.00 | 0.05 | 0.03 | 0.02 | 0.06 | 0.03 | 0.05 | 0.05 |
| MgO | 8.90 | 8.88 | 11.37 | 11.22 | 12.85 | 12.57 | 12.51 | 12.74 | 12.58 |
| CaO | 0.00 | 0.00 | 0.01 | 0.01 | 0.04 | 0.00 | 0.00 | 0.02 | 0.03 |
| MnO | 0.03 | 0.01 | 0.00 | 0.00 | 0.02 | 0.06 | 0.04 | 0.11 | 0.07 |
| FeO | 20.57 | 20.41 | 17.70 | 17.38 | 15.39 | 14.69 | 15.02 | 14.91 | 16.10 |
| BaO | 0.00 | 0.00 | 0.00 | 0.00 | 0.00 | 0.00 | 0.00 | 0.00 | 0.00 |
| Na2O | 0.21 | 0.23 | 0.16 | 0.19 | 0.20 | 0.17 | 0.17 | 0.13 | 0.15 |
| K2O | 8.64 | 8.47 | 8.59 | 8.72 | 9.11 | 9.14 | 9.20 | 9.34 | 9.30 |
| H2O | 3.71 | 3.65 | 3.71 | 3.74 | 3.87 | 3.73 | 3.81 | 3.80 | 3.76 |
| F | 0.25 | 0.38 | 0.37 | 0.29 | 0.21 | 0.42 | 0.29 | 0.25 | 0.43 |
| Cl | 0.04 | 0.04 | 0.02 | 0.01 | 0.06 | 0.03 | 0.01 | 0.04 | 0.02 |
| total | 97.21 | 96.93 | 97.02 | 96.72 | 98.19 | 97.07 | 97.41 | 96.98 | 98.54 |
| O = F | -0.11 | -0.16 | -0.16 | -0.12 | -0.09 | -0.18 | -0.12 | -0.11 | -0.18 |
| O = Cl | -0.01 | -0.01 | -0.01 | 0.00 | -0.01 | -0.01 | 0.00 | -0.01 | -0.01 |
| total | 97.10 | 96.76 | 96.86 | 96.60 | 98.09 | 96.89 | 97.28 | 96.87 | 98.35 |
| Si | 2.740 | 2.741 | 2.745 | 2.754 | 2.774 | 2.779 | 2.763 | 2.782 | 2.776 |
| Ti | 0.081 | 0.097 | 0.072 | 0.104 | 0.100 | 0.104 | 0.100 | 0.088 | 0.085 |
| Al | 1.686 | 1.676 | 1.652 | 1.613 | 1.587 | 1.604 | 1.627 | 1.587 | 1.584 |
| Cr | 0.003 | 0.000 | 0.003 | 0.002 | 0.001 | 0.003 | 0.002 | 0.003 | 0.003 |
| Mg | 1.035 | 1.035 | 1.306 | 1.293 | 1.444 | 1.426 | 1.416 | 1.450 | 1.416 |
| Ca | 0.000 | 0.000 | 0.001 | 0.001 | 0.003 | 0.000 | 0.000 | 0.001 | 0.003 |
| Mn | 0.002 | 0.001 | 0.000 | 0.000 | 0.001 | 0.004 | 0.003 | 0.007 | 0.005 |
| Fe | 1.342 | 1.335 | 1.141 | 1.124 | 0.970 | 0.936 | 0.954 | 0.952 | 1.016 |
| Ba | 0.000 | 0.000 | 0.000 | 0.000 | 0.000 | 0.000 | 0.000 | 0.000 | 0.000 |
| Na | 0.031 | 0.034 | 0.024 | 0.029 | 0.029 | 0.025 | 0.025 | 0.019 | 0.022 |
| K | 0.860 | 0.845 | 0.844 | 0.860 | 0.875 | 0.887 | 0.891 | 0.910 | 0.895 |
| total | 7.780 | 7.764 | 7.788 | 7.780 | 7.784 | 7.768 | 7.781 | 7.799 | 7.805 |
| <H> | 1.933 | 1.902 | 1.908 | 1.927 | 1.943 | 1.894 | 1.928 | 1.933 | 1.894 |
| <F> | 0.063 | 0.094 | 0.090 | 0.072 | 0.050 | 0.101 | 0.071 | 0.061 | 0.103 |
| <Cl> | 0.005 | 0.005 | 0.003 | 0.001 | 0.007 | 0.004 | 0.001 | 0.005 | 0.003 |

Appendix 1C: Biotite Analyses

| Sample: | A321 | | A933 | | | | A2061A | | |
|---|---|---|---|---|---|---|---|---|---|
| Analysis #: | 30 | 31 | 2 | 3 | 4 | 5 | 13 | 7 | 9 |
| SiO2 | 35.43 | 34.51 | 34.20 | 35.95 | 35.74 | 35.50 | 37.49 | 38.48 | 37.94 |
| TiO2 | 1.64 | 1.71 | 0.27 | 1.65 | 1.63 | 1.74 | 1.19 | 1.16 | 1.30 |
| Al2O3 | 16.81 | 16.82 | 17.45 | 18.23 | 17.86 | 17.50 | 16.41 | 16.74 | 16.40 |
| Cr2O3 | 0.07 | 0.09 | 0.01 | 0.01 | 0.03 | 0.03 | 0.02 | 0.07 | 0.00 |
| MgO | 9.40 | 9.19 | 9.02 | 9.74 | 9.46 | 9.59 | 15.68 | 15.78 | 16.32 |
| CaO | 0.08 | 0.01 | 0.27 | 0.03 | 0.07 | 0.17 | 0.02 | 0.04 | 0.01 |
| MnO | 0.04 | 0.01 | 0.06 | 0.10 | 0.03 | 0.03 | 0.30 | 0.46 | 0.37 |
| FeO | 21.29 | 21.92 | 21.55 | 19.28 | 19.51 | 19.45 | 11.78 | 11.52 | 11.73 |
| BaO | 0.00 | 0.00 | 0.00 | 0.00 | 0.00 | 0.00 | 0.00 | 0.00 | 0.00 |
| Na2O | 0.19 | 0.11 | 0.17 | 0.15 | 0.15 | 0.17 | 0.22 | 0.13 | 0.14 |
| K2O | 8.73 | 8.39 | 7.24 | 8.86 | 8.69 | 7.72 | 9.57 | 9.82 | 9.69 |
| H2O | 3.70 | 3.68 | 3.58 | 3.72 | 3.73 | 3.71 | 3.65 | 3.76 | 3.63 |
| F | 0.29 | 0.21 | 0.27 | 0.38 | 0.27 | 0.23 | 0.65 | 0.60 | 0.83 |
| Cl | 0.01 | 0.03 | 0.04 | 0.01 | 0.01 | 0.02 | 0.02 | 0.00 | 0.01 |
| total | 97.66 | 96.69 | 94.13 | 98.09 | 97.20 | 95.88 | 97.00 | 98.56 | 98.36 |
| O = F | -0.12 | -0.09 | -0.11 | -0.16 | -0.11 | -0.10 | -0.28 | -0.25 | -0.35 |
| O = Cl | 0.00 | -0.01 | -0.01 | 0.00 | 0.00 | -0.01 | -0.01 | 0.00 | 0.00 |
| total | 97.54 | 96.60 | 94.01 | 97.93 | 97.08 | 95.78 | 96.72 | 98.31 | 98.01 |
| Si | 2.768 | 2.732 | 2.761 | 2.762 | 2.774 | 2.780 | 2.832 | 2.853 | 2.827 |
| Ti | 0.096 | 0.102 | 0.016 | 0.095 | 0.095 | 0.103 | 0.068 | 0.064 | 0.073 |
| Al | 1.548 | 1.570 | 1.660 | 1.651 | 1.633 | 1.615 | 1.461 | 1.463 | 1.440 |
| Cr | 0.004 | 0.006 | 0.001 | 0.001 | 0.002 | 0.002 | 0.001 | 0.004 | 0.000 |
| Mg | 1.094 | 1.084 | 1.086 | 1.115 | 1.095 | 1.120 | 1.766 | 1.744 | 1.812 |
| Ca | 0.007 | 0.001 | 0.024 | 0.002 | 0.006 | 0.014 | 0.002 | 0.003 | 0.001 |
| Mn | 0.003 | 0.001 | 0.004 | 0.006 | 0.002 | 0.002 | 0.019 | 0.029 | 0.024 |
| Fe | 1.391 | 1.452 | 1.455 | 1.239 | 1.266 | 1.274 | 0.744 | 0.714 | 0.731 |
| Ba | 0.000 | 0.000 | 0.000 | 0.000 | 0.000 | 0.000 | 0.000 | 0.000 | 0.000 |
| Na | 0.028 | 0.017 | 0.026 | 0.022 | 0.023 | 0.026 | 0.031 | 0.019 | 0.021 |
| K | 0.870 | 0.848 | 0.746 | 0.869 | 0.860 | 0.772 | 0.922 | 0.929 | 0.921 |
| total | 7.809 | 7.813 | 7.779 | 7.762 | 7.756 | 7.708 | 7.846 | 7.822 | 7.850 |
| <H> | 1.929 | 1.944 | 1.926 | 1.907 | 1.932 | 1.940 | 1.841 | 1.860 | 1.805 |
| <F> | 0.070 | 0.053 | 0.069 | 0.091 | 0.066 | 0.057 | 0.156 | 0.140 | 0.194 |
| <Cl> | 0.001 | 0.004 | 0.006 | 0.002 | 0.002 | 0.003 | 0.003 | 0.000 | 0.001 |

Appendix 1C: Biotite Analyses

Sample: A1337

| Analysis #: | 13 | 14 | 15 | 16 | 18 | 19 | 4 | 11 |
|---|---|---|---|---|---|---|---|---|
| SiO2 | 36.70 | 35.96 | 36.32 | 36.25 | 35.81 | 36.15 | 36.03 | 36.11 |
| TiO2 | 1.42 | 1.46 | 1.35 | 1.57 | 1.78 | 1.19 | 1.41 | 1.28 |
| Al2O3 | 17.84 | 17.10 | 17.57 | 17.38 | 17.15 | 17.45 | 17.33 | 18.17 |
| Cr2O3 | 0.12 | 0.09 | 0.03 | 0.07 | 0.18 | 0.05 | 0.06 | 0.04 |
| MgO | 11.36 | 11.77 | 11.59 | 11.99 | 10.90 | 11.53 | 11.01 | 10.95 |
| CaO | 0.00 | 0.03 | 0.02 | 0.00 | 0.04 | 0.11 | 0.03 | 0.07 |
| MnO | 0.15 | 0.15 | 0.15 | 0.16 | 0.18 | 0.12 | 0.19 | 0.15 |
| FeO | 17.46 | 18.46 | 17.76 | 16.83 | 17.70 | 17.02 | 19.53 | 17.59 |
| BaO | 0.00 | 0.00 | 0.00 | 0.00 | 0.00 | 0.00 | 0.00 | 0.00 |
| Na2O | 0.14 | 0.08 | 0.15 | 0.16 | 0.11 | 0.18 | 0.13 | 0.11 |
| K2O | 9.22 | 8.78 | 8.83 | 8.63 | 8.67 | 8.34 | 8.60 | 8.42 |
| H2O | 3.80 | 3.89 | 3.87 | 3.78 | 3.79 | 3.80 | 3.85 | 3.85 |
| F | 0.32 | 0.02 | 0.09 | 0.27 | 0.13 | 0.14 | 0.11 | 0.10 |
| Cl | 0.02 | 0.02 | 0.02 | 0.00 | 0.05 | 0.02 | 0.02 | 0.01 |
| Total | 98.55 | 97.81 | 97.75 | 97.10 | 96.49 | 96.09 | 98.29 | 96.86 |
| O = F | -0.13 | -0.01 | -0.04 | -0.12 | -0.05 | -0.06 | -0.05 | -0.04 |
| O = Cl | 0.00 | 0.00 | 0.00 | 0.00 | -0.01 | 0.00 | 0.00 | 0.00 |
| Total | 98.41 | 97.80 | 97.71 | 96.99 | 96.42 | 96.03 | 98.25 | 96.82 |
| | | | | | | | | |
| Si | 5.572 | 5.521 | 5.556 | 5.561 | 5.559 | 5.596 | 5.526 | 5.554 |
| Ti | 0.163 | 0.169 | 0.155 | 0.181 | 0.208 | 0.139 | 0.163 | 0.148 |
| Al | 3.193 | 3.095 | 3.167 | 3.142 | 3.138 | 3.183 | 3.134 | 3.294 |
| Cr | 0.014 | 0.011 | 0.003 | 0.009 | 0.022 | 0.006 | 0.007 | 0.004 |
| Mg | 2.572 | 2.695 | 2.643 | 2.741 | 2.523 | 2.660 | 2.517 | 2.510 |
| Ca | 0.000 | 0.004 | 0.004 | 0.001 | 0.007 | 0.019 | 0.005 | 0.012 |
| Mn | 0.019 | 0.019 | 0.020 | 0.021 | 0.023 | 0.015 | 0.025 | 0.020 |
| Fe | 2.217 | 2.370 | 2.273 | 2.160 | 2.298 | 2.203 | 2.505 | 2.262 |
| Ba | 0.000 | 0.000 | 0.000 | 0.000 | 0.000 | 0.000 | 0.000 | 0.000 |
| Na | 0.040 | 0.025 | 0.043 | 0.047 | 0.034 | 0.054 | 0.037 | 0.034 |
| K | 1.786 | 1.721 | 1.723 | 1.689 | 1.718 | 1.647 | 1.683 | 1.652 |
| Total | 15.575 | 15.630 | 15.587 | 15.551 | 15.529 | 15.521 | 15.601 | 15.491 |
| <H> | 3.844 | 3.987 | 3.952 | 3.867 | 3.924 | 3.928 | 3.944 | 3.949 |
| <F> | 0.151 | 0.009 | 0.044 | 0.133 | 0.063 | 0.067 | 0.052 | 0.049 |
| <Cl> | 0.005 | 0.004 | 0.005 | 0.000 | 0.013 | 0.005 | 0.005 | 0.003 |

Appendix 1C: Biotite Analyses

Sample: A1435

| Analysis #: | 1 | 2 | 3 | 12 | 14 | 15 | 21 |
|---|---|---|---|---|---|---|---|
| SiO2 | 34.66 | 34.65 | 34.92 | 34.66 | 35.06 | 35.41 | 34.72 |
| TiO2 | 1.81 | 1.82 | 1.92 | 1.62 | 2.01 | 1.70 | 1.85 |
| Al2O3 | 16.82 | 16.99 | 16.99 | 17.25 | 17.33 | 17.56 | 17.06 |
| Cr2O3 | 0.12 | 0.07 | 0.02 | 0.10 | 0.00 | 0.06 | 0.01 |
| MgO | 8.10 | 8.42 | 8.11 | 8.38 | 8.51 | 8.41 | 8.37 |
| CaO | 0.02 | 0.01 | 0.00 | 0.15 | 0.04 | 0.03 | 0.09 |
| MnO | 0.05 | 0.02 | 0.08 | 0.06 | 0.04 | 0.01 | 0.07 |
| FeO | 22.17 | 22.12 | 22.24 | 21.19 | 21.52 | 21.03 | 21.56 |
| BaO | 0.00 | 0.00 | 0.00 | 0.00 | 0.00 | 0.00 | 0.00 |
| Na2O | 0.16 | 0.11 | 0.12 | 0.18 | 0.15 | 0.18 | 0.18 |
| K2O | 8.71 | 8.74 | 8.86 | 8.15 | 8.90 | 8.92 | 8.40 |
| H2O | 3.77 | 3.79 | 3.80 | 3.76 | 3.82 | 3.83 | 3.77 |
| F | * | * | * | * | * | * | * |
| Cl | 0.00 | 0.00 | 0.01 | 0.02 | 0.03 | 0.00 | 0.01 |
| Total | 96.39 | 96.75 | 97.08 | 95.54 | 97.43 | 97.14 | 96.09 |
| O = F | * | * | * | * | * | * | * |
| O = Cl | 0.00 | 0.00 | 0.00 | -0.01 | -0.01 | 0.00 | 0.00 |
| Total | 96.39 | 96.75 | 97.07 | 95.54 | 97.42 | 97.14 | 96.08 |
| | | | | | | | |
| Si | 5.513 | 5.488 | 5.515 | 5.518 | 5.495 | 5.544 | 5.512 |
| Ti | 0.216 | 0.217 | 0.228 | 0.195 | 0.237 | 0.200 | 0.221 |
| Al | 3.153 | 3.171 | 3.162 | 3.237 | 3.202 | 3.240 | 3.192 |
| Cr | 0.015 | 0.009 | 0.003 | 0.013 | 0.000 | 0.008 | 0.002 |
| Mg | 1.920 | 1.988 | 1.908 | 1.988 | 1.988 | 1.962 | 1.980 |
| Ca | 0.003 | 0.002 | 0.001 | 0.026 | 0.007 | 0.006 | 0.016 |
| Mn | 0.007 | 0.003 | 0.011 | 0.009 | 0.005 | 0.001 | 0.009 |
| Fe | 2.950 | 2.929 | 2.937 | 2.822 | 2.820 | 2.753 | 2.863 |
| Ba | 0.000 | 0.000 | 0.000 | 0.000 | 0.000 | 0.000 | 0.000 |
| Na | 0.050 | 0.034 | 0.036 | 0.056 | 0.047 | 0.056 | 0.055 |
| K | 1.768 | 1.765 | 1.786 | 1.655 | 1.780 | 1.782 | 1.700 |
| Total | 15.595 | 15.605 | 15.586 | 15.517 | 15.580 | 15.551 | 15.549 |
| <H> | 4.000 | 4.000 | 3.998 | 3.994 | 3.992 | 4.000 | 3.997 |
| <F> | * | * | * | * | * | * | * |
| <Cl> | 0.000 | 0.000 | 0.002 | 0.006 | 0.008 | 0.000 | 0.004 |

*Flourine not analyzed due to problem of interference between spectrometers.

Appendix 1C: Biotite Analyses

Sample: A1341

| Analysis #: | 10 | 13 | 14 | 15 | 22 | 25 | 26 | 28 | 30 |
|---|---|---|---|---|---|---|---|---|---|
| SiO2 | 35.70 | 35.36 | 35.97 | 35.99 | 35.76 | 36.04 | 35.96 | 36.01 | 35.77 |
| TiO2 | 2.33 | 1.37 | 1.68 | 1.63 | 1.64 | 1.44 | 1.69 | 1.54 | 1.76 |
| Al2O3 | 18.03 | 17.66 | 17.83 | 17.94 | 17.97 | 18.29 | 18.22 | 17.50 | 17.91 |
| Cr2O3 | 0.05 | 0.02 | 0.03 | 0.01 | 0.02 | 0.00 | 0.03 | 0.03 | 0.04 |
| MgO | 9.65 | 9.97 | 10.14 | 10.28 | 10.05 | 10.64 | 10.07 | 10.15 | 9.77 |
| CaO | 0.02 | 0.02 | 0.00 | 0.00 | 0.00 | 0.01 | 0.00 | 0.01 | 0.00 |
| MnO | 0.00 | 0.00 | 0.01 | 0.00 | 0.02 | 0.04 | 0.00 | 0.00 | 0.05 |
| FeO | 19.03 | 20.09 | 19.47 | 19.47 | 8.87 | 18.65 | 19.83 | 20.05 | 20.32 |
| BaO | 0.00 | 0.00 | 0.00 | 0.00 | 0.00 | 0.00 | 0.00 | 0.00 | 0.00 |
| Na2O | 0.25 | 0.26 | 0.22 | 0.23 | 0.23 | 0.26 | 0.31 | 0.23 | 0.22 |
| K2O | 9.48 | 8.66 | 9.29 | 9.21 | 9.18 | 9.10 | 9.20 | 9.16 | 9.17 |
| H2O | 3.91 | 3.85 | 3.91 | 3.92 | 3.89 | 3.93 | 3.94 | 3.91 | 3.91 |
| F | * | * | * | * | * | * | * | * | * |
| Cl | 0.02 | 0.02 | 0.01 | 0.02 | 0.01 | 0.00 | 0.00 | 0.00 | 0.02 |
| Total | 98.45 | 97.29 | 98.56 | 98.68 | 97.64 | 98.39 | 99.26 | 98.59 | 98.93 |
| O = F | * | * | * | * | * | * | * | * | * |
| O = Cl | 0.00 | 0.00 | 0.00 | 0.00 | 0.00 | 0.00 | 0.00 | 0.00 | -0.01 |
| Total | 98.44 | 97.29 | 98.56 | 98.68 | 97.64 | 98.39 | 99.26 | 98.59 | 98.93 |
| | | | | | | | | | |
| Si | 5.476 | 5.498 | 5.512 | 5.504 | 5.515 | 5.502 | 5.476 | 5.528 | 5.482 |
| Ti | 0.269 | 0.160 | 0.194 | 0.187 | 0.190 | 0.165 | 0.193 | 0.178 | 0.203 |
| Al | 3.260 | 3.237 | 3.220 | 3.233 | 3.267 | 3.290 | 3.270 | 3.167 | 3.235 |
| Cr | 0.006 | 0.002 | 0.004 | 0.001 | 0.003 | 0.000 | 0.003 | 0.004 | 0.005 |
| Mg | 2.206 | 2.310 | 2.315 | 2.343 | 2.311 | 2.421 | 2.285 | 2.324 | 2.231 |
| Ca | 0.003 | 0.004 | 0.001 | 0.000 | 0.000 | 0.001 | 0.000 | 0.001 | 0.000 |
| Mn | 0.000 | 0.000 | 0.002 | 0.000 | 0.002 | 0.006 | 0.000 | 0.000 | 0.006 |
| Fe | 2.441 | 2.612 | 2.496 | 2.491 | 2.433 | 2.381 | 2.526 | 2.574 | 2.605 |
| Ba | 0.000 | 0.000 | 0.000 | 0.000 | 0.000 | 0.000 | 0.000 | 0.000 | 0.000 |
| Na | 0.074 | 0.078 | 0.064 | 0.067 | 0.070 | 0.076 | 0.093 | 0.068 | 0.066 |
| K | 1.854 | 1.718 | 1.816 | 1.796 | 1.807 | 1.772 | 1.788 | 1.795 | 1.794 |
| Total | 15.587 | 15.620 | 15.623 | 15.623 | 15.598 | 15.613 | 15.634 | 15.639 | 15.626 |
| <H> | 3.996 | 3.996 | 3.999 | 3.996 | 3.998 | 4.000 | 4.000 | 4.000 | 3.994 |
| <F> | * | * | * | * | * | * | * | * | * |
| <Cl> | 0.005 | 0.004 | 0.001 | 0.004 | 0.002 | 0.000 | 0.000 | 0.000 | 0.006 |

*Flourine not analyzed due to problem of interference between spectrometers.

Appendix 1D: Muscovite Analyses

| Sample: | A114A | A1718 | A1945 | | | | | A2061A | | | |
|---|---|---|---|---|---|---|---|---|---|---|---|
| Analysis # | 24 | 29 | 19 | 15 | 16 | 22 | 23 | 10 | 11 | 12 | 8 |
| SiO2 | 45.86 | 46.77 | 45.52 | 45.06 | 45.88 | 46.11 | 46.20 | 45.50 | 45.21 | 45.98 | 46.19 |
| TiO2 | 0.30 | 0.46 | 0.49 | 0.49 | 0.49 | 0.43 | 0.30 | 0.47 | 0.42 | 0.41 | 0.35 |
| Al2O3 | 32.86 | 31.72 | 33.83 | 33.44 | 34.07 | 34.09 | 33.06 | 30.92 | 31.42 | 31.44 | 31.06 |
| Cr2O3 | 0.18 | 0.02 | 0.05 | 0.08 | 0.04 | 0.00 | 0.13 | 0.00 | 0.02 | 0.00 | 0.00 |
| MgO | 1.65 | 1.84 | 1.28 | 1.37 | 1.44 | 1.29 | 1.68 | 1.62 | 1.48 | 1.62 | 1.67 |
| CaO | 0.02 | 0.00 | 0.01 | 0.02 | 0.01 | 0.04 | 0.00 | 0.01 | 0.02 | 0.01 | 0.00 |
| MnO | 0.02 | 0.01 | 0.00 | 0.00 | 0.00 | 0.00 | 0.01 | 0.03 | 0.01 | 0.00 | 0.03 |
| FeO | 1.80 | 1.67 | 1.22 | 1.19 | 1.29 | 1.29 | 1.65 | 3.67 | 3.47 | 3.20 | 3.68 |
| BaO | 0.07 | 0.03 | 0.17 | 0.10 | 0.31 | 0.31 | 0.02 | 0.07 | 0.17 | 0.19 | 0.01 |
| Na2O | 1.26 | 0.70 | 1.34 | 1.14 | 1.00 | 1.28 | 1.18 | 0.89 | 1.10 | 1.36 | 0.82 |
| K2O | 9.40 | 10.12 | 9.35 | 9.26 | 9.73 | 9.51 | 9.56 | 9.91 | 9.48 | 9.31 | 10.12 |
| H2O | 4.35 | 4.38 | 4.40 | 4.36 | 4.35 | 4.42 | 4.43 | 4.28 | 4.32 | 4.33 | 4.38 |
| F | 0.12 | 0.05 | 0.03 | 0.01 | 0.22 | 0.08 | 0.00 | 0.10 | 0.01 | 0.09 | 0.00 |
| Cl | 0.00 | 0.00 | 0.02 | 0.01 | 0.00 | 0.01 | 0.00 | 0.03 | 0.02 | 0.00 | 0.00 |
| total | 97.90 | 97.77 | 97.70 | 96.53 | 98.82 | 98.84 | 98.23 | 97.49 | 97.15 | 97.95 | 98.30 |
| O = F | -0.05 | -0.02 | -0.01 | 0.00 | -0.09 | -0.04 | 0.00 | -0.04 | 0.00 | -0.04 | 0.00 |
| O = Cl | 0.00 | 0.00 | -0.01 | 0.00 | 0.00 | 0.00 | 0.00 | -0.01 | 0.00 | 0.00 | 0.00 |
| total | 97.85 | 97.74 | 97.69 | 96.52 | 98.73 | 98.81 | 98.23 | 97.44 | 97.14 | 97.91 | 98.30 |
| Cations? | | | | | | | | | | | |
| Si | 3.119 | 3.183 | 3.093 | 3.094 | 3.090 | 3.100 | 3.126 | 3.146 | 3.129 | 3.150 | 3.163 |
| Ti | 0.016 | 0.023 | 0.025 | 0.026 | 0.025 | 0.022 | 0.015 | 0.024 | 0.022 | 0.021 | 0.018 |
| Al | 2.634 | 2.545 | 2.709 | 2.707 | 2.704 | 2.701 | 2.636 | 2.520 | 2.562 | 2.538 | 2.506 |
| Cr | 0.010 | 0.001 | 0.003 | 0.004 | 0.002 | 0.000 | 0.007 | 0.000 | 0.001 | 0.000 | 0.000 |
| Mg | 0.168 | 0.186 | 0.129 | 0.140 | 0.145 | 0.130 | 0.170 | 0.167 | 0.153 | 0.165 | 0.171 |
| Ca | 0.002 | 0.000 | 0.001 | 0.001 | 0.001 | 0.003 | 0.000 | 0.000 | 0.001 | 0.000 | 0.000 |
| Mn | 0.001 | 0.001 | 0.000 | 0.000 | 0.000 | 0.000 | 0.001 | 0.001 | 0.001 | 0.000 | 0.001 |
| Fe | 0.102 | 0.095 | 0.069 | 0.068 | 0.073 | 0.072 | 0.093 | 0.212 | 0.201 | 0.183 | 0.211 |
| Ba | 0.002 | 0.001 | 0.004 | 0.003 | 0.008 | 0.008 | 0.001 | 0.002 | 0.004 | 0.005 | 0.000 |
| Na | 0.167 | 0.092 | 0.177 | 0.152 | 0.130 | 0.167 | 0.155 | 0.119 | 0.148 | 0.181 | 0.108 |
| K | 0.815 | 0.879 | 0.810 | 0.811 | 0.836 | 0.816 | 0.825 | 0.874 | 0.837 | 0.814 | 0.884 |
| total | 7.036 | 7.006 | 7.020 | 7.006 | 7.014 | 7.019 | 7.029 | 7.065 | 7.059 | 7.057 | 7.062 |
| <H > | 1.974 | 1.989 | 1.992 | 1.997 | 1.954 | 1.981 | 2.000 | 1.974 | 1.996 | 1.979 | 2.000 |
| <F > | 0.026 | 0.011 | 0.006 | 0.002 | 0.046 | 0.018 | 0.000 | 0.022 | 0.002 | 0.020 | 0.000 |
| <Cl> | 0.000 | 0.000 | 0.002 | 0.001 | 0.000 | 0.001 | 0.000 | 0.003 | 0.002 | 0.000 | 0.000 |

Appendix 1D: Muscovite Analyses

| Sample: | A1337 | A933 | A1341 | | | | A1435 | |
|---|---|---|---|---|---|---|---|---|
| Analysis # | 19 | 1 | 24 | 27 | 29 | 11 | 22 | 16 |
| SiO2 | 46.02 | 45.89 | 46.24 | 46.04 | 45.72 | 45.98 | 45.96 | 46.15 |
| TiO2 | 0.70 | 0.25 | 0.25 | 0.23 | 0.47 | 0.41 | 0.28 | 0.32 |
| Al2O3 | 34.00 | 33.46 | 33.54 | 34.83 | 35.35 | 33.83 | 33.12 | 31.90 |
| Cr2O3 | 0.15 | 0.43 | 0.03 | 0.00 | 0.07 | 0.02 | 0.05 | 0.01 |
| MgO | 1.21 | 1.42 | 1.24 | 1.02 | 0.89 | 1.24 | 1.09 | 1.39 |
| CaO | 0.00 | 0.03 | 0.02 | 0.00 | 0.00 | 0.00 | 0.01 | 0.04 |
| MnO | 0.04 | 0.03 | 0.00 | 0.06 | 0.00 | 0.03 | 0.00 | 0.00 |
| FeO | 1.54 | 1.97 | 2.09 | 1.90 | 1.48 | 1.90 | 2.69 | 2.85 |
| BaO | 0.32 | 0.11 | 0.12 | 0.17 | 0.19 | 0.16 | 0.00 | 0.00 |
| Na2O | 0.95 | 1.21 | 1.25 | 1.27 | 1.77 | 1.49 | 1.07 | 0.83 |
| K2O | 9.95 | 9.41 | 9.31 | 9.73 | 8.96 | 9.36 | 9.68 | 9.58 |
| H2O | 4.47 | 4.44 | 4.44 | 4.49 | 4.49 | 4.45 | 4.42 | 4.37 |
| F | 0.00 | 0.00 | * | * | * | * | * | * |
| Cl | 0.01 | 0.00 | 0.02 | 0.00 | 0.02 | 0.01 | 0.00 | 0.02 |
| total | 99.35 | 98.63 | 98.55 | 99.74 | 99.41 | 98.90 | 98.37 | 97.47 |
| O = F | 0.00 | 0.00 | * | * | * | * | * | * |
| O = Cl | 0.00 | 0.00 | 0.00 | 0.00 | -0.01 | 0.00 | 0.00 | 0.00 |
| total | 99.35 | 98.63 | 98.55 | 99.74 | 99.40 | 98.90 | 98.37 | 97.47 |
| Si | 6.178 | 3.100 | 6.241 | 6.151 | 6.103 | 6.192 | 6.239 | 6.321 |
| Ti | 0.071 | 0.013 | 0.026 | 0.023 | 0.047 | 0.042 | 0.029 | 0.033 |
| Al | 5.379 | 2.664 | 5.335 | 5.485 | 5.562 | 5.370 | 5.299 | 5.150 |
| Cr | 0.015 | 0.023 | 0.003 | 0.000 | 0.008 | 0.003 | 0.005 | 0.001 |
| Mg | 0.242 | 0.143 | 0.250 | 0.202 | 0.177 | 0.249 | 0.221 | 0.284 |
| Ca | 0.000 | 0.002 | 0.003 | 0.000 | 0.000 | 0.000 | 0.002 | 0.006 |
| Mn | 0.005 | 0.002 | 0.000 | 0.007 | 0.000 | 0.004 | 0.000 | 0.000 |
| Fe | 0.173 | 0.111 | 0.236 | 0.212 | 0.165 | 0.215 | 0.306 | 0.327 |
| Ba | 0.017 | 0.003 | 0.006 | 0.009 | 0.010 | 0.009 | 0.000 | 0.000 |
| Na | 0.246 | 0.158 | 0.327 | 0.329 | 0.459 | 0.389 | 0.282 | 0.221 |
| K | 1.703 | 0.811 | 1.603 | 1.658 | 1.526 | 1.607 | 1.677 | 1.674 |
| total | 14.029 | 7.030 | 14.029 | 14.077 | 14.058 | 17.078 | 14.060 | 14.018 |
| <H > | 3.998 | 2.000 | 3.995 | 4.000 | 3.994 | 3.999 | 4.000 | 3.996 |
| <F > | 0.000 | 0.000 | * | * | * | * | * | * |
| <Cl> | 0.002 | 0.000 | 0.005 | 0.000 | 0.006 | 0.002 | 0.000 | 0.004 |

*Fluorine not analyzed due to problem of interference between spectrometers.

Appendix 1E: Feldspar Analyses

| Sample: | A1337 | | | | | A933 | | | A791 | A321 | | |
|---|---|---|---|---|---|---|---|---|---|---|---|---|
| Analysis #: | 1 | 2 | 3 | 7 | 12 | 21 | 24 | 26 | 62 | 68 | 69 | 70 |
| SiO2 | 67.07 | 66.34 | 63.53 | 64.93 | 68.40 | 61.95 | 64.26 | 62.12 | 67.93 | 64.37 | 66.10 | 64.10 |
| Al2O3 | 20.66 | 20.64 | 22.75 | 22.18 | 19.72 | 23.20 | 22.04 | 23.36 | 19.74 | 21.87 | 20.86 | 22.12 |
| Fe2O3 | 0.00 | 0.15 | 0.02 | 0.11 | 0.06 | 0.09 | 0.20 | 0.07 | 0.09 | 0.07 | 0.06 | 0.12 |
| CaO | 1.24 | 1.38 | 3.49 | 2.87 | 0.18 | 4.31 | 2.87 | 4.40 | 0.12 | 2.78 | 1.41 | 2.87 |
| BaO | 0.05 | 0.07 | 0.02 | 0.00 | 0.00 | 0.07 | 0.00 | 0.08 | 0.00 | 0.00 | 0.00 | 0.12 |
| Na2O | 10.75 | 10.63 | 9.41 | 9.93 | 11.62 | 9.02 | 10.01 | 8.99 | 11.63 | 10.11 | 10.69 | 9.95 |
| K2O | 0.04 | 0.21 | 0.10 | 0.11 | 0.06 | 0.06 | 0.08 | 0.06 | 0.05 | 0.09 | 0.05 | 0.06 |
| total | 99.81 | 99.41 | 99.33 | 100.13 | 100.03 | 98.71 | 99.46 | 99.08 | 99.57 | 99.28 | 99.17 | 99.34 |
| | | | | | | | | | | | | |
| Si | 2.941 | 2.928 | 2.820 | 2.855 | 2.987 | 2.777 | 2.848 | 2.775 | 2.981 | 2.856 | 2.921 | 2.845 |
| Al | 1.068 | 1.073 | 1.190 | 1.149 | 1.015 | 1.226 | 1.151 | 1.229 | 1.021 | 1.144 | 1.086 | 1.157 |
| Fe | 0.000 | 0.005 | 0.001 | 0.004 | 0.002 | 0.003 | 0.007 | 0.002 | 0.003 | 0.002 | 0.002 | 0.004 |
| Ca | 0.058 | 0.065 | 0.166 | 0.135 | 0.008 | 0.207 | 0.136 | 0.211 | 0.006 | 0.132 | 0.067 | 0.137 |
| Ba | 0.001 | 0.001 | 0.000 | 0.000 | 0.000 | 0.001 | 0.000 | 0.001 | 0.000 | 0.000 | 0.000 | 0.002 |
| Na | 0.914 | 0.910 | 0.810 | 0.847 | 0.984 | 0.784 | 0.860 | 0.778 | 0.990 | 0.869 | 0.916 | 0.856 |
| K | 0.002 | 0.012 | 0.006 | 0.006 | 0.003 | 0.004 | 0.005 | 0.004 | 0.003 | 0.005 | 0.003 | 0.003 |
| total | 4.984 | 4.994 | 4.993 | 4.996 | 4.999 | 5.002 | 5.007 | 5.000 | 5.004 | 5.008 | 4.995 | 5.004 |
| | | | | | | | | | | | | |
| <Ab> | 93.8 | 92.2 | 82.5 | 85.7 | 98.8 | 78.8 | 85.9 | 78.4 | 99.1 | 86.4 | 93.0 | 86.0 |
| <Or> | 0.2 | 1.2 | 0.6 | 0.6 | 0.3 | 0.4 | 0.5 | 0.4 | 0.3 | 0.5 | 0.3 | 0.3 |
| <An> | 6.0 | 6.6 | 16.9 | 13.7 | 0.8 | 20.8 | 0.0 | 0.0 | 0.6 | 13.1 | 6.8 | 13.7 |

Appendix 1E: Feldspar Analyses

| Sample: | A2061 | | | | A1945 | GRUV | | | | |
|---|---|---|---|---|---|---|---|---|---|---|
| Analysis #: | 29 | 30 | 31 | 32 | 33 | 38 | 39 | 43 | 44 | 46 |
| SiO2 | 63.27 | 67.30 | 63.18 | 66.52 | 62.00 | 63.24 | 62.46 | 67.77 | 64.11 | 62.01 |
| Al2O3 | 22.39 | 20.27 | 21.18 | 20.73 | 22.96 | 22.64 | 23.21 | 19.58 | 22.03 | 23.23 |
| Fe2O3 | 0.61 | 0.07 | 0.14 | 0.06 | 0.07 | 0.06 | 0.09 | 0.01 | 0.03 | 0.07 |
| CaO | 1.26 | 1.36 | 2.37 | 1.32 | 4.29 | 4.01 | 4.39 | 0.02 | 3.32 | 4.68 |
| BaO | 0.00 | 0.07 | 0.00 | 0.10 | 0.02 | 0.00 | 0.00 | 0.04 | 0.08 | 0.00 |
| Na2O | 9.33 | 10.54 | 10.13 | 10.68 | 9.05 | 9.35 | 9.07 | 11.52 | 9.75 | 9.07 |
| K2O | 1.49 | 0.10 | 0.09 | 0.05 | 0.08 | 0.08 | 0.08 | 0.12 | 0.08 | 0.09 |
| total | 98.35 | 99.70 | 97.09 | 99.46 | 98.46 | 99.38 | 99.30 | 99.04 | 99.41 | 99.14 |
| | | | | | | | | | | |
| Si | 2.841 | 2.954 | 2.866 | 2.931 | 2.785 | 2.811 | 2.782 | 2.988 | 2.845 | 2.771 |
| Al | 1.185 | 1.049 | 1.132 | 1.076 | 1.216 | 1.186 | 1.218 | 1.018 | 1.152 | 1.223 |
| Fe | 0.021 | 0.002 | 0.005 | 0.002 | 0.002 | 0.002 | 0.003 | 0.000 | 0.001 | 0.002 |
| Ca | 0.060 | 0.064 | 0.115 | 0.062 | 0.206 | 0.191 | 0.210 | 0.001 | 0.158 | 0.224 |
| Ba | 0.000 | 0.001 | 0.000 | 0.002 | 0.000 | 0.000 | 0.000 | 0.001 | 0.001 | 0.000 |
| Na | 0.812 | 0.897 | 0.891 | 0.912 | 0.788 | 0.806 | 0.784 | 0.985 | 0.839 | 0.786 |
| K | 0.085 | 0.005 | 0.005 | 0.003 | 0.004 | 0.005 | 0.004 | 0.007 | 0.004 | 0.005 |
| total | 5.004 | 4.972 | 5.014 | 4.988 | 5.001 | 5.001 | 5.001 | 5.000 | 5.000 | 5.011 |
| | | | | | | | | | | |
| <Ab> | 84.8 | 92.8 | 88.1 | 93.3 | 78.9 | 80.5 | 78.5 | 99.3 | 83.8 | 77.4 |
| <Or> | 8.9 | 0.6 | 0.5 | 0.3 | 0.4 | 0.5 | 0.5 | 0.7 | 0.5 | 0.5 |
| <An> | 6.3 | 6.6 | 11.4 | 6.4 | 20.7 | 19.1 | 21.0 | 0.1 | 15.8 | 22.1 |

Appendix 1E: Feldspar Analyses

| Sample: | A1573 | | | | A1463 | | | | | A20 | |
|---|---|---|---|---|---|---|---|---|---|---|---|
| Analysis #: | 47 | 48 | 49 | 50 | 51 | 52 | 53 | 54 | 55 | 66 | 67 |
| SiO2 | 62.38 | 62.24 | 62.58 | 62.56 | 62.32 | 63.41 | 63.60 | 63.90 | 62.02 | 67.46 | 67.50 |
| Al2O3 | 23.41 | 23.25 | 22.60 | 23.23 | 22.29 | 22.44 | 22.67 | 22.37 | 21.46 | 19.87 | 19.70 |
| Fe2O3 | 0.07 | 0.06 | 0.19 | 0.04 | 0.33 | 0.22 | 0.24 | 0.31 | 1.29 | 0.30 | 0.12 |
| CaO | 4.77 | 4.58 | 4.21 | 4.53 | 4.04 | 3.86 | 3.84 | 3.60 | 4.42 | 0.26 | 0.11 |
| BaO | 0.00 | 0.08 | 0.11 | 0.18 | 0.20 | 0.19 | 0.00 | 0.02 | 0.13 | 0.11 | 0.04 |
| Na2O | 8.96 | 9.11 | 9.09 | 8.97 | 9.52 | 9.56 | 9.49 | 9.69 | 8.79 | 11.49 | 11.34 |
| K2O | 0.06 | 0.06 | 0.08 | 0.07 | 0.08 | 0.07 | 0.08 | 0.06 | 0.07 | 0.03 | 0.07 |
| total | 99.65 | 99.37 | 98.85 | 99.58 | 98.78 | 99.75 | 99.92 | 99.95 | 98.18 | 99.52 | 98.89 |
| | | | | | | | | | | | |
| Si | 2.772 | 2.775 | 2.801 | 2.782 | 2.799 | 2.814 | 2.812 | 2.824 | 2.807 | 2.968 | 2.981 |
| Al | 1.226 | 1.222 | 1.192 | 1.218 | 1.180 | 1.174 | 1.181 | 1.166 | 1.144 | 1.030 | 1.026 |
| Fe | 0.002 | 0.002 | 0.006 | 0.001 | 0.011 | 0.007 | 0.008 | 0.010 | 0.044 | 0.010 | 0.004 |
| Ca | 0.227 | 0.219 | 0.202 | 0.216 | 0.194 | 0.183 | 0.182 | 0.170 | 0.215 | 0.012 | 0.005 |
| Ba | 0.000 | 0.001 | 0.002 | 0.003 | 0.004 | 0.003 | 0.000 | 0.000 | 0.002 | 0.002 | 0.001 |
| Na | 0.772 | 0.787 | 0.789 | 0.773 | 0.829 | 0.823 | 0.814 | 0.831 | 0.771 | 0.980 | 0.971 |
| K | 0.004 | 0.003 | 0.004 | 0.004 | 0.004 | 0.004 | 0.004 | 0.003 | 0.004 | 0.002 | 0.004 |
| total | 5.003 | 5.009 | 4.996 | 4.997 | 5.021 | 5.008 | 5.001 | 5.004 | 4.987 | 5.004 | 4.992 |
| | | | | | | | | | | | |
| <Ab> | 77.0 | 78.0 | 79.3 | 77.6 | 80.4 | 81.2 | 81.4 | 82.7 | 77.9 | 98.6 | 99.1 |
| <Or> | 0.4 | 0.3 | 0.4 | 0.4 | 0.4 | 0.4 | 0.4 | 0.3 | 0.4 | 0.2 | 0.4 |
| <An> | 22.6 | 21.7 | 20.3 | 21.7 | 18.9 | 18.1 | 18.2 | 17.0 | 21.7 | 1.2 | 0.5 |

Appendix 1F: Chlorite Analyses

| Sample: | A1341 | | | | A1718 | | A933 | A2061 |
|---|---|---|---|---|---|---|---|---|
| Analysis #: | 1 | 3 | 4 | 5 | 20 | 22 | 10 | 11 |
| SiO2 | 24.93 | 24.20 | 24.48 | 24.29 | 24.73 | 24.60 | 24.00 | 25.86 |
| Al2O3 | 21.37 | 21.88 | 21.77 | 21.86 | 22.21 | 22.06 | 21.33 | 21.43 |
| Cr2O3 | 0.05 | 0.06 | 0.01 | 0.01 | 0.00 | 0.06 | 0.02 | 0.00 |
| MgO | 16.39 | 14.62 | 13.69 | 14.11 | 16.17 | 16.51 | 13.82 | 23.05 |
| MnO | 0.18 | 0.00 | 0.03 | 0.06 | 0.06 | 0.04 | 0.12 | 0.56 |
| FeO | 22.22 | 25.59 | 25.50 | 26.23 | 23.02 | 22.22 | 25.81 | 13.51 |
| H2O | 11.21 | 11.17 | 11.07 | 11.16 | 11.32 | 11.26 | 10.97 | 11.63 |
| total | 96.35 | 97.51 | 96.55 | 97.70 | 97.50 | 96.75 | 96.06 | 96.03 |
| Si | 2.667 | 2.599 | 2.652 | 2.611 | 2.621 | 2.619 | 2.625 | 2.667 |
| Al | 2.695 | 2.770 | 2.780 | 2.769 | 2.773 | 2.768 | 2.749 | 2.605 |
| Cr | 0.004 | 0.005 | 0.001 | 0.000 | 0.000 | 0.005 | 0.002 | 0.000 |
| Mg | 2.614 | 2.341 | 2.211 | 2.260 | 2.554 | 2.620 | 2.252 | 3.543 |
| Mn | 0.016 | 0.000 | 0.002 | 0.005 | 0.005 | 0.004 | 0.011 | 0.049 |
| Fe | 1.988 | 2.298 | 2.310 | 2.358 | 2.040 | 1.979 | 2.360 | 1.166 |
| total | 9.984 | 10.013 | 9.956 | 10.003 | 9.993 | 9.995 | 9.999 | 10.030 |
| <H > | 8 | 8 | 8 | 8 | 8 | 8 | 8 | 8 |

Appendix 1F: Chlorite Analyses

| Sample: | A114A | A791 | | A20 | | A1945 | | 1435 | |
|---|---|---|---|---|---|---|---|---|---|
| Analysis #: | 15 | 16 | 17 | 18 | 19 | 12 | 13 | 7 | 8 |
| SiO2 | 26.02 | 23.64 | 23.99 | 26.00 | 25.99 | 25.07 | 25.15 | 23.75 | 23.33 |
| Al2O3 | 21.79 | 21.99 | 21.32 | 20.59 | 20.39 | 21.65 | 21.63 | 21.68 | 20.86 |
| Cr2O3 | 0.10 | 0.00 | 0.05 | 0.18 | 0.20 | 0.03 | 0.02 | 0.01 | 0.00 |
| MgO | 22.28 | 13.03 | 12.46 | 21.01 | 21.15 | 18.71 | 18.37 | 12.75 | 12.27 |
| MnO | 0.08 | 0.07 | 0.08 | 0.09 | 0.11 | 0.11 | 0.13 | 0.11 | 0.11 |
| FeO | 14.96 | 27.04 | 27.12 | 16.90 | 17.06 | 19.31 | 19.89 | 27.34 | 28.63 |
| H2O | 11.69 | 10.99 | 10.88 | 11.49 | 11.49 | 11.36 | 11.37 | 10.95 | 10.78 |
| total | 96.92 | 96.77 | 95.91 | 96.26 | 96.40 | 96.23 | 96.55 | 96.59 | 95.98 |
| Si | 2.669 | 2.580 | 2.644 | 2.714 | 2.713 | 2.647 | 2.654 | 2.602 | 2.595 |
| Al | 2.635 | 2.829 | 2.768 | 2.533 | 2.508 | 2.695 | 2.689 | 2.799 | 2.735 |
| Cr | 0.008 | 0.000 | 0.004 | 0.015 | 0.017 | 0.002 | 0.002 | 0.001 | 0.000 |
| Mg | 3.407 | 2.120 | 2.047 | 3.269 | 3.290 | 2.945 | 2.890 | 2.081 | 2.034 |
| Mn | 0.007 | 0.007 | 0.008 | 0.008 | 0.010 | 0.010 | 0.011 | 0.010 | 0.010 |
| Fe | 1.283 | 2.468 | 2.499 | 1.475 | 1.489 | 1.705 | 1.755 | 2.505 | 2.663 |
| total | 10.009 | 10.004 | 9.970 | 10.014 | 10.027 | 10.004 | 10.001 | 9.998 | 10.037 |
| <H > | 8 | 8 | 8 | 8 | 8 | 8 | 8 | 8 | 8 |

Appendix 1G: Epidote Analyses

| Sample: | A2061 | | | | | | GRUV | | | | A1573 | | | |
|---|---|---|---|---|---|---|---|---|---|---|---|---|---|---|
| Analysis #: | 1 | 2 | 3 | 4 | *5 | 6 | 7 | 8 | 9 | 10 | 11 | 12 | 14 | 15 |
| SiO2 | 36.66 | 36.64 | 36.80 | 36.96 | 30.77 | 51.79 | 37.50 | 36.85 | 37.09 | 37.60 | 37.94 | 41.45 | 38.13 | 37.72 |
| TiO2 | 0.06 | 0.03 | 0.06 | 0.15 | 1.81 | 0.03 | 0.10 | 0.04 | 0.08 | 0.09 | 0.04 | 0.47 | 0.06 | 0.05 |
| CeO2 | 0.16 | 0.42 | 0.00 | 0.00 | 8.68 | 0.09 | 0.00 | 0.00 | 0.00 | 0.14 | 0.00 | 0.00 | 0.04 | 0.03 |
| Al2O3 | 24.44 | 24.20 | 23.51 | 23.92 | 17.34 | 17.79 | 26.13 | 23.82 | 25.59 | 26.44 | 28.45 | 27.21 | 28.52 | 28.03 |
| Y2O3 | 0.00 | 0.04 | 0.12 | 0.00 | 0.18 | 0.00 | 0.00 | 0.02 | 0.00 | 0.01 | 0.00 | 0.00 | 0.00 | 0.00 |
| La2O3 | 0.00 | 0.05 | 0.00 | 0.05 | 3.66 | 0.05 | 0.00 | 0.04 | 0.00 | 0.01 | 0.03 | 0.02 | 0.00 | 0.01 |
| MgO | 0.08 | 0.10 | 0.05 | 0.03 | 0.49 | 0.04 | 0.05 | 0.03 | 0.04 | 0.09 | 0.03 | 0.04 | 0.03 | 0.03 |
| CaO | 22.13 | 22.26 | 22.12 | 22.67 | 11.34 | 17.28 | 23.51 | 22.67 | 23.27 | 23.34 | 24.38 | 21.39 | 24.10 | 23.88 |
| MnO | 1.31 | 0.93 | 0.73 | 0.53 | 1.14 | 0.49 | 0.14 | 0.24 | 0.14 | 0.18 | 0.07 | 0.02 | 0.07 | 0.05 |
| FeO | 10.79 | 10.60 | 11.36 | 11.03 | 10.33 | 8.50 | 8.70 | 11.67 | 8.73 | 8.12 | 5.88 | 5.23 | 5.64 | 5.93 |
| H2O | 1.81 | 1.80 | 1.79 | 1.81 | 1.51 | 1.93 | 1.85 | 1.80 | 1.82 | 1.85 | 1.89 | 1.91 | 1.89 | 1.87 |
| total | 97.43 | 97.07 | 96.53 | 97.14 | 87.24 | 97.98 | 97.97 | 97.17 | 96.78 | 97.86 | 98.70 | 97.74 | 98.47 | 97.59 |
| | | | | | | | | | | | | | | |
| Si | 6.082 | 6.102 | 6.165 | 6.141 | 6.123 | 8.029 | 6.088 | 6.133 | 6.102 | 6.094 | 6.026 | 6.513 | 6.055 | 6.055 |
| Ti | 0.007 | 0.004 | 0.008 | 0.019 | 0.270 | 0.004 | 0.012 | 0.005 | 0.010 | 0.010 | 0.005 | 0.056 | 0.007 | 0.006 |
| Ce | 0.009 | 0.024 | 0.000 | 0.000 | 0.603 | 0.005 | 0.000 | 0.000 | 0.000 | 0.008 | 0.000 | 0.000 | 0.002 | 0.002 |
| Al | 4.779 | 4.750 | 4.641 | 4.684 | 4.067 | 3.250 | 5.000 | 4.673 | 4.961 | 5.050 | 5.326 | 5.039 | 5.338 | 5.304 |
| Y | 0.000 | 0.003 | 0.011 | 0.000 | 0.020 | 0.000 | 0.000 | 0.002 | 0.000 | 0.001 | 0.000 | 0.000 | 0.000 | 0.000 |
| La | 0.000 | 0.003 | 0.000 | 0.003 | 0.268 | 0.003 | 0.000 | 0.002 | 0.000 | 0.001 | 0.002 | 0.001 | 0.000 | 0.000 |
| Mg | 0.019 | 0.024 | 0.012 | 0.008 | 0.145 | 0.009 | 0.012 | 0.007 | 0.011 | 0.023 | 0.006 | 0.010 | 0.006 | 0.008 |
| Ca | 3.934 | 3.972 | 3.970 | 4.035 | 2.418 | 2.871 | 4.089 | 4.043 | 4.102 | 4.052 | 4.150 | 3.602 | 4.101 | 4.106 |
| Mn | 0.184 | 0.131 | 0.104 | 0.075 | 0.192 | 0.064 | 0.019 | 0.034 | 0.020 | 0.024 | 0.010 | 0.003 | 0.009 | 0.007 |
| Fe | 1.497 | 1.476 | 1.591 | 1.532 | 1.718 | 1.102 | 1.181 | 1.624 | 1.201 | 1.100 | 0.781 | 0.687 | 0.749 | 0.796 |
| total | 16.511 | 16.489 | 16.502 | 16.497 | 15.824 | 15.337 | 16.401 | 16.523 | 16.407 | 16.363 | 16.306 | 15.911 | 16.267 | 16.284 |
| <H > | 2 | 2 | 2 | 2 | 2 | 2 | 2 | 2 | 2 | 2 | 2 | 2 | 2 | 2 |

*Allanite core in epidote grain.

Appendix 1G: Epidote Analyses

| Sample: | A20 | | | | A1463 | | A114 | | |
|---|---|---|---|---|---|---|---|---|---|
| Analysis #: | 22 | 23 | 24 | 25 | 16 | 18 | 19 | 20 | 21 |
| SiO2 | 37.12 | 37.18 | 43.21 | 36.68 | 39.73 | 38.02 | 38.19 | 48.74 | 37.67 |
| TiO2 | 0.09 | 0.09 | 0.34 | 0.07 | 0.14 | 0.04 | 0.11 | 0.11 | 0.09 |
| CeO2 | 0.00 | 0.00 | 0.00 | 0.00 | 0.00 | 0.07 | 0.06 | 0.03 | 0.00 |
| Al2O3 | 24.62 | 24.42 | 11.41 | 23.88 | 26.19 | 28.45 | 28.55 | 22.88 | 27.58 |
| Y2O3 | 0.00 | 0.00 | 0.00 | 0.01 | 0.00 | 0.00 | 0.01 | 0.00 | 0.03 |
| La2O3 | 0.00 | 0.03 | 0.00 | 0.00 | 0.00 | 0.04 | 0.00 | 0.00 | 0.01 |
| MgO | 0.03 | 0.03 | 11.95 | 0.05 | 1.71 | 0.05 | 0.07 | 0.06 | 0.07 |
| CaO | 23.24 | 23.28 | 10.74 | 23.17 | 22.76 | 24.20 | 23.37 | 19.58 | 23.39 |
| MnO | 0.12 | 0.01 | 0.16 | 0.10 | 0.14 | 0.07 | 0.12 | 0.13 | 0.14 |
| FeO | 10.49 | 10.61 | 13.84 | 10.68 | 6.22 | 5.37 | 5.97 | 4.84 | 6.52 |
| H2O | 1.82 | 1.82 | 1.78 | 1.79 | 1.90 | 1.88 | 1.89 | 1.96 | 1.86 |
| total | 97.54 | 97.46 | 93.41 | 96.43 | 98.78 | 98.20 | 98.32 | 98.33 | 97.35 |
| Si | 6.116 | 6.134 | 7.293 | 6.130 | 6.277 | 6.053 | 6.070 | 7.460 | 6.077 |
| Ti | 0.011 | 0.011 | 0.043 | 0.009 | 0.016 | 0.005 | 0.013 | 0.013 | 0.011 |
| Ce | 0.000 | 0.000 | 0.000 | 0.000 | 0.000 | 0.004 | 0.003 | 0.002 | 0.000 |
| Al | 4.782 | 4.748 | 2.269 | 4.703 | 4.877 | 5.339 | 5.348 | 4.127 | 5.242 |
| Y | 0.000 | 0.000 | 0.000 | 0.001 | 0.000 | 0.000 | 0.001 | 0.000 | 0.002 |
| La | 0.000 | 0.002 | 0.000 | 0.000 | 0.000 | 0.002 | 0.000 | 0.000 | 0.000 |
| Mg | 0.008 | 0.007 | 3.006 | 0.011 | 0.403 | 0.012 | 0.016 | 0.013 | 0.017 |
| Ca | 4.102 | 4.115 | 1.942 | 4.149 | 3.853 | 4.128 | 3.979 | 3.212 | 4.042 |
| Mn | 0.017 | 0.001 | 0.023 | 0.014 | 0.019 | 0.009 | 0.016 | 0.016 | 0.019 |
| Fe | 1.446 | 1.463 | 1.953 | 1.493 | 0.822 | 0.716 | 0.794 | 0.619 | 0.880 |
| total | 16.482 | 16.481 | 16.529 | 16.510 | 16.267 | 16.268 | 16.240 | 15.462 | 16.290 |
| <H> | 2 | 2 | 2 | 2 | 2 | 2 | 2 | 2 | 2 |

# APPENDIX 2
## Structural Data

## Appendix 2A: Foliation Measurements

| DOME AREA | | DOME AREA | | DOME AREA | | DOME AREA | |
|---|---|---|---|---|---|---|---|
| STATION # | FOLIATION | STATION # | FOLIATION | STATION # | FOLIATION | STATION # | FOLIATION |
| 36 | S 35 W, 45 W | 125 | S 30 W, 45 W | 227 | N 52 E, 76 E | 329 | N 16 E, 45 E |
| 37 | S 18 E, 39 W | 126 | S 9 W, 39 W | 233 | S 34 W, 56 W | 330 | N 33 E, 80 E |
| 38 | S 16 W, 29 W | 127 | S 21 W, 35 W | 282 | S 38 E, 80 W | 331 | N 15 E, 69 E |
| 39 | S 68 W, 68 W | 128 | S 10 E, 34 W | 283 | S 42 E, 30 W | 332 | N 7 E, 52 E |
| 40 | S 5 W, 48 W | 129 | S 14 E, 29 W | 284 | S 48 W, 87 W | 333 | N 9 E, 52 E |
| 41 | N 68 E, 58 E | 130 | S 25 W, 34 W | 285 | N 44 W, 80 E | 334 | N 9 E, 54 E |
| 43 | S 72 E, 51 W | 132 | S 15 W, 25 W | 286 | N 35 E, 64 E | 335 | N 17 E, 63 E |
| 44 | N 78 E, 80 E | 133 | S 55 E, 15 W | 287 | N 65 W, 67 E | 337 | N 6 E, 64 E |
| 45 | S 85 E, 50 W | 135 | S 55 E, 37 W | 288 | N 5 E, 70 E | 338 | N 17 E, 75 E |
| 46 | S 28 W, 72 W | 136 | S 60 E, 40 W | 289 | S 69 E, 73 W | 339 | N 2 E, 60 E |
| 47 | S 5 W, 47 W | 137 | S 85 E, 49 W | 291 | N 15 E, 72 E | 340 | N 4 W, 40 E |
| 48 | S 22 W, 57 W | 138 | S 54 E, 47 W | 292 | S 62 W, 62 W | 341 | N 14 E, 52 E |
| 49 | N 19 E, 82 E | 139 | N 69 E, 54 E | 293 | S 47 W, 49 W | 342 | N 30 E, 32 E |
| 50 | N 15 E, 75 E | 141 | N 32 E, 52 E | 294 | N 12 W, 52 E | 343 | N 2 W, 60 E |
| 51 | S 9 W, 61 W | 142 | N 37 E, 72 E | 295 | S 8 W, 36 W | 344 | N 7 W, 50 E |
| 52 | S 6 W, 52 W | 143 | N 45 E, 63 E | 297 | S 53 W, 37 W | 345 | N 11 W, 54 E |
| 53 | N 37 W, 8 E | 144 | N 57 E, 33 E | 298 | S 85 W, 81 W | 346 | N 10 E, 54 E |
| 54 | S 23 W, 77 W | 145 | N 35 E, 68 E | 299 | N 86 W, 66 E | 347 | N 26 E, 57 E |
| 55 | S 12 W, 67 W | 146 | S 62 E, 19 W | 300 | N 86 W, 67 E | 348 | N 29 E, 81 E |
| 56 | S 24 W, 67 W | 147 | S 58 W, 69 W | 301 | S 77 E, 76 W | 349 | N 23 E, 49 E |
| 57 | S 12 W, 56 W | 148 | S 10 W, 20 W | 302 | S 18 E, 36 W | 350 | N 12 E, 63 E |
| 58 | S 24 W, 46 W | 150 | S 12 W, 22 W | 303 | S 79 E, 59 W | 351 | S 3 E, 60 W |
| 60 | S 5 W, 78 W | 151 | S 55 E, 12 W | 305 | S 13 W, 26 W | 352 | N 18 E, 72 E |
| 61 | S 7 E, 27 W | 152 | S 24 W, 17 W | 306 | S 10 E, 52 W | 353 | N 19 E, 73 E |
| 62 | S 17 E, 35 W | 153 | S 8 E, 25 W | 307 | S 60 E, 53 W | 354 | N 21 E, 81 E |
| 63 | S 26 W, 36 W | 154 | S 40 E, 11 W | 308 | S 8 W, 60 W | 355 | N 16 E, 64 E |
| 64 | S 24 W, 70 W | 155 | S 15 W, 52 W | 309 | N 50 E, 34 E | 356 | N 17 E, 60 E |
| 65 | S 22 W, 51 W | 156 | S 18 W, 20 W | 310 | N 70 E, 29 E | 357 | S 33 W, 84 W |
| 66 | S 30 W, 40 W | 157 | S 24 W, 27 W | 312 | S 6 E, 49 W | 358 | N 26 E, 60 E |
| 67 | S 15 W, 36 W | 158 | S 13 W, 26 W | 313 | N 45 E, 22 E | 359 | N 4 E, 42 E |
| 68 | N 10 W, 30 E | 159 | S 35 W, 26 W | 314 | N 44 E, 34 E | 360 | S 42 W, 76 W |
| 69 | S 9 W, 48 W | 160 | S 35 W, 35 W | 315 | N 45 E, 67 E | 361 | N 70 E, 45 E |
| 70 | S 12 E, 30 W | 161 | S 39 W, 33 W | 316 | N 14 E, 40 E | 362 | N 86 W, 40 E |
| 71 | S 17 W, 37 W | 162 | S 13 W, 32 W | 316 | N 60 E, 42 E | 363 | S 50 W, 70 W |
| 72 | S 30 E, 24 W | 163 | S 54 W, 33 W | 316 | N 10 W, 28 E | 364 | N 5 W, 59 E |
| 73 | S 26 W, 30 W | 164 | S 33 W, 30 W | 316 | N 20 E, 20 E | 365 | N 22 E, 85 E |
| 74 | S 30 W, 30 W | 165 | S 46 W, 26 W | 316 | S 46 E, 81 W | 366 | S 43 W, 66 W |
| 75 | S 5 E, 17 W | 166 | S 57 W, 32 W | 316 | S 5 E, 64 W | 367 | S 52 W, 65 W |
| 113 | S 54 E, 57 W | 167 | S 12 W, 19 W | 318 | N 20 E, 42 E | 368 | S 55 W, 55 W |
| 114 | S 67 E, 44 W | 168 | S 68 W, 15 W | 319 | N 13 E, 31 E | 369 | S 52 W, 44 W |
| 116 | N 85 E, 67 E | 169 | N 84 E, 9 E | 320 | N 33 E, 46 E | 370 | S 76 W, 44 W |
| 116 | S 86 E, 74 W | 170 | S 42 W, 62 W | 321 | N 64 E, 57 E | 371 | N 58 W, 48 E |
| 117 | S 89 E, 81 W | 171 | S 20 W, 36 W | 322 | N 72 W, 74 E | 372 | N 26 W, 60 E |
| 118 | S 75 E, 54 W | 172 | S 48 W, 32 W | 323 | N 10 E, 48 E | 372 | N 22 W, 34 E |
| 119 | S 65 E, 64 W | 221 | N 53 W, 47 E | 324 | N 14 E, 47 E | 372 | S 65 E, 52 W |
| 121 | S 10 E, 29 W | 222 | N 40 W, 42 E | 325 | N 12 E, 40 E | 373 | N 62 W, 55 E |
| 122 | S 40 W, 45 W | 223 | N 39 W, 57 E | 326 | N 20 E, 52 E | 374 | N 64 W, 50 E |
| 123 | S 24 W, 66 W | 224 | S 50 W, 70 W | 327 | N 22 E, 52 E | 375 | N 42 W, 55 E |
| 124 | S 29 W, 44 W | 228 | N 85 E, 27 E | 328 | N 9 E, 37 E | 376 | N 74 W, 44 E |

Appendix 2A, continued

| DOME AREA STATION # | FOLIATION | DOME AREA STATION # | FOLIATION | DOME AREA STATION # | FOLIATION | DOME AREA STATION # | FOLIATION |
|---|---|---|---|---|---|---|---|
| 753 | S 10 E, 34 W | 994 | S 16 W, 20 W | 1058 | S 14 W, 52 W | 1127 | S 2 E, 50 W |
| 754 | S 12 E, 29 W | 996 | S .0 E, 57 W | 1059 | S 74 E, 84 W | 1128 | S 31 E, 50 W |
| 755 | S 7 E, 34 W | 997 | S 9 E, 47 W | 1060 | S 69 W, 23 W | 1129 | S 28 E, 54 W |
| 756 | S 31 E, 26 W | 998 | S 21 E, 58 W | 1061 | N 16 W, 24 E | 1130 | S 12 E, 64 W |
| 757 | N 78 W, 26 E | 999 | S 2 W, 60 W | 1063 | S 62 W, 43 W | 1131 | S 54 E, 59 W |
| 758 | S 79 W, 31 W | 1000 | S 42 W, 40 W | 1064 | S 52 W, 57 W | 1133 | S 64 E, 59 W |
| 759 | S 70 E, 62 W | 1001 | S 42 W, 58 W | 1065 | S 35 W, 50 W | 1134 | S 46 E, 57 W |
| 760 | S 73 E, 50 W | 1002 | S 34 W, 36 W | 1066 | S 34 W, 64 W | 1135 | S 51 W, 27 W |
| 761 | S 77 W, 74 W | 1003 | S 38 W, 46 W | 1067 | S 53 W, 54 W | 1136 | S 15 E, 67 W |
| 762 | N 88 W, 89 E | 1005 | S 21 E, 25 W | 1068 | N 42 E, 72 E | 1137 | S 38 W, 52 W |
| 763 | S 58 W, 78 W | 1006 | S 21 E, 27 W | 1069 | S 50 E, 26 W | 1138 | S 39 W, 20 W |
| 764 | N 69 W, 51 E | 1007 | S 32 E, 19 W | 1070 | S 67 E, 42 W | 1139 | S 25 W, 52 W |
| 766 | S 44 W, 25 W | 1008 | S 42 E, 42 W | 1071 | S 15 W, 29 W | 1140 | S 12 W, 48 W |
| 767 | S 82 W, 12 W | 1009 | S 5 W, 41 W | 1072 | S 30 E, 40 W | 1142 | S 14 W, 45 W |
| 768 | S 82 W, 59 W | 1010 | N 13 E, 27 E | 1073 | S 77 E, 42 W | 1143 | S 44 E, 54 W |
| 769 | N 43 W, 50 E | 1020 | N 90 E, 44 S | 1074 | S 81 E, 36 W | 1145 | S 17 W, 66 W |
| 770 | N 70 W, 20 E | 1020 | S 43 W, 42 W | 1075 | S 27 W, 60 W | 1146 | S 11 W, 54 W |
| 771 | S 14 E, 52 W | 1022 | S 76 W, 27 W | 1076 | S 55 E, 23 W | 1147 | S 87 E, 57 W |
| 772 | N 76 W, 72 E | 1023 | S 31 E, 29 W | 1077 | S 25 W, 50 W | 1198 | S 59 W, 75 W |
| 773 | N 75 W, 57 E | 1024 | S 62 W, 63 W | 1079 | S 52 W, 48 W | 1199 | S 71 W, 71 W |
| 774 | N 8 E, 69 E | 1025 | S 80 W, 79 W | 1080 | S 46 E, 53 W | 1200 | N 81 E, 64 E |
| 775 | N 29 E, 56 E | 1026 | N 82 W, 83 E | 1081 | S 52 W, 70 W | 1201 | N 76 E, 25 E |
| 776 | N 36 E, 52 E | 1027 | S 6 W, 43 W | 1082 | S 7 E, 53 W | 1203 | S 28 W, 44 W |
| 778 | N 26 E, 51 E | 1028 | S 60 E, 61 W | 1083 | S 52 W, 70 W | 1227 | S 76 E, 38 W |
| 779 | N 22 E, 51 E | 1029 | S 43 E, 46 W | 1084 | S 48 W, 61 W | 1228 | S 7 E, 76 W |
| 780 | N 29 E, 56 E | 1030 | S 2 E, 32 W | 1085 | N 68 E, 58 E | 1229 | S 77 E, 59 W |
| 781 | N 25 E, 54 E | 1031 | S 82 E, 62 W | 1086 | N 48 E, 47 E | 1230 | S 48 E, 20 W |
| 782 | N .0 E, 40 E | 1032 | S 13 W, 32 W | 1086 | S 37 W, 44 W | 1231 | S 38 W, 27 W |
| 783 | N 36 E, 50 E | 1033 | S 2 W, 50 W | 1087 | S 28 W, 38 W | 1232 | S 47 W, 31 W |
| 784 | N 25 E, 56 E | 1034 | S 2 E, 34 W | 1102 | S 30 E, 50 W | 1233 | S 44 W, 49 W |
| 785 | N 24 E, 76 E | 1035 | S 82 E, 52 W | 1103 | S 66 E, 67 W | 1234 | S 53 W, 42 W |
| 786 | N 7 E, 53 E | 1036 | S 26 W, 61 W | 1104 | S 43 E, 24 W | 1235 | S 47 W, 48 W |
| 787 | N 5 E, 55 E | 1037 | S 6 E, 42 W | 1106 | S 39 E, 33 W | 1236 | S 54 W, 37 W |
| 788 | N 4 W, 54 E | 1039 | S 70 E, 35 W | 1107 | S 78 E, 59 W | 1237 | S 16 W, 49 W |
| 789 | N 4 E, 53 E | 1040 | S 72 E, 30 W | 1108 | N 87 E, 35 E | 1238 | S 62 W, 40 W |
| 790 | N 22 E, 73 E | 1041 | S 71 E, 30 W | 1109 | N 87 E, 63 E | 1246 | S 38 W, 48 W |
| 791 | N 13 E, 67 E | 1042 | S 25 W, 74 W | 1111 | N 62 E, 48 E | 1247 | S 46 W, 67 W |
| 792 | N 14 E, 67 E | 1043 | S 84 E, 52 W | 1112 | N 65 W, 62 E | 1248 | N 19 E, 59 E |
| 793 | S 73 W, 29 W | 1044 | S 59 E, 43 W | 1113 | N 62 E, 67 E | 1249 | S 20 W, 56 W |
| 794 | N 34 E, 75 E | 1047 | S 14 E, 25 W | 1114 | S 89 E, 25 W | 1250 | S 17 W, 36 W |
| 795 | S 52 W, 63 W | 1048 | S 30 E, 53 W | 1115 | N 60 E, 60 E | 1251 | S 52 W, 16 W |
| 796 | N 26 W, 26 E | 1049 | S 47 W, 59 W | 1116 | N 83 E, 63 E | 1253 | S 59 E, 10 W |
| 797 | N 4 E, 75 E | 1050 | S 25 W, 65 W | 1119 | N 55 E, 79 E | 1255 | S 74 E, 41 W |
| 798 | N 5 E, 44 E | 1051 | S 15 E, 35 W | 1120 | N 74 E, 60 E | 1257 | N 47 E, 40 E |
| 800 | N 10 E, 86 E | 1052 | S 27 W, 42 W | 1121 | N 48 E, 80 E | 1258 | S 17 W, 43 W |
| 806 | N 13 E, 68 E | 1054 | S 42 W, 55 W | 1122 | N 63 E, 72 E | 1259 | N 66 E, 33 E |
| 810 | N 30 E, 90 E | 1055 | S 45 W, 82 W | 1124 | S 40 W, 75 W | 1263 | N 32 E, 57 E |
| 993 | S 59 E, 56 W | 1056 | S 36 W, 53 W | 1125 | S 77 E, 55 W | 1265 | N 58 E, 22 E |
| 994 | N 71 E, 63 E | 1057 | S 41 W, 22 W | 1126 | S 21 E, 59 W | 1266 | N 52 E, 74 E |

Appendix 2A, continued

| DOME AREA | | DOME AREA | | DOME AREA | | DOME AREA | |
|---|---|---|---|---|---|---|---|
| STATION # | FOLIATION | STATION # | FOLIATION | STATION # | FOLIATION | STATION # | FOLIATION |
| 1267 | N 60 E, 65 E | 1321 | N 36 E, 58 E | 1629 | N 27 E, 54 E | 1698 | N 62 E, 44 E |
| 1268 | N 59 E, 67 E | 1322 | N 53 E, 63 E | 1630 | N 8 W, 70 E | 1701 | N 45 E, 41 E |
| 1269 | N 58 E, 40 E | 1324 | N 40 E, 54 E | 1630 | S 28 W, 85 W | 1702 | N 80 E, 63 E |
| 1270 | N 45 E, 57 E | 1325 | N 30 E, 47 E | 1631 | N 59 E, 35 E | 1703 | N 56 E, 75 E |
| 1272 | N 30 E, 40 E | 1326 | N 39 E, 52 E | 1632 | N 52 E, 37 E | 1704 | N 46 E, 61 E |
| 1273 | N 43 E, 46 E | 1327 | N 46 E, 52 E | 1633 | N 22 E, 40 E | 1707 | N 6 W, 21 E |
| 1274 | N 52 E, 76 E | 1328 | N 58 E, 55 E | 1636 | N 28 E, 41 E | 1708 | N 85 E, 18 E |
| 1275 | N 75 E, 49 E | 1329 | N 49 E, 43 E | 1637 | N 20 E, 38 E | 1709 | S 84 E, 44 W |
| 1276 | N 62 E, 52 E | 1330 | N 55 E, 47 E | 1638 | N 69 E, 62 E | 1711 | S 12 W, 50 W |
| 1277 | N 78 E, 57 E | 1331 | N 89 E, 12 E | 1639 | N 68 E, 30 E | 1712 | N 78 E, 44 E |
| 1278 | N 88 E, 39 E | 1333 | N 30 E, 42 E | 1640 | N 39 E, 83 E | 1713 | S 21 E, 70 W |
| 1279 | S 88 E, 46 W | 1335 | S 36 W, 79 W | 1641 | N 84 E, 40 E | 1714 | N 82 E, 40 E |
| 1280 | S 52 E, 20 W | 1336 | N 22 E, 64 E | 1642 | N 82 E, 34 E | 1715 | N 83 E, 42 E |
| 1281 | S 75 E, 27 W | 1337 | S 41 W, 68 W | 1643 | N 58 E, 47 E | 1716 | N 44 E, 68 E |
| 1283 | S 44 E, 36 W | 1338 | N 28 E, 78 E | 1644 | N 52 E, 54 E | 1719 | N 58 E, 61 E |
| 1284 | S 56 W, 15 W | 1339 | S 30 W, 88 W | 1645 | N 63 E, 37 E | 1720 | N 53 E, 35 E |
| 1286 | N 67 E, 60 E | 1340 | N 5 E, 72 E | 1646 | N 46 E, 36 E | 1721 | N 83 E, 36 E |
| 1286 | S 38 W, 45 W | 1341 | N 15 W, 54 E | 1647 | N 42 E, 52 E | 1722 | N 52 E, 50 E |
| 1288 | S 82 E, 20 W | 1342 | N 8 E, 67 E | 1648 | N 37 E, 35 E | 1723 | N 51 E, 42 E |
| 1290 | N 65 E, 43 E | 1343 | N 7 E, 57 E | 1649 | N 44 E, 45 E | 1724 | N 46 E, 34 E |
| 1291 | N 30 E, 36 E | 1344 | N 9 E, 64 E | 1650 | N 29 E, 49 E | 1725 | N 33 E, 52 E |
| 1292 | N 55 E, 51 E | 1345 | N 32 E, 70 E | 1651 | N 38 E, 59 E | 1728 | N 61 E, 65 E |
| 1293 | N 64 E, 53 E | 1346 | N 25 E, 54 E | 1652 | N 24 E, 62 E | 1730 | N 56 E, 56 E |
| 1294 | N 59 E, 54 E | 1347 | N 28 E, 84 E | 1653 | N 41 E, 59 E | 1731 | N 47 E, 38 E |
| 1295 | N 43 E, 53 E | 1348 | N 37 E, 80 E | 1654 | N 52 E, 58 E | 1734 | N 86 E, 50 E |
| 1296 | N 62 E, 53 E | 1349 | S 22 W, 71 W | 1655 | N 75 E, 61 E | 1736 | N 60 E, 68 E |
| 1297 | N 60 E, 51 E | 1350 | S 39 W, 57 W | 1656 | N 63 E, 53 E | 1738 | N 66 E, 68 E |
| 1299 | N 54 E, 37 E | 1351 | S 51 W, 56 W | 1657 | N 45 E, 27 E | 1739 | N 75 E, 52 E |
| 1300 | N 44 E, 48 E | 1352 | S 34 W, 45 W | 1658 | N 49 E, 51 E | 1741 | N 28 E, 87 E |
| 1301 | N 24 E, 62 E | 1354 | S 36 E, 47 W | 1659 | N 33 E, 58 E | 1743 | N 52 E, 45 E |
| 1302 | N 5 E, 54 E | 1355 | N 45 E, 89 E | 1660 | N 65 E, 52 E | 1901 | N 54 E, 29 E |
| 1303 | N 22 E, 63 E | 1356 | S 65 E, 19 W | 1661 | N 78 E, 75 E | 1903 | N 54 E, 50 E |
| 1304 | N 53 E, 68 E | 1357 | S 24 E, 57 W | 1662 | N 21 E, 70 E | 1904 | S 86 E, 45 W |
| 1305 | N 25 E, 64 E | 1358 | N 56 E, 30 E | 1663 | N 34 E, 54 E | 1905 | S 77 E, 46 W |
| 1306 | N 24 E, 63 E | 1359 | N 30 E, 63 E | 1664 | N 21 E, 72 E | 1918 | S 14 E, 56 W |
| 1307 | N 24 E, 61 E | 1360 | S 78 E, 60 W | 1665 | N 44 E, 57 E | 1920 | N 40 E, 47 E |
| 1308 | N 19 E, 60 E | 1361 | S 40 W, 70 W | 1666 | N 40 E, 57 E | 1921 | S 85 E, 27 W |
| 1309 | N 24 E, 53 E | 1362 | S 28 W, 51 W | 1667 | N 72 E, 52 E | 1923 | N 21 E, 54 E |
| 1310 | N 2 E, 40 E | 1363 | S 84 E, 65 W | 1668 | N 34 E, 74 E | 1924 | S 27 W, 59 W |
| 1311 | N 12 E, 68 E | 1365 | N 53 E, 74 E | 1669 | N 82 E, 45 E | 1926 | N 59 E, 89 E |
| 1312 | N 23 E, 70 E | 1366 | N 42 E, 69 E | 1670 | N 42 E, 65 E | 1928 | N 35 E, 48 E |
| 1313 | N 28 E, 84 E | 1367 | N 53 E, 39 E | 1671 | N 34 E, 50 E | 1930 | N 42 E, 70 E |
| 1314 | N 29 E, 84 E | 1368 | N 57 E, 36 E | 1673 | N 32 E, 44 E | 1931 | N 51 E, 28 E |
| 1315 | N 33 E, 66 E | 1370 | N 30 E, 45 E | 1674 | N 42 E, 52 E | 2102 | S 31 W, 51 W |
| 1316 | N 22 E, 69 R | 1621 | N 29 E, 50 E | 1675 | N 52 E, 35 E | 2103 | S 35 W, 44 W |
| 1317 | N 27 E, 65 E | 1622 | N 34 E, 42 E | 1676 | N 38 E, 56 E | 2104 | S 24 W, 58 W |
| 1318 | N 31 E, 59 E | 1625 | N 12 E, 51 E | 1695 | N 56 E, 42 E | 2105 | S 49 W, 73 W |
| 1319 | N 49 E, 53 E | 1626 | N 33 E, 43 E | 1696 | S 70 E, 36 W | 2106 | S 82 W, 64 W |
| 1320 | N 39 E, 67 E | 1628 | N 19 E, 68 E | 1697 | N 40 E, 39 E | 2107 | S 50 W, 44 W |

Appendix 2A, continued

| DOME AREA | | SAVALEN AREA | | SAVALEN AREA | | SAVALEN AREA | |
|---|---|---|---|---|---|---|---|
| STATION # | FOLIATION | STATION # | FOLIATION | STATION # | FOLIATION | STATION # | FOLIATION |
| 2108 | S 19 W, 44 W | 1 | N 27 E, 80 E | 104 | S 32 W, 85 W | 215 | N 22 E, 78 E |
| 2109 | S 21 W, 54 W | 2 | N 14 E, 63 E | 105 | N 22 E, 75 E | 216 | N 34 E, 89 E |
| 2110 | S 14 W, 79 W | 3 | N 18 E, 72 E | 105 | N 40 E, 87 E | 217 | N 26 E, 86 E |
| 2112 | S 18 W, 77 W | 4 | N 27 E, 67 E | 106 | N 30 E, 82 E | 218 | S 36 W, 80 W |
| 2114 | S 2 E, 62 W | 5 | N 36 E, 70 E | 107 | S 22 W, 60 W | 219 | S 42 W, 80 W |
| 2115 | S 30 E, 48 W | 6 | N 19 E, 56 E | 108 | N 29 E, 87 E | 220 | N 24 E, 74 E |
| 2116 | S 25 E, 63 W | 7 | N 40 E, 51 E | 109 | N 32 E, 75 E | 235 | S 9 W, 70 W |
| 2117 | N 37 E, 45 E | 8 | N 25 E, 70 E | 110 | N 20 E, 55 E | 236 | S 24 W, 74 W |
| 2118 | N .0 E, 61 E | 9 | N 24 E, 79 E | 111 | N 8 E, 85 E | 237 | S 10 W, 64 W |
| 2119 | N 31 E, 48 E | 10 | N 17 E, 60 E | 174 | N 14 E, 81 E | 238 | N 28 E, 82 E |
| 2120 | N 28 E, 63 E | 11 | N 25 E, 62 E | 175 | N 8 E, 81 E | 239 | S 42 W, 63 W |
| 2121 | N 2 W, 60 E | 12 | N 30 E, 61 E | 176 | N 35 E, 79 E | 240 | S 30 W, 76 W |
| 2122 | N 17 E, 84 E | 13 | N 29 E, 77 E | 177 | S 15 W, 78 W | 241 | S 38 W, 75 W |
| 2123 | N 5 E, 63 E | 16 | N 20 E, 90 E | 178 | S 14 W, 79 W | 242 | S 7 W, 42 W |
| 2124 | N 47 E, 79 E | 17 | S 8 W, 86 W | 179 | N 21 E, 86 E | 243 | S 24 W, 65 W |
| 2126 | N 49 E, 80 E | 19 | N 32 E, 76 E | 180 | N 20 E, 84 E | 244 | S 5 W, 69 W |
| 2129 | N 21 E, 74 E | 20 | N 32 E, 72 E | 181 | S 20 W, 78 W | 245 | S 22 W, 65 W |
| 2130 | S 8 W, 78 W | 21 | S 36 W, 78 W | 182 | N 8 E, 87 E | 246 | S 15 W, 74 W |
| 2132 | S .0 E, 58 W | 22 | N 22 E, 86 E | 183 | S 32 W, 82 W | 247 | S 22 W, 76 W |
| 2133 | S 14 W, 78 W | 23 | N 20 E, 80 E | 185 | N 18 E, 87 E | 248 | S 34 W, 76 W |
| 2134 | S 4 W, 82 W | 24 | N 28 E, 86 E | 186 | N 23 E, 56 E | 249 | S 34 W, 84 W |
| 2135 | S 11 E, 62 W | 25 | N 19 E, 87 E | 187 | N 34 E, 75 E | 250 | S 14 W, 56 W |
| 2136 | S 14 W, 66 W | 26 | S 42 W, 76 W | 188 | S 27 W, 88 W | 251 | S 27 W, 67 W |
| 2138 | N 9 E, 85 E | 27 | N 28 E, 83 E | 189 | S 27 W, 82 W | 252 | S 26 W, 59 W |
| 2139 | S 15 W, 76 W | 28 | N 38 E, 78 E | 190 | N 26 E, 74 E | 253 | S 24 W, 65 W |
| 2140 | S 22 W, 60 W | 29 | N 36 E, 87 E | 191 | S 19 W, 72 W | 254 | S 42 W, 72 W |
| 2141 | N 20 E, 48 E | 30 | N 43 E, 71 E | 192 | N 9 E, 80 E | 255 | S 40 W, 67 W |
| 2142 | N 4 E, 44 E | 31 | N 36 E, 74 E | 193 | S 28 W, 75 W | 256 | S 35 W, 72 W |
| 2143 | N 21 E, 47 E | 33 | S 16 W, 33 W | 194 | S 5 E, 39 W | 257 | S 54 W, 60 W |
| 2144 | N 7 W, 49 E | 34 | S 22 W, 80 W | 195 | N 29 E, 88 E | 258 | S 25 W, 86 W |
| 2145 | N 14 W, 32 E | 84 | N 24 E, 75 E | 196 | N 30 E, 89 E | 259 | S 17 W, 76 W |
| 2146 | N 7 W, 36 E | 86 | N 32 E, 82 E | 197 | N 31 E, 74 E | 260 | S 42 W, 73 W |
| 2148 | N 4 E, 37 E | 87 | N 17 E, 83 E | 198 | N 21 E, 84 E | 262 | N 55 E, 65 E |
| 2149 | N 43 W, 28 E | 88 | N 9 E, 81 E | 199 | S 31 W, 83 W | 263 | N 59 E, 89 E |
| 2150 | N 24 E, 45 E | 89 | N 36 E, 79 E | 200 | N 42 E, 89 E | 264 | S 34 W, 33 W |
| | | 90 | S 22 W, 78 W | 201 | S 23 W, 88 W | 265 | N 20 E, 85 E |
| | | 91 | N 26 E, 82 E | 202 | N 52 E, 68 E | 266 | N 24 E, 86 E |
| | | 92 | S 30 W, 75 W | 203 | S 28 W, 78 W | 267 | S 18 W, 87 W |
| | | 93 | S 48 W, 80 W | 204 | N 28 E, 81 E | 268 | S 30 W, 87 W |
| | | 94 | S 42 W, 72 W | 205 | S 26 W, 88 W | 269 | S 26 W, 87 W |
| | | 95 | N 23 E, 79 E | 206 | S 24 W, 87 W | 270 | S 31 W, 80 W |
| | | 96 | N 44 E, 81 E | 207 | N 23 E, 81 E | 271 | S 27 W, 81 W |
| | | 97 | N 19 E, 84 E | 208 | N 25 E, 88 E | 272 | S 22 W, 75 W |
| | | 98 | N 30 E, 80 E | 209 | S 22 W, 80 W | 273 | S 19 W, 84 W |
| | | 99 | N 30 E, 78 E | 210 | S 38 W, 62 W | 274 | S 31 W, 74 W |
| | | 100 | N 27 E, 75 E | 211 | S 28 W, 83 W | 275 | S 24 W, 80 W |
| | | 101 | N 44 E, 77 E | 212 | N 26 E, 72 E | 277 | S 29 W, 71 W |
| | | 102 | N 30 E, 87 E | 213 | S 18 W, 82 W | 278 | S 23 W, 87 W |
| | | 103 | N 24 E, 86 E | 214 | N 30 E, 68 E | 279 | S 34 W, 75 W |

Appendix 2A, continued

| SAVALEN AREA | | SAVALEN AREA | | SAVALEN AREA | | SAVALEN AREA | |
|---|---|---|---|---|---|---|---|
| STATION # | FOLIATION | STATION # | FOLIATION | STATION # | FOLIATION | STATION # | FOLIATION |
| 280 | S 42 W, 88 W | 461 | N 27 E, 79 E | 657 | S 24 W, 78 W | 726 | N 41 E, 87 E |
| 412 | S 47 W, 81 W | 462 | N 21 E, 83 E | 658 | S 17 W, 82 W | 727 | N 32 E, 72 E |
| 413 | N 44 E, 55 E | 463 | S 34 W, 88 W | 659 | N 30 E, 83 E | 728 | S 34 W, 87 W |
| 414 | N 22 E, 68 E | 464 | S 37 W, 76 W | 660 | N 22 E, 70 E | 729 | S 34 W, 72 W |
| 415 | N 39 E, 65 E | 465 | N 36 E, 57 E | 661 | S 15 W, 54 W | 730 | N 18 E, 70 E |
| 416 | N 47 E, 35 E | 466 | N 31 E, 47 E | 662 | S 27 W, 89 W | 731 | S 13 W, 87 W |
| 417 | S 18 W, 80 W | 468 | N 32 E, 62 E | 663 | S 37 W, 67 W | 732 | S 22 W, 73 W |
| 419 | S 25 W, 75 W | 469 | N 39 E, 64 E | 664 | N 10 E, 87 E | 733 | S 12 W, 60 W |
| 419 | N 27 E, 57 E | 470 | N 47 E, 71 E | 665 | S 22 W, 70 W | 734 | S 15 E, 60 W |
| 420 | N 26 E, 72 E | 471 | N 31 E, 66 E | 666 | N 30 E, 86 E | 735 | S 17 W, 73 W |
| 421 | S 11 W, 89 W | 472 | S 38 W, 87 W | 667 | S 5 W, 77 W | 736 | S 14 W, 81 W |
| 422 | N 25 E, 85 E | 473 | N 43 E, 62 E | 668 | S 8 W, 58 W | 738 | N 85 E, 57 E |
| 423 | N 38 E, 68 E | 474 | N 36 E, 56 E | 669 | S 2 W, 67 W | 739 | S 36 W, 77 W |
| 424 | N 49 E, 76 E | 475 | N 48 E, 59 E | 670 | S 16 W, 75 W | 740 | S 38 W, 84 W |
| 425 | S 28 W, 87 W | 476 | S 82 E, 56 W | 671 | S 32 W, 84 W | 741 | S 18 W, 89 W |
| 426 | N 42 E, 44 E | 477 | N 62 E, 65 E | 672 | S 33 W, 80 W | 742 | S 26 W, 78 W |
| 427 | N 48 E, 44 E | 478 | S 64 W, 84 W | 673 | S 33 W, 75 W | 743 | S 22 W, 71 W |
| 428 | N 35 E, 66 E | 479 | S 52 W, 74 W | 674 | S 24 W, 86 W | 744 | S 22 W, 60 W |
| 429 | N 53 E, 56 E | 480 | S 52 W, 80 W | 675 | S 21 W, 75 W | 745 | S 20 W, 40 W |
| 430 | N 44 E, 64 E | 481 | S 34 W, 52 W | 676 | N 33 E, 86 E | 746 | S 18 W, 62 W |
| 431 | N 45 E, 61 E | 482 | S 29 W, 63 W | 677 | S 24 W, 68 W | 814 | N 35 E, 47 E |
| 432 | N 52 E, 70 E | 483 | N 38 E, 80 E | 678 | N 35 E, 67 E | 815 | N 44 E, 61 E |
| 433 | N 51 E, 64 E | 484 | N 21 E, 70 E | 679 | S 24 W, 81 W | 816 | N 43 E, 67 E |
| 434 | N 58 E, 72 E | 485 | N 34 E, 42 E | 680 | N 25 E, 86 E | 817 | N 38 E, 69 E |
| 435 | N 38 E, 40 E | 486 | N 20 E, 76 E | 681 | N 26 E, 80 E | 818 | N 23 E, 81 E |
| 436 | N 48 E, 66 E | 487 | N 28 E, 85 E | 682 | N 24 E, 82 E | 819 | N 27 E, 80 E |
| 437 | N 54 E, 40 E | 488 | S 40 W, 74 W | 683 | N 4 W, 72 E | 820 | N 39 E, 80 E |
| 438 | N 23 E, 69 E | 489 | N 30 E, 75 E | 684 | N 51 E, 80 E | 821 | N 38 E, 71 E |
| 439 | N 65 E, 84 E | 490 | N 30 E, 67 E | 685 | N 28 E, 60 E | 822 | N 33 E, 64 E |
| 441 | N 47 E, 65 E | 491 | N 30 E, 85 E | 686 | S 30 W, 76 W | 833 | N 53 E, 82 E |
| 442 | N 40 E, 74 E | 492 | S 27 W, 85 W | 687 | N 45 E, 77 E | 844 | N 40 E, 63 E |
| 443 | N 48 E, 70 E | 493 | N 30 E, 80 E | 688 | N 35 E, 82 E | 825 | N 44 E, 80 E |
| 444 | S 53 W, 73 W | 494 | S 38 W, 72 W | 689 | S 41 W, 56 W | 826 | N 44 E, 71 E |
| 445 | N 40 E, 86 E | 495 | N 32 E, 82 E | 690 | N 24 E, 66 E | 827 | S 50 W, 89 W |
| 446 | S 29 W, 75 W | 497 | N 56 E, 73 E | 691 | N 31 E, 84 E | 828 | N 45 E, 53 E |
| 447 | S 19 W, 83 W | 498 | S 45 W, 60 W | 672 | N 44 E, 68 E | 829 | N 36 E, 84 E |
| 448 | S 29 W, 68 W | 499 | S 59 W, 71 W | 693 | S 33 W, 65 W | 830 | N 47 E, 84 E |
| 449 | S 28 W, 76 W | 500 | S 55 W, 60 W | 694 | N 40 E, 75 E | 831 | N 47 E, 82 E |
| 450 | S 41 W, 81 W | 503 | S 24 W, 51 W | 695 | N 29 E, 73 E | 832 | N 31 E, 84 E |
| 451 | N 30 E, 89 E | 503 | S 65 E, 80 W | 715 | S 15 W, 86 W | 833 | N 30 E, 76 E |
| 452 | S 16 W, 82 W | 504 | S 8 W, 37 W | 716 | S 17 W, 80 W | 834 | N 38 E, 81 E |
| 453 | N 50 E, 83 E | 505 | S 40 W, 73 W | 717 | S 12 W, 86 W | 834 | N 32 E, 88 E |
| 454 | N 45 E, 88 E | 506 | S 48 W, 67 W | 718 | S 18 W, 85 W | 835 | N 44 E, 63 E |
| 455 | N 30 E, 86 E | 507 | S 52 W, 89 W | 720 | S 24 W, 84 W | 836 | N 33 E, 84 E |
| 456 | N 24 E, 76 E | 655 | S 52 W, 77 W | 721 | S 26 W, 79 W | 838 | N 40 E, 71 E |
| 457 | N 33 E, 87 E | 656 | N 38 E, 59 E | 722 | S 19 W, 89 W | 840 | N 34 E, 74 E |
| 458 | S 17 W, 72 W | 656 | N 7 E, 51 E | 723 | N 23 E, 71 E | 841 | S 29 E, 39 W |
| 459 | N 8 E, 87 E | 656 | N 14 E, 76 E | 724 | S 18 E, 80 W | 844 | S 32 W, 76 W |
| 460 | N 37 E, 77 E | 656 | N 48 E, 35 E | 725 | S 12 W, 81 W | 846 | N 9 E, 84 E |

Appendix 2A, continued

| AVALEN AREA | | SAVALEN AREA | | SAVALEN AREA | | SAVALEN AREA | |
|---|---|---|---|---|---|---|---|
| STATION # | FOLIATION | STATION # | FOLIATION | STATION # | FOLIATION | STATION # | FOLIATION |
| 847 | S 86 E, 76 W | 898 | N 18 E, 89 E | 958 | S 33 W, 88 W | 1148 | N 30 E, 87 E |
| 848 | N 87 E, 60 E | 899 | N 28 E, 62 E | 959 | S 36 W, 60 W | 1149 | N 40 E, 84 E |
| 849 | S 83 E, 67 W | 900 | N 27 E, 67 E | 960 | N 46 E, 87 E | 1150 | S 17 W, 76 W |
| 850 | N 76 E, 81 E | 901 | N 32 E, 81 E | 961 | N 62 E, 81 E | 1151 | S 31 W, 71 W |
| 851 | S 76 E, 65 W | 902 | N 26 E, 66 E | 962 | S 48 W, 84 W | 1152 | S 30 W, 66 W |
| 852 | N 88 E, 87 E | 903 | N 32 E, 72 E | 963 | S 24 W, 75 W | 1153 | S 24 W, 80 W |
| 853 | S 51 W, 81 W | 904 | N 26 E, 72 E | 964 | N 37 E, 83 E | 1154 | S 42 W, 87 W |
| 854 | S 74 W, 35 W | 905 | N 31 E, 80 E | 965 | N 52 E, 73 E | 1155 | N 58 E, 72 E |
| 855 | S 50 W, 70 W | 906 | N 40 E, 70 E | 966 | N 22 E, 52 E | 1156 | N 33 E, 80 E |
| 856 | S 21 W, 84 W | 907 | N 41 E, 90 E | 967 | N 14 E, 77 E | 1157 | N 34 E, 82 E |
| 857 | S 25 W, 69 W | 908 | N 39 E, 86 E | 968 | N 23 E, 87 E | 1158 | S 30 W, 84 W |
| 858 | N 52 E, 65 E | 909 | N 38 E, 67 E | 969 | N 34 E, 68 E | 1159 | S 25 W, 89 W |
| 859 | S 38 W, 72 W | 910 | N 36 E, 70 E | 970 | N 53 E, 67 E | 1160 | S 34 W, 79 W |
| 860 | N 28 E, 64 E | 911 | N 43 E, 73 E | 971 | S 38 W, 66 W | 1161 | S 16 W, 61 W |
| 861 | N 40 E, 87 E | 912 | S 32 W, 72 W | 972 | N 54 E, 58 E | 1162 | S 28 W, 81 W |
| 862 | S 18 W, 55 W | 913 | N 30 E, 69 E | 973 | N 40 E, 68 E | 1163 | N 45 E, 71 E |
| 863 | S 15 W, 58 W | 914 | N 10 E, 72 E | 974 | N 43 E, 70 E | 1164 | S 39 W, 76 W |
| 864 | S 40 W, 81 W | 915 | N 23 E, 76 E | 975 | N 34 E, 77 E | 1165 | S 61 W, 60 W |
| 866 | N 27 E, 87 E | 916 | N 21 E, 77 E | 977 | N 28 E, 52 E | 1166 | S 11 W, 78 W |
| 867 | S 37 W, 87 W | 917 | N 23 E, 73 E | 978 | N 27 E, 77 E | 1167 | S 23 W, 72 W |
| 868 | N 40 E, 90 E | 918 | N 38 E, 71 E | 979 | S 7 W, 42 W | 1168 | S 41 W, 84 W |
| 869 | S 24 W, 74 W | 919 | N 42 E, 73 E | 980 | S 30 W, 50 W | 1169 | S 28 W, 85 W |
| 870 | S 40 W, 75 W | 920 | N 15 E, 84 E | 981 | N 32 E, 82 E | 1171 | S 26 W, 68 W |
| 872 | S 8 W, 76 W | 921 | N 23 E, 70 E | 982 | N 39 E, 66 E | 1172 | S 22 W, 70 W |
| 873 | S 26 W, 74 W | 922 | N 28 E, 77 E | 984 | N 38 E, 71 E | 1173 | S 19 W, 73 W |
| 874 | S 25 W, 70 W | 924 | N 38 E, 72 E | 986 | N 49 E, 74 E | 1174 | S 41 W, 77 W |
| 875 | S 14 W, 85 W | 925 | N 51 E, 54 E | 987 | N 31 E, 29 E | 1175 | S 37 W, 81 W |
| 876 | S 26 W, 75 W | 926 | N 32 E, 65 E | 988 | N 22 E, 68 E | 1176 | S 18 W, 82 W |
| 877 | S 16 W, 60 W | 927 | N 45 E, 61 E | 989 | N 39 E, 50 E | 1177 | S 34 W, 88 W |
| 878 | S 32 W, 86 W | 928 | N 53 E, 49 E | 990 | N 48 E, 61 E | 1179 | S 40 W, 75 W |
| 879 | S 14 W, 77 W | 930 | N 52 E, 78 E | 991 | S 45 E, 57 W | 1180 | N 48 E, 85 E |
| 880 | S 24 W, 72 W | 931 | N 52 E, 47 E | 992 | N 24 E, 39 E | 1181 | S 52 W, 72 W |
| 881 | S 10 W, 57 W | 932 | N 66 E, 25 E | 1011 | N 38 E, 48 E | 1184 | N 84 E, 86 E |
| 882 | S 21 W, 84 W | 932 | S 86 E, 50 W | 1012 | N 40 E, 63 E | 1185 | S 50 W, 27 W |
| 883 | S 9 W, 81 W | 942 | S 20 W, 67 W | 1013 | N 36 E, 47 E | 1186 | S 38 W, 30 W |
| 884 | S 26 W, 77 W | 943 | S 37 W, 76 W | 1014 | S 43 W, 43 W | 1187 | S 52 W, 87 W |
| 885 | S 18 W, 80 W | 944 | S 27 W, 81 W | 1088 | N 19 E, 76 E | 1188 | N 64 W, 80 E |
| 886 | S 17 W, 72 W | 945 | N 34 E, 90 E | 1090 | S 22 W, 74 W | 1189 | N 29 E, 31 E |
| 887 | S 27 W, 70 W | 946 | S 40 W, 64 W | 1091 | N 38 E, 83 E | 1191 | N 88 W, 72 E |
| 888 | S 31 W, 67 W | 947 | S 39 W, 75 W | 1092 | N 34 E, 76 E | 1192 | N 72 E, 86 E |
| 889 | N 26 E, 86 E | 948 | S 39 W, 80 W | 1093 | N 47 E, 63 E | 1193 | N 82 E, 71 E |
| 890 | N 30 E, 75 E | 950 | S 30 W, 72 W | 1094 | N 43 E, 80 E | 1194 | N 74 W, 50 E |
| 891 | N 23 E, 76 E | 951 | S 36 W, 81 W | 1095 | N 38 E, 87 E | 1195 | S 67 W, 60 W |
| 892 | S 32 W, 85 W | 952 | S 33 W, 76 W | 1096 | N 29 E, 82 E | 1196 | S 52 W, 58 W |
| 893 | N 29 E, 77 E | 953 | S 37 W, 62 W | 1097 | N 27 E, 73 E | 1204 | S 15 W, 69 W |
| 894 | N 68 W, 25 E | 954 | S 50 W, 88 W | 1098 | N 18 E, 80 E | 1205 | S 32 W, 77 W |
| 895 | N 19 E, 85 E | 955 | S 31 W, 73 W | 1099 | S 5 W, 82 W | 1206 | S 26 W, 76 W |
| 896 | N 16 E, 67 E | 956 | S 39 W, 79 W | 1100 | N 12 E, 85 E | 1207 | S 41 W, 80 W |
| 897 | N 10 E, 25 E | 957 | S 37 W, 78 W | 1101 | N 40 E, 74 E | 1208 | S 18 W, 85 W |

Appendix 2A, continued

| SAVALEN AREA | | SAVALEN AREA | | SAVALEN AREA | | SAVALEN AREA | |
|---|---|---|---|---|---|---|---|
| STATION # | FOLIATION | STATION # | FOLIATION | STATION # | FOLIATION | STATION # | FOLIATION |
| 1209 | S 24 W, 72 W | RDH 8/2/90 | N 33 E, 77 E | 1442 | N 44 E, 81 E | 1500 | S 33 W, 89 W |
| 1210 | N 24 E, 74 E | " | N 24 E, 81 E | 1444 | N 27 E, 81 E | 1501 | N 29 E, 79 E |
| 1211 | S 24 W, 75 W | " | N 37 E, 79 E | 1445 | N 34 E, 73 E | 1503 | N 33 E, 84 E |
| 1212 | S 34 W, 67 W | " | N 31 E, 78 E | 1446 | N 44 E, 79 E | 1504 | N 38 E, 87 E |
| 1213 | S 33 W, 78 W | " | N 31 E, 89 E | 1447 | N 21 E, 59 E | 1505 | N 31 E, 84 E |
| 1214 | S 29 W, 79 W | 1395 | N 49 E, 79 E | 1448 | N 38 E, 66 E | 1506 | S 37 W, 82 W |
| 1215 | S 24 W, 63 W | 1396 | N 40 E, 75 E | 1449 | N 41 E, 65 E | 1507 | S 29 W, 83 W |
| 1216 | S 34 W, 73 W | 1397 | N 31 E, 84 E | 1450 | N 56 E, 72 E | 1508 | N 23 E, 83 E |
| 1217 | S 15 W, 74 W | 1398 | N 58 E, 30 E | 1451 | N 41 E, 79 E | 1509 | N 33 E, 88 E |
| 1218 | S 18 W, 68 W | 1399 | N 39 E, 84 E | 1452 | N 34 E, 80 E | 1509 | S 30 W, 82 W |
| 1219 | S 26 W, 79 W | 1400 | N 44 E, 78 E | 1453 | S 43 W, 85 W | 1510 | S 37 W, 89 W |
| 1220 | S 20 W, 54 W | 1401 | N 42 E, 81 E | 1455 | N 44 E, 84 E | 1511 | N 35 E, 83 E |
| 1221 | S 19 W, 69 W | 1402 | N 29 E, 77 E | 1456 | N 51 E, 79 E | 1512 | N 45 E, 81 E |
| 1222 | S 38 W, 78 W | 1403 | N 32 E, 82 E | 1459 | N 52 E, 67 E | 1514 | N 15 E, 80 E |
| 1223 | N 12 E, 80 E | 1404 | N 31 E, 79 E | 1460 | N 51 E, 60 E | 1515 | S 50 W, 88 W |
| 1224 | S 36 W, 66 W | 1405 | N 31 E, 84 E | 1461 | N 44 E, 75 E | 1516 | N 21 E, 89 E |
| 1225 | S 28 W, 59 W | 1406 | N 34 E, 79 E | 1462 | N 51 E, 72 E | 1517 | N 34 E, 82 E |
| 1226 | S 41 W, 71 W | 1407 | N 32 E, 77 E | 1464 | N 32 E, 77 E | 1518 | N 43 E, 76 E |
| 1239 | S 2 W, 57 W | 1409 | N 38 E, 77 E | 1465 | N 44 E, 69 E | 1519 | N 33 E, 78 E |
| 1240 | S 39 W, 52 W | 1410 | N 41 E, 62 E | 1466 | N 60 E, 73 E | 1520 | S 23 W, 75 W |
| 1241 | S 20 W, 55 W | 1411 | N 36 E, 76 E | 1468 | S 29 W, 75 W | 1521 | N 52 E, 87 E |
| 1242 | S 32 W, 60 W | 1412 | N 31 E, 82 E | 1469 | N 42 E, 75 E | 1522 | S 42 W, 85 W |
| 1243 | S 30 W, 52 W | 1413 | N 39 E, 87 E | 1470 | N 39 E, 85 E | 1524 | N 36 E, 82 E |
| 1244 | S 65 W, 82 W | 1414 | N 38 E, 82 E | 1471 | N 27 E, 70 E | 1527 | S 39 W, 79 W |
| 1373 | N 56 E, 55 E | 1415 | N 61 E, 32 E | 1472 | N 43 E, 70 E | 1528 | N 26 E, 75 E |
| 1374 | N 74 E, 37 E | 1416 | N 42 E, 82 E | 1473 | N 39 E, 57 E | 1529 | N 34 E, 84 E |
| 1375 | N 39 E, 54 E | 1417 | N 44 E, 76 E | 1474 | N 39 E, 71 E | 1531 | S 26 W, 76 W |
| 1377 | N 43 E, 59 E | 1418 | N 39 E, 71 E | 1475 | N 45 E, 8 E | 1533 | N 28 E, 76 E |
| 1378 | N 19 E, 69 E | 1419 | N 42 E, 81 E | 1476 | N 36 E, 86 E | 1534 | N 57 E, 85 E |
| 1379 | N 20 E, 80 E | 1420 | N 48 E, 57 E | 1477 | N 38 E, 70 E | 1536 | N 29 E, 77 E |
| 1380 | N 21 E, 82 E | 1421 | N 41 E, 74 E | 1478 | N 47 E, 68 E | 1537 | N 43 E, 86 E |
| 1381 | N 40 E, 82 E | 1422 | N 33 E, 87 E | 1479 | N 38 E, 69 E | 1538 | N 50 E, 65 E |
| 1382 | N 38 E, 69 E | 1423 | N 34 E, 83 E | 1480 | N 37 E, 61 E | 1539 | N 47 E, 35 E |
| 1383 | N 25 E, 70 E | 1424 | N 27 E, 75 E | 1481 | N 24 E, 81 E | 1540 | N 44 E, 62 E |
| 1384 | N 35 E, 80 E | 1425 | N 21 E, 87 E | 1483 | N 36 E, 76 E | 1541 | N 42 E, 67 E |
| 1385 | N 53 E, 71 E | 1426 | N 13 E, 76 E | 1484 | N 40 E, 75 E | 1542 | N 55 E, 72 E |
| 1386 | N 23 E, 84 E | 1428 | N 30 E, 65 E | 1485 | N 41 E, 90 E | 1543 | N 38 E, 50 E |
| 1387 | N 39 E, 70 E | 1429 | N 39 E, 74 E | 1486 | N 48 E, 77 E | 1544 | N 62 E, 60 E |
| 1388 | N 33 E, 84 E | 1430 | S 10 W, 82 W | 1488 | N 36 E, 61 E | 1545 | N 61 E, 86 E |
| 1389 | N 34 E, 78 E | 1431 | N 31 E, 79 E | 1489 | N 50 E, 52 E | 1548 | N 59 E, 31 E |
| 1390 | S 51 W, 80 W | 1432 | N 14 E, 82 E | 1490 | N 52 E, 61 E | 1549 | N 55 E, 52 E |
| 1391 | N 34 E, 83 E | 1434 | N 17 E, 82 E | 1492 | N 21 E, 82 E | 1550 | N 56 E, 41 E |
| 1392 | N 37 E, 68 E | 1435 | N 43 E, 79 E | 1493 | N 55 E, 52 E | 1551 | N 48 E, 61 E |
| 1393 | N 34 E, 53 E | 1436 | N 42 E, 75 E | 1494 | N 37 E, 82 E | 1552 | N 34 E, 61 E |
| 1394 | N 40 E, 74 E | 1437 | N 34 E, 76 E | 1495 | N 36 E, 80 E | 1553 | N 80 E, 30 E |
| RDH 8/2/90 | N 46 E, 72 E | 1438 | N 42 E, 70 E | 1496 | N 47 E, 66 E | 1554 | N 34 E, 69 E |
| " | N 49 E, 79 E | 1439 | N 24 E, 76 E | 1497 | N 36 E, 59 E | 1555 | N 54 E, 47 E |
| " | N 33 E, 86 E | 1440 | N 47 E, 67 E | 1498 | S 35 W, 76 W | 1557 | N 75 E, 38 E |
| " | N 46 E, 81 E | 1441 | N 14 E, 53 E | 1499 | N 34 E, 87 E | 1559 | S 20 E, 57 W |

Appendix 2A, continued

| SAVALEN AREA | | SAVALEN AREA | | SAVALEN AREA | | SAVALEN AREA | |
|---|---|---|---|---|---|---|---|
| STATION # | FOLIATION | STATION # | FOLIATION | STATION # | FOLIATION | STATION # | FOLIATION |
| 1560 | N 52 E, 70 E | 1619 | N 38 E, 73 E | 1793 | S 23 W, 80 W | 1977 | N 46 E, 57 E |
| 1562 | N 45 E, 34 E | 1620 | N 13 E, 56 E | 1794 | N 47 E, 37 E | 1979 | N 29 E, 61 E |
| 1563 | N 44 E, 72 E | 1677 | S 41 W, 78 W | 1795 | S 17 W, 68 W | 1980 | N 36 E, 76 E |
| 1565 | N 44 E, 18 E | 1678 | S 35 W, 74 W | 1796 | S 15 W, 76 W | 1982 | N 31 E, 71 E |
| 1566 | N 54 E, 34 E | 1679 | S 27 W, 68 W | 1797 | S 8 W, 65 W | 1984 | N 29 E, 78 E |
| 1567 | N 58 E, 76 E | 1680 | S 36 W, 87 W | 1798 | S 23 W, 80 W | | |
| 1568 | N 42 E, 35 E | 1681 | S 23 W, 73 W | 1799 | N 35 E, 72 E | | |
| 1569 | N 28 E, 48 E | 1682 | S 29 W, 56 W | 1800 | N 16 E, 78 E | | |
| 1570 | N 51 E, 42 E | 1683 | S 35 W, 75 W | 1801 | N 21 E, 56 E | | |
| 1572 | N 25 E, 57 E | 1684 | N 28 E, 80 E | 1802 | N 26 E, 47 E | | |
| 1574 | N 31 E, 62 E | 1685 | N 54 E, 83 E | 1803 | N 24 E, 49 E | | |
| 1576 | N 53 E, 50 E | 1687 | S .0 E, 68 W | 1804 | N 31 E, 55 E | | |
| 1576 | N 24 E, 41 E | 1688 | N 18 E, 83 E | 1806 | N 27 E, 80 E | | |
| 1577 | N 60 E, 71 E | 1689 | S 21 W, 64 W | 1808 | S 23 W, 76 W | | |
| 1579 | N 29 E, 62 E | 1690 | S 20 W, 80 W | 1809 | S 29 W, 84 W | | |
| 1580 | N 55 E, 35 E | 1691 | S 24 W, 64 W | 1810 | N 23 E, 76 E | | |
| 1581 | N 25 E, 65 E | 1692 | S 10 W, 82 W | 1824 | S 18 W, 84 W | | |
| 1582 | N 39 E, 87 E | 1693 | S 24 W, 62 W | 1825 | N 19 E, 79 E | | |
| 1583 | N 41 E, 78 E | 1694 | S 23 W, 64 W | 1826 | S 11 W, 88 W | | |
| 1584 | N 41 E, 74 E | 1759 | N 38 E, 77 E | 1827 | N 23 E, 76 E | | |
| 1585 | N 45 E, 74 E | 1760 | S 42 W, 85 W | 1828 | N 25 E, 75 E | | |
| 1586 | N 46 E, 82 E | 1761 | S 35 W, 85 W | 1830 | S 15 W, 80 W | | |
| 1588 | N 42 E, 90 E | 1762 | S 6 W, 57 W | 1831 | S 27 W, 87 W | | |
| 1589 | N 26 E, 89 E | 1763 | S 22 W, 74 W | 1832 | S 27 W, 81 W | | |
| 1590 | N 38 E, 77 E | 1764 | S 25 W, 63 W | 1833 | S 21 W, 78 W | | |
| 1592 | N 40 E, 55 E | 1765 | S 12 W, 84 W | 1834 | N 19 E, 78 E | | |
| 1593 | N 23 E, 76 E | 1766 | S 34 W, 89 W | 1835 | N 11 E, 74 E | | |
| 1594 | N 34 E, 89 E | 1767 | S 29 W, 82 W | 1836 | N 31 E, 72 E | | |
| 1595 | S 2 W, 74 W | 1769 | N 35 E, 89 E | 1837 | N 28 E, 86 E | | |
| 1596 | N 44 E, 82 E | 1771 | N 35 E, 85 E | 1838 | N 17 E, 89 E | | |
| 1597 | N 30 E, 88 E | 1772 | S 38 W, 59 W | 1839 | N 25 E, 69 E | | |
| 1598 | S 15 W, 60 W | 1773 | S 32 W, 69 W | 1841 | N 40 E, 62 E | | |
| 1598 | N 29 E, 66 E | 1774 | S 30 W, 65 W | 1842 | N 46 E, 84 E | | |
| 1598 | N 32 E, 63 E | 1775 | N 29 E, 87 E | 1843 | N 31 E, 78 E | | |
| 1598 | N 41 E, 82 E | 1777 | N 27 E, 76 E | 1847 | N 27 E, 76 E | | |
| 1601 | N 42 E, 75 E | 1778 | S 36 W, 83 W | 1849 | S 20 W, 87 W | | |
| 1602 | S 53 W, 77 W | 1779 | S 28 W, 85 W | 1851 | S 24 W, 85 W | | |
| 1603 | S 63 W, 85 W | 1780 | N 20 E, 86 E | 1853 | S 15 W, 83 W | | |
| 1604 | S 52 W, 73 W | 1781 | N 29 E, 90 E | 1855 | N 38 E, 78 E | | |
| 1605 | S 67 W, 88 W | 1782 | N 25 E, 87 E | 1857 | S 35 W, 84 W | | |
| 1606 | S 37 W, 65 W | 1783 | N 28 E, 85 E | 1863 | S 20 W, 86 W | | |
| 1608 | N 15 E, 43 E | 1784 | N 27 E, 86 E | 1956 | S 16 W, 50 W | | |
| 1609 | N 32 E, 71 E | 1786 | S 32 W, 84 W | 1958 | S 10 W, 35 W | | |
| 1610 | N 27 E, 80 E | 1787 | S 24 W, 72 W | 1964 | S 35 W, 84 W | | |
| 1611 | N 11 E, 73 E | 1788 | S 25 W, 87 W | 1965 | S 26 W, 80 W | | |
| 1612 | S 4 W, 75 W | 1789 | N 28 E, 70 E | 1967 | S 18 W, 84 W | | |
| 1614 | N 27 E, 81 E | 1790 | S 28 W, 79 W | 1969 | S 30 W, 78 W | | |
| 1615 | N 36 E, 77 E | 1791 | S 29 W, 85 W | 1973 | S 34 W, 79 W | | |
| 1616 | S 21 W, 81 W | 1792 | S 24 W, 80 W | 1975 | S 27 W, 55 W | | |

Appendix 2A, continued

| DOME AREA | | DOME AREA | | DOME AREA | | DOME AREA | |
|---|---|---|---|---|---|---|---|
| STATION # | FOLIATION | STATION # | FOLIATION | STATION # | FOLIATION | STATION # | FOLIATION |
| 377 | N 62 W, 73 E | 521 | N 38 E, 45 E | 570 | N 41 E, 68 E | 623 | N 42 E, 50 E |
| 378 | N 70 W, 87 E | 522 | N 32 E, 47 E | 571 | N 62 E, 60 E | 624 | N 77 E, 42 E |
| 379 | N 34 W, 74 E | 523 | N 47 E, 66 E | 572 | N 43 E, 40 E | 625 | N 56 E, 52 E |
| 380 | N 7 W, 85 E | 524 | N 54 E, 51 E | 573 | N 64 E, 49 E | 626 | N 67 E, 49 E |
| 381 | N 15 W, 88 E | 525 | N 50 E, 77 E | 574 | N 58 E, 65 E | 627 | N 59 E, 57 E |
| 382 | N 43 W, 84 E | 526 | N 42 E, 64 E | 575 | N 85 E, 70 E | 628 | N 53 E, 59 E |
| 383 | N 17 W, 87 E | 527 | N 42 E, 62 E | 576 | N 58 E, 42 E | 630 | N 72 E, 62 E |
| 384 | N 2 W, 75 E | 528 | N 65 E, 35 E | 577 | N 44 E, 44 E | 631 | N 73 E, 44 E |
| 385 | S 12 W, 84 W | 529 | N 46 E, 46 E | 578 | N 82 E, 68 E | 632 | N 52 E, 44 E |
| 386 | S 15 E, 64 W | 530 | S 37 E, 32 W | 579 | S 52 W, 55 W | 633 | S 17 E, 4 W |
| 387 | S 7 E, 69 W | 531 | N 45 E, 53 E | 580 | S 44 W, 43 W | 636 | N 40 E, 43 E |
| 388 | S 20 W, 70 W | 532 | N 63 E, 57 E | 581 | S 52 W, 66 W | 637 | N 40 E, 85 E |
| 389 | N 7 E, 85 E | 533 | N 22 E, 66 E | 582 | N 27 E, 14 E | 642 | S 11 W, 14 W |
| 390 | N 14 W, 84 E | 534 | N 83 E, 50 E | 583 | N 32 E, 17 E | 642 | N 42 E, 55 E |
| 391 | S 2 E, 89 W | 535 | N 26 E, 54 E | 584 | N 18 E, 51 E | 643 | N 25 E, 56 E |
| 392 | S 22 W, 90 W | 536 | N 34 E, 70 E | 585 | N 47 E, 46 E | 644 | N 27 E, 43 E |
| 393 | S 10 W, 85 W | 537 | N 40 E, 69 E | 587 | N 69 E, 27 E | 645 | N 42 W, 22 E |
| 394 | N 2 E, 77 E | 538 | N 35 E, 64 E | 588 | N 33 E, 64 E | 646 | N 23 W, 24 E |
| 395 | N 7 E, 81 E | 539 | N 59 E, 51 E | 589 | N 28 E, 42 E | 647 | S 10 E, 15 W |
| 396 | N 3 W, 75 E | 540 | N 52 E, 57 E | 590 | N 40 E, 59 E | 648 | S 25 W, 37 W |
| 397 | N 6 W, 74 E | 541 | N 75 W, 36 E | 592 | S 60 W, 75 W | 649 | S 42 W, 30 W |
| 398 | N 1 W, 86 E | 542 | N 40 E, 46 E | 594 | N 20 E, 17 E | 650 | S 40 W, 35 W |
| 399 | N 10 E, 73 E | 543 | N 34 E, 53 E | 595 | N 60 E, 47 E | 651 | S 55 W, 21 W |
| 400 | N 7 E, 72 E | 544 | N 42 E, 48 E | 596 | S 37 W, 80 W | 652 | N 15 W, 34 E |
| 401 | N 10 E, 86 E | 545 | N 82 E, 45 E | 597 | N 84 E, 29 E | 654 | N 38 E, 60 E |
| 402 | N 22 E, 90 E | 546 | N 62 E, 48 E | 599 | N 85 E, 43 E | 697 | S 26 W, 43 W |
| 403 | N 10 E, 84 E | 547 | N 56 E, 72 E | 600 | N 39 E, 50 E | 697 | S 7 W, 47 W |
| 404 | N 22 E, 73 E | 548 | N 19 E, 69 E | 601 | N 43 E, 31 E | 698 | S 28 W, 54 W |
| 405 | N 2 W, 82 E | 549 | N 64 E, 53 E | 602 | N 50 E, 21 E | 699 | S 61 W, 52 W |
| 406 | N 5 E, 76 E | 550 | S 30 W, 70 W | 603 | N 16 E, 29 E | 700 | S 26 E, 70 W |
| 408 | N 14 E, 72 E | 551 | N 67 E, 47 E | 604 | N 38 E, 37 E | 701 | S 7 E, 45 W |
| 409 | N 17 E, 80 E | 552 | N 16 E, 77 E | 605 | N 15 E, 62 E | 702 | S 7 E, 59 W |
| 410 | N 7 E, 87 E | 553 | N 44 E, 49 E | 606 | N 50 E, 44 E | 703 | S 22 W, 26 W |
| 411 | N 12 W, 89 E | 554 | N 58 E, 64 E | 607 | N 20 E, 44 E | 704 | S 12 E, 56 W |
| 508 | N 12 E, 67 E | 555 | N 48 E, 59 E | 608 | N 38 E, 73 E | 705 | S 19 W, 60 W |
| 508 | N 35 W, 53 E | 556 | N 68 E, 38 E | 609 | N 26 E, 56 E | 706 | S 39 W, 69 W |
| 509 | N 60 E, 47 E | 557 | N 49 E, 66 E | 610 | N 13 E, 73 E | 707 | S 12 W, 49 W |
| 510 | N 67 E, 39 E | 558 | N 68 E, 49 E | 611 | N 40 E, 52 E | 708 | S 20 E, 44 W |
| 511 | N 2 E, 70 E | 559 | N 63 E, 42 E | 612 | N 12 E, 42 E | 709 | N 2 E, 21 E |
| 511 | N 15 E, 46 E | 560 | N 62 E, 52 E | 613 | N 24 E, 53 E | 710 | N 23 E, 48 E |
| 512 | N 22 E, 40 E | 561 | N 50 E, 55 E | 614 | N 29 E, 46 E | 711 | N 49 E, 56 E |
| 513 | N 70 E, 69 E | 562 | N 44 E, 65 E | 615 | N 41 E, 59 E | 712 | S 78 W, 38 W |
| 514 | N 80 E, 42 E | 563 | N 52 E, 66 E | 616 | N 33 E, 54 E | 713 | S 42 E, 43 W |
| 515 | N 40 E, 86 E | 564 | N 57 E, 58 E | 617 | N 42 E, 53 E | 714 | N 82 W, 15 E |
| 516 | N 72 E, 47 E | 565 | N 44 E, 40 E | 618 | N 49 E, 42 E | 747 | N 72 E, 78 E |
| 517 | N 48 E, 58 E | 566 | N 65 E, 73 E | 619 | N 54 E, 64 E | 748 | N 86 E, 87 E |
| 518 | N 36 E, 63 E | 567 | N 70 E, 40 E | 620 | N 48 E, 61 E | 750 | S 42 W, 53 W |
| 519 | N 26 E, 62 E | 568 | N 57 E, 82 E | 621 | N 22 E, 66 E | 751 | S 17 W, 45 W |
| 520 | N 42 E, 42 E | 569 | N 70 E, 56 E | 622 | N 40 E, 46 E | 752 | S 33 W, 67 W |

## Appendix 2B: Fold Measurements

| STATION # | AXIAL PLANE | AXIS | FOLD TYPE |
|---|---|---|---|
| 2 | N17E, 49SE | 39°, S66E | TIGHT |
| 14 | N64E, 85SE | 55°, N59E | ISO |
| 14 | N30E, 80NW | 54°, S58W | ISO |
| 16 | N47E, 76SE | 69°, S52E | TIGHT |
| 16 | N60E, 61SE | 52°, S49W | ASYM, S |
| 35 | N18E, 75NW | 24°, S9W | CREN |
| 35 | N65W, 30SW | 22°,S62W | ISO |
| 36 | N54W, 74SW | 30°, N76W | UPRIGHT |
| 37 | N60E, 80SE | 40°, S58W | OPEN (upright) |
| 38 | N80E, 12SE (?) | 28°, S50E | ASYM, Z |
| 41 | N44W, 19SW | 25°, S45W | ISO |
| 41 | N80E, 30SE | 34°, S16W | ASYM, Z |
| 41 | N41E, 82NW | | TIGHT |
| 41 | N45E, 62SE | 8°, N35W | TIGHT |
| 42 | | 68°, N30W | OPEN |
| 46 | N18E, 72NW | 40°, N20E | ASYM, Z |
| 46 | N10E, 60NW | 40°, N4W | ASYM, Z |
| 52 | N5W, 63SW | 47°, S15W | TIGHT |
| 53 | N32E, 58NW | 40°, N21W | TIGHT |
| 58 | N10W, 56SW | 51°, N20W | ASYM, Z |
| 59 | N38E, 64SE | 32°, N34E | ASYM, Z |
| 72 | | 25°, N20E | CREN |
| 77 | N64E, 44NW | 24°, S68W | ASYM, Z |
| 82 | N42E, 69NW | 57°, N24E | TIGHT |
| 82 | N50E, 76NW | 41°, S70W | TIGHT |
| 82 | N20E, 49 NW | 44°, N81W | ISO |
| 82 | N42E, 68NW | 56°, S81W | TIGHT |
| 82 | N73E, 72NW | 42°, N28E | TIGHT |
| 82 | N30E, 60NW | 46°, N77W | TIGHT |
| 82 | N65E, 52NW | 36°, S73W | TIGHT |
| 86 | N10W, 70SW | 46°, S20W | TIGHT |
| 87 | N43E, 85SE | 48°, S25W | TIGHT |
| 97 | N5W, 80SW | 34°, N2E | KINK |
| 104 | N10W, 56NE | 40°, N10E | KINK |
| 110 | N5W, 30NE | 17°, N40E | KINK |
| 112 | N18E, 72NW | 55°, S75W | CRE |
| 112 | N65E, 57NW | 20°, N78W | OPEN |
| 116 | N50W, 45SW | 49°, S35W | CREN |
| 119 | N28E, 61NW | 50°, N30W | ISO |
| 119 | N83E, 84SE | 45°, S70W | ASYM |
| 120 | N35E, 45NW | 45°, N85W | CREN |
| 138 | N52W, 83SW | 50°, S35W | ASYM |
| 147 | N18E, 59NW | 24°, S45W | ASYM |
| 149 | | 12°, S40W | OPEN |
| 152 | N47E, 70NW | 22°, S51W | ASYM |
| 154 | N30E, 87SE | 18°, S20W | OPEN |
| 155 | N29E, 85SE | 7°, S32W | CREN |
| 174 | N10E, 69NW | 29°, N10E | ISO |
| 201 | N50E, 72SW | 62°, N50E | KINK |
| 221 | N50W, 67SW | 13°, W | OPEN |

| STATION # | AXIAL PLANE | AXIS | FOLD TYPE |
|---|---|---|---|
| 1040 | | 25°, S55W | CREN |
| 1042 | N18W, 41SE | 8°, S33W | OPEN |
| 1045 | N82W, 75NE | 75, S62W | OPEN |
| 1053 | | 52°, S75W | CREN |
| 1102 | | 38°, S52W | CREN |
| 1104 | N68E, 76NW | 45°, S58W | OPEN |
| 1108 | | 36°, S62W | CREN |
| 1110 | | 14°, S75W | CREN |
| 1113 | | 48°, S58W | CREN |
| 1114 | N18E, 87NW | 53°, S23W | OPEN |
| 1116 | N62E, 75NW | 12°, S51W | KINK |
| 1106 | N52E, 27NW | 17°, N62W | ASYM, S |
| 1132 | N59W, 45SW | 35°, S64W | ASYM, S |
| 1133 | | 45°, S65W | CREN |
| 1141 | N68W, 62NE | 40°, S82W | ASYM, Z |
| 1228 | N34W, 69SW | 32°, N79W | TIGHT |
| 1228 | | 69°, S52W | CREN |
| 1229 | | 52°, S19W | CREN |
| 1231 | N50W, 40SW | 7°, S45E | OPEN |
| 1245 | | 10°, N38E | CREN |
| 1248 | | 34°, S20W | CREN |
| 1249 | | 32°, S86W | CREN |
| 1251 | | 34°, N8E | CREN |
| 1252 | | 7°, N52E | CREN |
| 1252 | | 4°, S50W | TIGHT |
| 1260 | | 12°, N56E | CREN |
| 1262 | | 25°, N41E | ASYM, Z |
| 1282 | N79E, 76SE | 10°, S70W | TIGHT |
| 1286 | | 12°, N46E | TIGHT |
| 1300 | | 9°, S58W | CREN |
| 1312 | | 33°, N18E | CREN |
| 1313 | N20E, 80SE | 50°, S | ASYM, Z |
| 1313 | N52E, 80SE | 30°, N42E | TIGHT |
| 1323 | N72E, 74NW | 24°, N63E | TIGHT |
| 1324 | | 14°, S30W | CREN |
| 1326 | N83E, 68NW | 42°, N45E | ASYM, Z |
| 1334 | | 7°, S41W | CREN |
| 1349 | N86E, 67NW | 48°, S74W | ASYM, Z |
| 1366 | N54E, 69SE | 24°, S44W | TIGHT |
| 1627 | N74E, 85SE | 13°, S82W | ASYM, Z |
| 1630 | | 24°, S24W | CREN |
| 1634 | | 14°, S71W | CREN |
| 1634 | N74E, 74SE | 67°, S74W | TIGHT |
| 1635 | N22E, 80SE | 53°, S7E | TIGHT |
| 1635 | | 32°, S38W | CREN |
| 1645 | | 47°, S37E | CREN |
| 1659 | | 49°, S34W | CREN |
| 1674 | N42E, 85SE | 80°, S60W | TIGHT |
| 1703 | | 41°, S56W | CREN |
| 1706 | N56E, 77SE | 71°, S55W | TIGHT |

Appendix 2B, continued

| | | | | | | | |
|---|---|---|---|---|---|---|---|
| 222 | N87E, 57NW | 78°, N42E | TIGHT | 1709 | N44W, 80SW | 39°, S | KINK |
| 225 | N70E, 34NW | 22°, N82W | ISO | 1709 | | 67°, S26E | CREN |
| 225 | N28E, 85SE | 32°, N28E | CREN | 1731 | | 17°, S48W | CREN |
| 226 | N37E, 21NW | 5°, S70W | ISO | 1739 | | 34°, S30W | CREN |
| 231 | N32E, 59SE | 57°, S32E | CHEVRON | 1904 | N86W, 34SW | 5°, S56E | ISO |
| 232 | | 19°, N52E | CHEVRON | 1906 | | 8°, S4W | ASYM |
| 240 | N45W, 89SW | 60°, N40W | KINK | 1908 | | 44°, S31E | CREN |
| 242 | N85E, 84NW | 55°, S70W | KINK | 1909 | | 49°, S30W | OPEN |
| 257 | N7W, 90° | 56°, N14W | KINK | 1910 | | 32°, S28W | CREN |
| 263 | N75W, 14SW | 16°, S48W | CREN | 1913 | | 35°, S61W | CREN |
| 287 | N64E, 82NW | 65°, N87E | OPEN | 1941 | N48E, 72NW | 25°, N47E | TIGHT |
| 290 | N10W, 36NE | 39°, S52E | TIGHT | 1945 | | 42°, N20E | CREN |
| 291 | N73W, 61NE | 9°, N85W | TIGHT | 1947 | N42E, 75SE | 25°, N49E | TIGHT |
| 295 | N72E, 57SE | 26°, S89W | ASYM, Z | 1952 | | 58°, S68W | ASYM, S |
| 295 | N68E, 85SE | 12°, S58W | AYM, Z | 1990 | N76E, 67NW | 24°, S43W | TIGHT |
| 295 | N1E, 21NW | 20°, S73W | TIGHT | 1994 | | 30°, N40E | CREN |
| 296 | N80E, 63NW | 36°, DUE W | CREN | 1994 | | 15°, N53E | TIGHT |
| 309 | N49W, 74NE | 6°, S50E | | 2006 | N20E, 75NW | 28°, N26E | OPEN |
| 309 | N36W, 83SW | 11°, S28E | | 2007 | | 3°, N10W | CREN |
| 316 | N29E, 12SSE | 3°, S15E | TIGHT | 2011 | | 19°, N51E | CREN |
| 316 | N53W, 70NE | 9°, S35E | | 2020 | | 15°, S7E | CHEVRON |
| 350 | N39E, 64SE | 4°, S7W | TIGHT | 2065 | N3E, 36SE | 23°, N30E | TIGHT |
| 352 | N25E, 75SE | 56°, S6W | TIGHT | 2074 | N33E, 80SE | 54°, N33E | ASYM, S |
| 372 | N7W, 50NE | 42°, N25E | | 2074 | N25E, 72SE | 41°, N31E | ASYM, S |
| 375 | N78E, 79NE | 47°, N82W | ISO | 2078 | | 44°, N25E | CREN |
| 382 | N71W, 69NE | 45°, S71E | ISO | 2104 | N36°E, 77NW | 56°, S48W | TIGHT |
| 382 | N79E, 83NW | 90°, S31W | TIGHT | 2131 | N11E, 56NW | 37°, N80W | TIGHT |
| 382 | N4W, 75NE | 52°, N14W | OPEN | 2140 | N25E, 81NW | 55°, S25W | TIGHT |
| 411 | N63E, 82SE | 81°, N78E | ASYM | 2190 | N12E, 77NW | 10°, N | TIGHT |
| 428 | N52E, 68SE | 45°, S11E | TIGHT | 2191 | | 7°, S40W | CREN |
| 456 | N29E, 87SE | 59°, S22W | ASYM, S | 2193 | N16E, 84SE | 60°, S14W | ISO |
| 462 | N16E, 87SE | 55°, N15E | ISO | 2194 | | 50°, N20E | CREN |
| 466 | N27E, 74SE | 35°, S21E | TIGHT | 2211 | | 6°, N27E | CREN |
| 472 | N37E, 84SE | 47°, S38W | KINK | 1181 | | 52°, S80W | CREN |
| 476 | 90°, N49E | 32°, S40W | OPEN | 1183 | N65E, 81NW | 19°, S67W | TIGHT |
| 501 | N18E, 77NW | 3°, S37W | TIGHT | 1183 | N22E, 75NW | 27°, S35W | TIGHT |
| 503 | N57E, 79NW | 28°, S55W | OPEN | 1185 | N75E, 74SE | 26°, N58E | TIGHT |
| 503 | N48E, 71NW | 27°, S50W | OPEN | 1189 | | 30°, S84E | CREN |
| 515 | N7E, 86SE | 52°, S7W | CREN | 1190 | N85W, 25SW | 3°, N85W | KINK |
| 519 | N5E, 74SE | 56°, S7W | CREN | 1196 | N81E, 75NW | 48°, S75W | OPEN |
| 520 | N61E, 55SE | 26°, N84E | TIGHT | 1196 | | 59°, N82W | CREN |
| 527 | N45E, 80SE | 5°, N47E | TIGHT | 1386 | | 9°, S45E | CREN |
| 536 | N63E,70SE | 33°, S32W | ASYM, S | 1396 | | 18°, S35W | CREN |
| 561 | N32E, 59SE | 53°, N50E | | 1426 | N14W, 70NE | 17°, S29E | TIGHT |
| 584 | N44E, 58SE | 54°, S81E | ASYM, S | 1433 | N30E, 85NW | 15°, S28W | TIGHT |
| 584 | N80W, 83NE | 41°, N82E | OPEN | 1442 | | 58°, S5E | KINK |
| 584 | N60E, 31SE | 30°, S3E | TIGHT | 1451 | | 10°, S37W | CREN |
| 584 | N35E, 34SE | 19°, S47E | TIGHT | 1465 | | 20°, S50W | CREN |
| 584 | N74W, 67NE | 15°, S74E | KINK | 1482 | N12W, 70SW | 32°, S7W | ASYM, S |
| 598 | N60E, 63SE | 27°, N60E | TIGHT | 1487 | N17E, 14NW | 12°, S68W | KINK |
| 611 | N27E, 44SE | 49°, S80E | ASYM, S | 1490 | N2E, 72NW | 43°, S7E | KINK |
| 619 | N33E, 48SE | 53°, S51E | ASYM, Z | 1523 | N2E, 50NW | 22°, S20W | TIGHT |

Appendix 2B, continued

| | | | |
|---|---|---|---|
| 620 | N59E, 51SE | 44°, S51E | ASYM, Z |
| 622 | N46E, 55SE | 43°, S80W | ISO |
| 646 | N85W, 29NE | 19°, N48E | ISO |
| 646 | N64W, 15NE | 10°, N78E | ISO |
| 647 | N32E, 38SE | 24°, N85W | CHEVRON |
| 648 | N6E, 50NW | 21°, S21W | ISO |
| 651 | N45E, 78SE | 16°, N20E | TIGHT |
| 651 | N20E, 76NW | 6°, N29E | ASYM |
| 651 | N18E, 68NW | 16°, N18E | TIGHT |
| 662 | N33E, 84NW | 51°, N26E | CREN |
| 662 | N37E, 74NW | 45°, N24E | ISO |
| 706 | N35E, 65NW | 51°, S72W | TIGHT |
| 706 | N34E, 75SE | 47°, S27W | OPEN |
| 706 | N37E, 76NW | 40°, N37E | KINK |
| 706 | N8E, 63NW | 44°, N87W | TIGHT |
| 718 | N68W, 78SW | 59°, N70W | OPEN |
| 719 | N62W, 70NE | 48°, N60W | TIGHT |
| 726 | N83W, 90° | 77°, N80E | KINK |
| 734 | N42W, 73SW | 53°, S32E | KINK |
| 737 | N66W, 54SW | 14°, S84W | OPEN |
| 737 | N54W, 51SW | 42°, S76W | OPEN |
| 744 | N24W, 52SW | | ISO |
| 752 | N75E, 60SE | 29°, S82W | OPEN |
| 752 | N66E, 88NW | 38°, S74W | ASYM, S |
| 765 | N65E, 87SE | 36°, S55W | OPEN |
| 806 | N36E, 86NW | 45°, N30E | TIGHT |
| 825 | N39E, 87SE | 65°, N20E | TIGHT |
| 837 | N8E, 71NW | 2°, S5W | OPEN |
| 840 | | 42°, S18W | ASYM, Z |
| 842 | N61W, 60SW | 61°, N65W | TIGHT |
| 843 | N66E, 44SE | 30°, S55W | KINK |
| 843 | N68E, 40SE | 21°, S35W | ASYM, S |
| 844 | N54E, 46SE | 39°, S24W | ASYM, S |
| 844 | N56E, 86SE | 61°, S38W | ISO |
| 845 | N21W, 84NE | 25°, N8E | KINK |
| 850 | N87E, 44SE | 18°, DUE W | KINK |
| 869 | N30E, 78NW | 42°, S40W | ISO |
| 884 | N28E, 24NE | 26°, N15E | KINK |
| 890 | N28E, 85SE | 65°, S36W | TIGHT |
| 895 | N21E, 70SE | | TIGHT |
| 895 | N32E, 73SE | 40°, S20W | TIGHT |
| 909 | N47E, 53SE | 55°, S36W | ISO |
| 910 | N15W, 6NW | 60°, N15E | KINK |
| 916 | N2E, 77NW | 41°, S18W | OPEN |
| 929 | N80E, 47SE | | TIGHT |
| 932 | N62W, 66SW | 36°, S52E | OPEN |
| 939 | N44E, 56SE | 43°, S60W | ASYM, S |
| 940 | N67E, 60SE | | OPEN |
| 993 | | 48°, S84W | CREN |
| 995 | N80E, 84SE | 39°, S65W | ASYM, S |
| 1530 | | 32°, S6W | TIGHT |
| 1532 | | 10°, S20W | OPEN |
| 1535 | N22E, 66NW | 37°, S40W | TIGHT |
| 1539 | | 9°, S9W | CREN |
| 1543 | N73E, 45SE | 14°, N80E | ISO |
| 1543 | N62E, 41SE | 34°, S53E | ASYM, S |
| 1547 | | 47°, S32W | TIGHT |
| 1572 | | 6°, S46W | CREN |
| 1576 | N84W, 30SW | 32°, S15W | TIGHT |
| 1578 | N48E, 50SW | 28°, S20E | KINK |
| 1578 | | 25°, S42W | CREN |
| 1579 | N75E, 32SE | 32°, S40E | TIGHT |
| 1582 | N51E, 82SE | 35°, N51E | TIGHT |
| 1584 | | 33°, S30W | CREN |
| 1593 | N40E, 40SE | 62°, S10W | TIGHT |
| 1598 | N46E, 80SE | 34°, S39W | TIGHT |
| 1599 | N36E, 85SE | 31°, S30W | TIGHT |
| 1613 | | 18°, S18W | CREN |
| 1617 | N27W, 50SW | 35°, S25E | KINK |
| 1869 | | 11°, S16W | CREN |
| 2034 | | 20°, S15W | CREN |
| 2083 | N31E, 70SE | 50°, S22W | TIGHT |
| 2092 | N49E, 82SE | 19°, N37E | OPEN |
| 2098 | | 44°, N30E | CREN |
| 2100 | | 64°, S67E | CREN |
| 2165 | N38E, 90° | 62°, N30E | ISO |
| 2214 | N45E, 80NW | 70°, S40W | CHEVRON |
| 2227 | | 32°, S20W | CREN |
| 2233 | | 34°, S38W | CREN |
| 995 | N71E, 80NW | 41°, S76W | ASYM, S |
| 996 | | 41°, S71W | ASYM, S |
| 997 | N60E, 68NW | 40°, S63W | OPEN |
| 1000 | | 5°, S50W | ISO |
| 1003 | | 24°, S57W | CREN |
| 1020 | | 25°, N73W | CREN |
| 1032 | N10W, 49SW | 20°, S36W | ISO |
| 1037 | | 20°, S82W | OPEN |
| 1038 | N51W, 8SW | 27°, N67W | TIGHT |

## Appendix 2C: Lineation Measurements

| STATION # | ORIENTATION | LINEATION TYPE |
|---|---|---|
| 6 | 30, S39E | INTERSECTION |
| 10 | 17, S24W | INTERSECTION |
| 12 | 62, S60E | INTERSECTION |
| 36 | 37, S70W | INTERSECTION |
| 37 | 37, S70W | INTERSECTION |
| 52 | 5, N24E | INTERSECTION |
| 76 | 34, W | INTERSECTION |
| 112 | 42, S70W | INTERSECTION |
| 120 | 30, S55W | MINERAL |
| 130 | 22, S72W | MINERAL |
| 132 | 19, S15W | MINERAL |
| 138 | 9, S46W | MINERAL |
| 146 | 17, S50W | MINERAL |
| 147 | 21, S56W | MINERAL |
| 149 | 10, S42W | MINERAL |
| 150 | 16, N85W | MINERAL |
| 154 | 15, S48W | MINERAL |
| 155 | 11, S52W | MINERAL |
| 159 | 10, S55W | MINERAL |
| 162 | 24, S72W | MINERAL |
| 163 | 25, S63W | MINERAL |
| 242 | 40, S2W | INTERSECTION |
| 320 | 14, S60E | INTERSECTION |
| 321 | 6, N | INTERSECTION |
| 328 | 2, S20W | MINERAL |
| 329 | 22, N40E | MINERAL |
| 362 | 30, N32E | MINERAL |
| 364 | 38, N22E | MINERAL |
| 608 | 9, S29W | MINERAL |
| 612 | 28, N38E | MINERAL |
| 624 | 10, S55W | MINERAL |
| 652 | 8, S19E | MINERAL |
| 745 | 29, S57W | MINERAL |
| 753 | 35, S85W | MINERAL |
| 776 | 14, S2W | MINERAL |
| 786 | 55, N62E | MINERAL |
| 787 | 50, N65E | MINERAL |
| 803 | 26, N68E | INTERSECTION |
| 818 | 56, S24W | INTERSECTION |
| 819 | 60, S21W | INTERSECTION |
| 840 | 43, S70W | INTERSECTION |
| 863 | 58, S82W | INTERSECTION |
| 876 | 12, S30W | INTERSECTION |
| 880 | 48, S55W | INTERSECTION |
| 907 | 40, S36W | MINERAL |
| 921 | 7, S23W | MINERAL |
| 1037 | 20, S82W | MINERAL |
| 1181 | 52, S80W | MINERAL |
| 1198 | 45, S67W | MINERAL |
| 1199 | 18, N57E | INTERSECTION |
| 1240 | 27, S32W | INTERSECTION |
| 1237 | 40, S34W | MINERAL |
| 1252 | 10, S52W | MINERAL |
| 1271 | 2, S60W | MINERAL |
| 1279 | 5, S72W | MINERAL |
| 1282 | 5, S72W | MINERAL |
| 1287 | 12, S36W | MINERAL |
| 1313 | 30, N42E | MINERAL |
| 1369 | 9, N29E | MINERAL |
| 1407 | 51, S33W | MINERAL |
| 1436 | 52, S14W | MINERAL |
| 1437 | 42, S35W | MINERAL |
| 1480 | 68, S12E | INTERSECTION |
| 1535 | 37, S40W | MINERAL |
| 1563 | 52, S39W | MINERAL |
| 1572 | 45, S40W | INTERSECTION |
| 1582 | 37, N47E | MINERAL |
| 1596 | 33, S30W | MINERAL |
| 1617 | 58, S9W | INTERSECTION |
| 1623 | 3, S35W | MINERAL |
| 1629 | 21, S39W | MINERAL |
| 1678 | 42, S38W | MINERAL |
| 1731 | 38, S12W | INTERSECTION |
| 1796 | 55, S80W | MINERAL |
| 1834 | 10, S35W | MINERAL |
| 1885 | 64, S5W | MINERAL |
| 1957 | 32, S47E | INTERSECTION |
| 1994 | 30, N30E | MINERAL |
| 2002 | 18, N18E | IINTERSECTION |
| 2067 | 10, N32E | MINERAL |
| 2211 | 6, N27E | MINERAL |

# APPENDIX 3
# Mineral Assemblages

# Appendix 3
# Mineral Assemblages

Mineral abbreviations used in following table:

| | |
|---|---|
| act | actinolite |
| an | anorthite |
| ap | apatite |
| bt | biotite |
| cc | calcite |
| chl | chlorite |
| ctd | chloritoid |
| epi | epidote/clinozoisite |
| gt | garnet |
| grap | graphite |
| hbl | hornblende |
| mus | muscovite |
| opq | opaque phase |
| pl | plagioclase |
| qtz | quartz |
| spn | sphene |
| tour | tourmaline |
| zir | zircon |

[ ] denotes accessory phases

Appendix 3, continued

| Unit | Lithology | Mineral Assemblage |
|---|---|---|
| Einunnfjellet quartzite/schist sequence | massive to thick-bedded quartzite | qtz + mus + bt ± pl + [zir + opq] |
| | schistose quartzite | qtz + pl + mus + bt + chl ± gt ± [epi + tour + opq] |
| | feldspathic metasandstone | qtz + pl + mus + bt + [zir + ap + opq] |
| | muscovite schist | mus + qtz + opq + chl + gt + [tour + epi] |
| | garnet-mica schist | qtz + mus + bt + gt + chl ± hbl ± pl ($an_{6-17}$) + [opq + tour + epi] |
| Einunna mafic complex | amphibole schist | qtz + hbl + bt + gt + pl ($an_{7-14}$) + opq + chl + [epi + zir] + cc (late, in veins) |
| | mica-epidote schist | qtz + pl ($an_{6-11}$) + mus + epi + opq + gt + bt + chl |
| Bangardsvola complex | amphibolite | hbl + bt + epi + chl + qtz + pl ($an_{16-22}$) ± cc ± mus + [spn] |
| | keratophyre | qtz + fsp + hbl + bt + chl + [epi + opq] |
| Svartlia schist | garnet-amphibole schist (garbenschiefer) | qtz + pl ($an_{21}$) + bt + mus + hbl + gt + chl ± grap + [tour + epi + opq] |
| Moskardsætra schist | garnet-graphite schist | qtz + grap + mus + bt + gt + chl + [tour + opq] |
| | graphitic quartzite | qtz + mus + grap + bt + chl + gt |
| | feldspathic meta sandstone | qtz + pl + mus + bt + chl + gt ± grap |
| Lomsjødalen complex | greenstone | hbl + act + chl + epi + pl ($an_{0.5-23}$) + qtz + cc + [spn] |
| | phyllite/schist (laminated) | qtz + pl + bt + mus + chl ± gt + [epi + opq] |
| | coticule (occurs as layers in phyllite above) | mn-gt + qtz |
| | chloritoid schist | qtz + pl + mus + bt + ctd + chl + gt + [epi + tour + opq] |
| Volengsvola phyllite | calcareous phyllite (laminated) | qtz + bt + mus + chl + cc ± grap ± gt + [tour + spn + epi] |
| Langåsen quartzite/marble | fuchsite quartzite | qtz + fuchsite + cc + bt + [zir + opq] |
| Savalen upper sequence | conglomerate | matrix: qtz + pl + chl + bt + epi + cc ± gt<br>lithic clast types: greenstone, keratophyre, quartzite, and marble |
| | graphitic phyllite | qtz + grap + chl + mus + bt ± cc + [epi + opq] |

# APPENDIX 4
# XRF Analytical Techniques

# APPENDIX 4
## XRF Analytical Techniques

Instrument: Philips sequential WD-spectrometer, PW 1480, with Sc/W dual anode sidewindow xray tube, and equipped with LIF220, LIF200, GE, PE, PX-1, PX-2 crystals.

Analysts: Bjørn Nilsen and technical staff, Analytical Chemistry Section, Norges Geologiske Undersøkelse, Trondheim, Norway.

Calibrations for major and trace elements based on international standards.

For major elements:

Major elements analyzed on fused disks melted with lithium tetraborate 1:7.
Accelerating voltage (kV) 50
Current (mA) 50
Measuring times:
24 seconds for Fe, Ti, Ca, K, Si, Al
48 seconds for Mn, P, Mg, Na
Measurements are drift-corrected with monitor measurement every sixth sample.

For trace elements:

Trace elements analyzed on pressed pellets.
Accelerating voltage (kV) 85
Current (mA) 30
measuring times:
20 seconds for all except:

| | | | |
|---|---|---|---|
| Sc | 100 | Co | 40 |
| S | 30 | Ce | 100 |
| Cl | 30 | Nd | 60 |
| F | 40 | Sb | 60 |
| Ba | 60 | | |

Note: FeO determined by titration, $H_2O$ using the Courville-Penfield method, and $CO_2$ by the rate of change of gas pressure liberated by adding sulfuric acid to sample in a closed vacuum system.

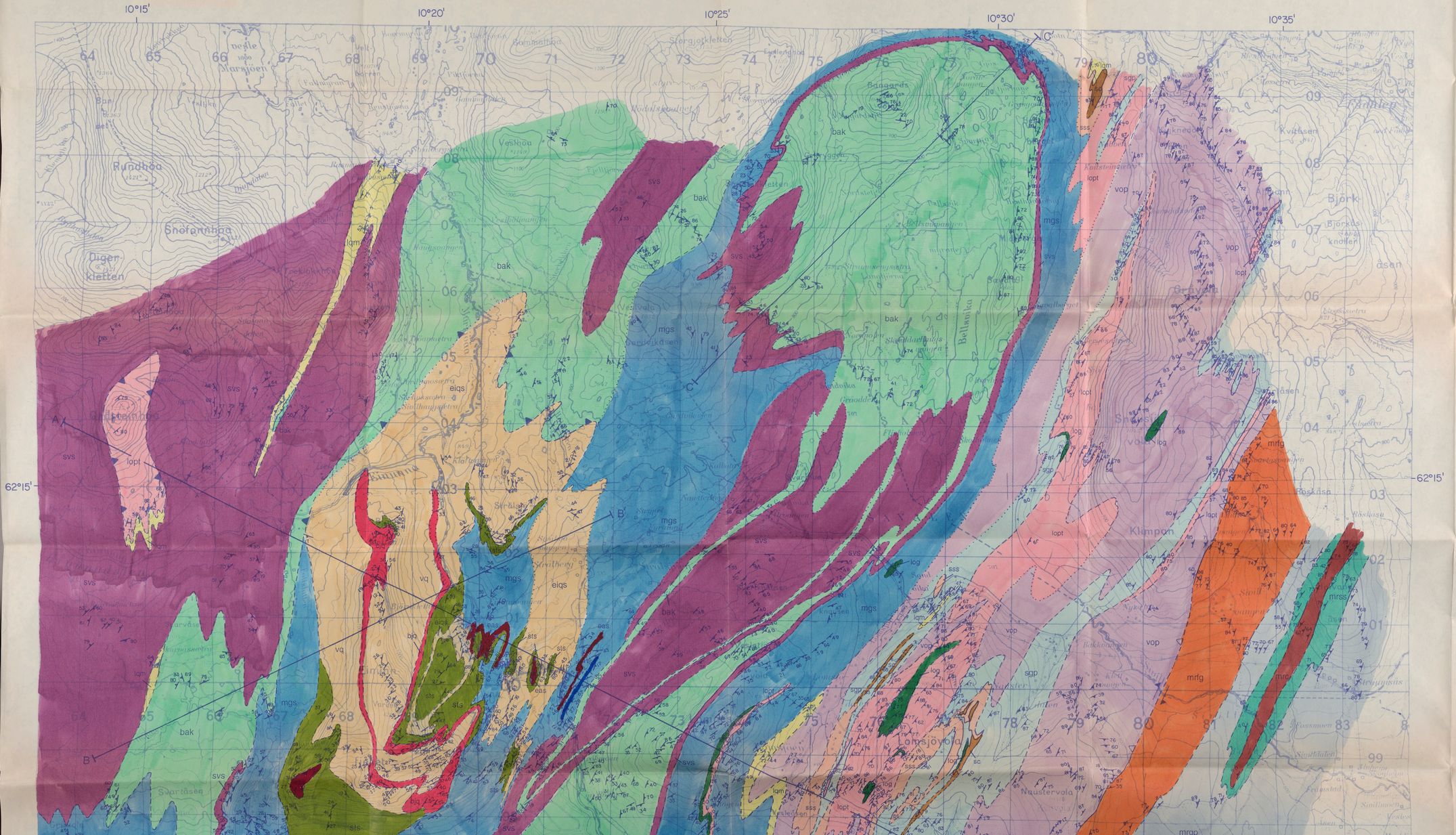
# VITA

Beth McClellan was born in the flatlands of south Georgia and was raised on the Gulf Coast, in Mobile, Alabama. She didn't discover mountains until she was 17 years old, but once she did, she was hooked on them. She began to study geology formally in 1981 at the University of Alabama in Birmingham, where she received a B.S. in 1985. After a year of graduate school at the University of South Carolina, she moved on to the University of Tennessee, Knoxville, where she received her M.S. in 1988. She is presently teaching geology at Western Kentucky University. She plans to continue her pursuit of an academic career, but also hopes to spend more time with her husband, her guitar, and the two dogs.

# PLATE I

## GEOLOGIC MAP OF PORTIONS OF THE ALVDAL AND KVIKNESKOGEN QUADRANGLES, NORWAY

by Elizabeth A. McClellan




## EXPLANATION

- mrp — gray phyllite
- mrss — sandstone
- mrc — conglomerate
- mrfg — Fundjsø group greenstone and keratophyre

Meråker nappe

- mgs — Moskardsætra graphitic schist
- serpentinite conglomerate
- serpentinite or conglomerate?
- sgp — graphitic phyllite
- sss — sandstone and phyllite
- sc — conglomerate

Savalen upper sequence

Unconformity

- svs — Svartlia mica schist
- bak — Bangardsvola amphibolite and keratophyre
- Einunna amphibole schist
- lqm — Langåsen quartzite and marble
- vop — Volengsvola phyllite
- lopt — Lomsjødalen phyllite and tuffite
- log — Lomsjødalen greenstone

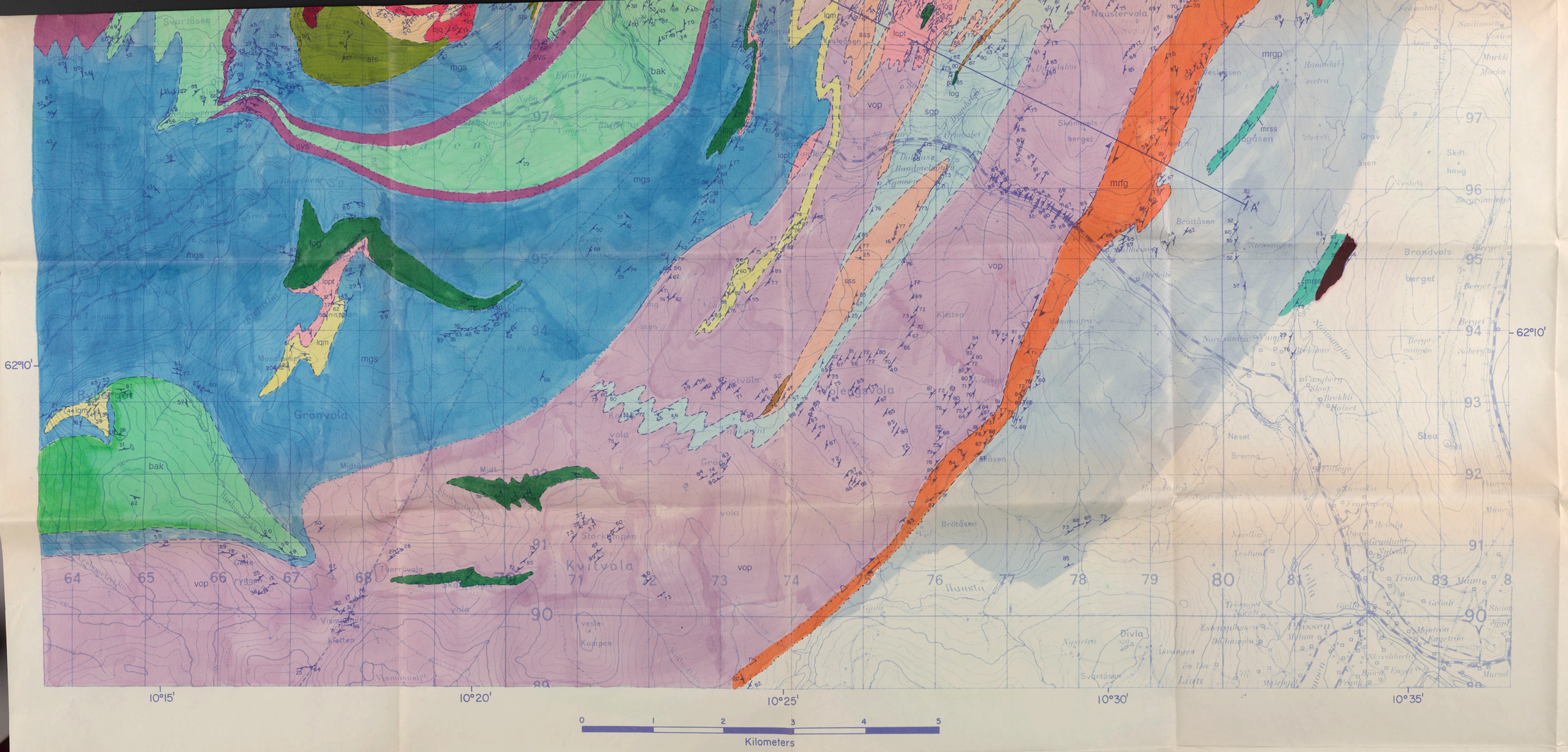
- sts — Strålsjøåsen schist
- bjq — Bjørnkletten quartzite
- vq — Varden quartzite
- eiqs — Einunnfjellet quartzite/schist sequence (undifferentiated)

### Contacts

- Lithologic: exact / approximate / inferred
- Pre-Scandian(?) thrust fault: exact / approximate / inferred
- Scandian oblique slip fault: exact / approximate / inferred

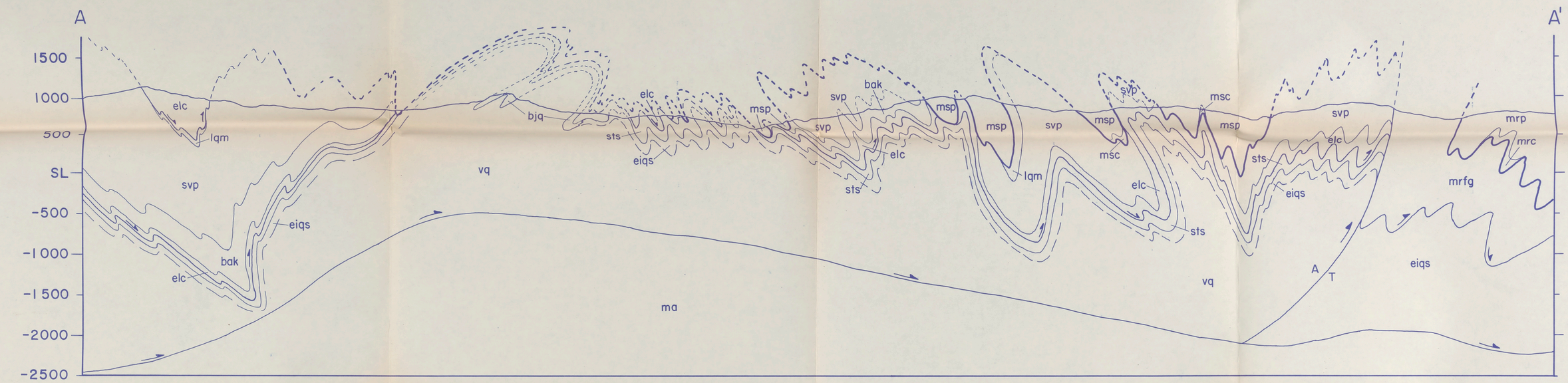
### Structure symbols

- Strike and dip of foliation
- Trend and plunge of mineral lineation
- Trend and plunge of intersection lineation
- Trend and plunge of upright antiform
- Trend and plunge of upright synform


Trend and plunge of upright antiform
Trend and plunge of upright synform
Trend and plunge of overturned antiform
Trend and plunge of overturned synform
Trend and plunge of crenulation axis
Trend and plunge of kink fold axis
Trend and plunge of Z fold
Trend and plunge of S fold
62°10'
10°15'
10°20'
10°25'
10°30'
10°35'
0 1 2 3 4 5
Kilometers
A
A'
mgs
bak
vop
sgp
sss
lopt
lqm
log
sls
svs
bjq
mrfg
mrgp
mrss
lgm
Grønvola
Kvitvola
Brøttåsen
Brandvola
Nuustervola
Svartåsen

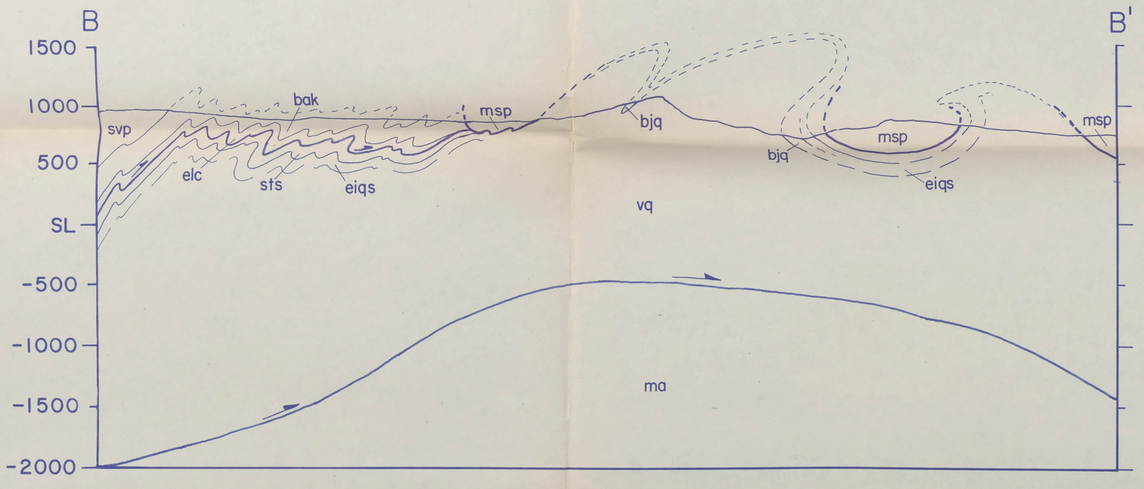
# PLATE II

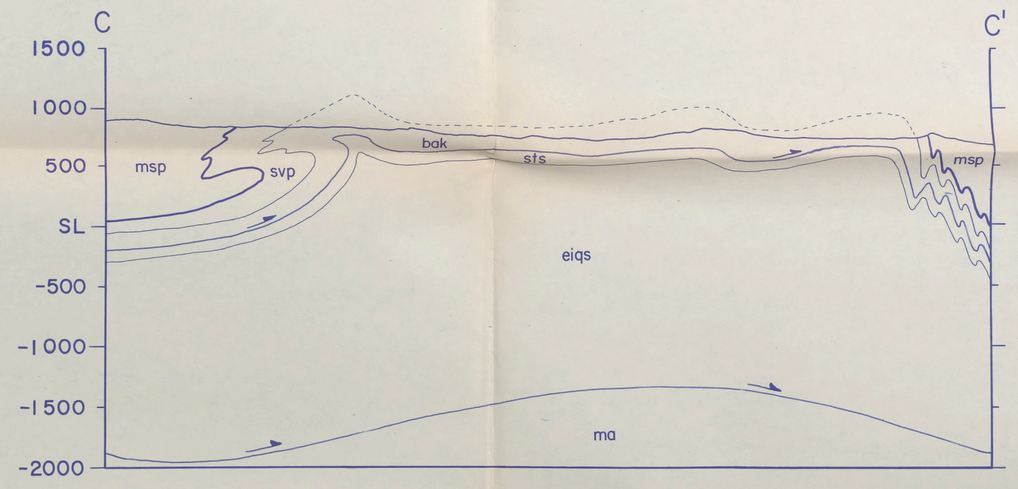
## CROSS SECTIONS ALONG LINES A-A', B-B', AND C-C' ON PLATE I




0 1 2 3

Kilometers
(No vertical exaggeration)




## COMBINED UNITS FROM GEOLOGIC MAP

(otherwise see Plate I for explanation of symbols)

| | |
|---|---|
| msp | Moskardsætra schist/Savalen phyllite |
| svp | Svartlia schist/ Volengsvola phyllite |
| elc | Einunna/Lomsjødalen complexes |
| ma | Middle Allochthon |

# PLATE III

## Bedrock Geologic Map of the Lomsjødalen Area, South of Lake Savalen (includes portions of the Lomsjøen, Naustervola, Svartknausen, and Sivilosen 1:5,000 maps, Hedmark Fylke, Norway)

by
Elizabeth A. McClellan
1993

### Explanation

**Savalen upper sequence**

- sgp — Slaty gray or black phyllite
- sss — Pebbly metasandstone, green phyllite
- sc — Conglomerate, dominantly polymict

→ sus — Upper sequence, undifferentiated

unconformity

**Savalen thrust sheet**

- lqm — Fuchsite-bearing, marble and quartzite (Langåsen quartzite/marble)
- bak — Amphibolite and metakeratophyre (Bangardsvola complex)
- vop — Calcareous gray phyllite. Contains mica schist and garbenscheifer to west (Volengsvola phyllite)
- lopt — Metatuff, phyllite, and metalliferous sediments (Lomsjødalen complex)
- log — Greenstone, with pillow basalt and breccia (Lomsjødalen complex)

### Lithologic contacts:

exact ————————

approximate – – – – – – – –

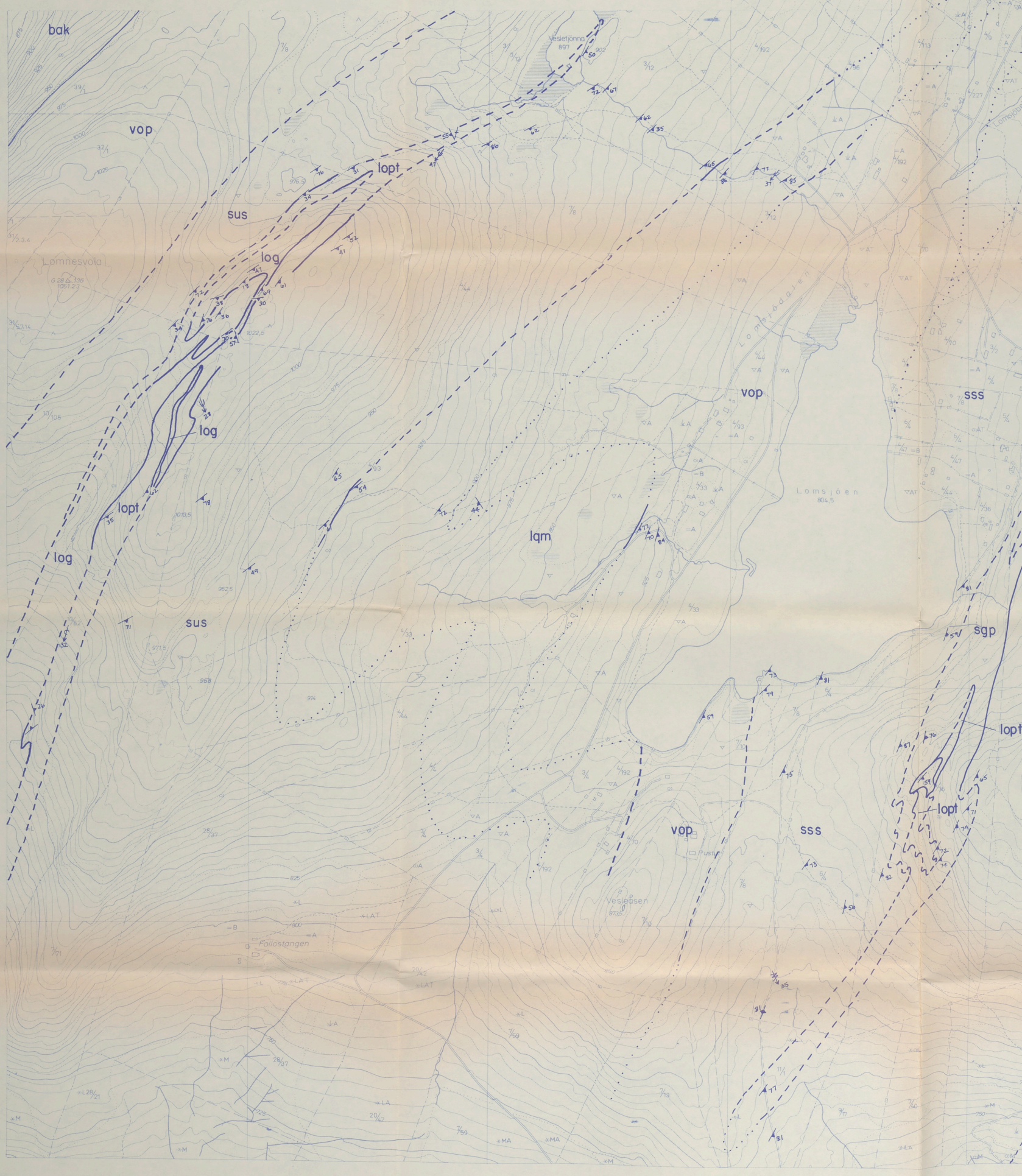
inferred · · · · · · · · · · · · ·

### Symbols:

strike and dip of foliation 70

trend and plunge of upright antiform 63

0 50 100 200 300 400 500
meters



bak
bak
log
vop
vop
sgp
sc
sus
log
sgp
lopt
lopt
sss
sgp
lopt
lopt
log
vop
Sandvika
Sandvika
sss
lqm
vop
Hammarodden
lopt
lopt
Lauvbekktangen
Lauvbekken
Golfbekken
Lomsjøbekken
Lomsjøvola
Lomsjøvola
Tangen
sss
sc
sc
sss
log
sc
sss
sgp
sgp
sgp
Nausterdalen
Nausterdalsbekken
lqm
Storstrypet
Djupdalen
Savalen
707